STRATEGIC ENVIRONMENTAL ASSESSMENT FOR MUNICIPAL WATER DEMAND BASED ON CLIMATE CHANGE

SALAH LAFTA FARHAN ZUBAIDI

A thesis submitted in partial fulfilment of the

requirements of Liverpool John Moores University

for the degree of Doctor of Philosophy

August 2018

DECLARATION

I, Salah Lafta Farhan Zubaidi, confirm that the work presented in this thesis is my own. Where information has been derived from other sources, I confirm this has been indicated in the thesis.

Salah Lafta Farhan Zubaidi

ACKNOWLEDGEMENT

PhD is a rewarding but challenging journey, which would not be possible without the help of many people.

First and foremost, I would like to express my sincere gratitude to my supervisors, Dr. Patryk Kot, Prof. Rafid Al Khaddar and Dr. Mawada Abdellatif for their continuous support, advice, and guidance throughout my candidature. They have built and directed an environment that granted me an opportunity to learn and practise research skills, meet and collaborate with brilliant researchers, and transfer the long journey of PhD to a great and lovely experience.

Special thanks go to Prof. Adnan Al-Samawi and Dr. Sandra Ortega-Martorell. They offered me guidance when I was struggling to choose an approach for implementing feasible solutions. Besides, I would like to thank my friends and colleagues in Liverpool John Moores University. It has been such a pleasure and a privilege to work with you all.

I appreciate the funding source that made my PhD work possible, the Ministry of Higher Education in Iraq and its representative in the United Kingdom the Iraqi cultural attaché in London.

I would like to thank my family. For the soul of my father who encouraged me to love science and supported me for chasing my dreams. For my beloved mother for all her love and encouragement.

Last but not the least, I would like to extend my heartfelt thanks to my lovely kids for making my life better and my wife for her encouragement during rough times, as we taste all the sweetness and bitterness of pursuing a PhD. I cannot imagine a greater fortune other than having them in my life. Their love and care are indispensable to any of my achievements.

ABSTRACT

Accurate urban water demand forecasting plays a key role in the planning and design of municipal water supply infrastructure. The reliable prediction of water demand is challenging for water companies, specifically when considering the implications of climate change (Zubaidi et al., 2018). Several studies have documented that weather variables drive water consumption in the short-term, and it enhances the accuracy of the prediction model when it is combined with socio-economic factors. However, the impact of climate change on the municipal water demand has yet to be challenged.

To surmount this challenge, more research work is needed to accurately estimate the required quantity of water with increasing water demands. Recently, Artificial Neural Networks (ANNs) have been found to be an innovative approach to predict water demand. This PhD study aims to develop a novel methodology to forecast the impact of climate change on municipal water demands for a long-term time series based on the baseline period 1980-2010. It should be highlighted that, based on our knowledge, this is the first study of substantial duration, based on data collected from 1980-2010, which focuses on the associations between monthly climate change and municipal water consumption.

A new approach is therefore proposed to quantifying municipal water demands through the assessment of climatic factors, using a combination of a Singular Spectrum Analysis (SSA) technique, three hybrid computational intelligence algorithms and an ANN model. These hybrid algorithms include a Lightning Search Algorithm (LSA-ANN), a Gravitational Search Algorithm (GSA-ANN) and Particle Swarm Optimisation (PSO-ANN). The SSA technique is adopted to decompose the time series of water consumption and climate variables to detect the stochastic signal for each time series. In the same context, the hybrid algorithms are used to find the best value of

learning rate coefficient and the number of neurons in both hidden layers of the ANN model. Based on the performance of each hybrid algorithm, the most accurate and reliable water demand forecast model will be selected and used for estimating future water consumption. The considered environments of this study are applied in Australia and the United States from America for mitigating the uncertainty associated with the geographic location (the data of the United States of America was used to support the reliability of developing the municipal water demands prediction model).

Furthermore, the Long Ashton Research Station Weather Generator (LARS-WG) model is utilised to simulate future climate factors over three periods (2011-2030, 2046-2065 and 2080-2099) based on the B1, A1B and A2 emission scenarios and seven General Circulation Models (GCMs). The future projection of these climate factors is applied directly to the impact model of water consumption to obtain the projected municipal water demand for different future periods and different greenhouse emission scenarios.

The principal findings of this research are the following: from the model perspective, 1) the SSA is a powerful technique when used to remove the effect of socio-economic factors and noise, and detect the stochastic signal time series for water consumption. 2) The ANN model has better performance in term of optimising the correlation between observed and predicted water consumption when using the (LSA-ANN) algorithm.

3) The evaluation of the ANN model (using a validation data set) for Melbourne and Columbia Cities gives a correlation coefficient of 0.96 and 0.95, and the root mean square errors are 0.025 and 0.016 respectively. These findings indicate the capability

of the proposed model to predict water demands with high accuracy in different continents.

4) The high performance of LARS-WG model results are found to be appropriate for the simulation of future climate variables.

5) The harmonisation between future monthly water demand (for the periods 2011-2030, 2046-2065 and 2080-2099) and stochastic signals of climate variables, relative to baseline period 1980-2010, emphasises the reliability of the present methodology.

However, from the water demand perspective, the water percentage demand (WPD) are likely to rise in winter, drop in summer and fluctuate in both spring and autumn seasons for all periods and under all greenhouse emission scenarios. The results of WPD distribute between -3.5% and 3% for all periods and emission scenarios. The A2 scenario shows the highest and lowest values of WPDs compared to the A1B and B1 scenarios, in particular, in the 3rd period. The mean of seasonal WPD values shows that there is no dominant scenario as the best or the worst case of water demand over all future periods. The highest amount of seasonal demand happens in winter (A2 scenario, 3rd period), and the lowest amount of seasonal demand occurs in autumn (A1B scenario, 3rd period).

In conclusion, this study facilitates the conception of the impact of climate change on municipal water demand from the baseline period 1980-2010.

List of Publications

- **Journals**

Zubaidi, S. L., Dooley, J., Alkhaddar, R. M., Abdellatif, M., Al-Bugharbee, H. & Ortega-Martorell, S. (2018) A Novel approach for predicting monthly water demand by combining singular spectrum analysis with neural networks. *Journal of Hydrology*, 561, 136-145. **(Published)**

Zubaidi, S. L., Gharghan, S. K., Dooley, J., Alkhaddar, R. M. & Abdellatif, M. 2018. Short-Term Urban Water Demand Prediction Considering Weather Factors. Water Resources Management, 32, 4527-4542. **(Published)**

Zubaidi, S. L., Kot, P., Alkhaddar, R. M., Abdellatif, M. & Ortega-Martorell, S. (2018) Methodology for Strategic Management of Municipal Water Demand Prediction under Climate Change. *Journal of Hydrology*. **(Under Review)**

- **International Conferences and Workshops**

Zubaidi, S. L., Kot, P., Alkhaddar, R. M., Abdellatif & M., Al-Bugharbee, "Short-Term Water Demand Prediction in Residential Complexes: Case Study in Columbia City, USA" in Developments in eSystems Engineering (DeSE), 2018 11th International Conference on, 2018.

Zubaidi, S. L., Kot, P., Alkhaddar, R. M. & Abdellatif, "Short-Term Water Demand Prediction Considering Climate Change Based on Particle Swarm Optimization Technique" in The Second International Conference for Science and Arts, 2018.

TABLE OF CONTENTS

LIST OF FIGURES

LIST OF TABLES

ABBREVIATIONS

ADF	Augmented Dickey-Fuller
AI	Artificial Intelligence
ANFIS	Adaptive Neuro-Fuzzy Inferences System
ANN	Artificial Neural Network
ANN-FLR	Artificial Neural Network-Fuzzy Linear Regression
AR4	IPCC Forth Assessment Report
ARIMA	Autoregressive Integrated Moving Average
ASCE	American Society of Civil Engineers
BP-NN	Backpropagation Neural Network
CCNN	Cascade Correlation Neural Networks
CNCM3	Centre National de Recherches France
DES	Deseasonalized
DET	Detrended
DETDES	Detrended and Deseasonalized
EKF	Extended Kalman Filter
Ɛ	noise
FFNN	Feed Forward Neural Networks
gbest	global best
GCMs	General Circulation Models
GFCM21	Geophysical Fluid Dynamics Lab USA
GLM-ANN	Generalised Linear Model and Artificial Neural Network
GP	Genetic Programming
GRNN	Generalized Regression Neural Networks
GSA	Gravitational Search Algorithm
HADCM3	UK Meteorological Office UK
HL	Hidden Layer
HLNs	Hidden Layer Neurons
INCM3	Institute for Numerical Mathematics Russia
IPCC	Intergovernmental Panel on Climate Change
IPCM4	Institute Pierre Simon Laplace France
KPSS	Kwiatkowski– Phillips–Schmidt–Shin
K-S	Kolmogorov-Smirnov
LARS-WG	Long Ashton Research Station Weather Generator
LM	Levenberg-Marquardt
LSA	Lightning Search Algorithm
LSSVM	Least Squares Support Vector Machine
M	Mean
MAE	Mean Absolute Error
ML	Megalitre
MLP	Multilayer Perceptron
MLP-MAF	Multilayer Perceptron- Multi-Activation Function
MLR	Multiple Linear Regression

MNLR	Multiple Nonlinear Regression
MPEH5	Max-Planck Institute for Meteorology Germany
MSE	Mean Squared Error
MW	Melbourne Water
MWPDs	Mean of the Water Percentage Demands
NCCCS	National Centre for Atmospheric USA
NN	Neural Network
OECD	Organisation for Economic Co-operation and Development
ORG	Original
Pbest	local best
PCs	Principle Components
PPP	Policy, Plan, or Program
PSO	Particle Swarm Optimisation
QPSO-LSSVM	Quantum Particle Swarm Optimization-Least Squares Support Vector Machine
QPSO-RBF	Quantum Particle Swarm Optimization-Radial Basis Function
R	Correlation Coefficient
Radi	Solar radiation
Rain	Rainfall
RBF	Radial Basis Function
RBNN	Radial Basis Neural Networks
RCM	Regional Climate Model
RMSE	Root Mean Square Error
SARIMA	Seasonal Autoregressive Integrated Moving Average
SCEM-UA	Shuffled Complex Evolution Metropolis
SD	Standard Deviation
SEA	Strategic Environmental Assessment
SPSS	Statistical Package for the Social Science
SVM	Support Vector Machine
Tmax	Maximum temperature
Tmean	Mean temperature
Tmin	Minimum temperature
TS	Time Series
TS-GRNN	General Regression Neural Network-Time Series
UNFCCC	United Nations Framework Convention on Climate Change
USA	United States of America
VIF	Variance Inflation Factor
WA-ANN	Wavelet-Artificial Neural Network
WDF-ANN	Water Demand Forecasts and Artificial Neural Networks
WPDs	Water Percentage Demands
YVW	Yarra Valley Water

Chapter 1: Introduction

1.1. Overview

Water is a fundamental element for the continuation of life on our planet, and an efficient municipal water system is essential for the social and economic development of any country. At present, many countries face numerous concurrent challenges in the management of, and access to, potable water. van Leeuwen et al. (2012), UNDP (2013) and Ferguson et al. (2013a) have identified the impact of global warming and related climate change, such as an increased frequency and severity of drought and flooding as one of the most significant impacts on our aquatic environment. As a result, considerable pressure is being placed on water infrastructure.

Climate change adversely affects the lives and livelihoods of human societies, and these impacts differ based on the region, significance and term. However, freshwater resources are widely influenced, especially in the centre of cities (UNDP, 2012). In addition, United Nations' reports show that, between 2009 and 2050, the level of urbanisation is expected to increase from 50% to 69% (Deng et al., 2015). Bougadis et al. (2005) pointed out that the prediction of municipal water consumption is very significant for decision makers in the water companies. Forecasting demand is therefore valuable in the operation and management of municipal water systems.

Previous studies have used traditional models and proved that water consumption is affected by weather variables throughout the year for example Gato et al. (2005); Gato et al. (2007a) and Gato et al. (2007b). However, Urich and Rauch (2014) stated that global warming causes considerable uncertainties regarding long-term planning projections for water demand in urban areas. These uncertainties can lead to significant

problems for systems (such as supply, operation and cost), which traditional planning methods cannot solve.

Several previous studies have established that artificial neural network (ANN) approaches outperform traditional methods (e.g. regression and time series) in different fields e.g. Jain et al. (2001), Mohammadi et al. (2005) and Azadeh et al. (2007). However, there has been disagreement on the criteria for selecting the factors of ANN model that could lead to over- or under-fitting the model (Gharghan et al., 2016a). In addition, the precise effect of climate change on municipal water demand for the long term is a much-debated topic and extremely challenging (Behboudian et al., 2014). Accordingly, much uncertainty still exists about the relationship between the capacity of municipal water systems and a potential rapid increase in water demand resulting from acute climate factors on a monthly, seasonal and yearly basis.

1.2. Strategic Environmental Assessment (SEA)

Increasing concerns about the impact of climate change have confirmed the need to plan and manage water ahead, to guarantee meeting municipal water demands to the satisfaction of the consumer (Babel and Shinde, 2011). Cutore et al. (2008) reported that this type of strategic planning means planning now for an uncertain future.

To provide sufficient information about the environmental implications of a potable water policy, plan or program, strategic environmental assessment (SEA) has been widely used by the decision makers. The aim behind the SEA is evaluation, identification and mitigation of these implications, as well as to protect the environment and encourage sustainability at the strategic level (Chaker et al., 2006; Li et al., 2014). In addition, WB (2005) defined the SEA as a formalised, systematic and

comprehensive process for evaluating the environmental impacts of a policy, plan, or program (PPP). A typical SEA methodological approaches diagram is revealed in Figure 1.1.

Figure 1-1: Strategic Environmental Assessment (SEA) (Partidário, 2007)

1.3. Research Problem

Fogden and Wood (2009) mentioned that the environmental outlook of the Organisation for Economic Co-operation and Development (OECD) to 2050 indicates that global demand for water is anticipated to increase by 55%, relative to 2000 as a baseline. Moreover, a high percentage of the universal population may be under acute water stress. The global population percentage that has a lack of access to safe drinking water is presented in Figure 1.2. It can be seen that the worldwide population percentage that has the lack of access to safe drinking water increases as we go into the future, and it is likely to be 50% in 2050.

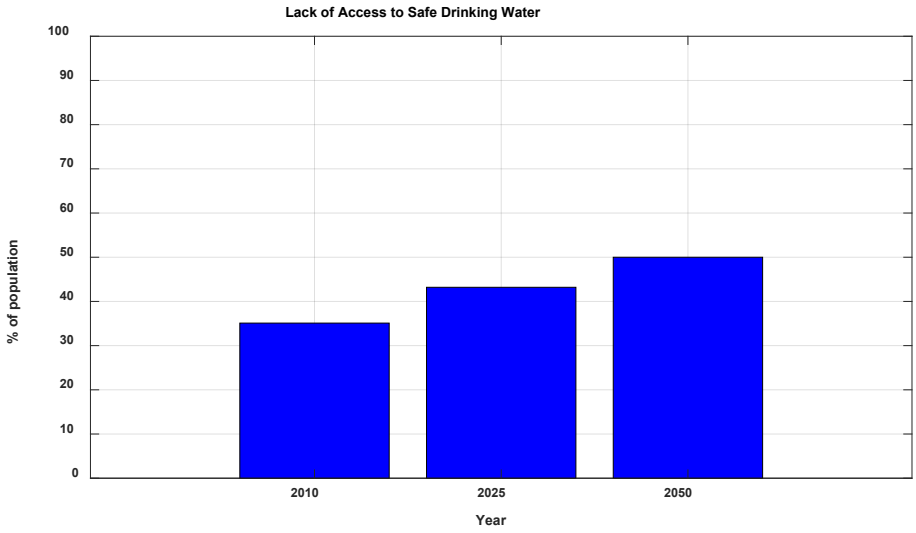

Figure 1-2: The global population percentage that has a lack of access to safe drinking water (Fogden and Wood, 2009)

The population is one of the significant factors that affecting the demand of municipal water and improving the prediction model as well as growing population lead to increase water demand (Adamowski, 2008; Firat et al., 2010). The majority of previous studies employed population factor as a model input to predict water demand (e.g., Jain et al. (2001), Liu et al. (2003), Firat et al. (2009) and Behboudian et al. (2014)). However, in this thesis, this factor has not been considered because it is out the scope of the study as the focus only on climate change assessment not the socio-economic factors.

Hot weather conditions, extended dry periods and a general reduction in rainfall, also increase the consumption and demand, for water. As it is anticipated that climate change will cause substantial increases in temperature, a decrease in rainfall and more droughts, it is necessary to analyse these issues and explore the relationships between climate and water consumption used to predict water demand (Zhoua et al., 2000). Adamowski et al. (2012) stated that successive dry days with high temperatures and a low number of rainy days can play a crucial role in increased water demand.

Accordingly, the urban water supply infrastructure faces increasing pressures related to the impact of extreme climate factors. Under these pressures, the present urban water supply infrastructure is probably insufficient to meet future water demands. However, conventional models are no longer fit to predict urban water demand under the pressures of climate change in the future (Marlow et al., 2013). Babel and Shinde (2011) and Bakker et al. (2014) stated that using the climate factors in the model input had significant impact on the forecast water demand by decease the scale of errors. The peak municipal consumption of Columbia City changes depend principally on how dry it is during the summer months (Jacobs and St. Louis, 2015). Gato et al. (2005), Gato et al. (2007a) and Gato et al. (2007b), have confirmed that weather factors drive water demand over the year. These studies were applied in different environments such as (Zhoua et al., 2000) in Australia, Adamowski et al. (2012) in Canada, Babel and Shinde (2011) in Thailand and Bakker et al. (2014) in Netherlands. As stated in aforementioned studies, we also believe that considering climate factors in a municipal water consumption has a significant effect on the forecasting water demand.

A search of the literature revealed that few previous studies deal with municipal water demand prediction. However, studies have used different types of factors as forecast model input in mid-term prediction models including socio-economic data e.g. Liu et al. (2003); Firat et al. (2009) and Firat et al. (2010), a mixture of socio-economic with weather variables for example Mohammed and Ibrahim (2013), Behboudian et al. (2014), Al-Zahrani and Abo-Monasar (2015), and a combination of previously recorded values of water consumption, e.g. Firat et al. (2010) and Sebri (2013). Most of these studies have weaknesses in terms of considering the impact of climate factors, which results in increasing the uncertainties of municipal water demand.

In the same context, these studies have ignored the impact of the climate change considering the baseline period 1980-2010, where this period was chosen to assess the impact of climate change. They apply the short or mid-terms e.g. Cutore et al. (2008) and Adamowski et al. (2012). Therefore, exactly how climate change affects municipal water demands is still not yet fully understood.

Although the previous studies have recognised weather factors, research has yet to systematically investigate the effect of these factors in terms of using adequate data preprocessing to remove the impact of socio-economic factors, which are insensitive to climate, in addition, applying a capable and effective forecasting technique that depended on a systematic basis instead of a trial and error approach. Accordingly, the studies to date have not been able to detect to what extent climate factors have driven municipal water demands.

Overall, previous studies of municipal water prediction have suffered from inadequate sample sizes, methodological limitations and a lack of a strong theoretical framework. So, the debate continues on the best strategies for the management of municipal water demands under the impact of climate change with a low level of certainty.

1.4. Aim and Objectives of this research

This research aims to forecast monthly municipal water demand for the long term considering several climatic variables including temperature, rainfall and solar radiation, by using a combination of techniques that have various types of hybrid Artificial Neural Network (ANN) models to provide water companies with the right strategic decision in operations and planning for municipal water systems.

The specific objectives for realising the aim of the thesis as stated above are:

1. To conduct a comprehensive literature review to identify gaps in this research field and to select the best approach. Many researchers have studied the prediction of water demand either for short-term, considering weather variables, or for mid-term, considering socio-economic factors and sometimes combined with some weather variables.
2. To assess the long-term influence of climate change on monthly municipal water demands it is important to be compared relative to the baseline period (1980-2010). This period was chosen by scientists to assess climate change because there is no variation in the climate pattern in this period. Furthermore, there is more data available during this period for climate change assessment.
3. To identify the stochastic signals for water consumption and different climate factors. The stochastic signal of a water consumption time series is detected after removing the effect of socioeconomic factors (which are insensitive to weather and have a deterministic relation with water consumption), and noise from water consumption for a long-term monthly time series.
4. To examining extra climate variables in the model inputs, and to select the best model input based on statistical techniques that increase forecasting accuracy compared with a trial and error approach.
5. To optimise the prediction of long-term monthly municipal water demand with high accuracy and minimum error where it is applied to different continents (different environments).
6. To simulate the rainfall, temperature and solar radiation variables in the future that are used in the water demand-forecasting model to investigate the climate change impact on municipal water consumption.

7. To increase the forecasting range and decrease the uncertainty of results for municipal water demands by using different models of hybrid ANN, general circulation models and different greenhouse emissions scenarios.
8. To provide the decision maker with a clear scientific view about municipal water demand in the future that is affected by climate change, as accurately as possible.

1.5. Contribution to Knowledge

This section describes the thesis contributions to the body of knowledge of the municipal water demand under climate change research field.

1. This research project investigates the municipal water demand prediction considering monthly data of climate factors on a long-term basis. In particular, a baseline period between 1980 and 2010 was used.
2. This thesis employs a powerful technique, namely singular spectrum analysis (SSA), which has the ability to detect the stochastic signal of water consumption and climate factors after removing trend, seasonality and noise. In contrast, previous studies have used the traditional methods to remove trend and seasonality from time series, which have less accuracy in terms of the scale of errors.
3. This research develops a new technique which includes cross-correlation and variance inflation factor. This technique was carried out to ensure that as many of the potential variables as possible were properly included in the map of the input-output relationship, to avoid multicollinearity, which can lead to incorrect conclusions.

4. Applying and comparing three hybrid intelligence algorithms to select the optimum parameters of the ANN model (i.e., Lightning Search Algorithm, Gravitational Search Algorithm and Particle Swarm Optimisation). The ANN parameters include the learning rate coefficient and number of neurons in both hidden layers. These parameters are responsible for mapping the relationship between the input and output variables adopted to develop the ANN model and minimise the error.
5. Using the combination model, SSA and hybrid ANN, to forecast municipal water demand based on climate factors under three emission scenarios and over three periods 2011-2030, 2046-2065 and 2080-2099.

1.6. Thesis Organisation:

The overview, aim and novelty of this thesis are already discussed in the previous sections. Next, the thesis chapters are organised as follows:

Chapter 2: The literature review presents different studies on climate change, and highlights the practical implications for freshwater resources and the different methods that are used to simulate future climate variables. The main techniques for predicting municipal water demand have been discussed in detail, includes current research contributes to it by introducing an innovative forecasting technique more consistent with the sustainable path.

Chapter 3: This chapter presents the steps for conducting the research methodology that includes developing a new combination model to forecast municipal water demands regarding climate change, as well as, the process and approaches that are used to simulate future climate factors under different emission scenarios.

Chapter 4: This chapter focuses on the study area, which offers the essential issues regarding municipal water consumption such as the location of the city, its weather, freshwater resources and municipal water system for two different cities. In addition, the chapter presents the data preprocessing technique that helps to prepare the data set before employing it in the municipal water prediction model.

Chapter 5: This chapter presents results and discussion, which show the development and validation of the proposed frameworks divided into three sections. 1) The evaluation of the combination model of forecasting the municipal water demands. 2) The calibration and validation of the downscaling model and the simulating future climate variables. 3) The forecasting of future municipal water demand using results of the future climate factors (step 2) in the model of water forecasting (step 1). This chapter also discusses the outcome of the results from the different experimental scenarios.

Chapter 6: The thesis conclusion contains the attained research aim and the contribution to fill the gap in this research field regarding the forecasting of municipal water demand considering climate change. Moreover, this chapter shows the limitations that are found in this research and the essential recommendations that should be considered to overcome these limitations.

Appendices: Detailed appendices that contain copies of additional figures and tables concerning this study are displayed at the end of the thesis. The organisation of the chapters in this thesis is presented in Figure 1.3.

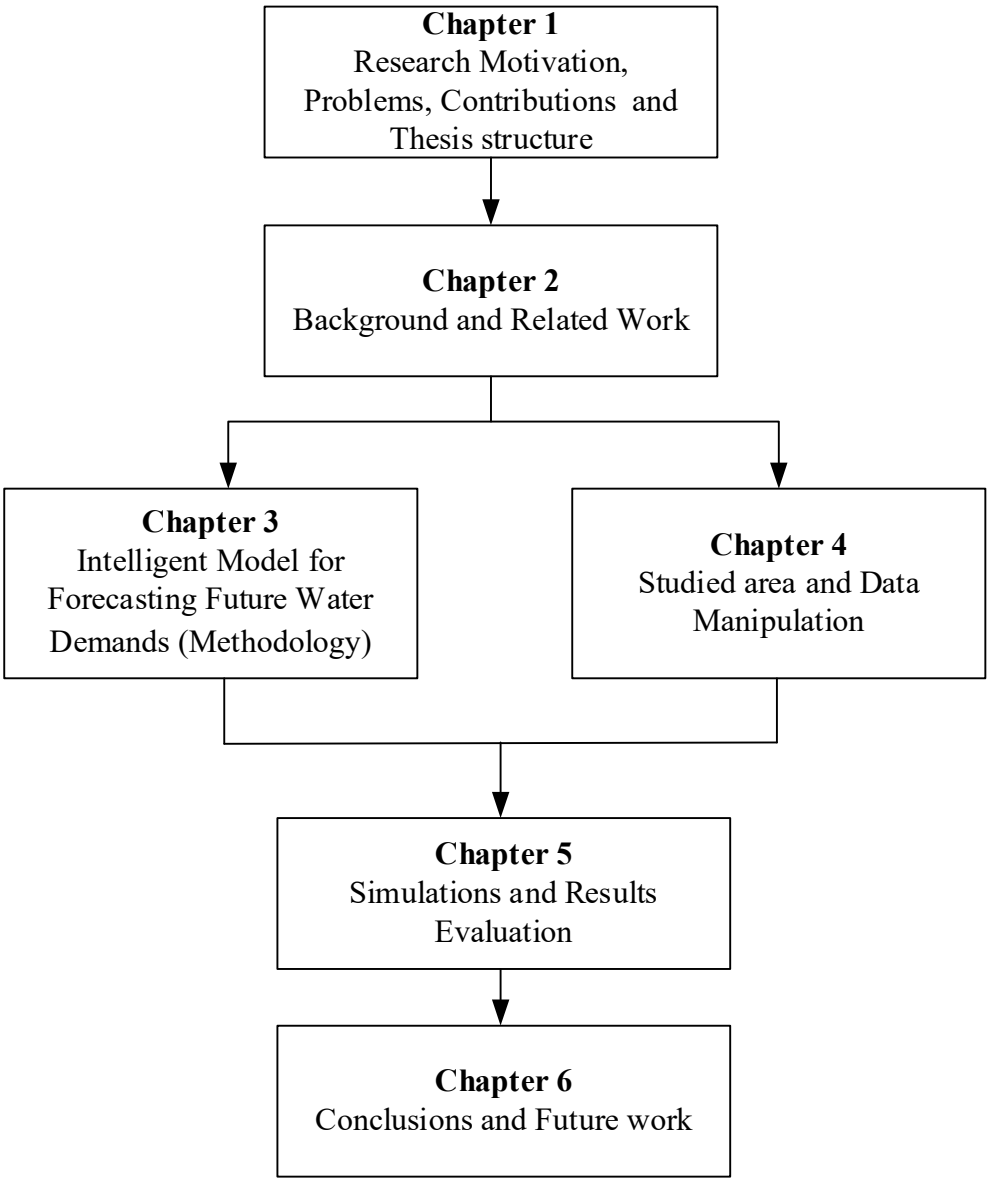

Figure 1.3: The thesis organization

Chapter 2: Literature Review

2.1. Introduction

This chapter highlights the advantages of the literature review to find out the principles, usefulness and reliability of the suggested project, which is forecasting municipal water demand over the long term taking into consideration the impact of climate change on different scenarios of greenhouse emissions. Accordingly, this chapter focuses on a short overview of methods relevant to the methodologies defined in this thesis. It is organised as follows:

Section 2.2 focuses on what climate change is and its implications. It covers the downscaling of the climate factors from large scale General Circulation Models (GCMs) and the approaches that are used for this purpose. Municipal water consumption and its priority to water companies are covered in section 2.3 and section 2.4 reviews the water consumption simulation models that were used to predict water demand.

Section 2.5 explores the water projection and its benefits for the municipal water system. Finally, section 2.6 discusses the time series analysis techniques that include data set and data preprocessing.

All the above mentioned helps to discover more about the software programmes that are currently used, and the ideas developed for the different approaches that are applied in the field of water demands prediction. This is taken into consideration to ensure the performance techniques for the proposed solution in this research study are valid. As a result, it illustrates the differences between the proposed study and previous studies.

2.2. Climate Change

Since the beginning of time, humanity has faced worldwide challenges, and one of the most significant problems is climate change. Climate change, which is also known as global warming, is the phenomenon of an increase in atmospheric temperature and change in magnitude and patterns of rainfall that causes modifications in the ecosystem. These modifications affect both people and their surrounding environment both directly and indirectly (Borbora and Das, 2014; Jewitt et al., 2015).

UNFCCC (2007) stated that climate change has harmful effects on atmospheric stability, the aquatic environment and the wild environment. The long-term effects of elevated CO_2 levels determine the world's vulnerability to climate change. As the effects of climate change are expected to increase, they continue to have wide-ranging impacts on ecosystems and human societies. These impacts vary in terms of the zone, the effects and the seriousness, and they can be either short-term disasters or long-term variations in the climate system. However, one of the substantial impacts is that freshwater resources are widely affected, particularly in cities (UNDP, 2012). Climate change causes considerable problems for the ecosystem, for example, fluctuation of precipitation where scarce precipitation can lead to drought, which can in turn cause desertification, freshwater resources are widely depleted, particularly in city centres, the problems this causes are likely to be exacerbated because of increasing demands on freshwater (Davies and Simonovic, 2011).

For example, in Australia the rainfall has shown different patterns from region to region. It increased in the north of Australia especially in summer, monsoon rainfall. While in contrast, precipitation dropped in the southern region. This reduction in

rainfall is likely because of raised the concentrations of greenhouse gas and land-use change (IPCC, 2007).

Figure 2.1 presents the projected maximum temperature for Australia. The left-hand graph shows the change in maximum temperature under the B1, A1B and A2 scenarios. This change is related to the stability in the concentrations of CO_2 at different values 450 ppm (WRE450), 550 ppm (WRE550), 650 ppm (WRE650), 750 ppm (WRE750) and 1,000 ppm (WRE1000). The graphical diagram of evaluating the relative coping range, adaptive capacity and vulnerability regarding the potential of global warming is shown in the right hand chart. The maximum temperature in 2100 is likely to increase by about 2, 3 and 4°C for the B1, A1B and A2 scenarios respectively, and the vulnerability of water security becomes considerable for 2 to 2.3°C of global warming (IPCC, 2007).

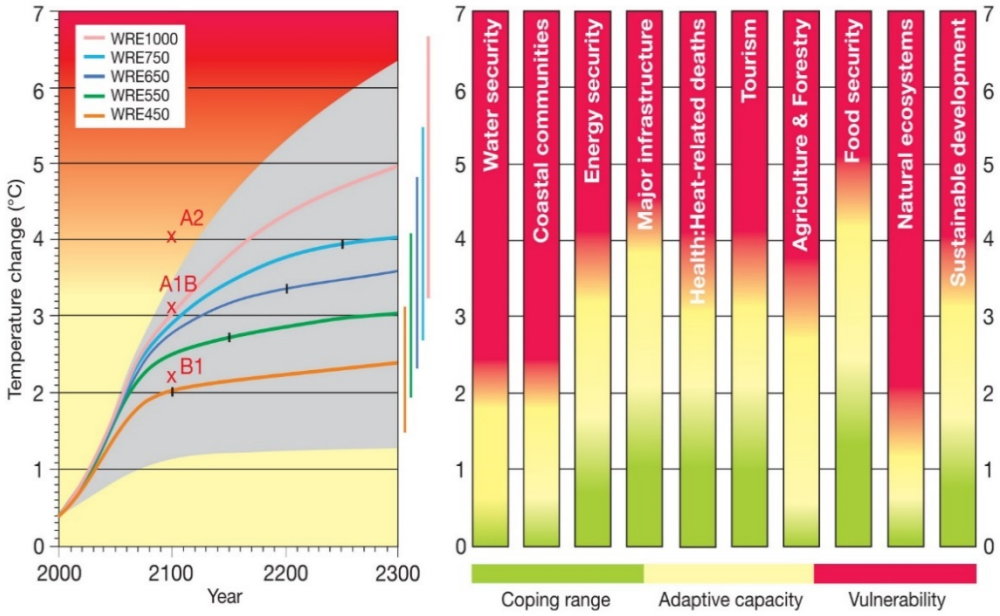

Figure 2-1: The expected maximum temperature for Australia and the coping range, adaptive capacity and vulnerability regarding of potential global warming (IPCC, 2007)

Antecedent research, such as Gato et al. (2005), Gato et al. (2007a) and Gato et al. (2007b), have confirmed that weather factors drive water demand over the year. Bakker et al. (2014) applied three varying models: a Multiple Linear Regression, a Transfer/-noise model, and an Adaptive Heuristic, with and without utilising weather input. The models' outcomes demonstrated that, when weather inputs are used, the average errors can be decreased by 7% and the largest predicting errors by 11%. Ferguson et al. (2013b) stated that currently, water managers and stakeholders are struggling to adapt municipal water systems to the increasingly complicated challenges of climate change.

Partidário (2007) claimed that baseline details are collected as proof to confirm environmental deterioration. However, it is necessary to collect and arrange baseline data which represent all necessary information that is collected about past and current situations concern, and it is especially concerned with describing all related aspects. (Partidário, 2012) believed that baseline data could help to predict and extrapolate likely influences in the future, and prediction will contribute to building a desirable future. In this research, the baseline data for any factor will be divided into two groups, which comprise calibrating and verifying models.

Climate change has placed considerable pressure on the environment in different areas of the world. These issues have increased the motivation of researchers to analyse and forecast the changes in critical climatic factors, such as temperature, rainfall and solar radiation, in order to offer valuable reference outcomes for management and planning in the future (Jewitt et al., 2015).

There are many efforts to reduce the emission of greenhouse gases such as Paris Agreement on Climate Change This agreement dealing with mitigation, adaptation,

and finance of greenhouse-gas-emissions, agreed upon by more than 180 countries within the United Nations Framework Convention on Climate Change (UNFCCC) in 2015 and starting in the year 2020. The long-term aim of this agreement is for keeping the rise in global average temperature to well below 2 °C above pre-industrial levels. Also, it discussed the technology transfer, financial transfer and enhance building capacity in the developing countries. Accordingly, it is expected that little decrease in the emissions will occur making the world may face rising difficulties (Jayaraman, 2015).

2.2.1. (Chen et al., 2011)Climate Projection

Several approaches have been utilised to assess global climate simulations and to downscale different global climate scenarios (from the different emissions scenarios) for evaluating the climate influences on hydrologic systems (Salathe et al., 2007). Daniels et al. (2012) mentioned that the downscaling methods depend on several General Circulation Models (GCMs) and Intergovernmental Panel on Climate Change (IPCC) scenarios. These methods can be divided into two main types as shown in Figure 2.2:

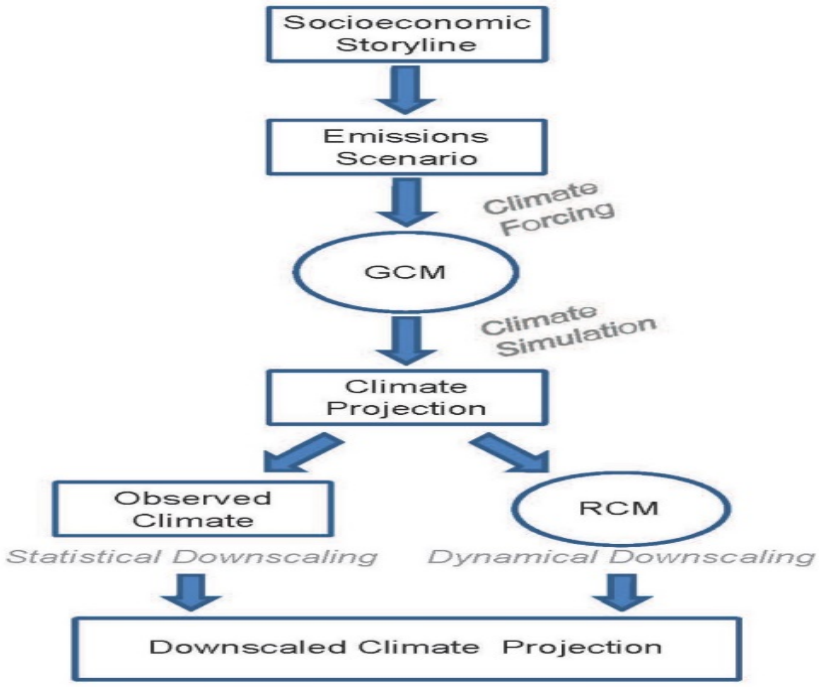

Figure 2-2: Downscaling methodologies flow chart (Daniels et al., 2012)

- The dynamical downscaling approach depends on the utilisation of a regional climate model that is similar to the GCM principles, but it has much higher resolution than GCM, and it covers particular regions of the global. The regional climate model (RCM)generates climate information at a spatial resolution of approximately 20–50 kilometres using the large-scale atmospheric information that is produced by the GCM model. Additionally, the regional climate model is dependent on the outputs of GCM, which causes the overall results to be affected by the quality of the GCM model.
- The statistical downscaling method includes establishing statistical relationships between the historical large-scale atmospheric and local climate factors. After determining and validating the relation, the model is ready to simulate future climate factors at a site-specific level. However, this method depends on the critical assumption that the relationship between the local

climate and present large-scale circulation remains valid at various conditions for simulating future climates.

A GCM is the main tool applied to project the influences of emissions on future climates. It provides information at a scale of 100-500 kilometres for one grid size and temporal scales of monthly means and longer. Accordingly, it is considered too coarse for planning and assessment of the impact for almost all decision makers. The downscaling technique, however, has been used to obtain information on climate change at a scale more relevant to stakeholders. It is utilised spatially, with a resolution of 20 kilometres or even at a specific location, and temporally (e.g., daily temperature sequences from monthly or seasonal temperature figures) (Trzaska and Schnarr, 2014). Roy and Majumder (2016) point out that the IPCC offers various climate change scenarios and attempts to forecast the result of that variation on different related natural phenomena. These scenarios are based on pollution and land use dynamics, population and the influence of climate change on these activities. These scenarios are:

- The A2 scenario depicts a very heterogeneous world, with continuously growing global population and economic development is oriented regionally.
- The B1 scenario describes a convergent world, global population will reach its peak mid-century and the introduction of clean technologies.
- The A1B scenario is balanced between using fossil and non-fossil energy across all sources.

More details about the IPCC scenarios can be found in IPCC (2007).

Chen et al. (2011) stated that the main sources of uncertainty are connected to greenhouse gases emissions and General Circulation Models (GCMs), while

downscaling approaches have been considered to have less influnce on the uncertainty. Accordingly, in this thesis seven GCMs and three greenhouse emission scenarios are considered to mitigate the uncertainties.

For hydrologic impact researches, temperature and rainfall are the most significant climate factors that are obtained from downscaling models (Salathe et al., 2007). Therefore, the temperature, solar radiation and rainfall have been used as a model input to forecast municipal water demand.

Many studies have applied downscale approaches to simulate future climate factors, such as Abdellatif et al. (2015) who investigated the spilling volume of urban drainage catchment in northwest England, under different climate change scenarios and climate models, using a generalised linear model and an ANN (hybrid GLM-ANN) model. In addition, Räisänen (2015) used 12 Regional Climate Model simulations (RCM) and baseline (1980–2010) monthly mean temperatures to investigate the changes in snowfall in northern Europe. Also, Masanganise et al. (2014) utilised 10 regional climate models (RCM) and monthly temperature and rainfall to describe climate changes in Zimbabwe for the 2040-2070 period, relative to the 1980-2010 baseline.

Daniels et al. (2012) stated that the statistical downscaling method has advantages such as being efficient, computationally inexpensive and offering various emissions scenarios and GCM pairings, while the dynamic downscaling method needs high computational resources, expertise and a high volume of data inputs. The Long Ashton Research Station Weather Generator (LARS-WG) model considers one of the statistical downscaling methods that were used by several researchers in different areas.

Several studies tested the LARS-WG performance and confirmed that the model is reliable. For example, Chen et al. (2012) used the LARS-WG model with seven GCMs, A1B scenario and the baseline period 1980-2010 to examine the ability of the model to simulating precipitation and (maximum, minimum) temperature in Sudan and South Sudan over three periods (2011-2030, 2046-2065 and 2080-2099). Osman et al. (2017) employed the LARS-WG model with seven GCMs, the A2 scenario and baseline the period 1980-2010 to investigate the capability of the model to simulate precipitation over three future periods in different areas in Iraq. Behboudian et al. (2014) used the LARS-WG model under a HADCM3 (A1B) scenario to downscale the monthly observation value of maximum temperature depending on baseline period to predict its monthly value from 2011-2030. These future values are adopted with some socio-economic values to predict monthly municipal water demand during this period.

Fenta Mekonnen and Disse (2018) Use LARS-WG version (5.5) to analyse the future climate change by projection maximum temperature, minimum temperature and rainfall of upper Blue Nile river basin. The result shows that the model is capable to simulate climate factors.

For this study, a set of CMIP4 GCMs and LARS-WG software version 5.5 have been used, which was the latest version available when this research project has started. In order to assess the reliability and capability of our proposed methodology to accurately predict long-term monthly water demand, we considered necessary to maintain, the same CMIP4 GCMs that was used previously to thoroughly evaluate the proposed methodology. Moreover, other researchers are also currently using the same version, as an example please see Fenta Mekonnen and Disse (2018). However, we would also

like to stress that, even when not the latest CMIP5 GCMs was used, this study is proposing a novel method for the strategic management of municipal water demand under climate change; therefore, its novelty goes beyond the data used, to provide a method that anyone can use and translate to any future CMIPx GCMs. Extra details about the LARS-WG model can be found in section 3.6.1.

2.3. Municipal Water Consumption

Municipal water consumption can be divided into domestic, industrial and commercial sectors (Gato, 2006). Liu et al. (2003) defined residential water consumption include all uses of water both inside residences and in gardens. In addition, the demand of residential water may account for more than half of the total municipal use in many societies.

Forecasting can be divided into short- and long-term. Short-term forecasting is fundamentally associated with scheduling operations related to pumping and decreasing the time that water is retained in storage tanks, which can improve the water quality (Bougadis et al., 2005). Long-term prediction is desired fundamentally to plan, design and make expansion plans for present municipal water systems (Jain et al., 2001). In addition, to date, many reviews have been carried out in the field of water demand forecasting, but most of these studies have focused on the short-term forecast and have used self-correlation models in forecasting (Behboudian et al., 2014).

Nowadays, increasing concerns about the impact of climate change have confirmed the need to plan and manage water ahead to guarantee meeting municipal water demands to the satisfaction of the consumer (Babel and Shinde, 2011).

2.4. Water Consumption Simulation

Hot weather conditions, extended dry periods and a general reduction in rainfall, also increase the consumption of, and demand, for water. As it is anticipated that climate change will cause substantial increases in temperature, a decrease in rainfall and more droughts, it is necessary to analyse these issues and explore the relationships between climate and water consumption used to predict water demand (Zhoua et al., 2000). Prediction is a significant topic in the water industry. One of the primary applications of forecasting is the estimation of municipal water demand, yet achieving the anticipated prediction accuracy is quite challenging (Behboudian et al., 2014).

Different techniques have been applied to forecast water demand, and these methods can be divided into three main kinds: Traditional, Artificial Intelligent and Hybrid models.

2.4.1. Traditional Prediction Techniques

Several researchers have examined the impact of weather factors on the water demand using conventional methods. More precisely, time-series and regression analysis, or a combination of the two methods, were most frequently adopted as the traditional modelling techniques by studies in the past (Jain et al., 2001).

Zhoua et al. (2000) developed a time series model to predict daily water demand for greater Melbourne, Australia, that includes residential, industrial and commercial consumption. Water consumption was divided into base use, weather-insensitive, that represented the lowest month's consumption; and seasonal use, weather-sensitive, which contains seasonal, climatic, and persistence components. The prediction model of daily water time series comprises a set of equations that represents the impacts of

four factors on water use containing trend, seasonality, climatic correlation, and autocorrelation. A polynomial was adopted to represent a yearly trend in base use consumption as a function of time. Seasonal, climatic and persistence components were utilised to model the seasonal water use. The study adopted the daily historical data of water consumption and three meteorological factors maximum temperature, precipitation and class A pan evaporation from 1st July 1989 to 31th January 1997. The results showed that Antecedent Precipitation Index improves the model and efficiency R^2= 89.6% for cross-validation data.

Gato et al. (2005) used a simple time series to develop a simple model of regression analysis for forecasting short-term water demand. The approach has potential to be utilised as a tool to determine the effects of water restrictions and conservation initiatives on water consumption, both base and seasonal use, that are allowed to be a function of weather factors. The study adopted the daily historical data of water consumption and two weather factors: maximum temperature and rainfall, from April 1991 to December 2001. In addition, it focuses on the distribution zone of East Doncaster that is a large residential suburb of Melbourne City, Australia; while Zhou et al., (2000) covered Greater Melbourne, which contains mix areas. This study confirmed the next three postulates: (1) urban water consumption can be split into base use, during winter months, and seasonal use. Also, the outcomes indicate that base use is sensitive to weather variables. (2) Rainfall occurrence causes a temporary decrease in seasonal water use that minimises over time and is finally negligible. (3) During the rainfall absence, the alteration in seasonal water use follows the air temperature pattern.

Two years later, Gato et al. (2007a) applied the same postulation of total water used that is assumed in Zhou et al. (2000) to develop the model of Gato et al., (2005) with the same data. In addition, this study used the Zhou et al. (2000) deseasonalising approach, which was Fourier analysis to calculate the potential component of seasonal water use instead of the heat function approach that was used in Gato et al., (2005). Also, Stepwise regression analysis was adopted in this study. The outcomes showed that base use was significantly affected by the maximum temperature, rainfall and the day of the week. It confirmed the findings of Gato et al.'s (2005) that base use is weather sensitive. Furthermore, the efficiency of the model had been improved.

Gato et al. (2007b) then evolved the simple time series model in Gato et al., (2005) by using the same period and zone of daily data. The study aimed to examine the threshold levels of maximum temperature and precipitation that drive the total water demand. The results show that domestic water demand was not influenced by maximum temperature changes at 15.3°C or below and at precipitation levels of 4.8 mm or higher.

Sarker et al. (2013) employed the Gato et al., (2007b) model for checking to what extent the base use component is weather-sensitive for mixed areas, i.e. residential, industrial and commercial. This study used the daily historical data of water consumption, maximum temperature and precipitation for Greater Melbourne City, Australia from 1980-2009. The results showed that the threshold levels of temperature and rainfall were 15.53°C and 4.08 mm respectively. The maximum temperature threshold concerning residential water use was a little bit lower than that for mixed water use, While, the precipitation threshold corresponding to residential water use was higher than that of mixed water use.

The studies confirmed that water demand was driven by weather factors during the year by using various traditional methods, which offered results that have different prediction accuracy. The accuracy of the model has encouraged researchers to look for more accurate methods to forecast water demand, especially as climate change challenges increase, and Artificial Intelligence (AI) is one of the most important prediction techniques.

2.4.2. Artificial Neural Network

Artificial neural networks (ANNs) are an information processing technique that aims to emulate human brain functionality by adopting the same connectivity and operations as biological neurones. It can capture nonlinear relationships by system input and output training (Ahmed et al., 2016; Cutore et al., 2008). Mohammadi et al. (2005) stated that the ANN is a new approach for urban water modelling, which has the ability to deal with a large number of input and output patterns. These techniques are:

- Faster in comparison to their conventional counterparts.
- Robust in noisy environments.
- Flexible in terms of solving different problems.
- Highly adaptive to newer environments.

These specifications make the ANN technique more efficient and viable in the comprehension of hydrologic issues (Mohammadi et al., 2005). Ghiassi et al. (2008) advised utilising the Artificial Neural Network (ANN) technique in water demand modelling because nonlinear relationships occur among the factors that determine the variation in water consumption. Moreover, the ANN approaches have been shown to be an efficient technique to analyse a variety of nonlinear time series events, including water demand prediction. Unlike many hydrological applications, it has been noted

that the artificial neural network technique has only limited application in terms of water demand modelling (Firat et al., 2010).

Several previous studies have investigated and compared conventional and ANN models to predict water demand, and they found that ANN techniques have the ability to predict water demand better than the traditional model:

Jain et al. (2001) examined three models, ANN, regression and time series. The study employed weekly historical data for water consumption and weather variables (total rainfall and average maximum air temperature) from 1989 to 1998 for Kanpur City, India. The findings show that the rainfall occurrence is a more effective indicator than the amount of rainfall itself and also that the ANN technique consistently outperformed both the traditional methods.

One year later, Jain and Ormsbee (2002) presented an ANN model and compared it with two traditional models, regression and time series. The study employed the historical daily data for water consumption and weather variables in Kentucky state, USA, from 1982-1992. The results indicated that the simple ANN model produce more accurate prediction than the conventional techniques.

Bougadis et al. (2005) investigated three methods: time series analysis, linear and multiple linear regression, and artificial neural networks. The research adopted the historical weekly data of water consumption, for summer months only, for the city of Ottawa, Canada, from 1993-2002. It also used the climate variables and antecedent water consumption as model inputs. The performance of the ANN models in predicting water demand consistently outperformed the traditional models.

Adamowski (2008) compared three approaches: time series analysis, multiple linear regression, and artificial neural networks to predict peak daily water demand in summer months only. Historical daily data of water consumption for the city of Ottawa, Canada from 1994-2002 were adopted in this study. Weather variables and previous water consumption were used as model inputs. Depending on results, ANNs techniques offered a better forecasting model for predicting peak daily water demand than the other approaches.

These applications clearly show that ANN models consistently outperformed the conventional models. Babel et al. (2007) stated that traditional forecast models are often unable to adequately provide precise and reliable outcomes, as they tended to overestimate water demand. This causes the production and transmission of more drinking water than is needed and leads to pressure on previously stressed water resources. Thus, an accurate and reliable technique is required. This has promoted the use of different types of ANN methods to predict water demand.

Msiza et al. (2007) investigated two types of artificial neural network: the multilayer perceptron (MLP) and the radial basis function (RBF). The study used data from Gauteng Province, in the Republic of South Africa for short- and medium-term water demand. Different activation functions, learning algorithms and numbers of neurons in the hidden layer were employed in this research. A comparison on the best networks from each type showed that the RBF network had the best accuracy and faster convergence.

A year later, Msiza et al. (2008) applied and compared two types of machine learning include ANN and Support Vector Machine (SVM) to predict municipal water demand for Gauteng Province, South Africa. The models were built and assessed by using

daily historical data of municipal water consumption from January 1997 to July 2006. The findings revealed that the ANN model offered better performance than SVM techniques in term of its ability to generalise municipal water time series prediction.

Firat et al. (2009) evaluated three types of ANN; Generalized Regression Neural Networks (GRNN), Feed Forward Neural Networks (FFNN) and Radial Basis Neural Networks (RBNN). This study used monthly socio-economic and weather variables as model inputs, from 1997-2005, for Izmir City, Turkey. The outcome, when using 25 different input variables, revealed that a model consisting of multiple input variables is better than a single variable input. The GRNN outperformed all other ANN techniques and Multiple Linear Regression (MLR) when predicting monthly water demand.

A year later, Firat et al. (2010) assessed three ANN models, including two of the techniques evaluated previously (FFNN, GRNN) and Cascade Correlation Neural Networks (CCNN). This study also used historical monthly data from Izmir City, Turkey, over the same period (1997-2005). The model input for the ANN techniques included several combinations of previous water consumption values. The results showed that using five of these values resulted in the best model input, CCNN consistently outperforming both FFNN and GRNN.

Yurdusev et al. (2010) proposed the generalised regression neural networks (GRNN) model to predict municipal water consumption in Izmir City, Turkey. This study used historical monthly socio-economic and weather variables from 1997 to 2004 to build and examine the model. The data included water bills, population, number of households, gross national product, average temperature and rainfall. The results

reveal that the GRNN model is capable of successfully simulating municipal water demand.

Babel and Shinde (2011) applied different artificial neural network (ANN) architectures, with various explanatory variables, to forecast daily and monthly water demands in Bangkok City, Thailand. This study used daily water consumption data and weather factors from October 2005 to August 2008 for daily predictions, and monthly water consumption data, meteorological variables and socioeconomic factors from October 2002 to August 2008, for monthly predictions. Cross-correlational and sensitivity analyses were applied to minimise the model input set to forecast water demand accurately. The results showed that weather factors had a more significant impact on the medium-term forecast as compared to short-term estimates.

Mohammed and Ibrahim (2013) used a multilayer perceptron neural network model with a multi-activation function (MLP-MAF), to predict both daily and monthly municipal water demand in Tampa City, USA. Various combinations of activation functions were used in the hidden layer of the model. To estimate the capability of the developed model over both the short and mid-term, daily water consumption data and four climatological factors over the period 1992 to 2004, were used. The results showed that the set of linear, sine and cosine activation functions within the MLP-MAF and Radial Basis Function (RBF) models were better than other groups. Turning to the models in general, the combined MLP-MAF model was better than the MLP and RBF models, even though the MLP-MAF model did not perform particularly well.

Ajbar and Ali (2015) applied ANN and compared with an econometric model to predict the monthly and yearly municipal water demand for Mecca City, Saudi Arabia. Both models were assessed using historical data of city population, persons per

household, household income, maximum temperature and a likely number of visitors each month over the period from 2003 to 2010. The results of the models showed that performance of the ANN was better than the performance of the econometric model based on monthly and yearly data.

Prediction of water demand is a substantial topic for policy-makers in the water industry. It is still extremely challenging to achieve the expected forecasting accuracy with respect to the prediction trends (Behboudian et al., 2014). Accordingly, different optimisation methods can be used to tackle problems in applications. The aim of optimisation algorithms is to locate the optimum values for a system's parameters, under different conditions (Ahmed et al., 2017). Recently, different hybrid models have been used to predict water demand accurately.

2.4.3. Hybrid Models

The need for increased reliability, capability and accuracy regarding data-driven techniques has encouraged researchers to evolve innovative models. Hybrid models are being developed to meet new requirements; their prime objective is to integrate the advantages of two or more techniques in such a way as to improve the capability of single models. These hybrid models are commonly an integration of techniques in a series where traditionally, one technique is deemed as the primary technique, the others functioning as pre-processing or post-processing methods (Araghinejad, 2014).

Liu et al. (2003) proposed a combined model that included water demand forecasts and artificial neural networks (WDF-ANN). This study used historical monthly water consumption and socio-economic data for Weinan City, China, from 1991 to 2000, to establish a water prediction model. The results indicated that a WDF-ANN model had the ability to simulate monthly water consumption patterns.

Cutore et al. (2008) developed a novel hybrid model that shuffled complex evolution metropolis algorithm (SCEM-UA) with an artificial neural network to predict daily municipal water demand. The new technique was compared with three approaches containing a traditional ANN, regression and an adaptive neuro-fuzzy inferences system (ANFIS). The study used daily weather variables and antecedent water consumption data from 2003 to 2004 in Catania City, Italy. The outcomes obtained show that the predictive ability of the hybrid model was better than the predictive capability of the other models.

Nasseri et al. (2011) developed a coupled model that combines the Extended Kalman Filter (EKF) and Genetic Programming (GP) to predict municipal water demand in Tehran City, Iran. Historical monthly data of municipal water consumption from 1992 to 2002 were used to build and assess the model. The data were divided randomly into two sets of 70% for training and 30% for verification. In addition, three lags of measured municipal water consumption were employed as likely and independent of the model inputs. The results showed that the hybrid model was effective and capable of simulating municipal water demand (R=0.87).

Azadeh et al. (2012) developed a relatively new technique of hybrid fuzzy linear regression–artificial neural network (FLR-ANN) and compared this with the artificial neural network (ANN) and fuzzy linear regression (FLR). This study employed daily historical data of municipal water consumption in Tehran City, Iran from 5th April 2004, to 21th March 2009, to build and assess the model. The hybrid approach consistently outperformed the ANN and FLR techniques for both cold and warm days.

Campisi-Pinto et al. (2012) applied a combined wavelet-denoising and ANN model and compared it with ANN and Multiple Linear Regression (MLR) models to predict

urban water demand in Syracuse City, Italy. The model employed 84 historical monthly-observed data from January 2002 to December 2008 for building and assessing the models. The results showed that the wavelet-denoising had a significant impact on ANN that leads to making the combined model offering better results than the ANN and MLR models.

Adamowski et al. (2012) developed a novel hybrid technique, a combination of discrete wavelet transforms and artificial neural networks (WA-ANNs) model, to predict municipal water demand for Montreal City, Canada. The daily historical data of rainfall, maximum temperature and previous water consumption over summer only (May to August) from 2001 to 2009 were employed to build the model. The WA-ANN model was tested and compared with the ANN, autoregressive integrated moving average (ARIMA), MLR and multiple nonlinear regression (MNLR). The results showed that the WA-ANN model was more accurate.

Zhu and Xu (2012) established an effective technique (QPSO-RBF) using combined quantum particle swarm optimisation algorithm (QPSO) and radial basis function (RBF) artificial neural networks. These models were employed to predict municipal water consumption in a city in southern China. The daily historical data for water consumption and weather factors from April to July 2010 were used to build and assess the models. The QPSO algorithm was utilised to optimise the parameters for the RBF and this led to improvements in the speed and accuracy of the hybrid model. The results demonstrated that QPSO-RBF hybrid techniques are better than both PSO-RBF and RBF models based on the root mean square error, which is 2.14, 2.76 and 3.5 for QPSO-RBF, PSO-RBF and RBF respectively.

A year later, Zhu and Chen (2013) proposed a hybrid model (QPSO-LSSVM) combining a QPSO algorithm and a least squares support vector machine (LSSVM). This study used the same data set from the last research to build and examine the new hybrid model. QPSO technique was employed to select the optimum parameters for the LSSVM. The results depict that the speed of computation and the accuracy of prediction for the hybrid model (QPSO-LSSVM) are better than SVM, and LSSVM approaches based on the average relative error that is 1.76, 2.18 and 3.16 respectively.

Al-Zahrani and Abo-Monasar (2015) established a model that combined the GRNN and time series (TS) techniques. Historical daily data of water consumption and weather variables for Al-Khobar City in the Kingdom of Saudi Arabia from 2006 to 2009 were used. The results confirm that the combined model (TS-GRNN) is superior to both the GRNN and TS approaches alone in simulating water demand pattern and seasonal water demand trend.

Brentan et al. (2017) proposed a novel hybrid model, which is support vector regression and adaptive Fourier series to predict short-term municipal water demand in France and Brazil. Historical meter data (every 20 minutes) from May 2012 to December 2013 were employed to build and evaluate the model. The findings showed that the model was viable and valid to use in both areas of study (France and Brazil).

Various optimisation approaches can be adopted to handle a range of issues for different applications. Recently, the Lightning Search Algorithm (LSA) is a new nature-inspired meta-heuristic optimisation algorithm, based on the natural phenomenon of lightning, for tackling constraint optimisation issues. This algorithm has been applied in various areas such as: improving a fuzzy logic speed controller for an induction motor drive (Abd Ali et al., 2015), home energy management (Ahmed et

al., 2016) and a wind power model (Sirjani and Okonkwo, 2016). The Gravitational Search Algorithm (GSA), which is inspired by the Newtonian law of gravity and proposed by Rashedi et al. (2009), has been used to tackle various optimisation problems such as wireless sensor networks (Gharghan et al., 2016a), image processing (Zhao, 2011) and the electricity market (Vijaya Kumar et al., 2013). Also, Particle Swarm Optimisation (PSO) algorithm has been used in different fields such as municipal water prediction (Zubaidi et al., 2018), wireless sensor localisation mechanisms (Gharghan et al., 2016b) and estimating results of biological treatment (Ethaib et al., 2016).

Based on these findings three optimisation techniques have been used in this thesis to estimate the best value for learning rate coefficient and the number of neurons in each hidden layer of the ANN model, for predicting long-term municipal water demand under climate change.

2.5. Future Projection of Water Demand

Forecasting municipal water demand aims to minimise the risks involved in decision-making (Walker et al., 2015). Marlow et al. (2013) point out that accurate prediction can improve the performance of water distribution systems and encourage better water management in addition to urban water sustainability. However, the problems faced by the water sector as a result of global warming, has increased pressure on its infrastructure.

Prediction of water demand can play a significant role in optimising the design, operation and management of urban water supply infrastructures. It can minimise the

uncertainty that results from a rapid increase in water demand due to climate effects (Bougadis et al., 2005).

Behboudian et al. (2014) used a stationary chain and ANN to develop a municipal water demand model to predict water demand between 2011-2030. In addition, a linear regression model was utilised to compare and decrease the forecast uncertainty. Monthly data for maximum mean temperature, inflation index, income (economic growth) and water price of Neyshabour City, Iran, from 1997 to 2008, was adopted to assess the model. The values of maximum temperature were forecasted from downscaling the model of LARS-WG software (using HADCM3 General Circulation Model (GCM), A1B scenario) for the period 2011-2030. The results show that (1) for data preprocessing, normalising the data by logarithm and then detrending was better that detrending only (without normalising). (2) For different structures of ANN, statistical values indicate that ANN was more accurate than the regression model.

The drawbacks of this study are:

1) the prediction model was dependent on trial and error processes that may not offer an optimal solution;

2) the study used small sample sizes and it employed maximum temperature and combined it with socio-economic factors;

3) it used one GCM to simulate future maximum temperature and that increased the uncertainty.

On examination of previous researches, no existing study has investigated the influence of climate change on municipal water demand over a recommended baseline

period. These studies have suffered from inadequate sample sizes, evidence for climate change impact has been mixed with socioeconomic factors and several conceptual and methodological weaknesses. So, the municipal water demand under the effect of climate change is still poorly understood.

2.6. Time Series Analysis Techniques

2.6.1. Data Set

Many methods have employed different data sets of model inputs over various periods to predict water demands.

Most studies of water demand prediction have only investigated the impact of socio-economic factors (e.g. Liu et al. (2003); Firat et al. (2009); Firat et al. (2010)), or a mixture of socio-economic and weather variables such as, Bougadis et al. (2005); Cutore et al. (2008); Firat et al. (2009); Babel and Shinde (2011); Mohammed and Ibrahim (2013); Behboudian et al. (2014); Al-Zahrani and Abo-Monasar (2015). Some of the previous research into water demand has focused on a combination of previously recorded values of water consumption for example, Firat et al. (2010) and Sebri (2013).

Few studies have adopted weather variables only in their water demand models as well as employing limited variables includes (maximum temperature and total rainfall only) e.g. (Jain et al., 2001; Jain and Ormsbee, 2002; Adamowski, 2008; Adamowski et al., 2012). Adamowski (2008) advised using extra weather variables in the water demand model to include evaporation, humidity, wind speed, and the amount of cloud cover and sunshine.

Much of the current literature on simulation of water demand pays particular attention to either short-term prediction such as Jain et al. (2001); Bougadis et al. (2005); Cutore et al. (2008); Adamowski (2008); and Firat et al. (2010), or mid-term prediction e.g. (Jain and Ormsbee, 2002; Adamowski et al., 2012; Mohammed and Ibrahim, 2013; Behboudian et al., 2014).

Overall, these studies highlight the need for assessing the impact of climate change on municipal water consumption over the long term that needs a robust technique for data manipulation (data preprocessing).

2.6.2. Data Preprocessing

Maier and Dandy (2000) stated that it is vital to pre-process data in an appropriate form before it is utilised in an ANN. These techniques are essential to confirm that all the data receives equal attention in the learning mode. Data cleaning includes identifying and removing trends and non-stationary components from a data set, as explained in Abrahart et al. (2004). Time series can be decomposed into trend (T), oscillatory (O), stochastic (S) and noise (Ɛ) components, with trend and oscillatory are considered deterministic signals (Araghinejad, 2014).

Zhang and Qi (2005), used ANN to evaluate the effect of two preprocessing techniques; the detrending and deseasoning of nonlinear monthly data. Their results showed that both techniques can minimise prediction errors, and the combination of both was found to be the most efficient preprocessing method. Sebri (2013) investigated the impact of data preprocessing to include original (ORG); detrended (DET); deseasonalized (DES); and detrended and deseasonalized (DETDES) in an ANN. They compared the results with the traditional Box–Jenkins method, which is Seasonal Autoregressive Integrated Moving Average (SARIMA). Trimester data was

adopted in this study during (1983-2010) for Tunisia City, Tunisia. Four time-series step lags were used as the input for all models in this study because the time series of residential water consumption is quarterly. The results depict that the (SARIMA) model with (ORG) data is better than the ANN approach with (ORG), (DET), and (DES) data. The ANN technique with (DETDES) data was superior to all the other models.

In this thesis, Singular Spectrum Analysis technique (SSA) is used for detrending, deseasoning and noise removal to detect the stochastic signals of water consumption and climate factors time series.

2.6.2.1. Singular spectrum analysis (SSA) method

SSA is a robust technique used to decompose the original time series, which may exhibit nonlinear properties, and to uncover the stochastic component after the removal of noise, trend and oscillatory components, as shown in Khan and Poskitt (2017).

The SSA contains two main stages, decomposition and reconstruction. In the decomposition stage the time series is decomposed into a number of components, where the first components have the larger portion of the original signal variance while the last components have the lower portion. In the reconstruction stage, only the first few components are used to re-build the signal. The last components are neglected as they represent the noise. This will improve the prediction performance of the time series. Additionally, it has the ability to work well even for samples that are small in size (Hassani et al., 2015).

This approach does not require the imposition of any statistical assumptions such as normality or linearity. It has been successfully applied in different sectors including industry (Al-Bugharbee and Trendafilova, 2016), groundwater prediction (Polomˇcic´ et al., 2017) and hydrology (Baratta et al., 2003).

No previous study has considered the impact of climate on water demands or employed a pretreatment signal technique, which has the ability to decompose the time series into different components such as trend, oscillatory behaviour (periodic or quasi-periodic components) and noise filtering. These components help to determine the effect of climate volatility on water consumption, to improve the accuracy of prediction, and to reduce the scale of error between observed and forecast water demand.

Table 2.1: Summary of previous studies

Period	No.	Authors	Methods	Factors
Short-term	1	Yurdusev et al. (2010)	GRNN	A and B
	2	Firat et al. (2010)	CCNN	C
	3	Al-Zahrani and Abo-Monasar (2015)	TS-GRNN	B and C
	4	Azadeh et al. (2012)	ANN-FLR	C
	5	Adamowski et al. (2012)	WA-ANNs	B and C
Mid-term	1	Liu et al. (2003)	WDF-ANN	A and C
	2	Nasseri et al. (2011)	EKF- GP	C
	3	Msiza et al. (2008)	ANN	C
	4	Bougadis et al. (2005)	ANN	C
	5	Jain and Ormsbee (2002)	ANN	B and C

A=Socio-economic, B=Weather and C=Previous water consumption

The research efforts discussed above are promising as shown in table 2.1. However, they all have one weakness or another. Unlike the existing proposals, the solution introduced in this thesis contains the climate factors only as model inputs and for the long-term time series (1980-2010). Additionally, to the best of the author's knowledge this work is a uniquely that addresses the data preprocessing, considering the pretreatment signal, to detect the stochastic signal of water consumption and climate factors. Also, the selection of the ANN model input is based on statistical criteria (cross-correlation and variance inflation factor).

2.7. Summary

Climate change has adversely impacted freshwater resources especially in city centres. Therefore, there is a desire to activate solutions that protect freshwater resources and achieve sustainability. Prediction of municipal water demand is one of the best solutions for conserving water resources, which and has been given attention by both academia and decision makers.

Many of the climate change studies have focused on identifying and evaluating the impacts of increasing temperature and decreasing rainfall. They consider how these factors affect the environment, in particular freshwater resources. Other researches have studied the prediction of municipal water demand where they pay attention to the impact of socio-economic factors more than weather factors.

In this chapter, The relevent literature was briefly summarised as to its impacts and downscaling approaches for simulating future climate factors. The significance of water prediction for the water utilities was discussed, and different types of water demand prediction techniques, with a variety of different inputs, were discussed. The

results confirmed the effect of weather variables on water consumption, and more emphasis was given to the time series analysis techniques, especially the SSA method and the hybrid-ANN methods to forecast long-term municipal water demand under climate change.

Based on the above, gaps have been identified along with suggested technical solutions to forecast long-term municipal water demand under different IPCC scenarios for three future time periods. The methodology of the proposed work is explained in Chapter 3.

Chapter 3: Inteligent Model for Forecasting Future Water Demand (Methodolgy)

3.1. Introduction

This chapter presents the research methodology to highlight the routes undertaken to complete forecasting municipal water demands based on climate change factors. This methodology is based on combination techniques of Singular Spectrum Analysis (SSA) and hybrid Artificial Neural Network (ANN) utilising monthly time series data for water consumption and five climate factors over the baseline period 1980-2010. The techniques of data preprocessing such data normalisation, data cleaning and pretreatment signal are presented in chapter 4. The first stage in this chapter shows all the fundamental issues regarding the ANN model. Next, three computational intelligence algorithms were adopted to optimise the best factors of the ANN model for reducing the uncertainty of municipal water demand prediction models regarding climate change. These algorithms are Lightning Search Algorithm (LSA), Gravitational Search Algorithm (GSA) and Particle Swarm Optimisation (PSO). Then, the ANN model runs to capture the relation between water consumption and climatic variables, in order to use it to forecast future municipal water demands.

In the second stage, daily time series data of climate factors over the period 1980-2010 were employed in statistical downscaling to simulate future weather data. The Long Ashton Research Station Weather Generator (LARS-WG) model is applied to simulate the future climate factors for three periods (2011-2030, 2046-2065 and 2080-2099). In addition, seven General Circulation Models (GCMs) are used to mitigate the uncertainty for different assumptions. Also, several Intergovernmental Panel on Climate Change (IPCC) scenarios are employed to cover all options of greenhouse

emission scenarios that are supported by the selected model. Finally, the simulated climate data applied in the ANN model that resulted from the first stage is used to forecast municipal water demands in the future.

The diagrammatic representation of the municipal water demands model is presented in Figure 3.1. It contains two stages: the first one provides the steps for building the model of water prediction, and the second stage refers to the steps for building a model of downscaling the future climate factors based on the IPCC scenarios.

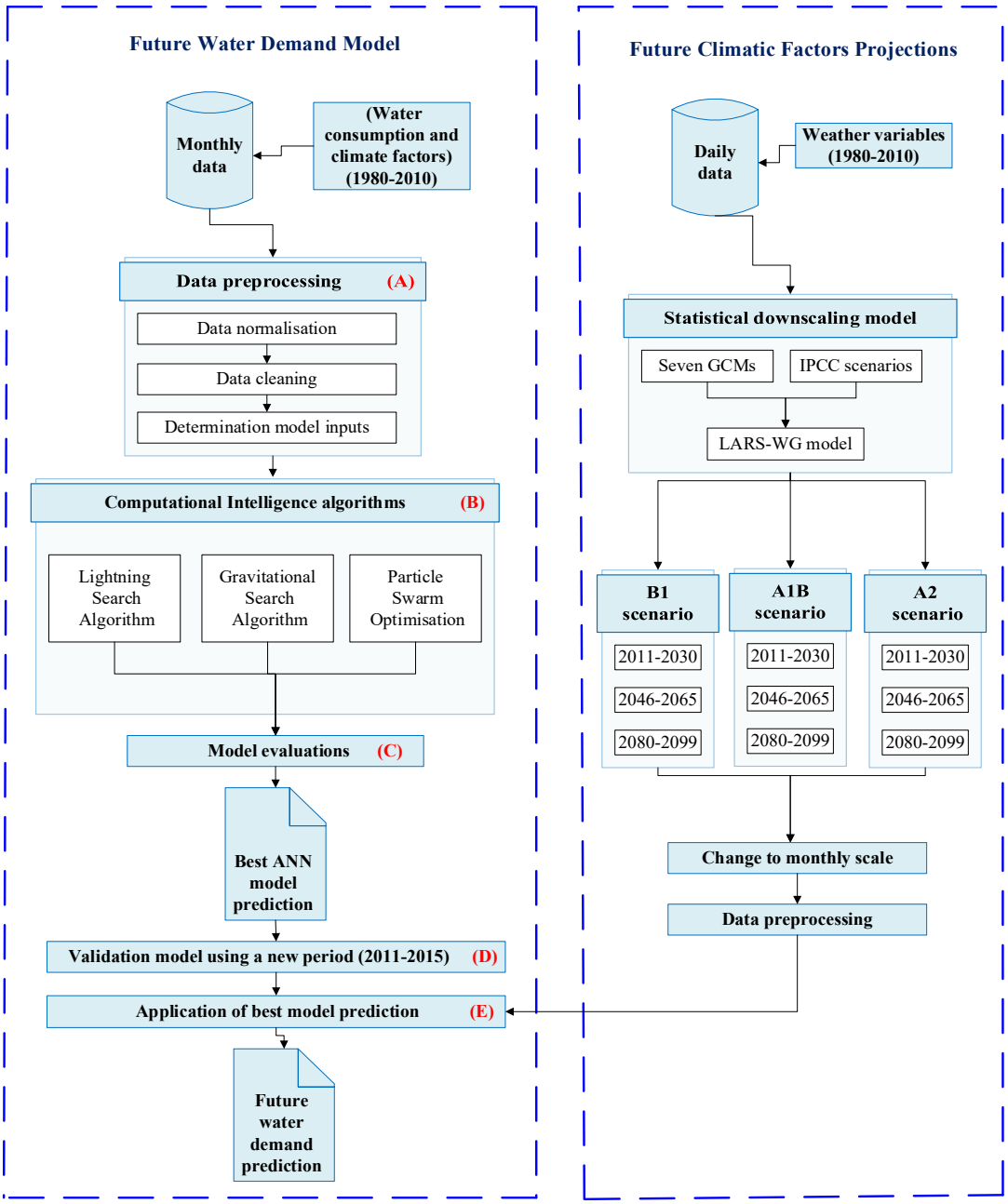

Figure 3-1: A flowchart shows the methodology steps of forecasting future municipal water demand under three scenarios over three future periods (2011-2030, 2046-2064 and 2080-2099)

3.2. Artificial Neural Network Technique

The ANN is a subsystem of artificial intelligence (AI). Its approach is a system of information processing that attempts to mimic the brain's neurons by utilising a network of artificial neurons, which are regular in layers. It has the ability to adequately map the non-linear water demand trend (Babel and Shinde, 2011), As it is

capable of handling different complex nonlinear environmental problems, and is appropriated for long-term prediction (Mutlu et al., 2008).

3.2.1. Basis of Artificial Neural Network

ANN has a layered structure, and the multilayer perceptrons (MLP) type is the most commonly applied in hydrological engineering (Adamowski et al., 2012). Each layer includes one or more processing units named neurons or perceptrons. The input layer contains the problem effective variables, whereas the output (last) layer contains objective variables. The one or two hidden layers contain the neurons that represent the components of computation (black box). All of the perceptrons in the separate layers are fully or partially interconnected with one another by a series of synaptic weighted connections. The scale of these weights refers to the connections strength between neurons that are interconnected. A weight of zero means that there is no connection between these neurons. There are no connections between its neurons in the same layer (Sayadi et al., 2013). Figure 3.2 illustrates a classic ANN structure.

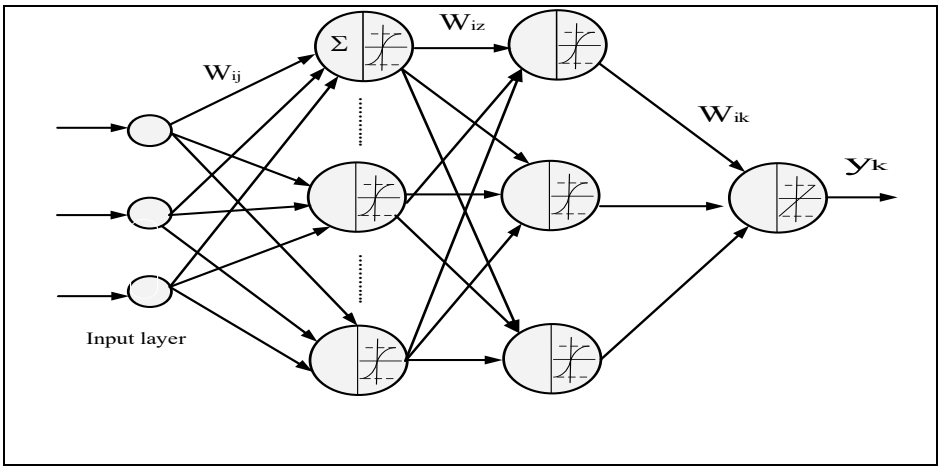

Figure 3-2: The ANN model architecture

A neuron comprises many components: input variables with bias, the synaptic weights of the inputs, the summation function, the activation function and the desired output

(Bennett et al., 2013; Zhang and Qi, 2005). Hagan et al. (2014), stated that training is used to optimise the connection synaptic weights. Kingston et al. (2005) points out that once the learning (optimisation) phase has been successfully completed, the learning model's performance has to be validated to ensure that the model is able to simulate data or generate forecasts robustly.

3.2.2. Modelling Issues in ANNs

Several refinements for ANN models should be conducted to overcome impediments, which badly affect the prediction results. This study endeavours to develop the ANN model in a systematic manner that leads to an improved performance. Such an approach requires remedying main factors such as the activation function, the determination of the model architecture, the learning rate, the data division, the stopping criteria and the model optimisation (Abrahart et al., 2004; Araghinejad, 2014; Hagan et al., 2014). These factors are clarified and discussed in sections 3.2.2.1 to 3.2.2.6.

3.2.2.1. Activation Function

The activation (or transfer) function is employed to transform the activation level of the neuron, the input summation term, to produce an output signal that arranges either [0,1] or [−1, 1] depending on the kind of transfer function used. This helps the network map any nonlinear process (Bennett et al., 2013). Jain et al. (2001) indicated that the transfer function is assumed to be continuous, differentiable, and bounded from above and below. Hagan et al. (2014) mentioned that the hyperbolic *tangent*, *sigmoid* and *linear* activation functions are commonly applied in the neural network (NN) models. The linear activation function is typically used in the output layer, and non-linear activation function are normally used in the hidden. Whereas, the input layer does not

contain an activation function. Noise has an adverse effect on the performance of the activation function.

To understand how climate variables regulate water consumption, two types of activation functions were employed. These are the *tansigmoidal* activation function in both the hidden layers to cover all ranges of the negative input values, while the output layer utilised the *linear* activation function to cover the positive values of water demand. Araghinejad (2014) presented the *tansigmoidal* and *linear* activation functions as the equations below respectively.

$$f(x) = \left(\frac{2}{1 + e^{-\alpha x}}\right) - 1 \quad \alpha > 0 \tag{3.1}$$

$$f(x) = x \tag{3.2}$$

3.2.2.2. Determination of Model Architecture

The choice of the network architecture is a substantial and complicated issue in the development of an ANN model. Generally, it is conducted by determining the optimum number of hidden layers and the number of neurons in each of these. The determination of the network architecture affects the ability to locate the globally optimal set of synaptic weights during learning. This leads to capturing the relationship among dependent and independents variables (ASCE, 2000; Shahin et al., 2008). There are two kinds of ANN models: i) a simple ANN models comprising only one hidden layer, and ii) a complex ANN model comprising two or more hidden layers (Bennett et al., 2013).

A) Hidden Layer (HL)

The addition of intermediate layers between the input and output layers was to deal with nonlinearly separable issues. One HL is adequate to approximate continuous functions. It will be insufficient when the relationship among the variables involved is complicated. In this situation, more than one HL may be necessary for providing the modelling flexibility needed (Basheer and Hajmeer, 2000). Smaller networks have a higher processing speed, but more local minima. Large networks have advantages of speed training and an improved capability for avoiding local minima in the error surface, but it needs a large number of learning samples to fulfil perfect generalisation (Maier and Dandy, 2000). There is no systematic way to choose the number of HL, but several studies that have developed multi-layers' perceptron (MLP), such those by Jain et al. (2001); Firat et al. (2010), examined several models and reported that two hidden layers present better results than one hidden layer. Many researchers have applied ANN with two HL in different aspects, and the results confirm the accuracy and robustness of these models (Gharghan et al. (2016a); Gharghan et al. (2016b); Ahmed et al. (2017) and Zubaidi et al. (2018)). Accordingly, two hidden layers were adopted to ensure that the ANN model could capture the nonlinear relation between water consumption and climate variables for a long-term period.

B) Hidden Layer Neurons (HLNs)

The number of HLNs significantly affects network performance; a network with few hidden neurons only resulting in a linear estiamtion of the actual trend. In contrast, with too many hidden neurons the network will overfit the learning data and lead to a poor generalisation of unlearned data (Basheer and Hajmeer, 2000). Figure 3.3 shows the impact of HLNs number on network generalisation. Choosing ANN parameters is not totally predicable and required trial and error, which can give a high level of error

in water demand prediction. To avoid this issue, computational intelligence algorithms were used to select the best number of neurons in both hidden layers to achieve accurate prediction models.

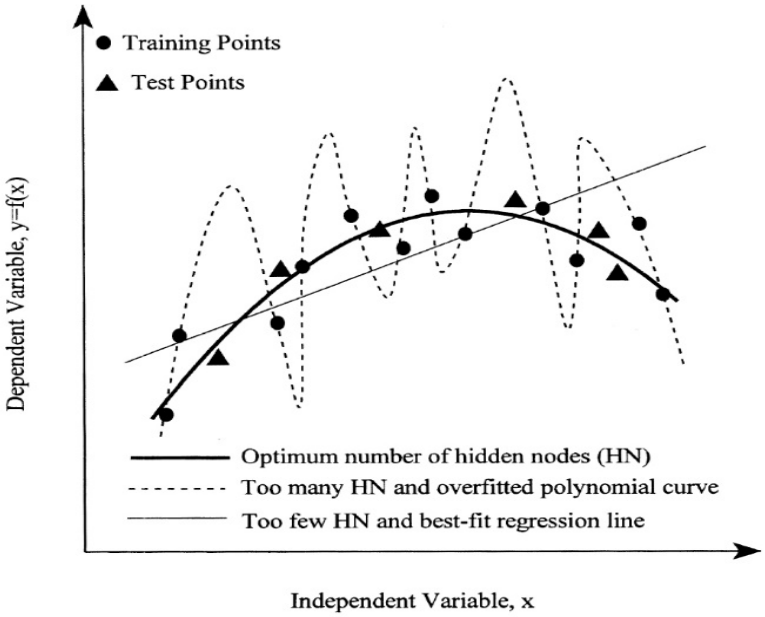

Figure 3-3: Impact of HLN number on network generalisation (Basheer and Hajmeer, 2000)

3.2.2.3. Learning Rate

Hagan et al. (2014) stated that the learning rate coefficient is a factor that is used to preserve the learning speed by significantly altering the size of the steps taken in weight space from one cycle to another. It is utilised to help prevent the learning process being trapped at a local minima instead of on global minimum. The learning rate coefficient remains constant during the learning. A small value of learning rate will slow the training; in contrast, a large value may cause unstable weights (W) that oscillate about the optimal value (Basheer and Hajmeer, 2000).

Many researchers such as Jain et al. (2001); Bougadis et al. (2005) and Adamowski et al. (2012) have utilised the trial and error technique, which is unsystematic, to locate

the optimum learning coefficients, But computational intelligence algorithms were applied to find the optimum coefficient of learning that avoids the learning process being trapped in local minima and offers a better generalisation model.

3.2.2.4. Data Division

Data division is a vital process that needs to be addressed in the ANN model. It is general practice to divide the obtainable data into three independent subsets, namely: learning, testing and validation. The learning data is used to adjust the weights; the test data is utilised to examine the performance of the network at different stages of training; the validation data is required to examine the generalisation capability of the model network (Basheer and Hajmeer, 2000). The training set should be adequately large to properly represent the data. All the three data sets must all be representative because the ANN model does not have the capability to extrapolate outside the range of data that is employed for training. Poor forecasts can be predicted if the validation data contain values outside of the range of those applied for learning (Maier and Dandy, 2000). In this study, the data were divided randomly into the training, testing and validation sets 70%, 15% and 15% respectively (Babel and Shinde, 2011; Behboudian et al., 2014; Zubaidi et al., 2018).

3.2.2.5. Stopping Criteria

Stopping criteria are required for ending the learning process. It was used to locate whether the model was optimally or sub-optimally learned. Learning can be stop when the learning error reaches an acceptable small value, after the display of a specific number of learning records, or when no, or only small alterations in the learning error occur. These definitions of stopping criteria either end training prematurely or overtrain. To unravel this problem, the cross-validation technique is commonly

recommended. It is deemed to be the most reliable tool to cease learning when the network starts to overtrain. This technique often needs abundant data and the data to be separated into three groups; learning, testing (cross training) and validation. In general, the error on the learning data set reduces indefinitely with rising learning cycles (epochs) or number of hidden neurons, as shown in (Figure 3.4). The primary considerable drop in error resulted from training, but the next slow decrease in error may be referred to two phenomena named memorisation and overtraining: (i) the excessive use of considerable numbers of epochs leads to network memorisation, and/or (ii) utilising a large number of hidden neurons causes overfitting (Basheer and Hajmeer, 2000).

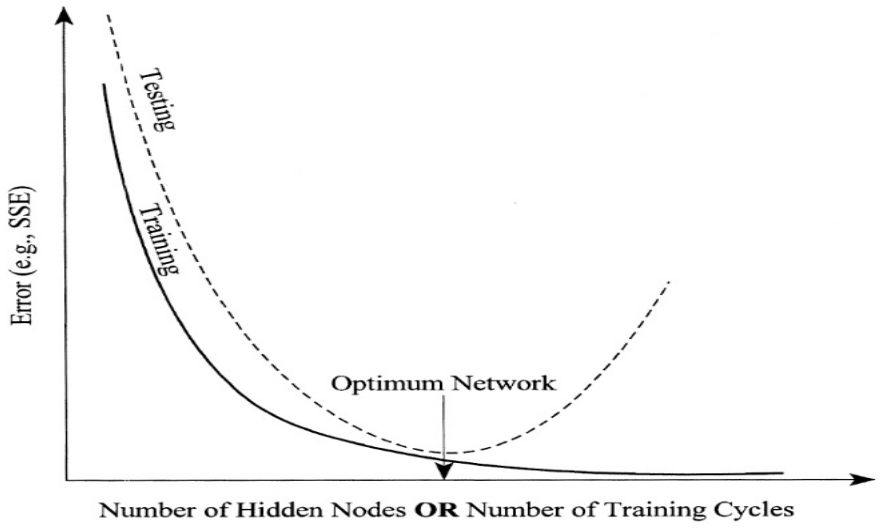

Figure 3-4: Criteria for stopping of learning and chosen of optimum NN architecture (Basheer and Hajmeer, 2000)

Stopping criteria were designed according to the procedure used by Gharghan et al. (2016a). Two different techniques have been employed to cease learning containing cross-validation technique, and root mean square error RMSE as an objective function (i.e., error not more than RMSE value in the testing phase). These techniques was approved by Zubaidi et al. (2018).

3.2.2.6. Model Optimisation (Training & Validation)

Training is the approach that is used to optimise the connection synaptic weights. This process is equal to the parameter assessment stage in the traditional models. There are two primary kinds of training (supervised and unsupervised). Supervised learning algorithm needs an external teacher to guide the learning mode. This type typically requires a large number of input and output data. An unsupervised training algorithm does not include a teacher, it only needs an input data set. The purpose of the training is to achieve a set of connection weights and nodal thresholds so that the ANN produces outputs that are adequately close to the target values and also attain a global solution. The dataset employed for the training process should have sufficient patterns to enable it to predict the targets with adequate precision. A cross-training approach is recommended to avoid overtraining as this causes poor prediction through memorising the individual examples (Hagan et al., 2014). Kingston et al. (2005) stated that once the learning (optimisation) phase has been successfully completed, the learning model's performance has to be validated. The validation data set should be an independent set which has not been utilised as part of the learning phase in any capacity. The training data set and validation data set should represent the same data patterns. Shahin et al. (2008) indicated that the aim of the model validation process is to ensure that the model is able to simulate data or generate forecasts robustly. All equations and additional details can be found in Hagan et al. (2014).

In this research, the supervisor-learning approach and the Backpropagation Neural Network (BP-NN) kind were used. The BP algorithm has a number of attractive features such as various choices of transfer function, and it can locate the weight that approximates observed values of output with a choice in the level of accuracy (Nawi et al., 2013). The Levenberg-Marquardt (LM) learning algorithm was employed for

training, testing and validation. The major advantages of the LM training algorithm is that it offers minimum error, speed and efficiency, as proven in Payal et al. (2015). This technique was approved in Zubaidi et al. (2018).

3.3. Computational Intelligence Algorithm

Optimisation is the process of determining the optimum solution to issues relying on input variables after locating the objective function as a constraint. Often, this function is formulated depending on the particular application and can take the style of minimal error or cost, optimal design or management and so on. Various methods have been applied to deal with optimisation difficulties. Finding the optimal answer with traditional techniques becomes difficult because the size of the search space increases with the dimension of the optimisation problem (Kanzow et al., 2004; Shareef et al., 2015). More recently, algorithms for computational intelligence optimisation have been widely applied for solving complicated optimisation issues in different fields such as; home energy management (Ahmed et al., 2016), wireless sensor networks (Gharghan et al., 2016a) and biological treatment (Ethaib et al., 2016), because of their ease of employment, global perspective and broad applicability. These algorithms include swarm intelligence methods, which are nature-inspired computational methodologies that can handle complicated problems of the real world (Shareef et al., 2015). To find the best learning rate and the number of neurons in both hidden layers, the following new swarm intelligence techniques have been used in this work. These algorithms are the Lightning Search Algorithm (LSA), the Gravitational Search Algorithm (GSA) and Particle Swarm Optimisation (PSO).

3.3.1. Lightning Search Algorithm (LSA)

LSA is a new nature-inspired meta-heuristic optimisation algorithm for tackling constraint optimisation issues. The lightning analogy is due to the mechanism of step leader propagation, virtual fast particles, known as projectiles, in the figuration of the binary tree structure of a step leader. There are 3 kinds of the projectiles: Transition projectiles, create the 1st step leader population N, the space projectiles try to be the leader, and the lead projectile, which represents the optimum positioned projectile found amid N number of step leaders (Mutlag et al., 2016; Shareef et al., 2015).

LSA, like to other meta-heuristic algorithms, needs a population to start the search (Ahmed et al., 2016). More details about the LSA algorithm can be found in (Shareef et al., 2015).

This algorithm has been applied in various areas such as; improving the fuzzy logic speed controller for an Induction motor drive (Abd Ali et al., 2015), home energy management (Ahmed et al., 2016) and wind power model (Sirjani and Okonkwo, 2016).

The formation of the step leaders is set in the first stage because transition projectiles are released from the cell of thunder in a random direction. The standard of uniform distribution can be expressed by Equation (3.3) (Ahmed et al., 2016; Shareef et al., 2015):

$$f(x^T) = \begin{cases} \dfrac{1}{(b-a)}\ , & for\ a \leq\ x^T \leq b \\ 0\ , & elsewhere \end{cases} \tag{3.3}$$

where x^T: random number, which may offer the solution.

a and b: lower and upper levels of the solution space, respectively.

And the probability density function f(x^s) of an exponential distribution is presented by Equation (3.4):

$$f(x^s) = \begin{cases} \frac{1}{\mu}\, e^{\left(\frac{x^s}{\mu}\right)}, & for\ x^s \geq 0 \\ 0\,, & for\ x^s \leq 0 \end{cases} \tag{3.4}$$

Once the initial is evaluated, then the position and direction are updated with Equation (3.5)

$$p_{i-NEW}^{s} = p_i^s \pm exp\ rand\ (\mu_i) \tag{3.5}$$

where the p_{i-NEW}^{s} is a new projectile and p_i^s : old projectile.

Both the projectiles and the step leaders that have travelled near to the ground do not have sufficient potential for ionising considerable sections in front of the leading edge. In this method, the lead projectile can be created as a random number taken from the standard normal distribution. The function of normal probability density $f(x^L)$ is revealed as:

$$f(x^L) = \left\{ \frac{1}{\sigma\sqrt{2\pi}}\, e^{\frac{-(x^L-\mu)^2}{2\sigma^2}} \right\} \tag{3.6}$$

Where:

f(x^L): the normal probability density function.

σ: scale parameter.

μ: shape parameter.

From Equation (3.6), a randomly generated lead projectile has the ability to search in all directions from the existing position defined via the shape parameter. The scale parameter, σ, reduces exponentially to locate the best solution. So, the position of pL in step + 1 can be revealed in Equation (3.7):

$$p_{NEW}^{L} = p^{L} + normrand(\mu_L, \sigma_L) \tag{3.7}$$

p_{NEW}^{L}: the new lead projectile.

Figure 3.5 displays the flow chart of the suggested hybrid LAS-ANN model.

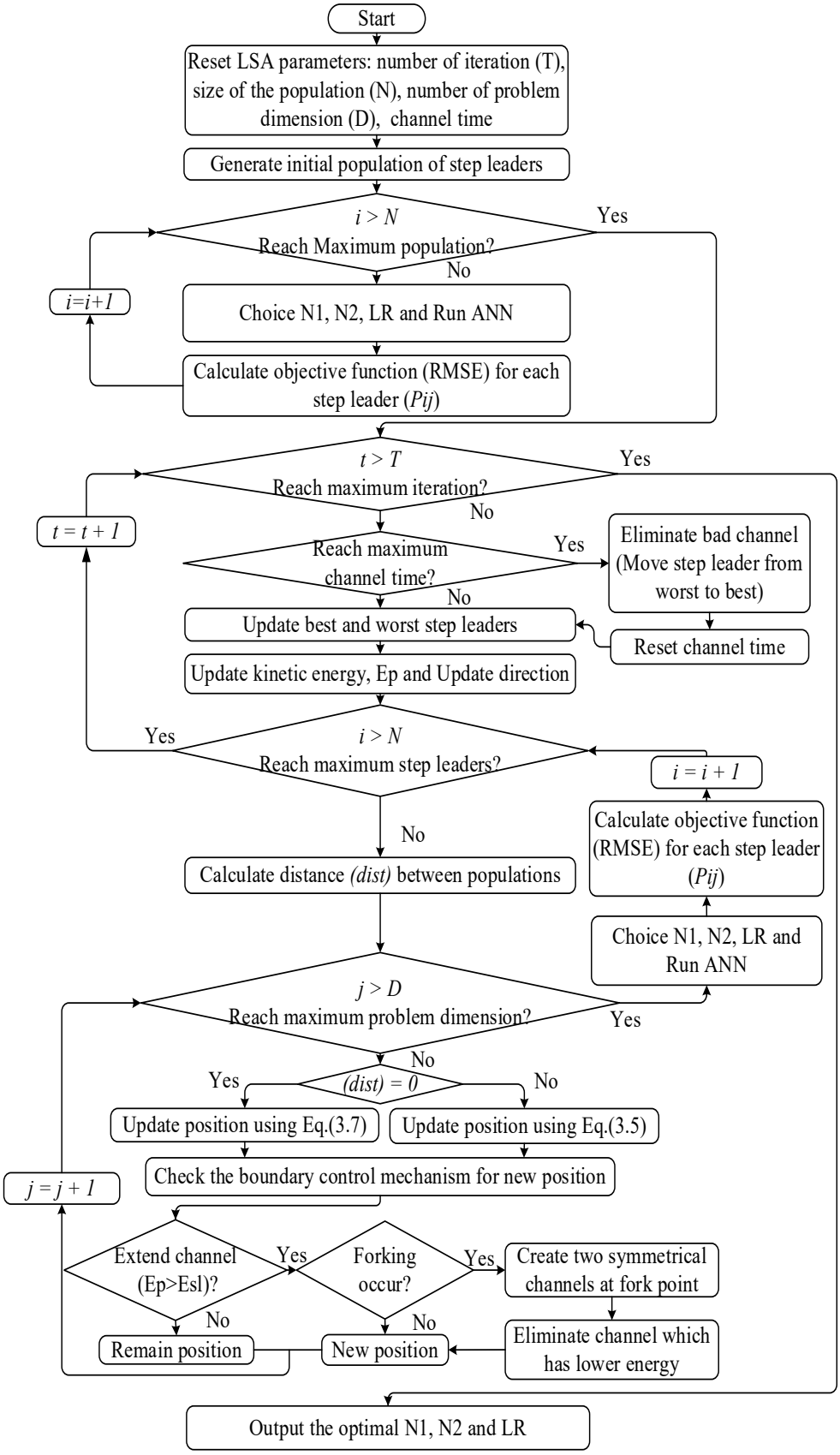

Figure 3-5: flow chart of the LAS-ANN model (Ahmed et al., 2016)

3.3.2. Gravitational Search Algorithm (GSA)

Rashedi et al. (2009) proposed the GSA algorithm, which is based on the Newtonian law of gravity: "Every particle in the universe attracts every other particle with a force that is directly proportional to the product of their masses and inversely proportional to the square of the distance between them". GSA has been used in different sectors such as image enhancement (Zhao, 2011), optimal power flow (Duman et al., 2012) and business (Vijaya Kumar et al., 2013).

The mathematical principle of the GSA is dependent on the Newtonian law of gravity, which is given in Equation (3.8):

$$F = G\frac{M_1 M_2}{R^2} \tag{3.8}$$

Where

F = gravitational force,

R = the distance between the first and second particles of mass (M_1) and (M_2) respectively, and

G = the gravitational constant value.

Newton's second law, Equation (3.9), states that "acceleration is inversely proportional to mass M and directly proportional to force F", as follows:

$$a = \frac{F}{M} \tag{3.9}$$

Due to the influence of declining gravity, the real value of the "gravitational constant (G)" relies on the universe's real age. Equation (3.10) offers a reduction of the gravitational constant with age (Gharghan et al., 2016a):

$$G(t) = G(t_0) \times (\frac{t_0}{t})^{\beta} \qquad \beta < 1 \tag{3.10}$$

Where

G (t) = the gravitational constant at time t.

G (t_0) = the gravitational constant at the first cosmic quantum-interval of time t_0, and

β = is a function of time.

The agents' positions are initialised (i.e., the masses are chosen randomly within the offered search interval). The i^{th} agent position it defined by Equation (3.11):

$$X_i = \left(X_i^1, \ldots\ldots\ldots, X_i^d, \ldots\ldots\ldots, X_i^k\right), \quad for\ i = 1,2,3, \ldots\ldots, N \tag{3.11}$$

Where

N = the number of agents,

$X^d{}_i$= the i^{th} agent position in the d^{th} dimension, and

k = the space dimension.

To compute the GSA fitness function, a root mean square error (RMSE) can be adopted to select the best and the worst fit for each iteration. The purpose of the computations is to reduce the problems and locate the masses of each agent as follows (Shuaib et al., 2015):

$$RMSE = \sqrt{\frac{1}{n}\sum_{i=1}^{n} e^2} \tag{3.12}$$

$$best(t) = \min_{j\in\{1,\dots,N\}} fit_j\,(t) \tag{3.13}$$

$$worst(t) = \max_{j\in\{1,\dots,N\}} fit_j\,(t) \tag{3.14}$$

$$m_i(t) = \frac{fit_i(t) - Worst(t)}{best(t) - Worst(t)} \tag{3.15}$$

$$M_i(t) = \frac{m_i(t)}{\sum_{j=1}^{N} m_j(t)} \tag{3.16}$$

Where

e = the predicted water error, and

n = the number of samples.

The actual water consumption was obtained based on observation, whereas the predicted water was gained using the GSA-ANN algorithm. The gravitational constant G at iteration t was calculated as follows:

$$G(t) = G_0 e^{(-\alpha t/T)} \tag{3.17}$$

The computation of the total force in different directions for the i^{th} agent, calculation of the velocity and acceleration, and the position of the agents in the next iteration are given by Eqaution (3.18):

$$F_{ij}^{d}(t) = G(t)\frac{M_{pi}(t) \times M_{aj}(t)}{R_{ij} + \varepsilon}(X_j^d(t) - X_i^d(t)) \tag{3.18}$$

$$F_i^d(t) = \sum_{j \epsilon Kbest, j \neq i} rand_j F_{ij}^d(t) \tag{3.19}$$

$$a_i^d(t) = \frac{F_i^d(t)}{M_i(t)} \tag{3.20}$$

$$v_i^d(t+1) = rand_i \times v_i^d(t) + a_i^d(t) \tag{3.21}$$

$$x_i^d(t+1) = x_i^d(t) + v_i^d(t+1) \tag{3.22}$$

Figure 3.6 presents the flowchart that shows the details of the GSA-ANN operation based on the previous equations.

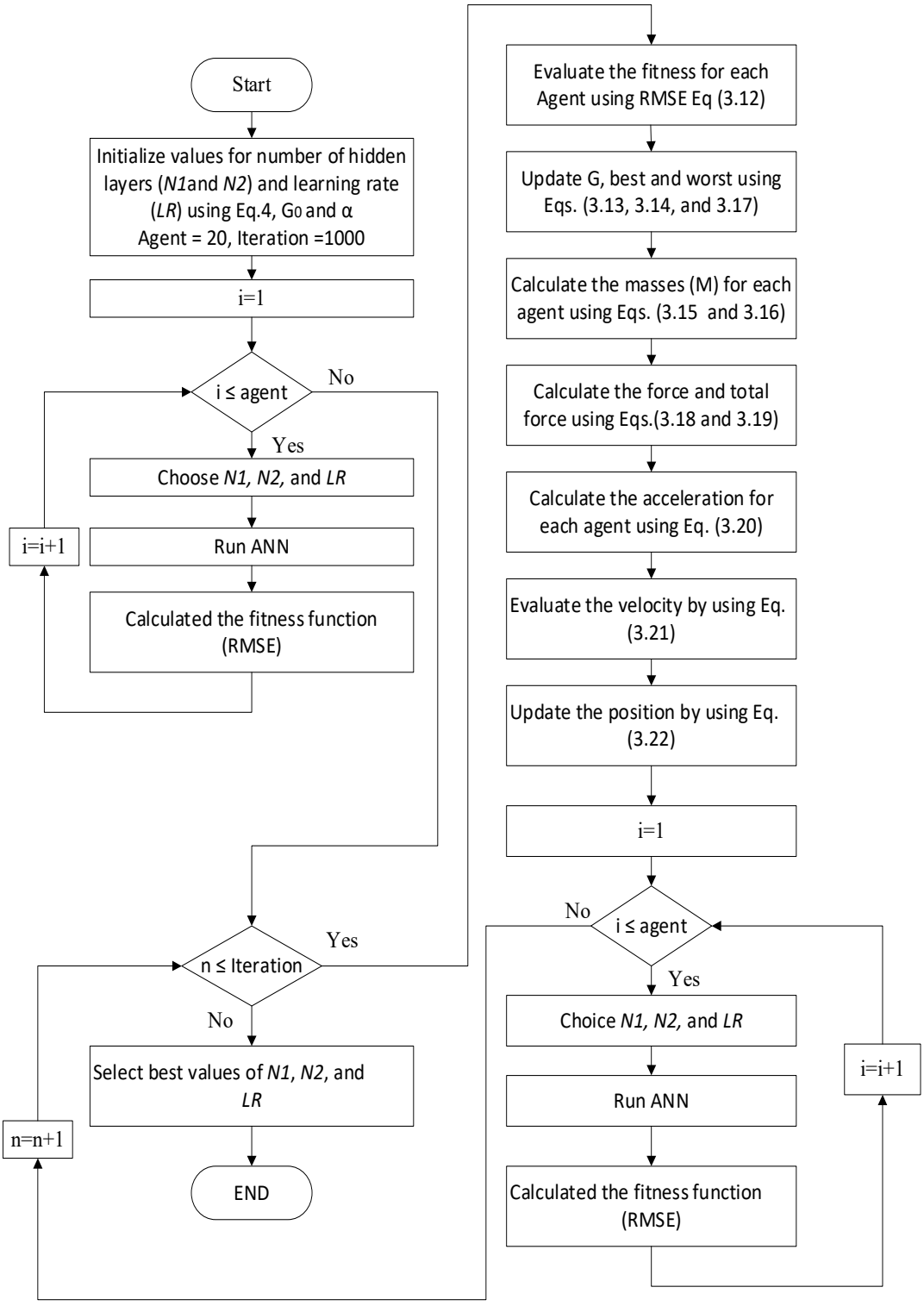

Figure 3-6: The GSA-ANN algorithm flowchart (Gharghan et al., 2016a)

3.3.3. Particle Swarm Optimisation (PSO)

A PSO algorithm is a computational iterative search and optimisation technique. It is biologically inspired by the social behaviour of animal societies such as flocks of birds or schools of fish. This method comprises a swarm of particles where a particle denotes a possible solution (Rini et al., 2011). The PSO algorithm is commonly utilised to settle optimisation issues (Eberhart and Shi, 2001). Recently, studies have emphasised the positive use of hybrid PSO–ANN models to tackle engineering issues such as improving the precision of wireless sensor localisation mechanisms (Gharghan et al., 2016b), estimating results of biological treatment (Ethaib et al., 2016) and home energy management (Ahmed et al., 2016).

In each process of iteration, the velocity and position of each particle in the swarm is updated according to the two "best" values. The first one is the local best (Pbest) which indicates particle's memory about its own best position (best fitness). The second is the global best (gbest) denoting global knowledge of the best position or the best position in their neighbourhood. Particle positions are altered by adding velocity, updating dependent on Equations 3.23 and 3.24 from Wang et al. (2010) and Gharghan et al. (2016b). The updating process continues until either an appropriate *gbest* is attained or the pre-set number of iterations (*k*max) is reached.

$$V_{id}(k+1) = \omega V_{id}(k) + c_1\, r_1(k)(Pbest_{id} - X_{id}) + c_2\, r_2(k)(gbest_{id} - X_{id}) \tag{3.23}$$

$$X_{id}(k+1) = X_{id}(k) + V_{id}\,(k+1) \tag{3.24}$$

where V_{id} is the velocity of the particle, X_{id} indicates the position of the particle; k is the iteration number; ω the inertia weight; $r_1(k)$ and $r_2(k)$ are random values ranging between 0 and 1; c_1 and c_2 are acceleration constants which are often equal; $c_1 r_1(k)(Pbest_{id} - X_{id})$ and $c_2 r_2(k)\ (gbest_{id} - X_{id})$ represent the update of particle velocity. Eberhart and Shi (2001) and Lavanya and Udgata (2011) both recommend ω =0.5, and $c_1 = c_2 = 1.494$ to achieve faster convergence. Figure 3.7 shows the proposed hybrid PSO–ANN algorithm flow chart used to enhance water demand prediction accuracy.

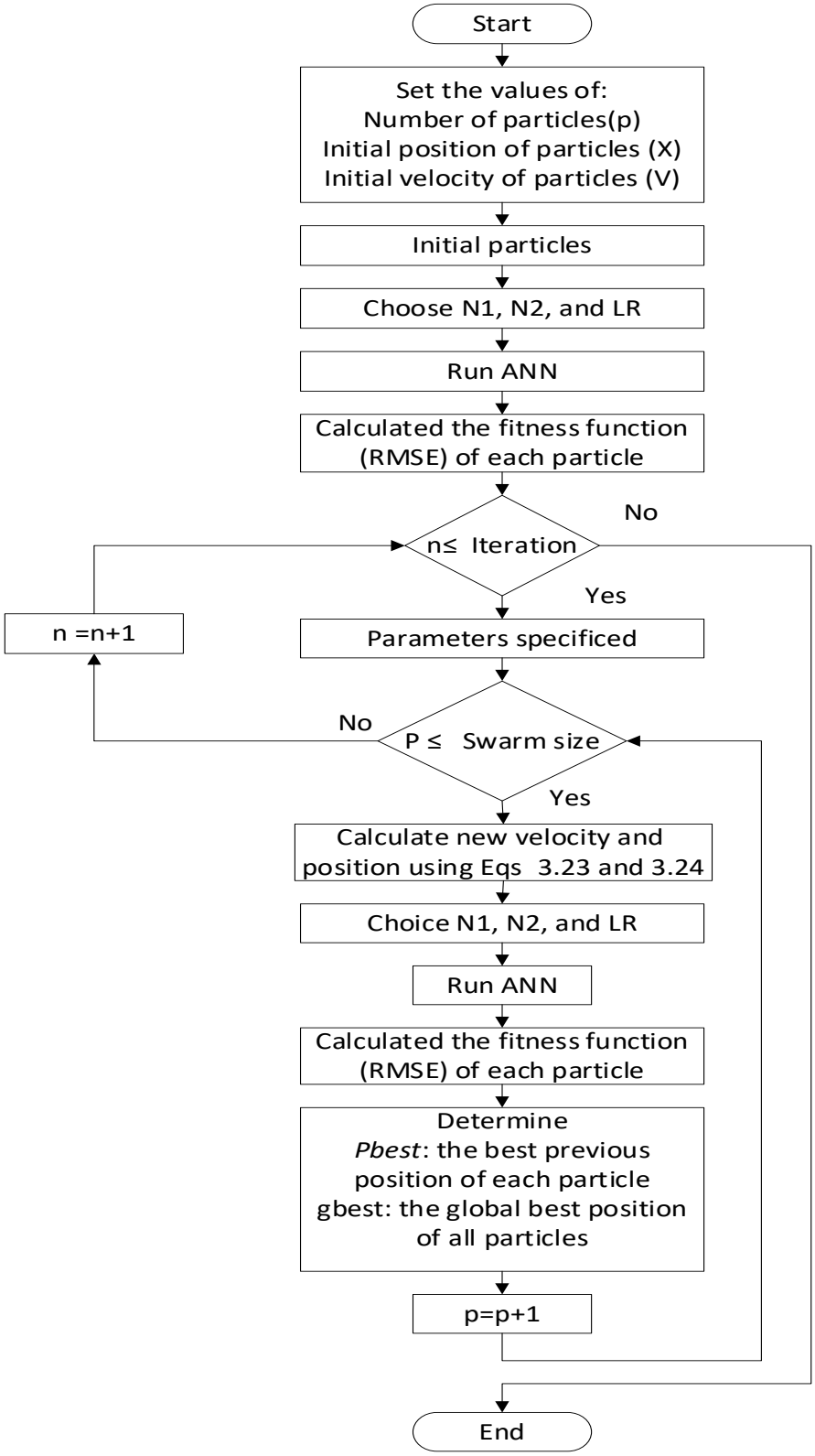

Figure 3-7: Flow chart of hybrid PSO–ANN algorithm, adapted from Gharghan et al. (2016b)

3.4. Proposed Computational Intelligence Algorithm-Base Artificial Neural Network

In this research study the ANN technique has been employed to predict long-term municipal water demand considering climatic variables as model inputs. The number of neurons in the hidden layers and the learning rate coefficient are considered essential factors of ANN architecture. They are responsible for mapping the relation between the input and output variables that are adopted in developing the ANN model and avoids the local minima (Jain et al., 2001). The computational intelligence algorithms were hybridised with the ANN to select the optimum parameters of the ANN (i.e., the learning rate value and the number of neurons in both hidden layers). It addresses such an issue to enhance the performance of the ANN model, which can be utilised in forecasting future water demand. Choosing ANN parameters is not totally reliable and is dependent on trial and error, which in return gives a high level of error in water demand prediction.

Five population sizes: 10, 20, 30, 40 and 50, were applied to let each algorithm determine the population that could attain the minimal fitness function value. The fitness function for optimising the model minimising was the root-mean-squared error (Wang et al., 2010).

3.5. Model Performance and Accuracy Measurements

After calibrating all the model structures via the calibration/training data set, their performance was assessed in terms of several standard statistical criteria, which depict the errors related to model predictions (Adamowski, 2008). The statistical criteria parameters provide a means of measuring prediction accuracy, so prediction errors

play a considerable role in the choice of suitable models and in providing insights in advising alterations to present models to minimise deviations in future predictions (Donkor et al., 2014). Several statistical parameters will be applied in the model's calibration such as Mean Absolute Error (MAE), Mean Squared Error (MSE), Root Mean Squared Error (RMSE) and Correlation Coefficient (R). These indicators are defined in Equations. (3.25) through (3.28).

$$MAE = \frac{\sum_{m=1}^{N}|x_o - x_p|}{N} \tag{3.25}$$

$$MSE = \frac{\sum_{m=1}^{N}(x_o - x_p)^2}{N} \tag{3.26}$$

$$RMSE = \sqrt{\frac{\sum_{m=1}^{N}(x_o - x_p)^2}{N}} \tag{3.27}$$

$$R = \left[\frac{\sum_{m=1}^{N}(x_o - \overline{x_o})(x_p - \overline{x_p})}{\sqrt{\sum(x_o - \overline{x_o})^2 \sum(x_p - \overline{x_p})^2}}\right] \tag{3.28}$$

Where x_o= observed water consumption, x_p= predicted water demand, N= sample size, $\overline{x_p}$= mean of predicted demand, and $\overline{x_o}$= mean of observed consumption.

The stationarity of stochastic time series for all variables will be examined by two digital tests, the Augmented Dickey-Fuller (ADF) test and Kwiatkowski– Phillips–Schmidt–Shin (KPSS) test. A residual analysis will be utilised to check the goodness of fit of the ANN model, and Bland–Altman analysis, which is a scatter plot test employed to locate the area of agreement between (observed- predicted) versus ([observed+ predicted]/2), and the percentage of data that is distributed inside the limits of the agreement area (Bland and Altman, 2007).

3.6. Statistical Downscaling Technique

The statistical downscaling technique employed to simulate the future climate factors was performed as recommended in Daniels et al. (2012). Trzaska and Schnarr (2014) reported that there are several types of statistical downscaling models such as the Long Ashton Research Station Weather Generator LARS-WG, MarkSim GCM and Nonhomogeneous Hidden Markov Mode. There are major caveats related with MarkSim GCM and Nonhomogeneous Hidden Markov Models. For MarkSim GCM model, high rainfall variances are not well projected and since the model simply matches future climate projections with a present climate cluster that is the most similar, future climate that is various from current day weather cannot be simulated. For Nonhomogeneous Hidden Markov Model, the methodology of this model depend on the hidden state, which is difficult to interpret and determine number of states. For, Long Ashton Research Station Weather Generator LARS-WG, Semenov et al. (2013) reported that this model was used successfully with same baseline period 1980-2010 in different regions (environments). Accordingly, LAR-WG (version 5.5) uses in this thesis.

3.6.1. The Long Ashton Research Station Weather Generator (LARS-WG) Model

LARS-WG is a stochastic weather generator utilised to generate a long series of synthetic data in three periods (2011-2030, 2046-2065 and 2080-2099). It was designed to study the impact of climate change and it has been tested for various sites across the world, and shown to give reasonal approximations (Semenov, 2008).

A reference baseline period is necessary to define the measured climate from which to calculate any scenario changes in climate. The availability of the required municipal

water consumption data will govern the baseline period choice. Accordingly, the period 1980-2010 was used as a reference baseline to compare with future climate scenarios. Semenov et al. (2013) suggested this period is valid for generating future climatic factors. Additionally, several researchers, such as (Masanganise et al., 2014); (Kadiyala et al., 2015) and (Räisänen, 2015), have adopted this period in other different environments.

For this research, a new version (5.5) of LARS-WG and 7 GCMs will be used to reduce the uncertainty for three different periods. In addition, three scenarios (A2, B1 and A1B) will be applied to represent all possible emission scenarios that are supported by the LARS-WG model. These scenarios will be investigated to show its influence in municipal water demand prediction. Use of more than one GCM and IPCC scenario is required to eliminate the uncertainty that result from the assumptions for long-term period projection.

The generation of synthetic weather data using the LARS-WG model can be divided into three stages:

1. Calibration: to calibrate the LARS-WG model, daily historical data of climate variables were employed over the period 1980-2010. Model calibration is achieved to employ the function "SITE ANALYSIS" in LARS-WG, which analyses measured climate data (e.g., maximum and minimum temperature, solar radiation and precipitation) to determine the statistical characteristics of these climate factors, and to store them in a files for use in the next stage.
2. Validation: the parameter files that were derived from measured weather data during the model calibration stage, are employed for generating synthetic weather data with the same statistical characteristics as the original measured

data. A statistical comparison between historical weather data and synthetic weather data generated by LARS-WG model will be performed to ensure that the model can simulate climate data probability distributions that are close to the real long-term measured distributions for the selected site. Graphical tests based on mean and standard deviation as well as P-value and Kolmogorov-Smirnov (K-S) are used to do the comparison between measured and synthetic climate data.

3. Generation: the model becomes ready to generate synthetic weather data based on B1, A1B and A2 scenarios and 7 GCMs over three periods 2011-2030, 2046-2065 and 2080-2099. The first period of the B1 scenario is chosen and the first GCM to simulate the first time series for all climate factors for period 2011-2030. The process is repeated 7 times based on seven different GCMs. Accordingly, we get 7 simulate time series for each climate factor and calculate the ensemble mean of these 7 time series (e.g., rainfall). These processes are repeated for second and third periods of the B1 scenario. In the same context, all the above procedure are repeated for A1B and A2 scenarios to reduce the uncertainty of assumptions. The daily future projection will be accumulated to monthly before being used with ANN.

Extra details about the modelling procedure and the basic ideas can be referred to Semenov and Barrow (2002). Table (3.1) presents the seven GCMs that were chosen from the IPCC Fourth Assessment Report (AR4).

Table 3.1: Selected 7 global climate models from IPCC AR4

No.	GCM	Research centre	Grid
1	CNCM3	Centre National de Recherches France	1.9×1.9°
2	GFCM21	Geophysical Fluid Dynamics Lab USA	2.0×2.5°
3	HADCM3	UK Meteorological Office UK	2.5×3.75°
4	INCM3	Institute for Numerical Mathematics Russia	4×5°
5	IPCM4	Institute Pierre Simon Laplace France	2.5×3.75°
6	MPEH5	Max-Planck Institute for Meteorology Germany	1.9×1.9°
7	NCCCS	National Centre for Atmospheric USA	1.4×1.4°

Melbourne City has a considerable number of meteorological stations that are spread around the area of the city. The Yarra Valley Water Company provided this study with the average daily value of all the climate factors that covered its service area. It requested the data from the Australia Bureau of Meteorology, and applied the arithmetic mean method to calculate the average value. In this technique, each climate variable for each meteorological station was added and then divided by the total number of stations, to get the mean value of that variable as in Equation (3.29). In addition, it is the simplest and easiest technique to calculate the average daily value. Each meteorological station had equal weight regardless of its location (Bhavani, 2013).

$$p_m = \{(p_1 + p_2 + p_3 + \cdots + p_n)/n\} \tag{3.29}$$

3.7. Summary

This chapter described the methodology to investigate the extent that climate change influences municipal water demand. The chapter covered the steps of the research methodology in order to meet the objectives set out in Chapter one based on the

literature review of current and previous studies on the ANN, computational intelligence algorithm and weather downscaling as mentioned in Chapter two.

Artificial Neural Network (ANN)

Several studies recommended using ANN to predict water demand because of its ability to map the non-linear relation between water demand and climate factors, and it is also appropriated for long-term prediction.

This section presented a short background about ANN, and explored the main components: model architecture, activation function, learning rate, data division, stopping criteria and model optimisation (training and validation). It also discussed its strengths, and how to select better choices.

Computational Intelligence Algorithms

The optimisation technique is adopted to choose the best learning rate coefficient and number of hidden neurons that enhance the performance of the ANN. Three different algorithms for computational intelligence optimisation were used to mitigate the model prediction uncertainty. These algorithms are: Lightning Search Algorithm (LSA), Gravitational Search Algorithm (GSA) and Particle Swarm Optimisation (PSO). The selection of the best computational intelligence algorithm is based on the minimum error of the objective function.

Weather Downscaling

This section discussed the methodology adopted for weather downscaling. The statistical downscaling approach was employed in this study to simulate future climate variables. Several studies have recommended using the Long Ashton Research Station

Weather Generator (LARS-WG) model. Three emission scenarios (A2, B1 and A1B) with seven GCMs were applied to reduce the uncertainty. Daily data for maximum temperature, minimum temperature, rainfall and solar radiation, which are supported by the LARS-WG model, over the period 1980-2010 were employed.

The next chapter presents the studied area and data manipulation that includes normalisation, cleaning and the determination model inputs, as well as demonstrating the results of model input developments.

Chapter 4: Studied Area and Data Manipulation

4.1. Introduction

This chapter illustrates the study field of the proposed methodology. The study investigates the impact of climate change on municipal water demands in Melbourne City in Australia and Columbia City in the United States of America. These two studied catchments were chosen based on the size of each city. It is important to assess the impact of climate change on different scale of water consumption such as big city like Melbourne and small city like Columbia. Also the availability and reliability of long-term data for those two cities is another reason for the selection. The reliability of data is a significant issue for forecasting models. The data sets gained from the Yarra Valley Company for the areas that are served in Melbourne City and from the city council for Columbia City. This data comes from reliable establishments and it is observed data not calculated or estimated data. Chapter five will confirm its reliability. Several techniques need to be conducted on the data before using it in the prediction model. This chapter describes the essential issues regarding the municipal water consumption, such as the location of the city, the weather, the freshwater resources, the municipal water system and the percentage of customer types. Then, monthly historical data is presented, which includes the water consumption and five climate factors: maximum, mean and minimum temperature; rainfall and solar radiation.

The data preprocessing techniques such as data normalisation, data cleaning and pretreatment signal are presented with the results of the model input.

Note that, the data for Melbourne City is used by all data preprocessing steps. All the results of data preprocessing for Columbia City are presented in Appendix 4-A.

4.2. Study Area

The Two areas selected for this work are described in more details in the following sections:

4.2.1. Melbourne City, Victoria, Australia

Melbourne City is the coastal capital of Victoria state, which is located in south-eastern Australia (Figure 4.1). The city has an area of around 9,992.5 km² as well as its coordinates are 37.8136° S, 144.9631° E. The Melbourne City region has experienced an increase in population, which was 2,765,000 capita in 1980 to 3,276,000 capita in 2010. The average yearly water consumption of Melbourne is estimated at 40,000 Megalitre. This was dominated by urban and residential water use, which was approximately 60%. Of the remainder, 28% was accounted for by industry and cooerence, 8% by leakage and 4% is miscellaneous. Melbourne City has faced a drought since 1998 that has pushed the city water authorities to enforce water restrictions after a long time of unrestricted supply (Gato et al., 2007a; MW, 2017).

Figure 4-1: Location Map of Melbourne City

4.2.1.1. Climate of Studied Catchment

The weather in Melbourne City varies from summer, which is warm, to winter, which is cold and windy. The seasons in Australia are spring - the three transition months September, October and November, summer - the three hottest months December, January and February, autumn - the transition months March, April and May and finally, winter - the three coldest months June, July and August. As for temperature, the warm period is statistically between 15th December to 16th March with an average daily high temperature higher than 23°C. Statistically the coldest period is from 23th May to 7th September with an average daily high temperature less than 15°C. Rainfall occurs throughout the year, but the most rain occurs during the 31 days around 3rd November, with an average total accumulation of 56 millimetres. The wet seasons called the monsoon seasons are hotter than the dry seasons with, temperatures around 30-50°C and it continues from November to March. This is due to the high humidity during the wet seasons. Frequent flooding occurs during the monsoon period (Diebel et al., 2013). Table 4.1 presents the statistical indicators for the four climate variables data that will be employed in this study over the period from 1980-2010. These variables are maximum temperature (Tmax), minimum temperature (Tmin), rainfall (Rain) and solar radiation (Radi).

Table 4.1: Max., Min. and Ave. values for four climate factors for a period (1980-2010)

	Tmax (°C)			**Tmin (°C)**			**Rain (mm)**			**Radi (MJ/m^2)**		
	Max.	**Min.**	**Ave.**	**Max.**	**Min.**	**Ave.**	**Max.**	**Min.**	**Ave.**	**Max.**	**Min.**	**Ave.**
J	30	22	27	16	12	14	97	1	50	26	21	23
F	31	24	27	16	12	14	153	0	40	23	19	21
M	28	21	24	15	11	12	113	14	48	18	15	16
A	24	17	21	12	7	10	140	18	59	13	10	12
M	19	16	17	11	7	8	120	16	58	9	7	8
J	16	13	14	9	4	6	150	19	67	7	6	7
J	14	12	13	7	3	6	109	20	56	8	6	7
A	17	13	15	8	5	6	104	25	65	12	9	10
S	19	14	17	9	6	7	151	19	69	16	11	14
O	22	17	19	10	7	9	149	10	71	22	17	18
N	27	20	22	14	9	11	170	27	73	24	19	21
D	27	21	24	14	10	12	189	15	71	26	19	23

4.2.1.2. Water Supply System

Melbourne Water Company has provided water services to the community of Melbourne for over 125 years. It delivers bulk water and sewage services to three retail water utilities, Yarra Valley Water, South East Water and City West Water.

The supply network of the Melbourne Water Company consists of 11 large storage facilities, treatment facilities and transfer infrastructure as shown in Figure 4.2.

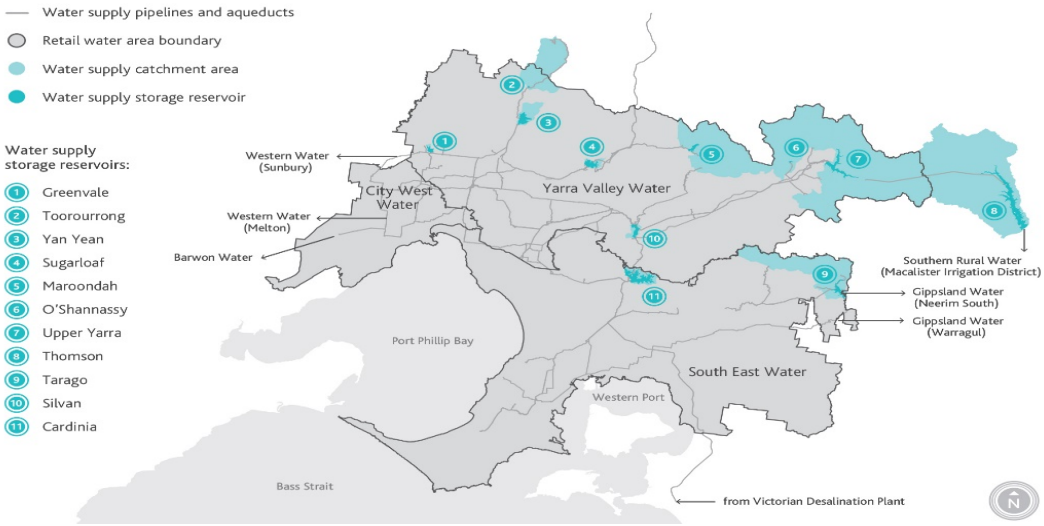

Figure 4-2: Melbourne's Water Services Area (MW, 2017)

The company has a program of work (2010 to 2020) to upgrade and maintain dams to meet standards and cover the future demand of Melbourne's residents.They also have the Victoria Desalination Plant which delivers a rainfall-independent source of water for Melbourne. In 2016, the Minister declared the first water order, 50 gigalitre, from the desalination plant to mix with the Thomson and Upper Yarra catchments (MW, 2017).

Melbourne Water Corporation has made a considerable investment in promoting alternative sources of water for non-potable uses. It is primarily achieved by: 1) storm water harvesting, which represents more than 2 gigalitre of water per year; 2) recycling treated water from sewerage networks, which is approximately 20 gigalitre annually. The recycled water is used in different sectors such as a) residential estates for toilet flushing and garden watering, b) irrigating pastures and public open spaces, c) intensive agriculture and horticulture and d) industrial processes and wash down facilities (MW, 2017).

Melbourne has faced dry climatic conditions since 1998, which led the authorities to push water restrictions after twenty years of unlimited supply. This strategy was evolved to guarantee a continuation of a reliable, safe and cost-efficient water supply that is environmentally sustainable in the long-term period (Gato, 2006).

One catchment area in Melbourne (Yarra Valley Water) has been used to develop the water demand model. Yarra Valley Water is one of three retail water utilities that delivers essential municipal water supplies and sewerage services to more than 1.8 million capita and 50,000 businesses who live in the catchment area of Yarra River, Melbourne City. The Yarra Valley Water buys wholesale water from Melbourne Water, this water is usually harvested from protected catchments in the mountains. The service area managed by the company is approximately 4,000 km^2, and covers the northern area of Melbourne and the eastern suburbs, from Wallan in the north to Warburton in the east (YVW, 2017).

4.2.2. Columbia City, Missouri State, United States of America:

Columbia is a small city in northern mid-Missouri, which is located in the middle of the United States of America (Figure 4.3). The city lies near the Missouri River and has an area of around 164.5 km^2; its coordinates are 38.9517° N, 92.3341° W. Columbia City experienced an increase in population from 62,061 capita in 1980 to 108,500 capita in 2010. In addition, the total number of customers for all the different services inside the city was 44,360 in 2010 and 92% of them are residential customers. Columbia's water company supplies water services to residential, institutional, commercial and industrial, within the limits of Columbia City, and utilises the groundwater as a freshwater resource (Jacobs and St. Louis, 2015).

Figure 4-3: Location Map of Columbia City

4.2.2.1. Climate of Studied Catchment

Weather in Columbia City varies from summer, which is hot, muggy and wet to winter, which is very cold. The hottest period is statistically from 31th May to the 17th September with an average daily high temperature above 26°C and the coldest period is from 28th November to 26th February with an average daily high temperature below 10°C. Rainfall occurs throughout the year, but the most rain happens during the 31 days concentrated around 18th May, with an average total accumulation of 111 millimetres. While the period of snow is from 15th November to 22nd May with a sliding 31-day liquid-equivalent snowfall of at least 3 millimetres. During the period from 22nd May to 22nd September the humidity is approximately 67% (Diebel et al., 2013). Table 4-2 presents the statistical indicators for the four climate variables data that have been employed in this study over the period from 1980-2010. These variables are maximum temperature (Tmax), minimum temperature (Tmin), rainfall (Rain) and solar radiation (Radi).

Table 4.2: Max., Min. and Ave. values for four climate factors for a period (1980-2010)

	Tmax (°C)			**Tmin (°C)**			**Rain (mm)**			**Radi (MJ/m^2)**		
	Max.	**Min.**	**Ave.**	**Max.**	**Min.**	**Ave.**	**Max.**	**Min.**	**Ave.**	**Max.**	**Min.**	**Ave.**
J	10	-3	3	1	-11	-5	147	1	45	10	6	8
F	10	0	6	2	-8	-3	157	3	52	13	8	11
M	17	5	12	7	-2	2	191	19	69	17	10	14
A	25	12	19	11	4	7	245	33	102	22	13	18
M	28	20	25	16	9	12	320	40	134	26	15	22
J	34	26	30	19	15	17	261	3	113	28	22	25
J	40	29	34	23	17	20	337	2	109	27	20	24
A	37	29	33	22	16	19	245	14	105	24	18	22
S	32	23	27	17	11	14	298	11	100	20	16	17
O	22	15	20	11	5	8	283	17	93	15	9	13
N	18	8	12	6	-1	3	265	6	79	11	5	8
D	8	-6	5	0	-12	-3	177	8	66	9	5	7

4.2.2.2. Water Supply System

Columbia water company supplies water services to all types of customers such as residential, institutional, commercial and industrial within the limit of Columbia City. Additionally, extra water providers in the area consist of rural water districts for the surrounding rural regions, and Missouri University, which has its own private deep well water system (Jacobs and St. Louis, 2015). Figure 4.4 presents the water services area of Columbia City.

Figure 4-4: Columbia's Water Services Area (Jacobs and St. Louis, 2015)

The city uses groundwater as a freshwater resource. It has fifteen shallow alluvial wells located near the Missouri River, and three additional alluvial wells for future use. It also has one deep well inside the metropolitan area that is utilised during excessive demand periods. The city has changed two of their deep wells into aquifer storage and recovery facilities that allow the city to store municipal water from the water treatment plant during off-peak demand periods. The total capacity of these two deep wells is around 7.5 Megalitre per day (Jacobs and St. Louis, 2015).

The city receives the municipal water from the McBaine water treatment plant, which is located about 20 kilometres southwest of the city near the Missouri River. The capacity of the plant was expanded in 2006 to become 121 Megalitre per day. The water distribution system has four pump stations with different capacities. From 2002 to 2012, water loss accounted from for approximately 7.1%-17.4% of total consumption. The peak municipal consumption changes depend principally on how dry it is during the summer months, which tends to occur between July and October.

The city has an additional system of raw water to irrigate the gardens (Jacobs and St. Louis, 2015).

4.3. Data Set

This study will employ monthly historical data containing information such as municipal water consumption (Megalitre, ML), maximum temperature (°C), minimum temperature (°C), mean temperature (°C), rainfall (mm) and solar radiation (MJ/m^2) over the periods (1980-2010) and (2011-2015). The period (2011-2015) was only used for extra validation. These data were collected from the Yarra Valley water company for the areas that are served in Melbourne City and from the city council for Columbia City (i.e. daily climate factors will be employ to simulate future climate factors).

These climate factors have been adopted by several researchers in different areas of study for example, (Masanganise et al., 2014); (Kadiyala et al., 2015); and (Räisänen, 2015), to assess the impact of climate change. They are considered robust predictors, able to simulate municipal water demand as shown in Zubaidi et al. (2018). The socioeconomic variables such as population, water price and household income are deterministic signals (Zhoua et al., 2000; Gato et al., 2005). For this reason, these factors were not included in our analysis, as these signals are out of the scope of this study.

A reference baseline period is necessary to define the measured climate from which to calculate any scenario changes in climate. The availability of the required data for municipal water consumption will govern the baseline period choice. Accordingly, the period 1980-2010 was used. Semenov et al. (2013) suggested that the period from 1980-2010 is valid as a baseline period for generating future climatic factors. Several

researchers, including (Masanganise et al., 2014); (Kadiyala et al., 2015) and (Räisänen, 2015), have adopted this period in other different studies and areas.

The reliability of data is a significant issue for forecasting models. The data sets gained from the Yarra Valley Company for the areas that are served in Melbourne City and from the city council for Columbia City. This data is assumed to be reliable as it comes from reliable establishments. Chapter five will confirm its reliability. Several techniques need to be conducted on the data before using it in the prediction model.

The distribution of any quantitative variable can be presented using a box and whisker plot, which is a graphical plot used for five number summary to offer a quick numerical description. The five number are the minimum value, the first quartile, the median, the third quartile, and the maximum value of a data set. Figures from (4.5) to (4.10) show the distribution for all selected variables.

Figure 4.5 shows the average monthly maximum temperature. What stands out in this figure is both data sets have no outliers and have approximately the same median. The distribution of the dataset for Columbia City is around double that of Melbourne City. Unlike Melbourne City, the dataset of Columbia City includes negative temperatures.

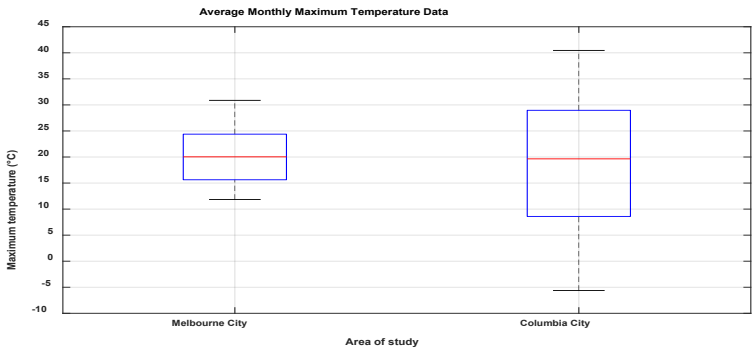

Figure 4-5: Box plot of average monthly maximum temperature for both cities

Figure 4.6 displays the average monthly mean temperature. It is very similar to Figure 4.5 but its median is approximately 5°C lower.

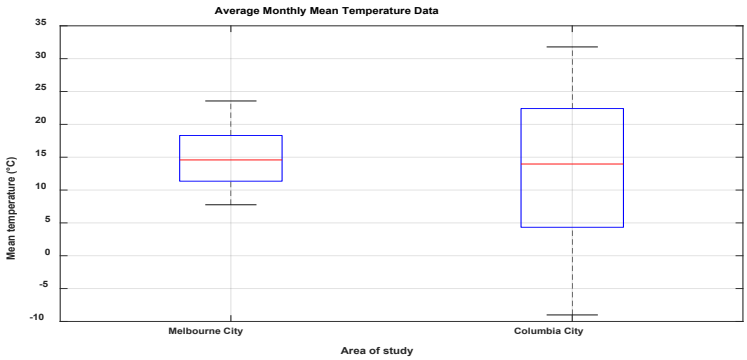

Figure 4-6: Box plot of average monthly mean temperature for both cities

The box plot of average monthly minimum temperature for both cities can be seen in Figure 4.7. It is apparent from the figure that there are no outliers for both cases. The dataset is distributed between 4 and 16°C and the median is 9°C for Melbourne City. While, the distribution of the data set for Columbia City is from -13 to 23°C and the median is 7°C.

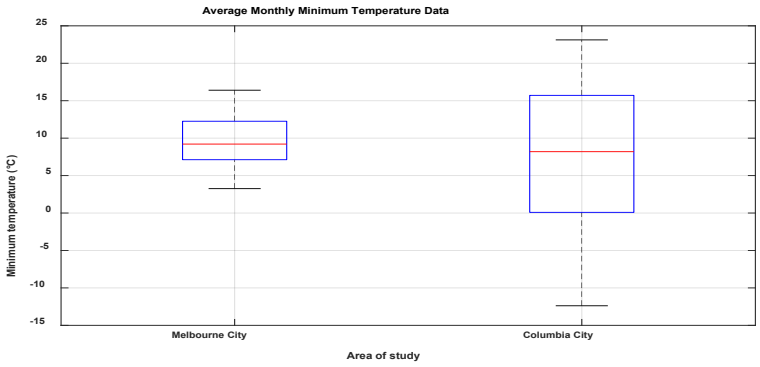

Figure 4-7: Box plot of average monthly minimum temperature for both cities

Figure 4.8 illustrates the solar radiation for both cities. It is apparent that there is no significant variation between the plot of both cities and there are no outliers. For

Melbourne City, the median is 15MJ/m^2 and the quartiles are between 9 to 21MJ/m^2. For Columbia City, the median is 16MJ/m^2 and the quartile range is 9 to 22MJ/m^2.

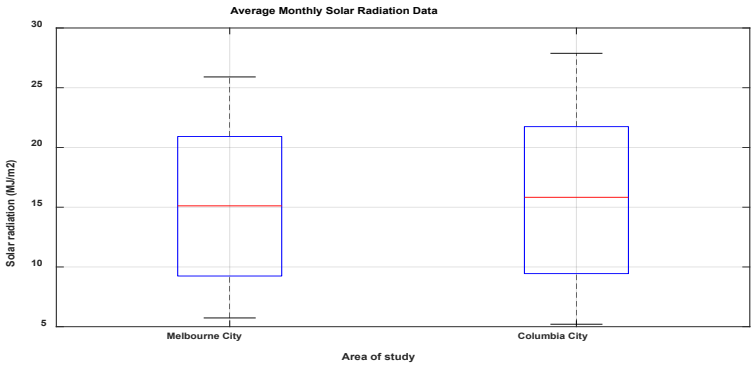

Figure 4-8: Box plot of average monthly solar radiation for both cities

As shown in Figure 4.9, the median value of rainfall for Columbia City is 75mm and its more than the median of Melbourne City with around 15mm. The maximum value of precipitation is 220mm for Columbia City while it is equal to about 140mm for the Melbourne City. The outliers in Columbia City are higher in comparison with Melbourne City.

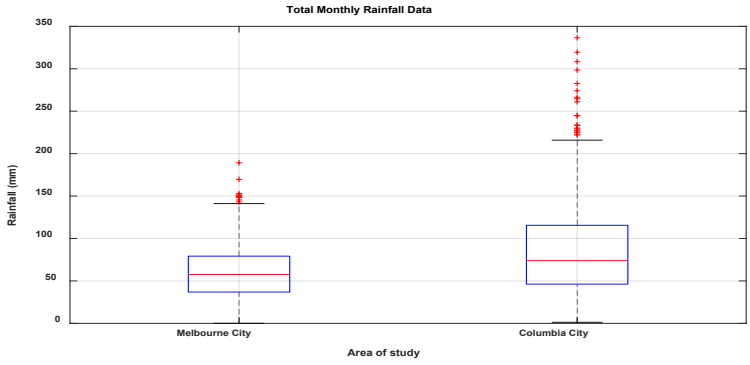

Figure 4-9: Box plot of total monthly rainfall for both cities

It is apparent from Figure 4.10 that the water consumption for Melbourne City is significantly higher than Columbia because of the population variance and the size of the serviced area. The median value of Melbourne City is around 14,100ML compare

with 1,190ML for Columbia City. Melbourne City has many more outliers than Columbia City, and that is considered a normal condition regarding the magnitude of the delivered municipal water.

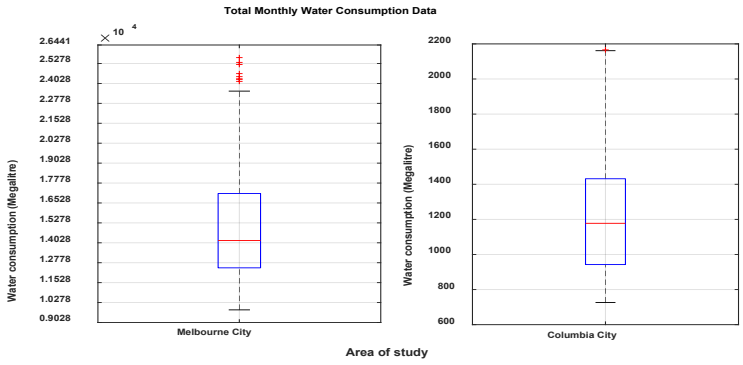

Figure 4-10: Box plot of total monthly water consumption for both cities

4.4. Data Pre-processing Techniques

Data preprocessing techniques are a significant step in the data mining process. These techniques play an important role in ANNs' performance by improving precision with minimal computational cost of the training stage. Noisy and unreliable information that could be present in data records will adversely affect the learning phase and result in a poor model (Kotsiantis et al., 2006). In spite of the ability of artificial neural networks to forecast any kind of relationship in the data with high accuracy, several experimental studies have highlighted the role of data preprocessing before employing them as inputs to neural network models (Sebri, 2013). Abrahart et al. (2004) stated that data preprocessing is steps include: data normalisation, cleaning, and identifying convenient model inputs. A novel technique will be applied in this study, that was successfully proven in Zubaidi et al. (2018)

4.4.1. Data Normalisation

Normalisation rescales the model input data to that each input has zero mean and unity variance. It aims to smooth the answer space and minimise the effects of noise (Araghinejad, 2014). Tabachnick and Fidell (2013) mention that transforming the continuous variables is important in making the time series normally, or near normally, distributed. The results of the model are degraded when the time series of variables are not normally, or near normally, distributed. In this research, the natural logarithm method was adopted to conduct the normalisation for the input data. A major advantage of the natural logarithm technique is that it makes data more static and removes collinearity between variables. In addition, it could rescale back the output values of ANN to the similar water demand unit (Behboudian et al., 2014).

4.4.2. Data Cleaning

Data cleaning techniques comprise detection and treatment of irrelevant or meaningless data, such as noise or outliers, to improve the outcomes of data analysis (Xiong et al., 2006). Extreme data has adverse effects on the regression solution and influences the accuracy of the model (Pallant, 2011). Donkor et al. (2014) ; Bakker et al. (2014) and Ghiassi et al. (2008) referred to the fact that sometimes the total system contains leaks and other system flaws, which cannot be deemed as actual demand. Taking this into consideration, it would be more suitable to predict the actual water demand including leakages to facilitate the actual system optimisation and revenue.

Based on Abrahart et al. (2004) data cleaning includes identifying and removing trends and non-stationary components within a data set. The time series can decompose to trend (T), oscillatory (O), stochastic (S) and noise (Ɛ) components (i.e.

trend and oscillatory are considered deterministic signals) as shown in Equation (4.1) (Araghinejad, 2014).

$$Y_t = T_t + O_t + S_t + \varepsilon_t \tag{4.1}$$

To identify outliers, the box and whisker method was used, and the then outliers were treated. The Singular spectrum analysis (SSA) technique was used to detect the stochastic signals for municipal water consumption and climate variables time series that was proven in Zubaidi et al. (2018). After that, the Augmented Dickey-Fuller (ADF) test and Kwiatkowski–Phillips–Schmidt–Shin (KPSS) test were employed to investigate the stationarity of the stochastic time series.

Box et al. (2016) state that "Stochastic" means having a random probability function or pattern that may be analysed statistically. A stochastic model is a tool for describing the probability structure of potential outcomes by letting for random variation in one or more inputs through time. Stochastic models were used to describe the time series that has received a great deal of importance, includes what are named stationary models. These models suppose that the mean level and variance should be constant over the time series. This technique applied initially in physics and now applied in different sectors such as engineering and environmental sciences (meteorology). In this study, the stochastic model used to characterise, analyse and understand the dynamic relationships among municipal water consumption and climate factors for long term, also enhance the accuracy of prediction.

Noise is an undesirable variance in the time series that comes from flied measurements Tabachnick and Fidell (2013). Noise signals represent very small percent from the total time series (e.g., it about 0.0001% of the total municipal water consumption time series as shown in Figure 4.12 B).

4.4.2.1. Singular spectrum analysis (SSA) method

SSA is a powerful method used to analyse time series to uncover significant prediction characteristics. It can be used for both linear and nonlinear time series and small sample sizes. It does not rely on any statistical assumptions based on the stationarity and linearity of the series, or on the normality of the residuals (Hassani et al., 2009).

SSA has been used in different fields including medical engineering (Ghodsi et al., 2009), economics (Hassani et al., 2015) and hydrology (Marques et al., 2006). SSA is utilised for decomposing the original time series into a number of independent components; the principal components (PCs). These PCs including trend, oscillatory components and irregular components. Then, a number of PCs can be used to reconstruct the initial time series (Rocco S, 2013).

The main reason for using SSA is to uncover the stochastic component, which is considered a significant prediction characteristic of the time series. This process is achieved by removing noise and a slowly varying components (trend, and oscillatory components).

The SSA approach consists of two stages: decomposition of the original time series into different principle components (PC_s) including trend, oscillatory components and irregular components, and noise removal and reconstruction of a new time series that has less noise (Al-Bugharbee and Trendafilova, 2016). Extra details about SSA and the basic ideas are explained in Golyandina et al. (2001).

A) Decomposition stage

In the decomposition step, a sub-signal y of length T, y_1, y_2, …., y_T, is mapped onto a length window (L) to create the so-called trajectory matrix, Hankel matrix, X (L×K) where K=T-L+1 (Equation (4.2)).

$$X=\begin{bmatrix} y_1 & y_2 & y_3 & \cdots & y_K \\ y_2 & y_3 & y_4 & \cdots & y_{K+1} \\ \vdots & \vdots & \vdots & \ddots & \vdots \\ y_L & y_{L+1} & y_{L+2} & \cdots & y_T \end{bmatrix} \tag{4.2}$$

The Hankel matrix (X) undergoes to singular value decomposition to get L eigenvectors ($\mathbf{U_i}$, i= 1, 2…., L) corresponding to L eigenvalues (λ_i, i=1, 2…, L). Any λ_i refers to the partial alteration of the original time series in the $\mathbf{U_i}$ direction. The corresponding principal components (PC_i) can be obtained by projecting the Hankel matrix onto every eigenvector:

$$PC_i(m) = \sum_{j=1}^{L} X'(m+j-1) * U_i(m) \tag{4.3}$$

where i=1,2….L, m= 1,2…T, j=1,2…L, and the prime means transpose.

Projecting the PC_s on the eigenvectors (U) gives the primary matrices L ($EI_i=U_i\,PC'_i$) where i= 1,2…..L and the prime denotes transposition.

In this study, L will be equal to 12 so as to extract together all seasonal components (12, 6, 4, 3, 2.4, and 2-months harmonics), trend and noise (Golyandina et al., 2001) .

The contribution of these primary matrix norms to the original Hankel matrix norm follows the singular values' trend, meaning that the highest contribution will go to the first matrix while the lowest contribution will go to the last.

B) Reconstruction stage

As mentioned above, the signals can be reconstructed via a linear combination of several, or all, the PCs. When choosing the number of PCs, there are various criteria to observe (Kilundu et al., 2011). In this study, valuable insight is offered via inspection breaks testing in the eigenvalue spectra to select the number (w) of PCs. A slight decrease in the singular sequence values indicates pure noise according to the latter test. The seasonal signal of the original sub-signal is contained in the new reconstructed signal (yr). The process of reconstruction is achieved via the diagonal averaging mechanism that is depicted in Equation (4.4) (Ghil et al., 2002).

$$yr(m) = \frac{1}{N_m}\sum_{i\in w}\sum_{j=Lm}^{Um} PC_i\,(m-j+1)\times U_i(m) \quad ,m = 1,2,,,n-1 \tag{4.4}$$

The normalisation factor (Nm) and the upper (Um) and the lower (Lm) limits y the inner of sum vary for the centre and edges of the signal. They are defined as shown below:

$$\left(\frac{1}{Nm}, Lm, Um\right) = \begin{cases} \left(\frac{1}{m}, 1, m\right), & for\ 1 \le m \le L-1 \\ \left(\frac{1}{L}, 1, K\right), & for\ L \le m \le K \\ \left(\frac{1}{n-m+1}, m-n+L, L\right), & for\ K+1 \le m \le n \end{cases} \tag{4.5}$$

4.4.3. Determination of Model Inputs

The selection of explanatory variables that influence water demand as model input data is one of the most significant stages in evolving a satisfactory forecasting model (Zhang et al., 2006). Maier and Dandy (2000) pointed out that the selection of suitable model inputs is highly significant in the ANN prediction model. The criteria for selecting the model inputs were as follows: cross-correlation was used to investigate the relation between dependent and independents variables. The variance inflation

factor (VIF) technique was applied to examine the multicollinearity among independents variables. These stages of the process were carried out to ensure that as many of the potential variables as possible were properly included in the map of the input-output relationship, to avoid multicollinearity, which can lead to incorrect conclusions. This technique of selection for model inputs was successfully proven in Zubaidi et al. (2018).

4.5. Results of Model Inputs Developments

This section corresponds to step A in Figure 3.1. Five monthly climate factors have been used to assess the impact of climate change on monthly water consumption. These factors are maximum temperature (Tmax), minimum temperature (Tmin), mean temperature (Tmean), solar radiation (Radi) and rainfall (Rain). The followings are the methods for data pre-processing:

1) Normalisation by natural logarithm to treat some of outliers and mitigate the rest of outliers.
2) Cleaning data outliers by using box and whisker method to identify the outliers. Each outlier was treated by calculate the mean of three recorded data (outlier, data before and data after). The average monthly data for water consumption and all climate factors after normalisation and cleaning can be found in Appendix 4-B. Pre-treatment signal analysis (SSA) then was used to uncover the stochastic component. Components of the original time series were examined to detect the stochastic signal. It represents the third signal in water consumption and all the climate factors time series except the solar radiation time series which was the second signal. The stationarity of the stochastic signal has been examined by the Augmented Dickey-Fuller (ADF) and Kwiatkowski–Phillips–Schmidt–Shin

(KPSS) tests. Figure 4.11 presents the original time series and the first four components of water consumption and all climate factors.

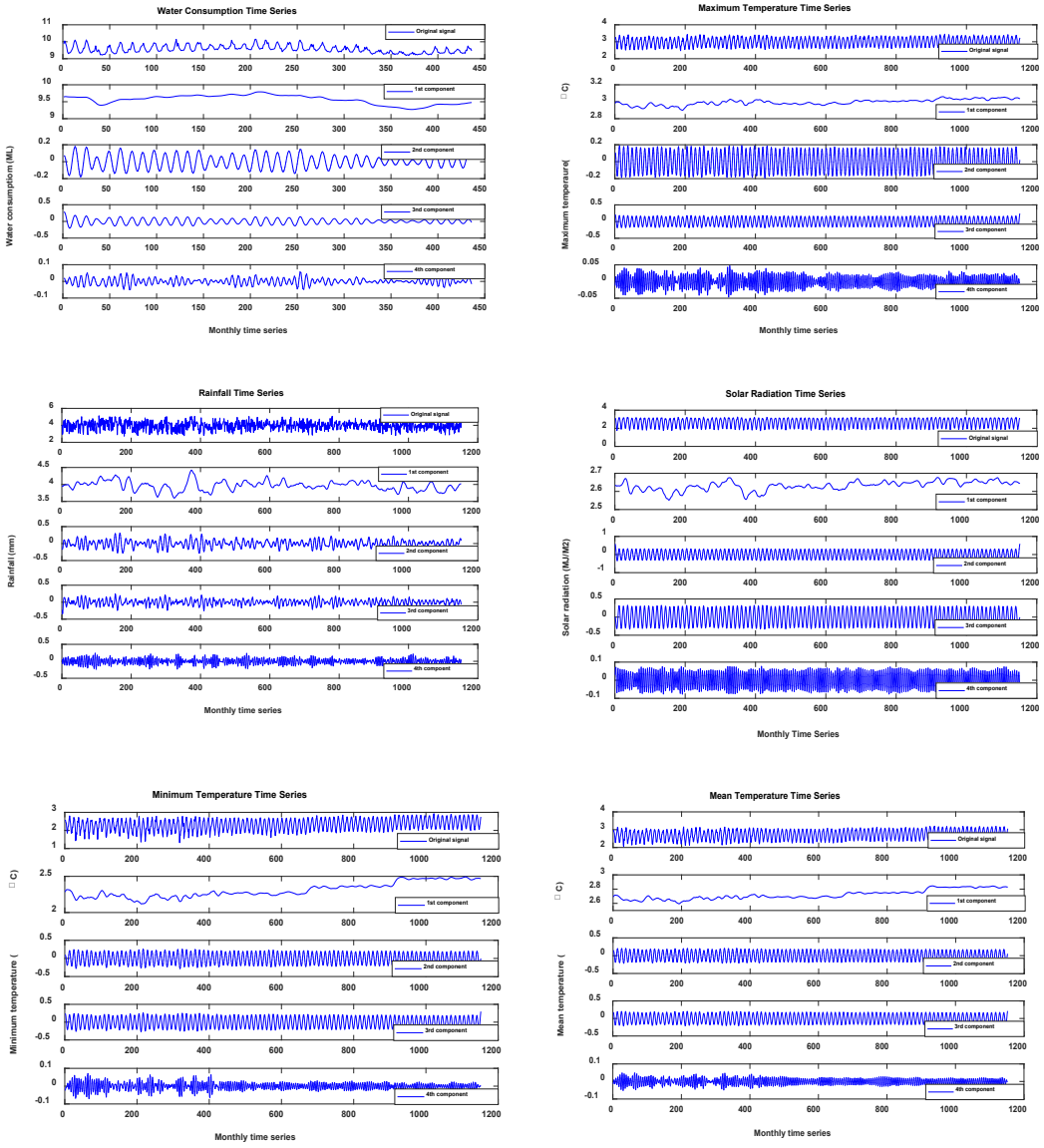

Figure 4-11: Original signal and the first four components obtained by SSA (Melbourne City)

To detect noise components, Ghodsi et al. (2009) pointed out that a significant drop in eigenvalue spectra values could be assumed as the beginning of pure noise. Figure 4.12 A shows the graph of eigenvalue spectra for the water consumption time series, where it can be seen that the first signal, which represents a trend, was prevailing and covered all the details. Therefore, the first signal was removed and the graph was

redrawn in section B. In this section, a significant drop occurred in the third signal, this representing the beginning of the noise floor. The figures for climate variables time series are presented in Appendix 4-C.

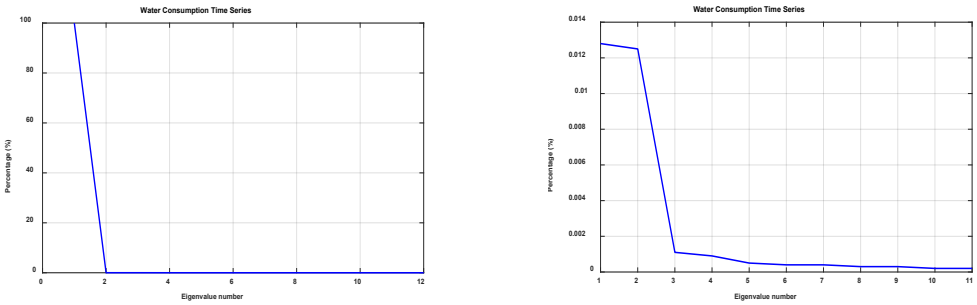

A B

Figure 4-12: Eigenvalues of water consumption time series (Melbourne City)

Figure 4.13 gives the descriptive statistics (maximum, minimum, median, upper quantile and lower quantile) for the monthly box plot of the stochastic signal for water consumption and all climate variables. The median for all factors is approximately zero and there are no outliers.

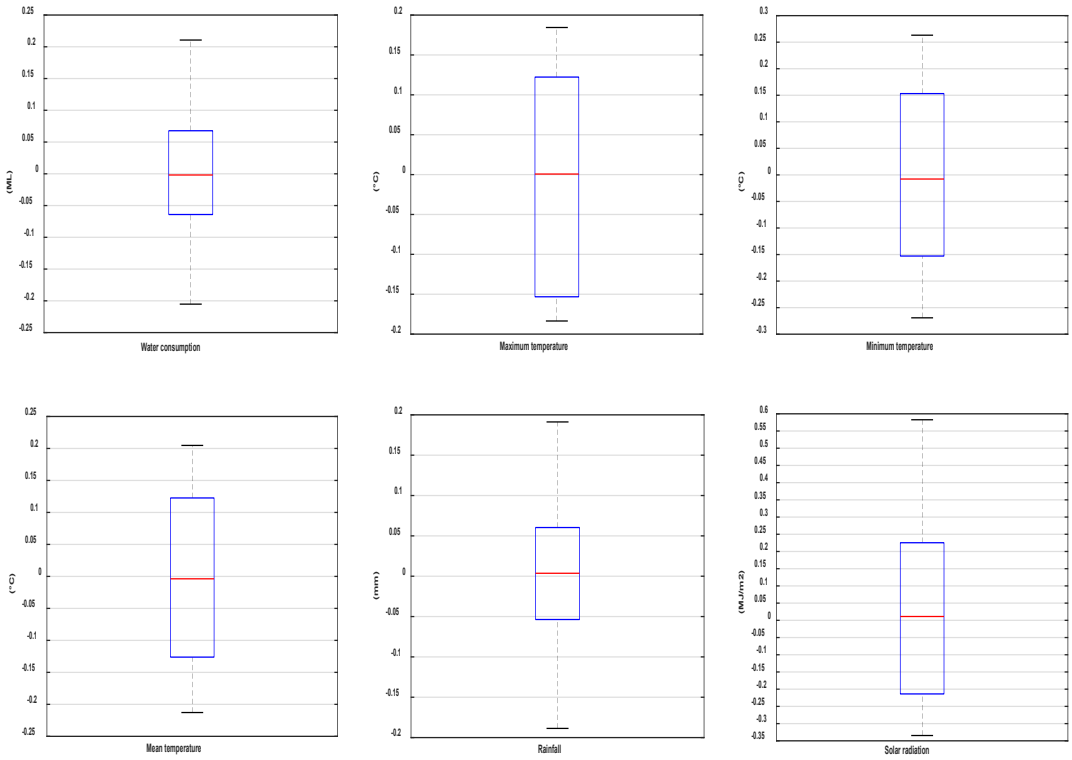

Figure 4-13: The monthly box plot of the stochastic signal for water consumption and all climate variables (Melbourne City)

3) A variance inflation factor (VIF) was applied to examine the multicollinearity between the independent variables. Three independent factors, i.e. Tmax, Radi and Rain, were selected as the model input. To decide on the appropriate sample size needed for developing a good ANN model, Tabachnick and Fidell (2013) proposed a sample size for the model that is dependent on the number of predictors, as shown in Equation (4.6).

$$N \geq 104 + m \tag{4.6}$$

Where N= sample size and m= number of independent variables.

The sample size required for the model was estimated by using Equation (4.6), obtaining that 107 (104+3) were needed. In this study the number of cases is N=372, which is more than three times the minimum required.

A Pearson product-moment correlation coefficient was used to determine the relationship between the stochastic components of water consumption and chosen climate variables. Figure 4.14 shows the correlation between the independent and dependent variables. We can see in this figure the strong correlation between water consumption and the climatological variables, especially with maximum temperature (R=0.94).

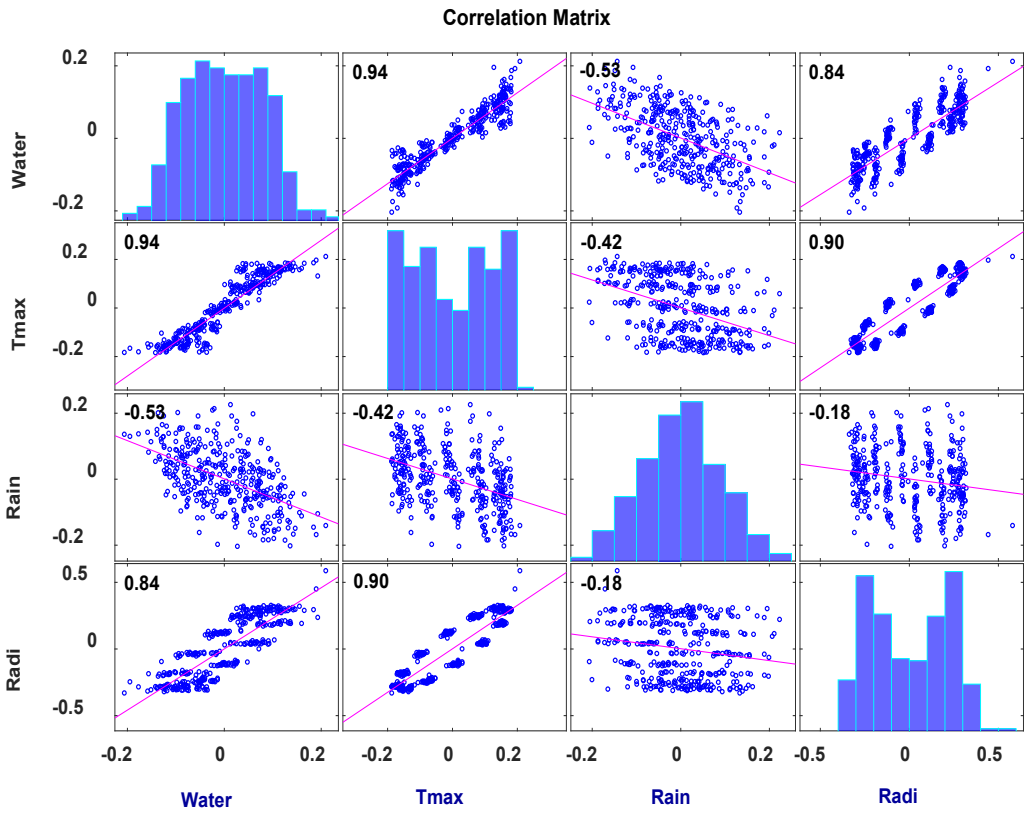

Figure 4-14: Correlations between water consumption and climate factors (Melbourne City)

A correlation matrix was used for water consumption and the selected weather variables with the raw data and compared with the stochastic phases (after preprocessing) to show the impact of the SSA on the data (Table 4.3). What stands out in this table is the significant increase in the correlation coefficient between water consumption and climate factors (e.g. maximum temperature correlation increases from 0.69 to 0.94 after removing trend, seasonal and noise signals by using SSA). These results confirm that adopting the SSA method as a pretreatment signal, helps to improve the correlation between the dependent and independent variables, when forecasting water demand models.

Table 4.3: Correlation matrix analysis results for raw and stochastic data (Melbourne City)

Data	Municipal water	Maximum temperature	Rainfall	Radiation
Raw	1	0.69**	-0.24**	0.63**
Stochastic		0.94**	-0.53**	0.84**

**Correlation is significant at the 0.01 level (2-tailed).

From these results, we can see that water demand (dependent variable) can be expressed as a function of Tmax, Radi and Rain (independent variables) and the process of optimisation to select the optimum parameters for the ANN model is ready now.

4.6. Discussion

Data preprocessing techniques have a significant role to play in the ANN input model, specifically the SSA method, to uncover the stochastic signal and remove the effect of socio-economic factors and noise (e.g. Tmax correlation increases from 0.69 to 0.94). The selection methods of explanatory variables (i.e., Tmax, Rain and Radi) are reliable predictors based on cross corealtion and VIF techinques to use to simulate long-term municipal water demand. Accordingly, data pre-processing techniques are effectively associated with the accuracy and robustness of the results.

4.7. Summary

This chapter described the areas of study that were chosen to assess the impact of climate change on municipal water consumption (i.e. background, climate condition, freshwater resources and municipal water supply system). It presented the data

preprocessing that is employed to prepare raw data before using it in the municipal water prediction model.

Area of Study

The availability and reliability of data lead to the selection of Melbourne City as a case study. It is a significant city located in Australia, summer months are December, January and February, rainfall harvesting is the primary freshwater resource, and 60% of water customers are residential (i.e. comprise the catchment area of Yarra River only, which is served by YVW company).

The next city selected was Columbia City. It is a small city located in the American continent, summer months are June, July and August, groundwater is the primary freshwater resource, and 92% of water customers are residential.

Data Set

This part of the chapter presented the type of data that will be used as independent variables in the prediction model over a specific period and their reliability. The independent variables comprise maximum temperature, mean temperature, minimum temperature, rainfall and solar radiation (i.e. these variables were used in several previous studies) over the recommended baseline period 1980-2010.

Data Preprocessing

A novel process of data manipulation was discussed, which included several techniques to prepare the raw data before employing it in the forecasting model. The main idea from data preprocessing is to detect the stochastic signal of dependent and independents variables because the relation between water consumption and climate

variables is stochastic (i.e. remove the effect of socioeconomic factors, which represent deterministic signals).

The findings highlight the significance of the data preprocessing technique especially the SSA approach to uncover the stochastic signal of water consumption and all climate factors time series. In addition, the data preprocessing technique helps to select the best model input that has the ability to simulate municipal water demand accurately.

The next chapter presents the results of the municipal water demand model development, simulation of the future climate factors and the expected future municipal water demand.

Chapter 5: Development of Water Consumption and Downscaling Models (Results and Discussion)

5.1. Introduction

This chapter describes the results and discussion of the thesis, which are divided into three main groups:

first group, develop municipal water demands model by using three computational intelligence algorithms include Lightning Search Algorithm (LSA), Gravitational Search Algorithm (GSA) and Particle Swarm Optimisation (PSO) to support the primary model, which is an Artificial Neural Network (ANN).

Second, simulate future climate factors by employing the Long Ashton Research Station Weather Generator (LARS-WG) model. In addition, seven General Circulation Models (GCMs), daily data of climate factors for the baseline period 1980-2010 and three of the Intergovernmental Panel on Climate Change (IPCC) scenarios A2, A1B and B1.

Third, forecast municipal water demands over three future periods and under three of the IPCC scenarios to cover all options of emission scenarios that are supported by the selected model.

The author would highlight that all the data through this chapter belong to the Melbourne City. While the data results from Columbia City are presented in Appendix 5-A.

5.2. Development of Municipal Water Demand Model

5.2.1. Application of the Hybrid PSO-, GSA- and LSA-ANN Algorithms

This section corresponds to step B in figure 3.1. We used the MATLAB toolbox to run the LSA-ANN, GSA-ANN and PSO-ANN algorithms. For estimating the best number of hidden neurons and the optimum learning rate coefficient of all three techniques, we used five population sizes (10, 20, 30, 40 and 50). Note that these population sizes relate to the size of the swarms, which is different to the sample size mentioned earlier (section 4.5). As can be seen in Figure 5.1, a population size of 50 provides the best solution for all three algorithms. Closer inspection of the fitness function values for all algorithms shows that the RMSE for the LSA-ANN algorithm (after 40 iterations) is 0.0236, whereas GSA-ANN does not improve a RMSE of 0.0241, and PSO-ANN algorithm only reaches its best RMSE of 0.0245 after 62 iterations, as presented in Figure 5.2. Accordingly, LSA-ANN algorithm outperforms GSA-ANN and PSO-ANN, as it achieves a smaller error (better performance) in a smaller number of iterations (making it a less complex model). Table 5.1 compiles the design parameters of the ANN model based on the LSA-ANN algorithm.

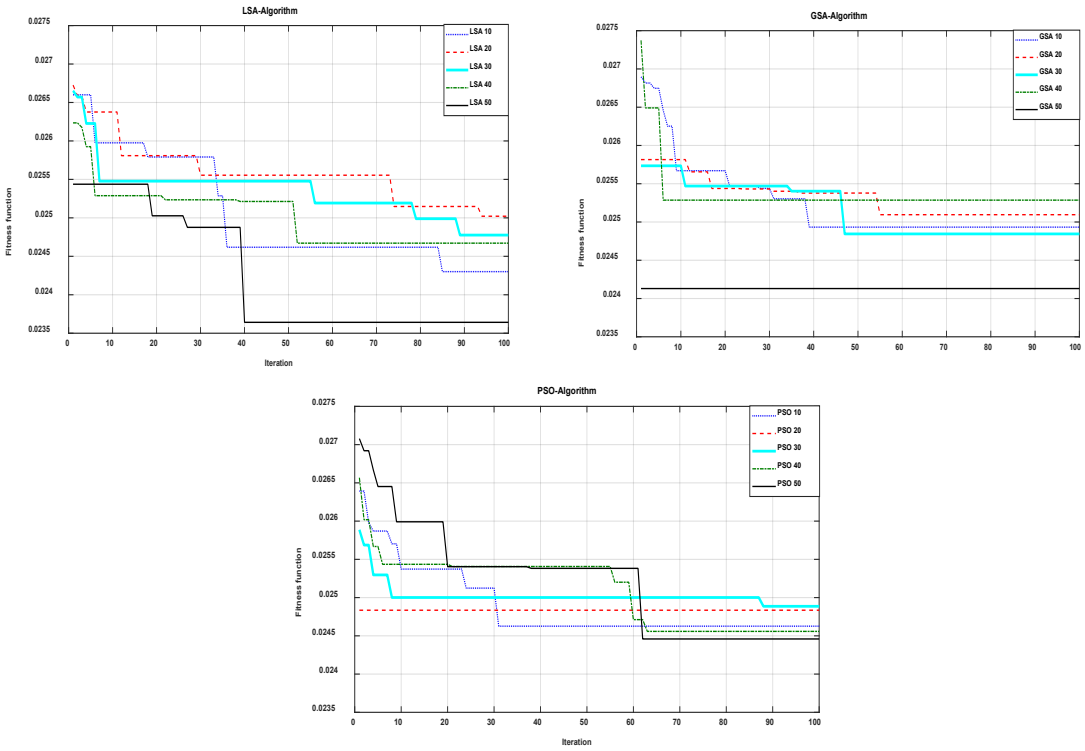

Figure 5-1: Fitness function for various populations using the computational intelligence algorithms (Melbourne City)

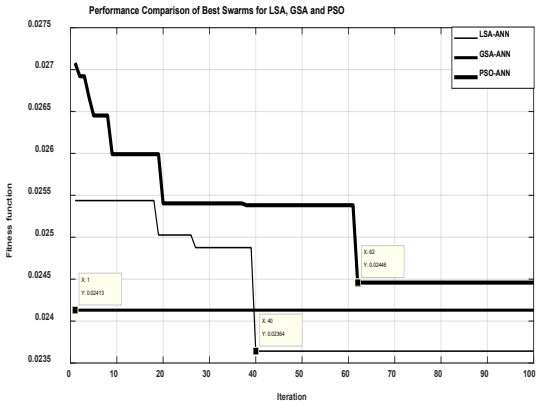

Figure 5-2: Comparison of the performance of the best swarm size of LSA, GSA and PSA algorithms (Melbourne City)

Table 5.1: ANN-designed parameters (Melbourne City)

Parameter	Value	Type
Number of inputs	3	As discussed in section 4.5
Number of outputs	1	Our target, which is water demand
Number of hidden layers	2	As used in Zubaidi et al. (2018)
Number of neurons in hidden layer N1	3	Estimated by LSA
Number of neurons in hidden layer N2	4	Estimated by LSA
Learning rate coefficient	0.1988	Estimated by LSA

The ANN model now is ready to simulate municipal water demand based on three climate factors.

5.2.2. Application of Artificial Neural Networks

This section corresponds to step C and D in figure 3.1. After identifying the parameters for the ANN, the model was run several times to find the best neural network architecture to forecast municipal water demand. A range of statistical tests was applied to evaluate the performance of the model. Firstly, the coefficient of regression (R) and residual distribution were determined between the measured and predicted water demands, as shown in Figure 5.3. The observed water consumption (i.e., the target on the x-axis) is plotted against the predicted water demand (i.e., the output on the y-axis). The combination model was significant R=0.96 at the validation stage. This figure emphasises the ability of the hybrid LSA-ANN technique to accurately predict municipal water demand.

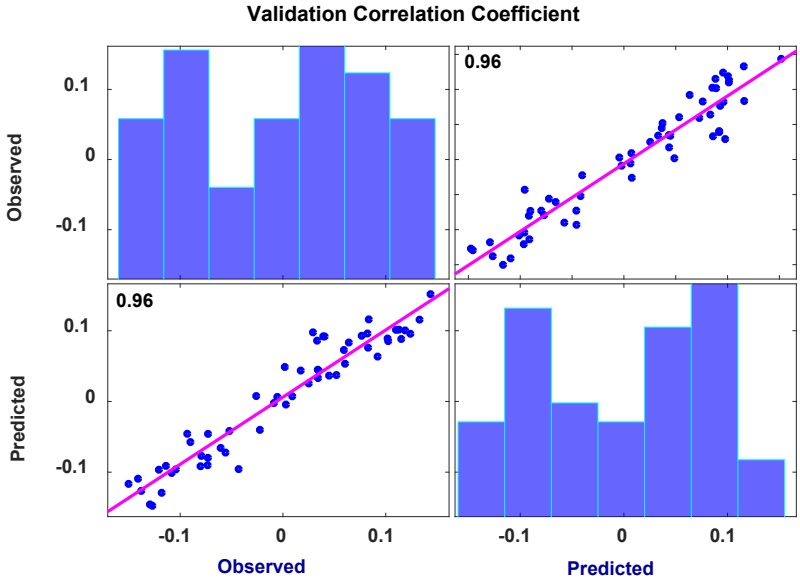

Figure 5-3: ANN algorithm performance for the validation data (Melbourne City)

In order to examine the goodness of fit of the model, an error analysis was performed. The scatter plots of error, versus a number of samples for validation, are presented in Figure 5.4. Three important patterns have emerged from the data; the data had a smaller error scale between -0.04 and 0.04 except for some data, no special trend exists for the pattern of distribution and the distribution of error density for all data is regular.

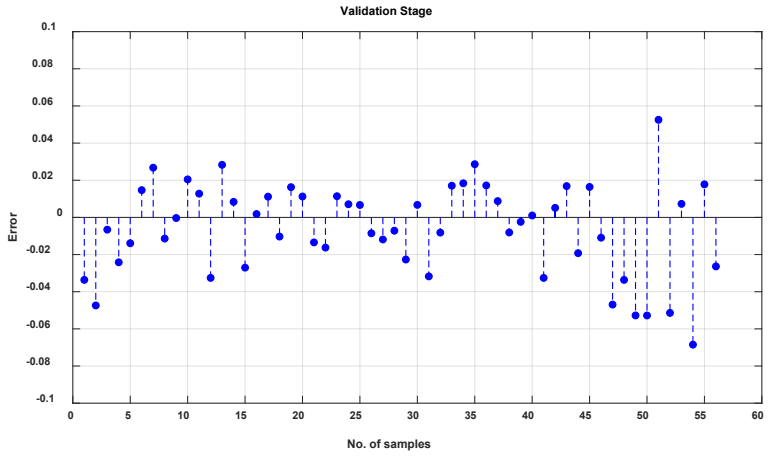

Figure 5-4: Residual scatterplots for validation data stage (Melbourne City)

Figure 5.5 provides a graph of the results for the observed and simulated water demands for the validation data. What stands out in this figure is the ability of the

model to capture the pattern of the observed data. The simulated data is a close match to the observed data regarding the scale of error. There is some deviation in the plot for the last months. It may come from the impact of additional climate factor in this period not included in the model like humidity (i.e., Melbourne City suffered from the impact of climate change). However, it is not statistically significant when the deviation has been assessed by T-test and shows that around 98% distribution fit between agreement limits of a Bland–Altman scatters plot as shown in Figure 5.6.

Figure 5-5: Observed and predicted stochastic signal of municipal water demands for the validation data (Melbourne City)

A Bland–Altman scatter plot was employed to examine the agreement of the model for validation data. It has the ability to reveal the systematic and random differences as well as the merit of exhibiting the variation in the outcomes. In this plot, mean (m) and standard deviation (SD) of the differences were obtained by applying the T-test technique that used to assess the difference between the mean of observed and predicted water values. In addition, m+1.96 SD and m−1.96 SD represent the upper and lower limits of agreement. From this plot, it is quite easy to evaluate the level of

(systematic) variation, the scatter of the values, and to display whether there is a relation between the observed and predicted error.

The most obvious finding to emerge from the analysis is that scattered data suggests an excellent distribution fit between agreement limits with percentage range values around 98%, as shown in Figure 5.6.

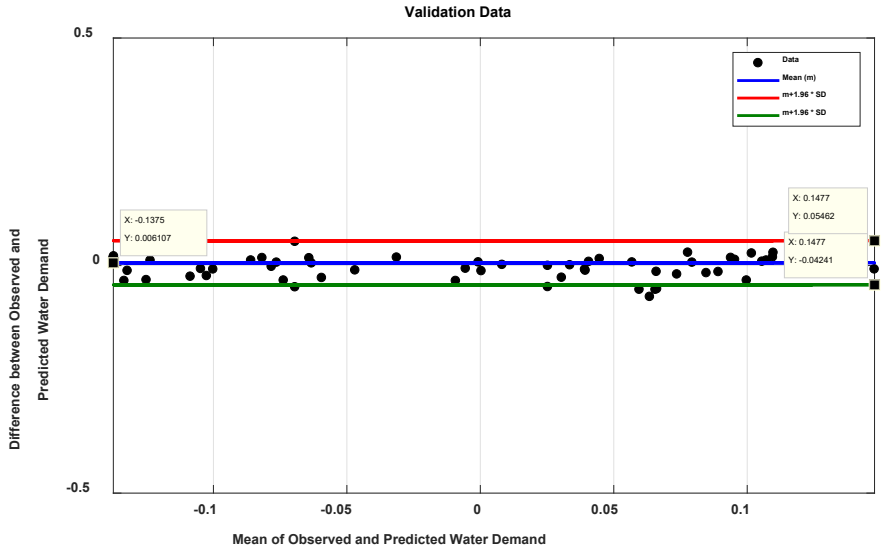

Figure 5-6: Bland–Altman plot of the relation between observed and predicted stochastic signal of municipal water (Melbourne City)

For more statistical support, Table 5.2 provides three measures of the differences between the predicted and observed time series, to evaluate the model performance. We can see that the differences between the observed and predicted water demands are negligible (MSE= 6.3911 10^{-04}). Up to this point in this section, we were covering step C from figure 3-1.

Table 5.2: Three statistical criteria for the validation data (Melbourne City)

Data	MAE	MSE	RMSE
Validation	0.0201	6.3911 10^{-04}	0.0253

MAE: mean absolute error, MSE: mean square error, RMSE: root mean square error

Finally, the model was also validated by evaluating an independent set of data from 2011 to 2015, and this corresponds to step D of our proposed methodology (figure 3.1). Two copies of water consumption data were adopted, the first one has the same 12 original signals. The second one contains the same components for the first one except for the stochastic signal, which was replaced by the predicted signal that was produced by the ANN model. Both sets were reconstructed, rescaled and the correlation coefficient between them was 0.98, which is sufficient assurance that the ANN network can generalise accurately as shown in Figure 5.7.

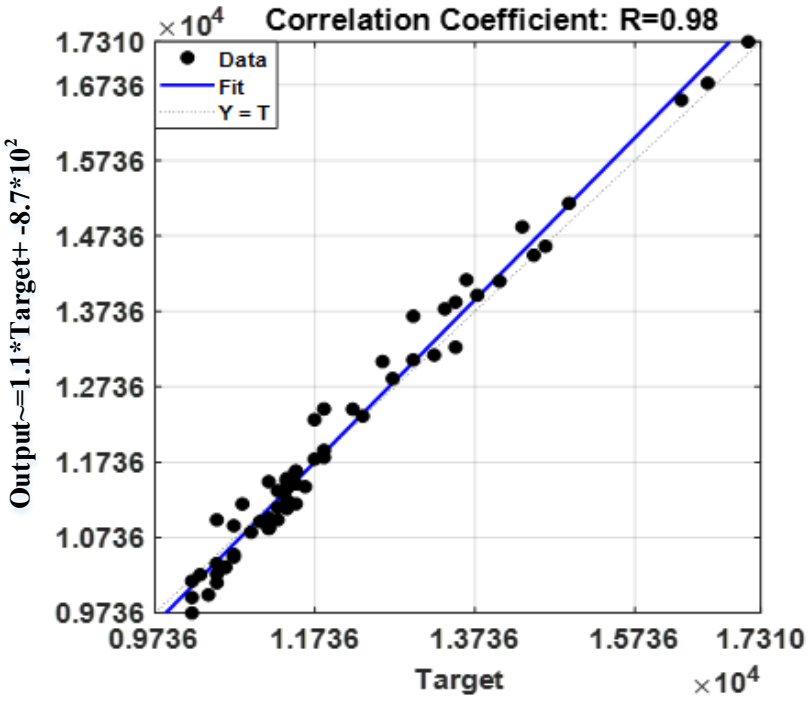

Figure 5-7: ANN algorithm performance for the independent set of data (2011-2015) (Melbourne City)

As shown in Figure 5.8, the graphical form was employed to display the outcomes in terms of measured and predicted water demands. The figure shows an excellent fit between actual and predicted municipal water supplies demonstrating the capacity of this model to capture the pattern of water consumption for the period 2011-2015 accurately.

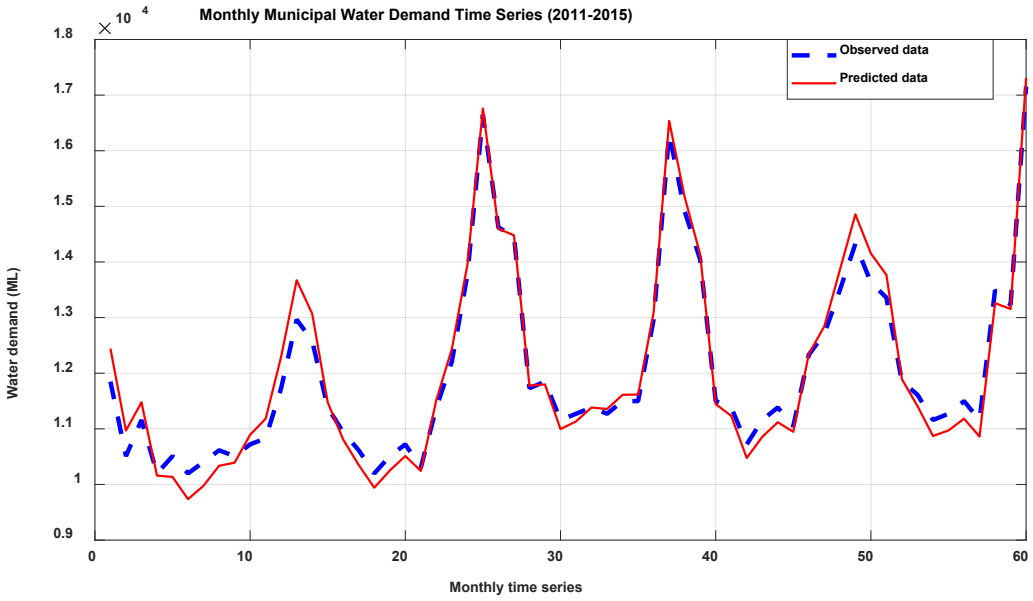

Figure 5-8: Observed and predicted municipal water demands for the independent set of data (2011-2015) (Melbourne City)

5.2.3. Municipal Water Demand Model Validation

Two cities (Melbourne and Columbia) were employed to validate the proposed methodology in Chapter 3, where they apply to show the impact of using different geographical locations and environments on the performance of the municipal water demands model. Melbourne City is different from Colombia City in a number of facts as presented in Table 5.3. It notices from the table that Melbourne has a higher population than Columbia city. In addition, in terms of the water consumption, Columbia City has indoor use only (i.e. it has an additional system of raw water to irrigate the gardens), while the Melbourne City has indoor and outdoor consumption (Jacobs and St. Louis, 2015; YVW, 2017).

Table 5.3: Different facts of Melbourne and Columbia Cities

Factors	**Melbourne City***	**Columbia City**
Location	Australia	United States of America
Population (capita)	1,800,000	108,500
Fresh water resource	harvested from protected catchments	groundwater
Customers	60% of them are residential	92% of them are residential
Water consumption	indoor and outdoor	indoor only
Median value of water consumption (1980-2010) (ML)	14,100	1,190

*These data are considered for the areas that are served by the Yarra Valley water company in Melbourne City.

The performance of the current methodology, applied to Melbourne and Columbia Cities is illustrated in Table 5.4. It appears from the table that the model inputs have the same climate factors for both cities include (Tmax, Rain and Radi). However, the correlation between the stochastic signal for water consumption and climate factors are slightly different from city to another, because of these cities have different climate conditions. The results confirm that the data preprocessing techniques to detect a stochastic signal and select the best model inputs are reliable because it has a significant correlation between dependent and independents factors. Moreover, as shown in the table, the hybrid algorithm LSA-ANN (Swarm=50) has a better performance compared with the other types of hybrid algorithms in respect of fitness function (i.e., based on RMSE) for both cities.

Different statistical criteria (e.g., R, MAE and RMSE) are used to evaluate the performance of the combination SSA and LSA-ANN model. An important point that emerged from the data was that the model has the ability to predict the water demands accurately in both cities. The R is approximately the same for both cities, while the MAE and RMSE for Columbia City are slightly better than the values of Melbourne City. The reason behind that is regarding the variation in the population, size of the serviced area and climate factors.

Table 5.4: The details comprising the results of the proposed methodology in different cities

Factors		**Melbourne City**	**Columbia City***
Model input (presented in chapter 4)	Tmax	0.94	0.92
	Rain	-0.53	0.59
	Radi	0.84	0.78
Hybrid algorithm		LSA-ANN (swarm 50)	LSA-ANN (swarm 50)
ANN Model Performance	R	0.96	0.95
	MAE	0.0201	0.0126
	RMSE	0.0253	0.0163

* These results are presented in Appendix 4-A and 5-A.

5.2.4. Results Comparison to Previous published work

The results' performance of the current methodology that are presented in Chapter 3 are compared to the two recently published works. Both studies have confirmed the effectiveness of data preprocessing (i.e. make the time series stationary). Sebri (2013) used detrend and deseasonal for preprocessing data, Trimester from 1983 to 2002 as a model input and ANN model. Behboudian et al. (2014) applied normalised by natural logarithm and detrend to make the series stationary. Monthly socio-economic and

Tmax from 1997 to 2008 used a model input and ANN model. The details of the compared results are present in Table 5.5. As can be seen from the table the reported results of the group of the present methodology significantly outperform the other two groups, although the previous studies used socio-economic factors over mid-term, in term of correlation coefficient and three statistical criteria to check the error between observed and predicted water consumption. Accordingly, the comparison of the findings with those of the other studies confirms the present methodology to forecast municipal water demand under climate change for the long term.

The significant drawbacks of previous approaches are that these works have not dealt with SSA to remove trend, seasonal factors and noise. In addition, these studies suffer from unsystematic techniques to choose the parameters of the ANN model.

Table 5.5: The details of the compare results of present methodology and previous work

No.	Author	Method	Data Preprocessing	Data set	R	MSE	RMSE	MAE
1	Sebri (2013)	ANN	DETDES	Trimester, 1983-2002	-	-	1,741.12	1,467.68
2	Behboudian et al. (2014)	ANN	Stationary chain	Monthly, 1997-2008	0.92	0.03	-	-
3	Our research study	The methodology present in Ch.3		Monthly, 1980-2010	0.96	$6.3911\ 10^{-4}$	0.0253	0.0201

5.3. Simulation of Future Climate Factors

5.3.1. LARS-WG model Calibration and Validation

This section relates to the second column in figure 3.1: "Statistical downscaling model". Historical daily climate variables data over the period 1980-2010 (31 years) were employed for calibration and validation of the LARS-WG model for the selected area. Two statistical criteria tests and graphics comparisons between observed and synthetic weather data generated by LARS-WG model were adopted for maximum temperature (Tmax), rainfall (Rain) and solar radiation (Radi) to assess how well the model performs.

For the two statistical criteria tests, the Kolmogorov-Smirnov (K-S) test was performed to test the equality of the distributions of daily climate factors calculated from measured data and simulated data. In addition, a p-value was utilised for acceptance or rejection of the hypothesis that both sets of data (i.e., observed and simulated) could have come from the same distribution. A very high p-value and a corresponding low K-S value indicate that the simulated climate is likely to be the same as the measured climate; hence must be accepted (Semenov et al., 2013). Semenov et al. (2013) recommended that a p-value of 0.01 should be employed as the significance level of acceptance instead of 0.05, which was applied in most statistics to increase the accuracy.

Table 5.4 presents the results of the statistical analysis for model performance in simulating the Tmax, Rain and Radi observed from the data. It can be seen from the assessment results in the table that the performance of the model in simulating the distribution of the daily Tmax, Rain and Radi is perfect.

Table 5.6: K-S and P-value tests for daily Tmax, Rain and Radi distributions

	Daily Tmax distributions		**Daily Rain distributions**		**Daily Radi distributions**	
Month	K-S	P-Value	K-S	P-Value	K-S	P-Value
J	0.106	0.9989	0.056	1	0.044	1
F	0.105	0.9991	0.016	1	0.087	1
M	0.053	1	0.042	1	0.044	1
A	0.105	0.9991	0.031	1	0.087	1
M	0.105	0.9991	0.081	1	0.087	1
J	0.106	0.9989	0.015	1	0.087	1
J	0.105	0.9991	0.039	1	0.044	1
A	0.053	1	0.056	1	0.087	1
S	0.053	1	0.011	1	0.044	1
O	0.106	0.9989	0.041	1	0.044	1
N	0.053	1	0.056	1	0.087	1
D	0.106	0.9989	0.056	1	0.044	1

In addition for statistical parameters, which contain mean and standard deviation for observed and synthetic data as shown in Figure 5.9. It can be seen in the figure that the model is able to accurately fit the three variables (Tmax, Rain and Radi), especially maximum temperature and solar radiation.

The LARS-WG model reveals an adequate performance in replicating the observed Tmax, Rain and Radi in this study, which obviously emphasises that the model is appropriate for this region. Similar reliable performances in generating climate factors have been found for the LARS-WG model in various locations around the world, as

mentioned in Osman et al. (2017). Accordingly, confidence was increased to employ the downscaling model in this study.

The model is ready to simulate future daily data for Tmax, Rain and Radi using seven GCMs and three IPCC scenarios (B1, A1B and A2) over three periods (2011-2030, 2046-2065 and 2080-2099) as in the next section.

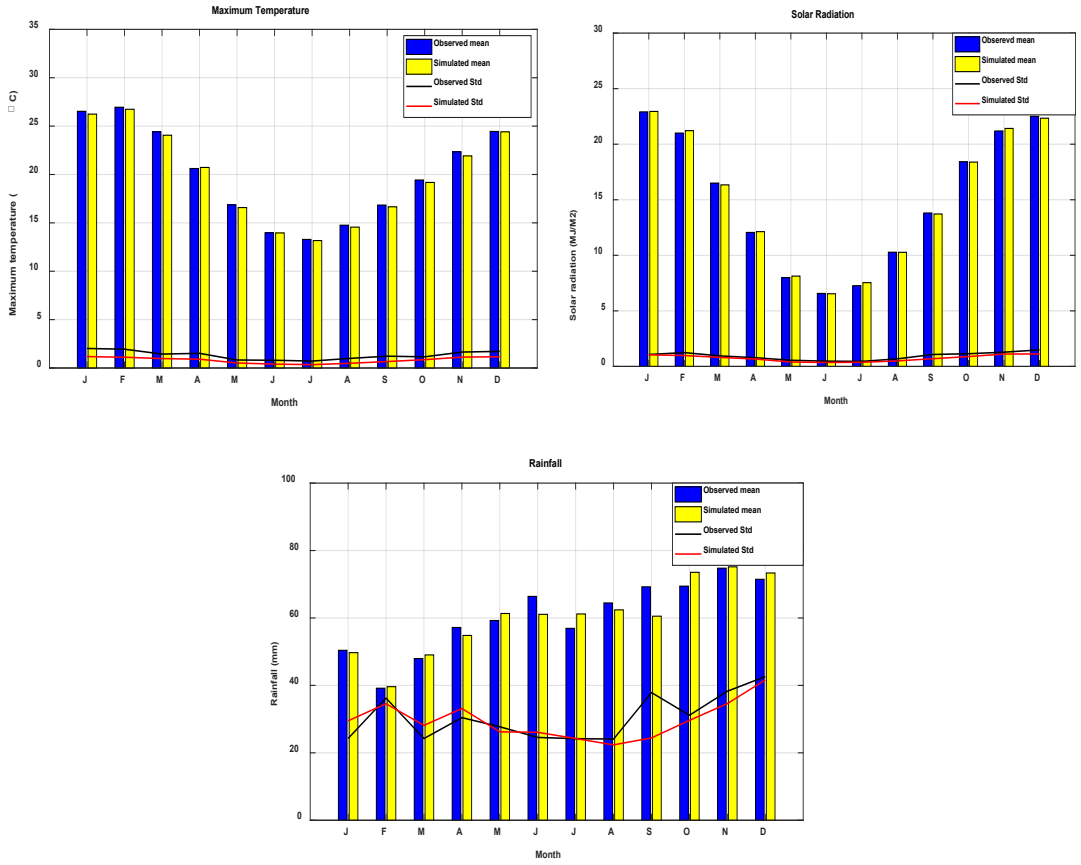

Figure 5-9: Calibration and validation of the LARS-WG model by using measured and simulated mean and standard deviation of maximum temperature, solar radiation and rainfall at study area (1980-2010)

5.3.2. Projection of Future Climate Factors

After calibration and validation of the model, the LARS-WG model was employed to simulate future daily data for Tmax, Rain and Radi over three periods 2011-2030, 2046-2065 and 2080-2099, depending on the A1B, B1 and A2 scenarios generated from seven GCMs (Table 3.1).

The results of the yearly maximum temperature, rainfall and solar radiation forecasting data for all GCMs and their ensemble mean under A1B scenario over 2011-2030 period are plotted in Figure 5.10. For maximum temperature, the figure shows that all the GCMs' projected data over the period 2011-2030, in general, are closer to each other. While the INCM3 model has approximately the same pattern but it is not close to them. In addition, all GCMs models exhibit anomalous behaviour in the first quarter of the period. The limitation of ensemble is projected between around 19.7-20.6°C (i.e. it means the maximum and minimum values over the 20 years).

The results for the rainfall, present that all GCMs show approximately the same pattern compare with INCM3 model, which has considerable variation. In addition, the GCMs exhibit anomalous behaviour in the first quarter of the period. The limitation of ensemble is projected to be approximately 47-75mm. The solar radiation results present that all the GCMs' projected data over the chosen period except MPEH5 and INCM3 models, in general, have little variation except some years such as years (3^{rd}, 7^{th}, 10^{th} and 18^{th}). The MPEH5 model has the same pattern but it is not close to others primarily in the first half of period while, the INCM3 model has an irregular pattern along the period. The limitation of ensemble is projected around 14.7-15.7MJ/m^2. The results of yearly data for all climate factors under A1B, B1 and A2 scenarios and over three future periods are shown in Appendix 5-B.

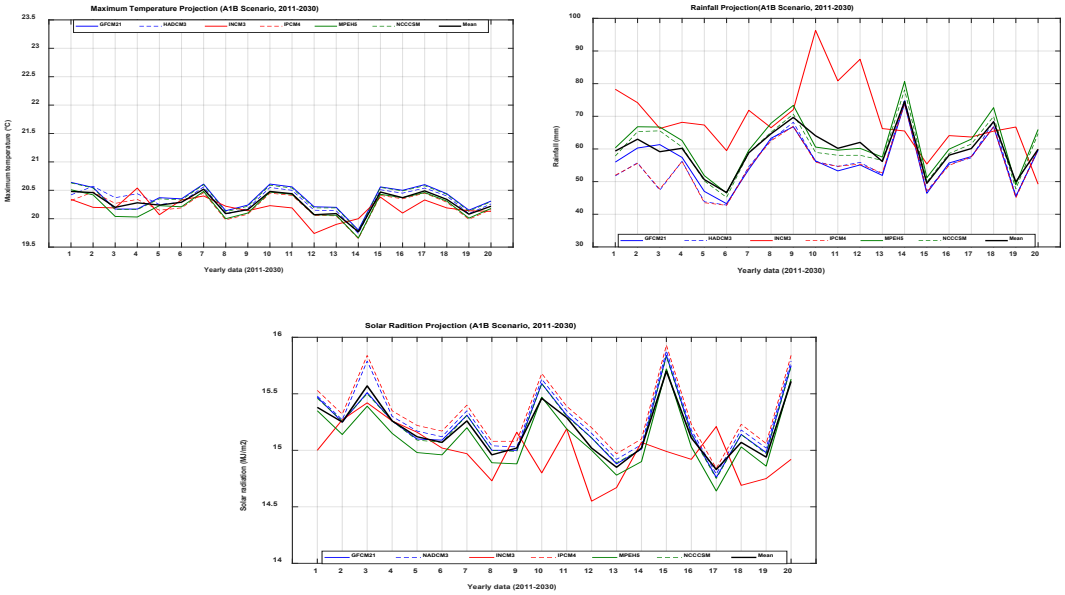

Figure 5-10: Projected yearly Tmax, Rain and Radi data under A1B scenario and over 2011-2030 period

The scale of the future climate variables over three periods for all three scenarios then changes from daily to monthly data (i.e. the scale of water prediction model is monthly). The monthly average mean with confidence interval level, 0.95% for A1B scenario, for all climate factors and over the three periods was drawn to increase the knowledge about how the climate variables will change in the future, as shown in Figure 5.11. The figure shows that Tmax is expected to increase as we go into the future, e.g. the values for the month of July, Tmax= 13.7, 14.3 and 14.9°C for the 1st, 2nd and 3rd period, respectively. Radi is also expected to increase over the three periods, e.g. for the month of December, Radi= 22.4, 22.7 and 23MJ/m^2 for the 1st, 2nd and 3rd period, respectively; and the confidence interval level was excellent for both factors over all periods. In contrast, Rain is expected to decrease, e.g. the values for the month of December, Rain= 85, 56.6 and 42.5mm for the 1st, 2nd and 3rd period, respectively, and the confidence interval level is approximately the same for all periods. All these show LARS-WG capabilities of simulating future climate variables very accurately. The figures regarding B1 and A2 scenarios are displayed in Appendix 5-C.

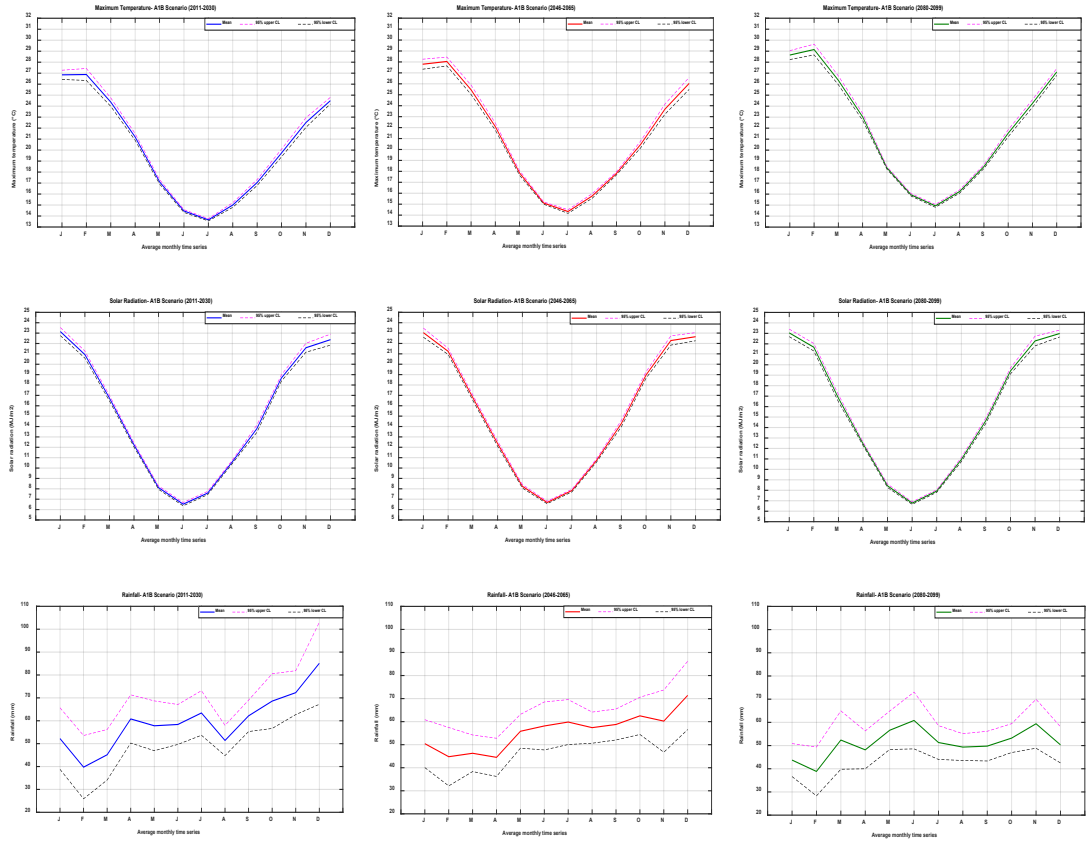

Figure 5-11: The average monthly mean for three simulated climate factors of A1B scenario over the future periods (2011-2030, 2046-265 and 2080-2099)

Figure 5.12 shows the average monthly maximum temperature has the same pattern under B1 scenario for 2011-2030, 2046-2065 and 2080-2099 periods, but it has variation in magnitude of degrees Celsius from one period to another. Tmax is likely to rise gradually from the first period to the last one, e.g. the values for the month of July, Tmax= 13.5, 14.3 and 14.5°C for the 1st, 2nd and 3rd period, respectively. The probable effects of climate change on future maximum temperature under A1B and A2 scenarios are similar to those of the B1 scenario for all future periods. However, the value of average monthly maximum temperature is different for each period under B1, A1B and A2 scenarios depending on the scenarios' assumptions. Accordingly, for the month of July, the expected difference between 1st and 3rd period is 1, 1.2 and 1.8°C for B1, A1B and A2 scenarios respectively. In addition, the average monthly

maximum temperature is likely to reach a peak at 15.6°C in the 3rd period under the A2 scenario.

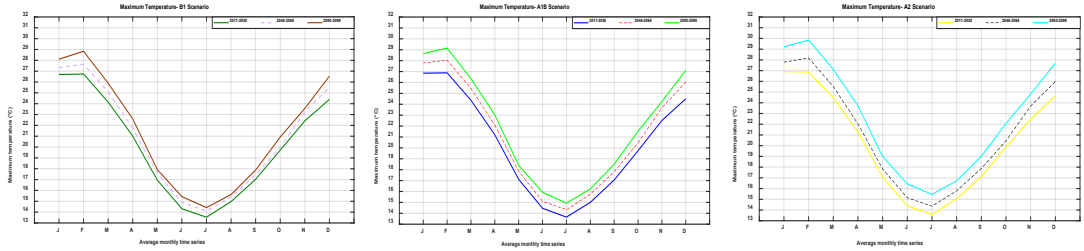

Figure 5-12: The average monthly maximum temperature under B1, A1B and A2 scenarios over three future periods

The average monthly values of solar radiation under B1, A1B and A2 scenarios for the three future periods are presented in Figure 5.13: In general, the results of B1 scenario are similar to those projected by A1B and A2 scenarios. In addition, there is a little variation among the three periods for any month regarding all IPCC scenarios. June tends to have less solar radiation, while January has a higher value. Also, solar radiation was expected to reach a peak in January under A2 scenario for the first period about 23.3MJ/m^2.

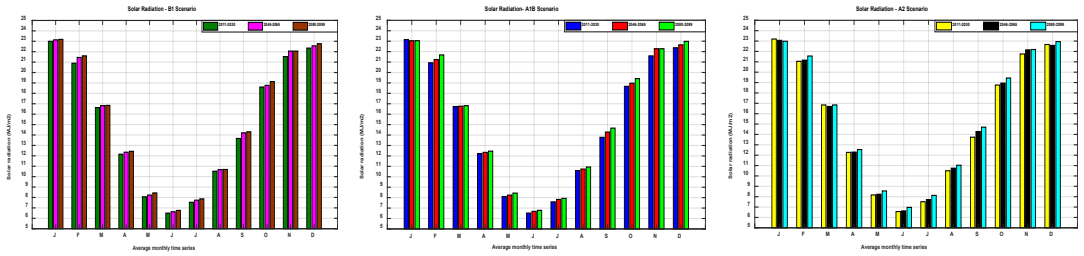

Figure 5-13: The average monthly of solar radiation under B1, A1B and A2 scenarios over three future periods

Figure 5.14 displays the average monthly data of rainfall under B1, A1B and A2 scenarios for 2011-2030, 2046-2065 and 2080-2099 periods. What can be clearly seen in this figure is the expected decline in rainfall amount as we go into the future (i.e. 1st period has rainfall more than 2nd and 3rd periods) for all three scenarios. The range of precipitation is likely to fall between (38 and 80) mm, (39 and 85) mm and

(35 and 78) mm for B1, A1B and A2 scenarios respectively. Therefore, the A2 scenario is projected to be a drier scenario compared with the B1 and A1B scenarios. Also, the month of February is probably going to be driest month compare with other months of the year under all IPCC scenarios.

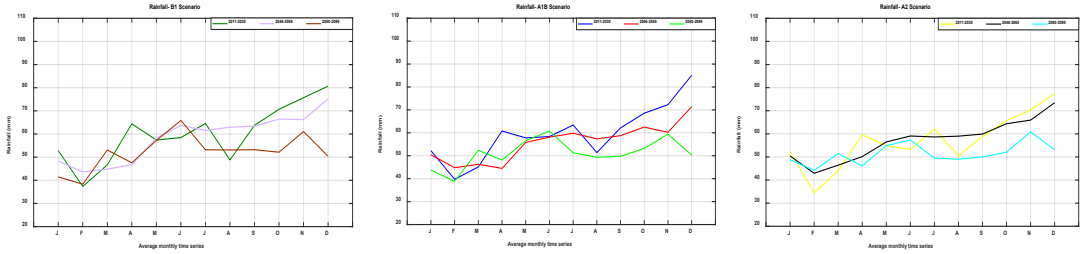

Figure 5-14: The average monthly of rainfall under B1, A1B and A2 scenarios and over three future periods

Monthly data of simulated climate factors for each period will be presented and compared to provide a clear scientific view about the impact of climate change in the future in two phases, which are expected time series and its stochastic signal time series.

5.3.2.1. Expected Time Series

The expected climate variables time series will be divided into three groups based on the periods 2011-2030, 2046-2065 and 2080-2099. In any period, each expected climate factor under a specific IPCC scenario will be compared with the two additional IPCC scenarios. Four months were chosen during the year to display the projected climate factor in each period. These months are January, April, July and October to represent summer, autumn, winter and spring seasons respectively (in the southern hemisphere). The figures regarding the rest of the months are displayed in Appendix 5-D.

A) First Period 2011-2030

The maximum temperature for the 1st period (20 years) for four months is shown in Figure 5.15. In general, January has the higher expected value of Tmax, July the lower and April more than October. In addition, the variation in the value of Tmax among B1, A1B and A2 scenarios for each month is no more than 1°C and July is likely to have less variation. In approximately half of these time series for each month, the expected Tmax value under A2 scenario exceeds other scenarios. The values of Tmax under B1, A1B and A2 scenarios fall between (25.8 and 28.5) °C, (19.5 and 22.2) °C, (13 to 14.1) °C and (18.7 and 21.2)°C for (January, summer), (April, autumn), (July, winter) and (October, spring) respectively.

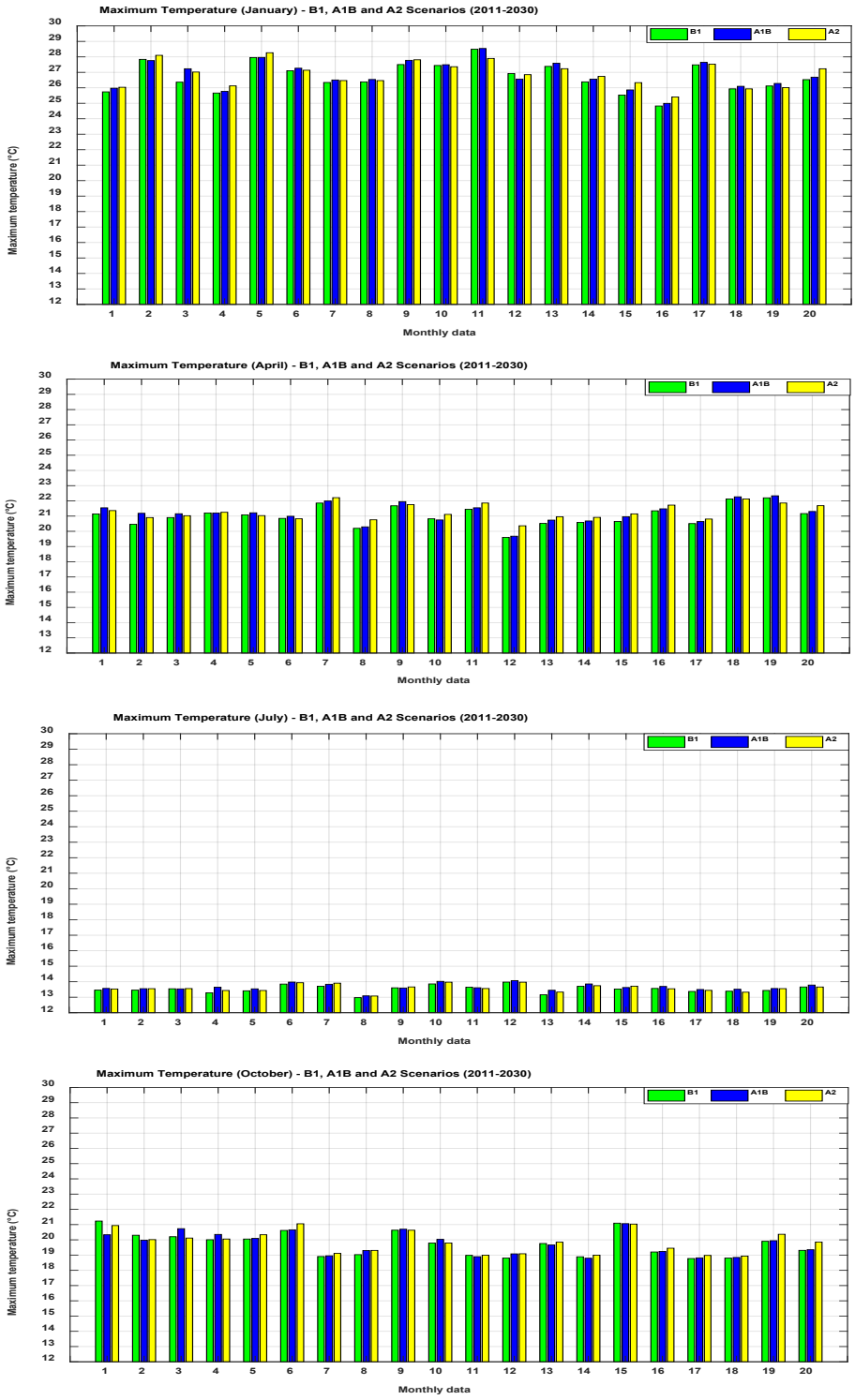

Figure 5-15: The maximum temperature projection under B1, A1B and A2 scenarios for the future period (2011-2030)

The rainfall time series is sorted based on a monthly basis and presented in Figure 5.16. It can be seen that projection of precipitation under various scenarios shares a

number of key features such as rainfall distributed over the year, there is no trend over these months (rainfall fluctuated).

In addition, there is little variation among the value of rainfall under B1, A1B and A2 scenarios for each month except some anomalous months. The range of rainfall is (8-142) mm, (30-123) mm, (32-115) mm and (23-108) mm for January, April, July and October months respectively.

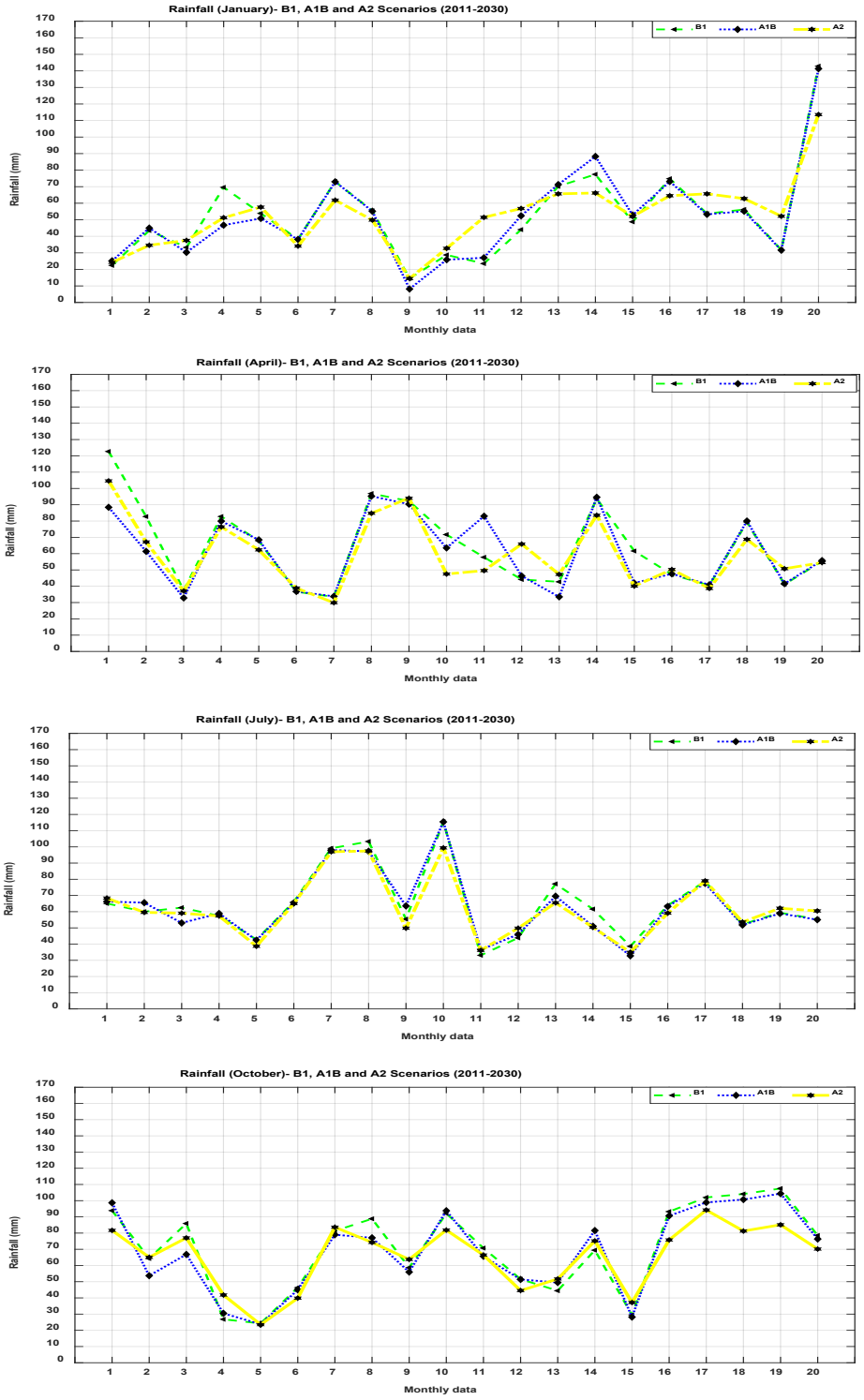

Figure 5-16: The rainfall projection under B1, A1B and A2 scenarios for the future period (2011-2030)

Figure 5.17 shows the probable solar radiation for four months representing the seasons over the year for the first period. The solar radiation has the same distribution of maximum temperature except for its magnitude in (October, spring) more than in

(April, autumn). The limitation for projected Radi is 21-24.3MJ/m^2, 11.2-13.1MJ/m^2, 7-8.5MJ/m^2 and 17.5-19.6MJ/m^2 for January, April, July and October respectively.

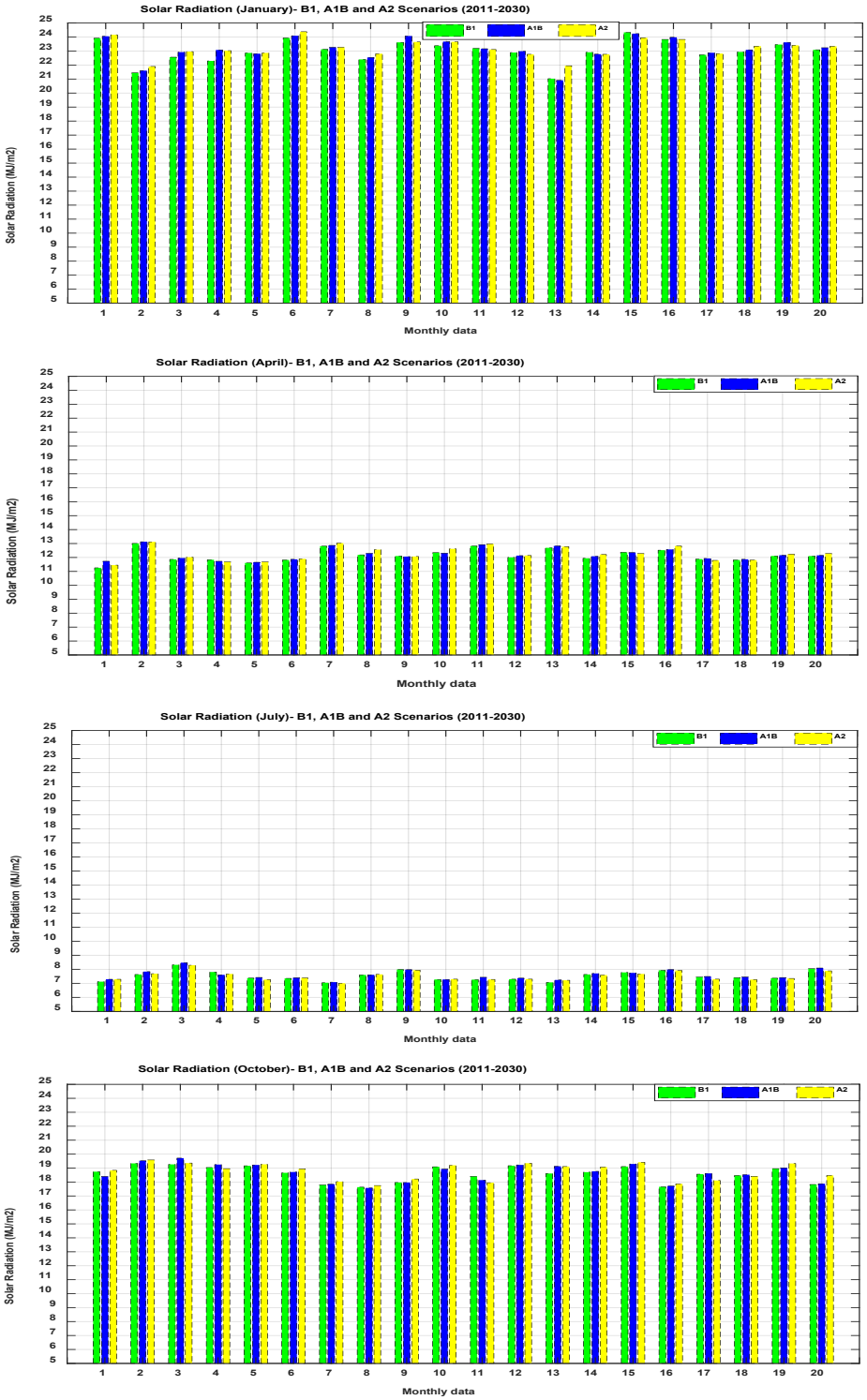

Figure 5-17: The solar radiation projection under B1, A1B and A2 scenarios for the future period (2011-2030)

B) Second period 2046-2065

The maximum temperature for the 2nd period (20 years) for four months is shown in Figure 5.18. The expected monthly results of Tmax are similar to those reported in the first period regarding the pattern and the variation in the value of Tmax among B1, A1B and A2 scenarios for each month, but differ in values. In addition, in approximately half of these time series for each month, the expected Tmax value under A2 scenario exceeds other scenarios. The values of Tmax under B1, A1B and A2 scenarios fall between (25.2 and 30) °C, (20.2 and 23.4) °C, (13.3 and 14.9) °C and (18.2 and 21.5) °C for January, (summer), April, (autumn), July, (winter) and October, (spring) respectively.

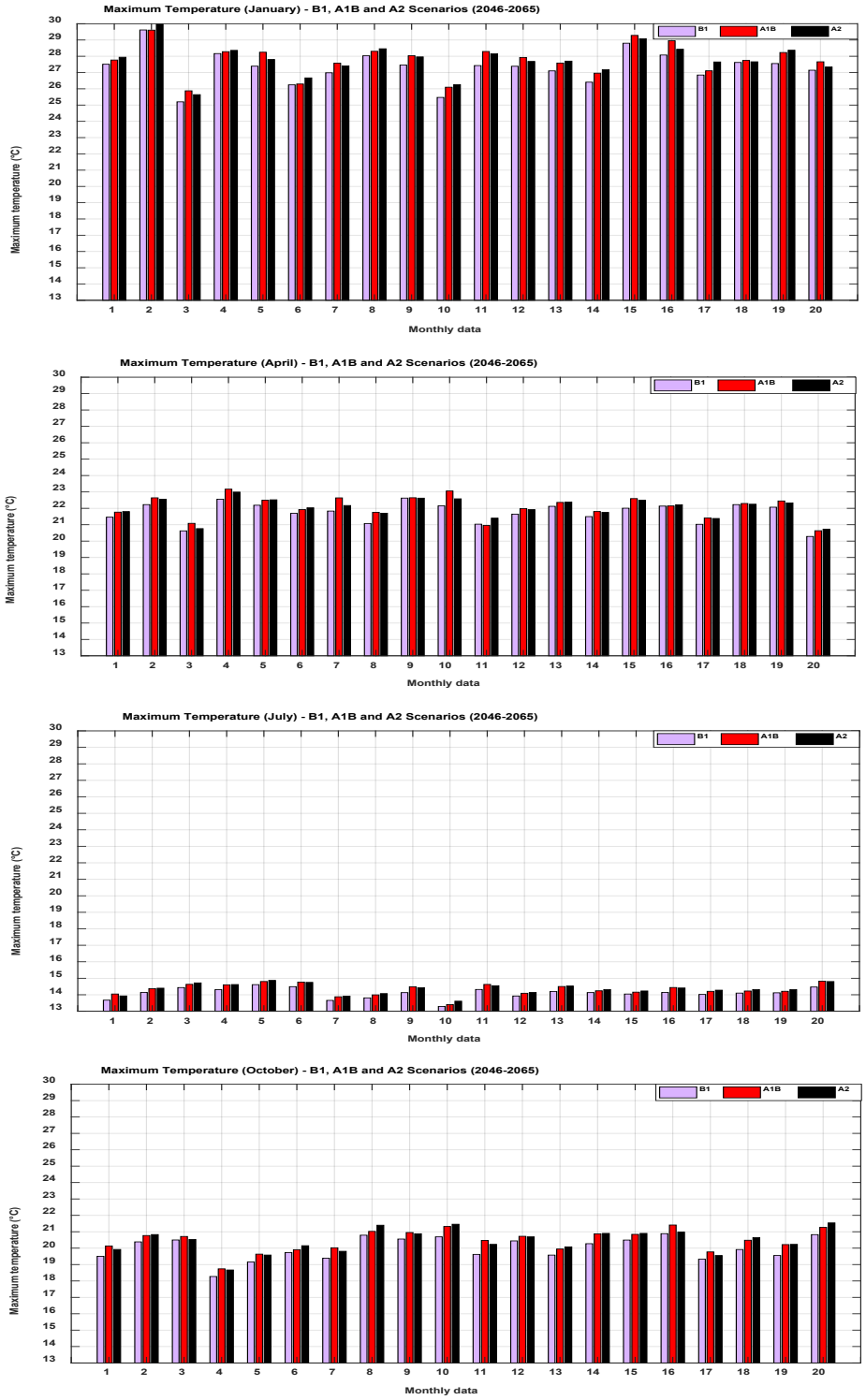

Figure 5-18: The maximum temperature projection under B1, A1B and A2 scenarios for the future period (2046-2065)

Rainfall time series for the three scenarios are presented in Figure 5.19. What is interesting about the data in this figure is that all months are wet over the year. It can be seen that the expected rainfall fluctuates between all IPCC scenarios during the

year. The figure shows that there has been a slight increase in the trend of precipitation for January and July and no clear direction for other months. The range of rainfall is 15-106mm, 8-104mm, 30-128mm and 28-94mm for January, April, July and October respectively. Accordingly, a higher percentage of precipitation is likely happen in winter and a lower ratio in autumn.

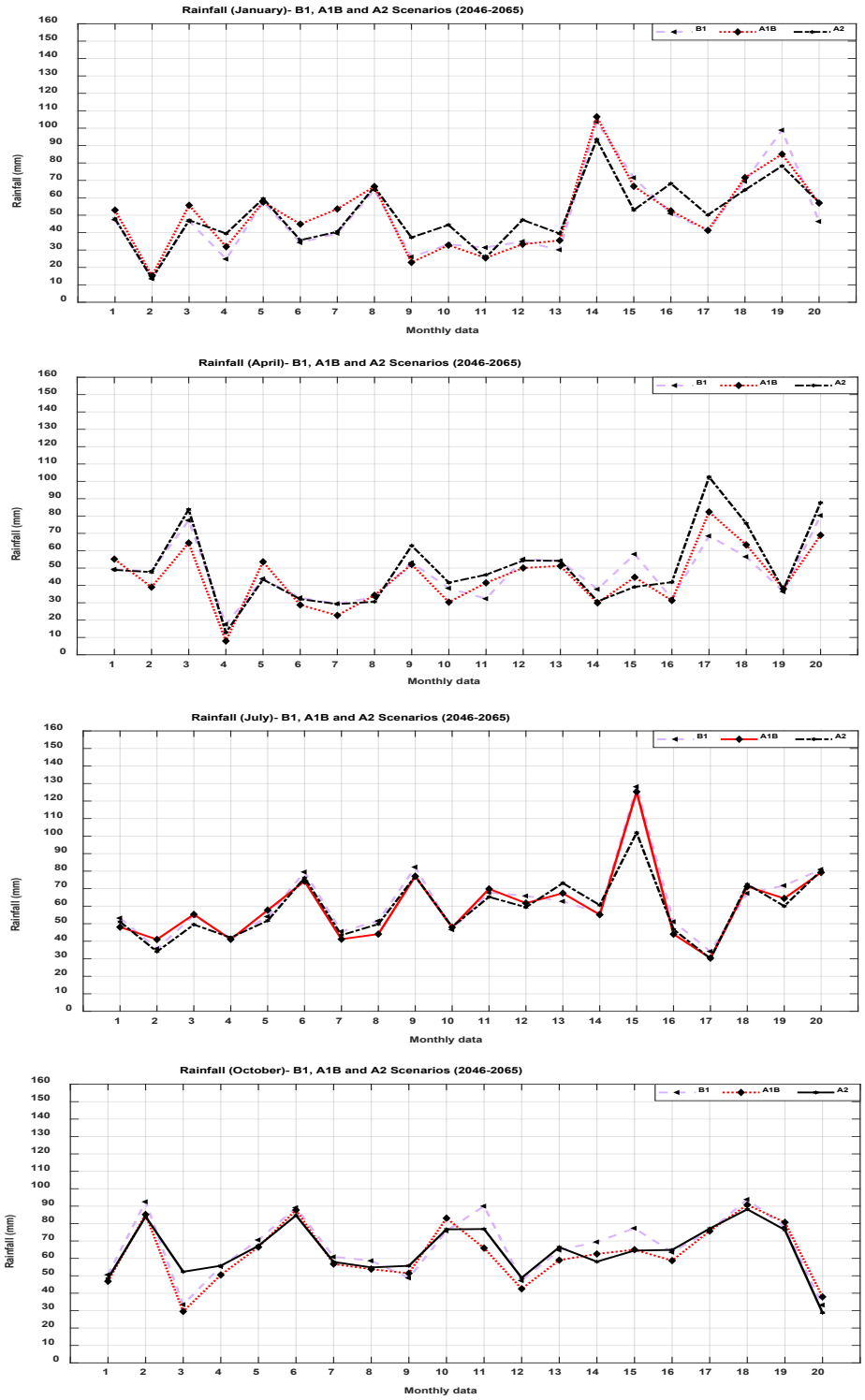

Figure 5-19: The rainfall projection under B1, A1B and A2 scenarios for the future period (2046-2065)

Figure 5.20 displays the probable monthly solar radiation data for the second period under three various IPCC scenarios. In general, the data have a similar pattern to those in the first period, and there is no significant difference in values over four months.

The distribution of data are 21-24.5MJ/m^2, 11-13.4MJ/m^2, 7.2-8.3MJ/m^2 and 17.5-20.2 MJ/m^2 for January, April, July and October respectively.

Figure 5-20: The solar radiation projection under B1, A1B and A2 scenarios for the future period (2046-2065)

C) Third Period 2080-2099

Figure 5.21 shows the projected monthly maximum temperature data for the third period under B1, A1B and A2 scenarios. The pattern of Tmax is similar to the Tmax in the first and second periods but has some differences. These differences include the variation in the value of Tmax among B1, A1B and A2 scenarios for each month up to approximate 2°C and July is likely to have less variation. In addition, look at the figure it realised that the A2 scenario in common has the highest values in all the seasons. The values of Tmax under B1, A1B and A2 scenarios fall between (26.3 and 31.5) °C, (20.3 and 24.6) °C, (13.7 and 16) °C and (20 and 24.6)°C for January, April, July and October respectively.

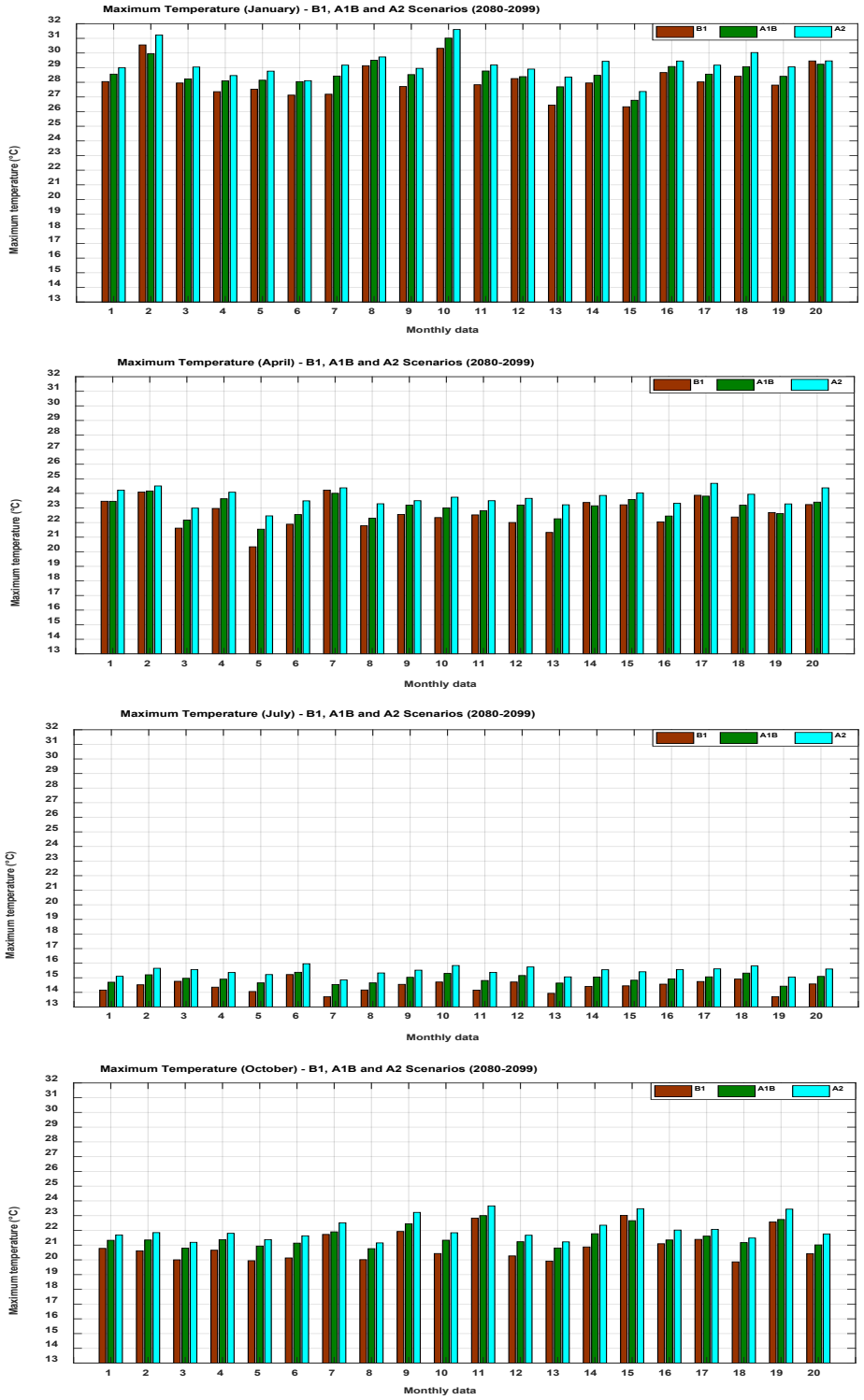

Figure 5-21: The maximum temperature projection under B1, A1B and A2 scenarios for the future period (2080-2099)

Projected rainfall time series for the B1, A1B and A2 scenarios over the 2080-2099 period are presented in Figure 5.22. Closer inspection of the figure shows that there is no clear direction to an increase or decrease in rainfall for all months. The expected

peak value will happen under the A2 scenario in January while, it occurs in July under the B1 scenario. In the same context,there is no dominant scenario for other months, and in October, the time series for all scenarios are close to each other.

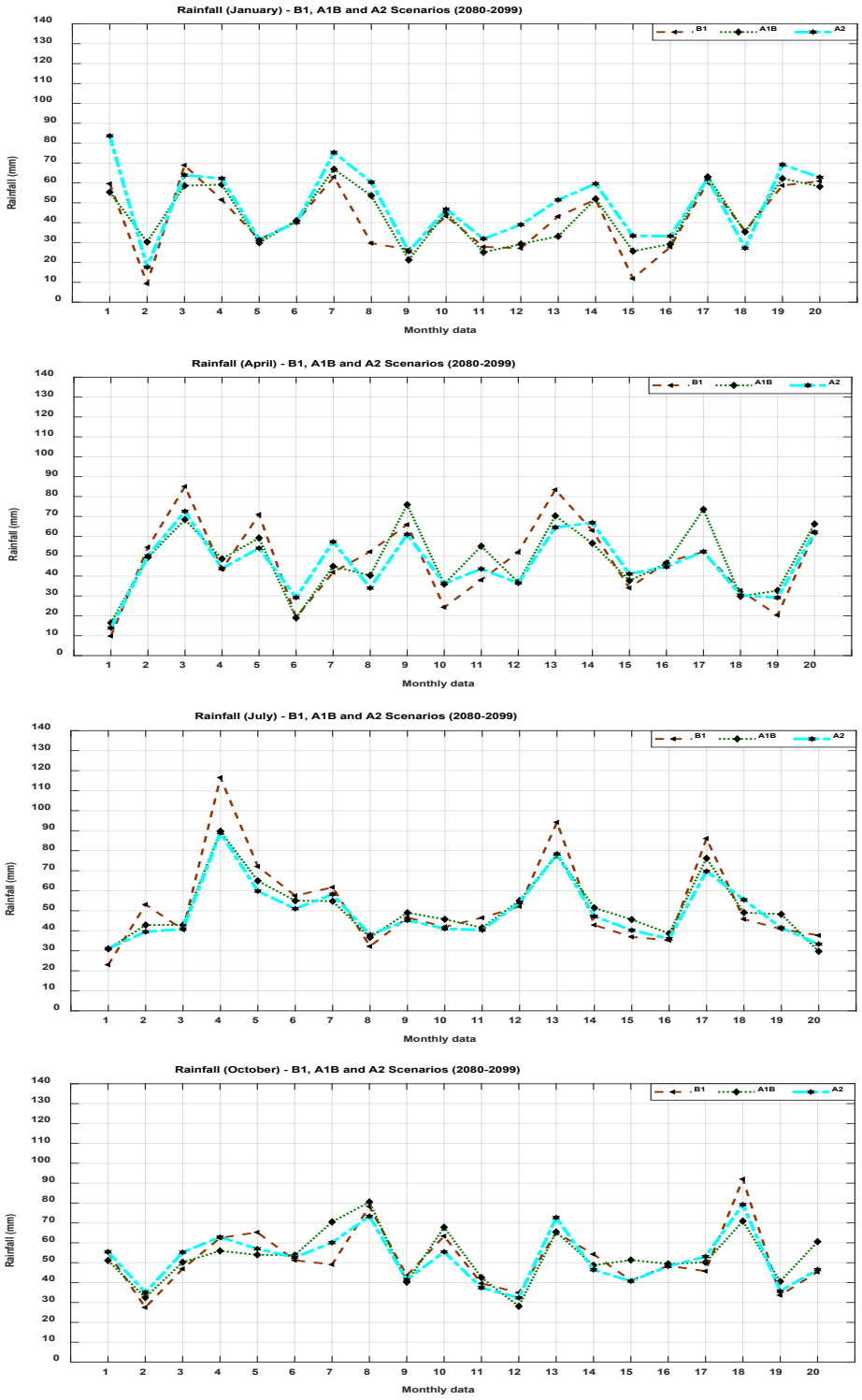

Figure 5-22: The rainfall projection under B1, A1B and A2 scenarios for the future period (2080-2099)

Figure 5.23 displays the probable monthly solar radiation data for the third period under three various IPCC scenarios. In general, data have a similar pattern to those in the first and second periods, and there is no significant difference in values over four months. The distribution of the data are 21.6-24.7MJ/m^2, 11.9-13.1MJ/m^2, 7.2-8.5MJ/m^2 and 18.1-20.5MJ/m^2 MJ/m^2 for January, April, July and October respectively.

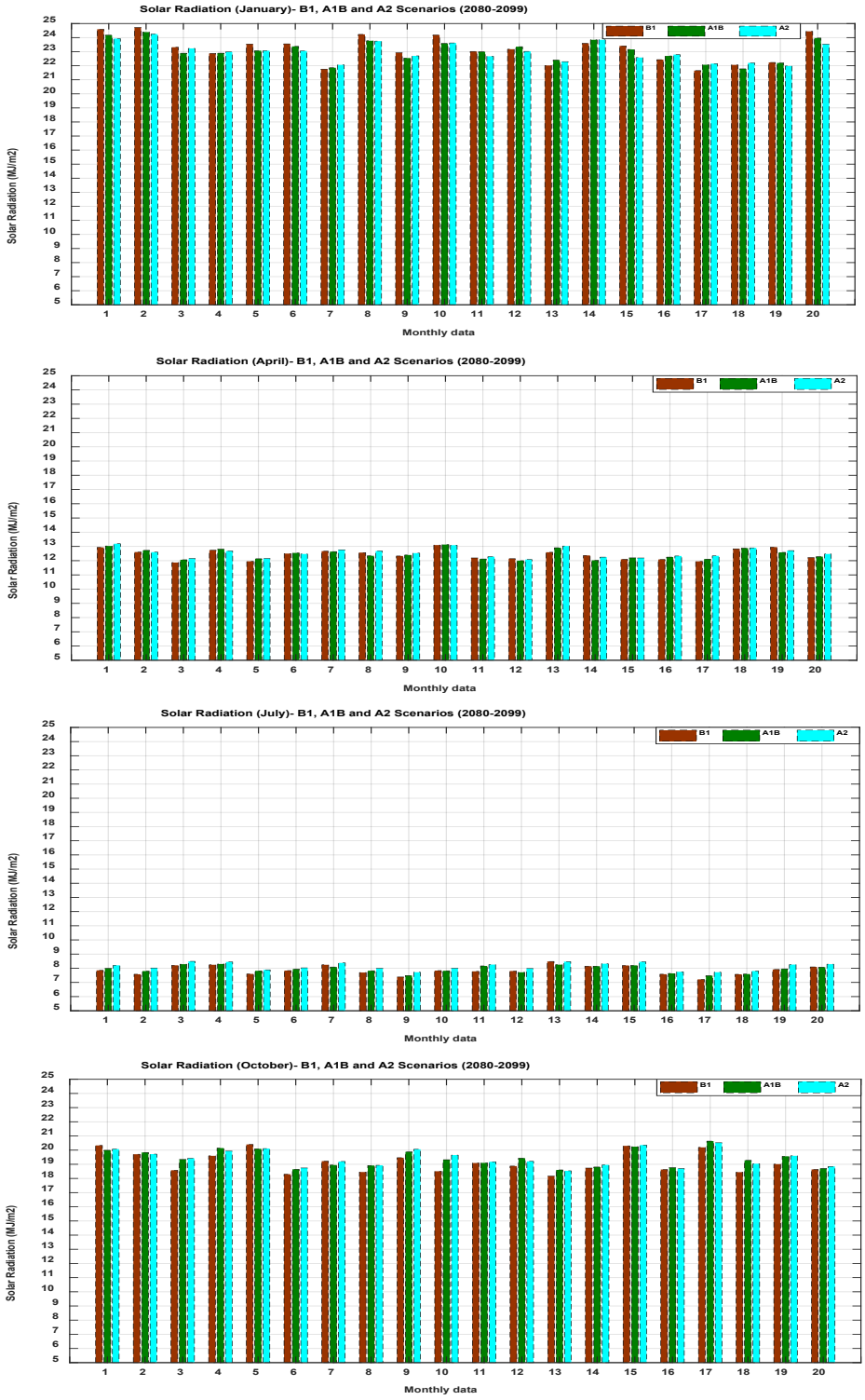

Figure 5-23: The solar radiation projection under B1, A1B and A2 scenarios for the future period (2080-2099)

These monthly time series of all climate factors under B1, A1B and A2 scenarios and over three future periods were normalised and decomposed by the SSA technique to

detect their stochastic signals. The monthly stochastic signals will be used in the ANN model to forecast future municipal water demand over three periods.

5.3.2.2. Stochastic Time Series

The stochastic signals of the ensemble means for Tmax, Rain and Radi that were simulated from the three IPCC scenarios and the seven GCMs were considered. The differences between the stochastic signals of the ensemble means for B1, A1B and A2 scenarios over all simulated periods and the stochastic signals of the baseline (1980-2010) were plotted, as shown in Figures 5.24, 5.25 and 5.26 respectively.

Figure 5.24 shows that Tmax will rise in general based on the average monthly basis for all months in winter and spring seasons (i.e., 2046-2065 is the hottest period), and it will decrease in summer and autumn. Radi will increase during the months May to September, and it increases even more as the prediction moves into the future. Rain has a non-uniform pattern for the three periods; it will increase for the first period except the months from March to September. For the second period, it will increase except the months May to June. For the third period, it will increase from February to July months and reduce from August to December months. Compared to other periods, the final period has the highest increase, which happens in March, and has the highest decrease, which happens in November.

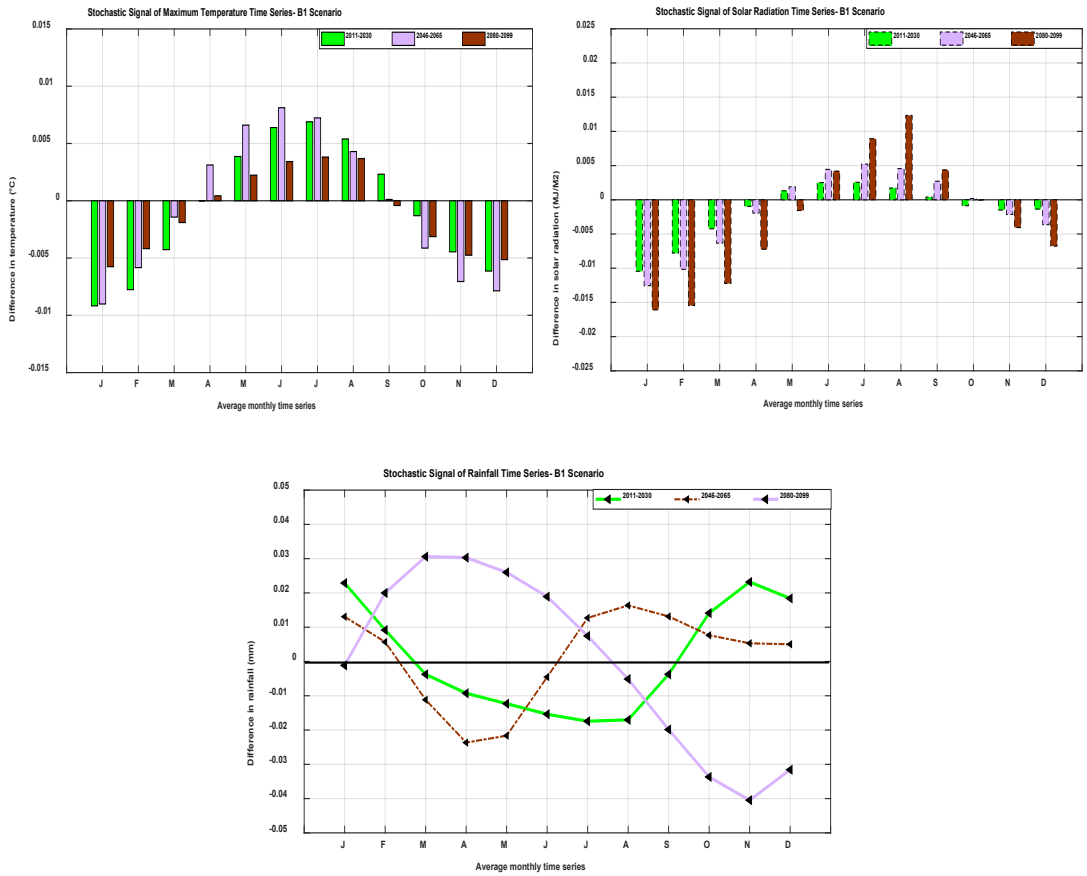

Figure 5-24: The differences in average monthly stochastic signal for three climate factors under B1 scenario between the future periods (2011-2030, 2046-265 and 2080-2099) and the current period (1980-2010)

Figure 5.25 presents that Tmax will increase in general based on the average monthly basis for all months in winter and spring seasons (i.e., 2080-2099 is the hottest period), and it will decrease in summer and autumn. Radi will increase during the months May to October, and it increases even more as the prediction moves into the future. However, Radi will decrease over the rest of the months, and the third period has the highest and lowest signals. Rain has a non-uniform pattern for the three periods; it will increase for the first period except the months from March to September. For the second period, it will decrease except the months August, December and from January to March. For the third period, it will increase for the first six months and reduce for last six months. Compared to the rest of the periods, the final period has the highest

increase, which happens in March, and has the highest decrease, which happens in October.

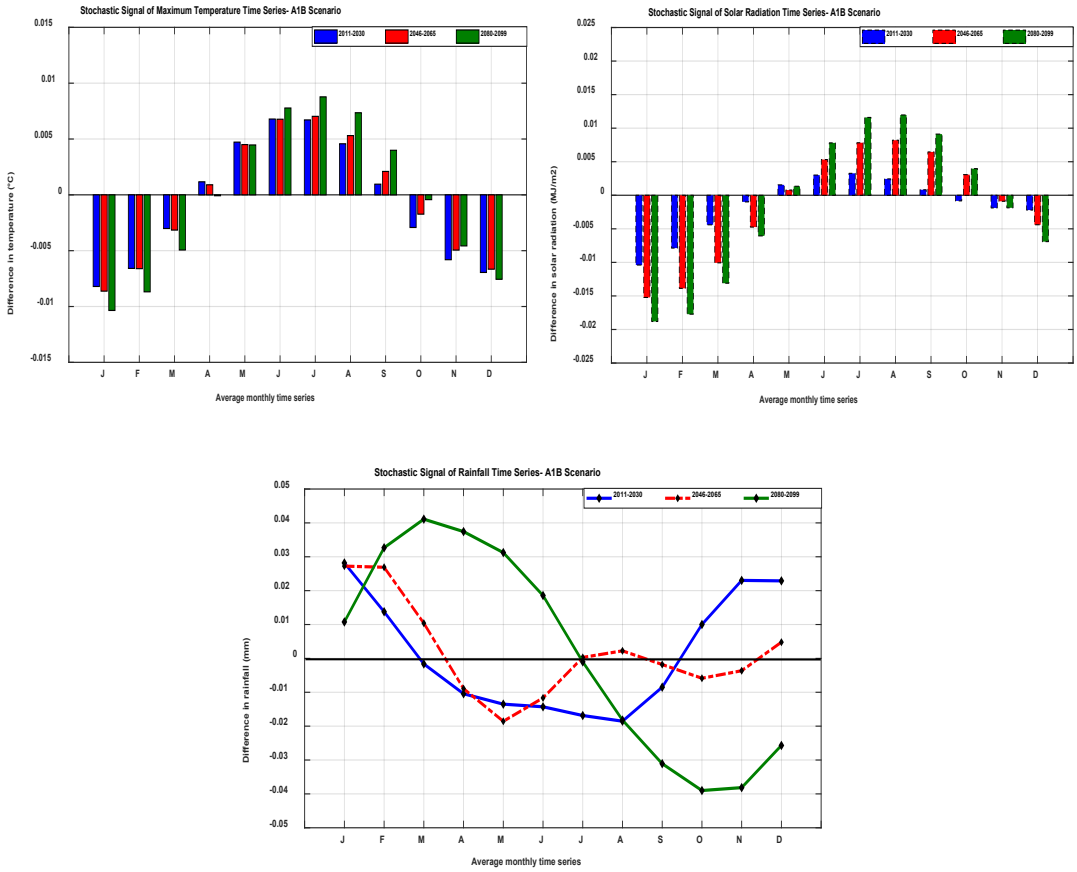

Figure 5-25: The differences in average monthly stochastic signal for three climate factors under A1B scenario between the future periods (2011-2030, 2046-265 and 2080-2099) and the current period (1980-2010)

Figure 5.26 displays that Tmax will increase in general based on the average monthly basis for all months in winter and spring seasons (i.e., 2080-2099 is the hottest period), and it will decrease in summer and autumn. Radi will increase during the months May to October (except some months for the first period), and it increases even more as the prediction moves into the future. However, Radi will decrease over the rest of the months, and the third period has the highest and lowest signals. Rain has a non-uniform pattern for the three periods; it will increase for the first period except the months from April to September. For the second period, it will increase except the months from April to October. For the third period, it will increase for the first six

months and reduce for last six months. Compared to the rest of periods, the final period has the highest increase, which happens in February, and has the highest decrease, which happens in October.

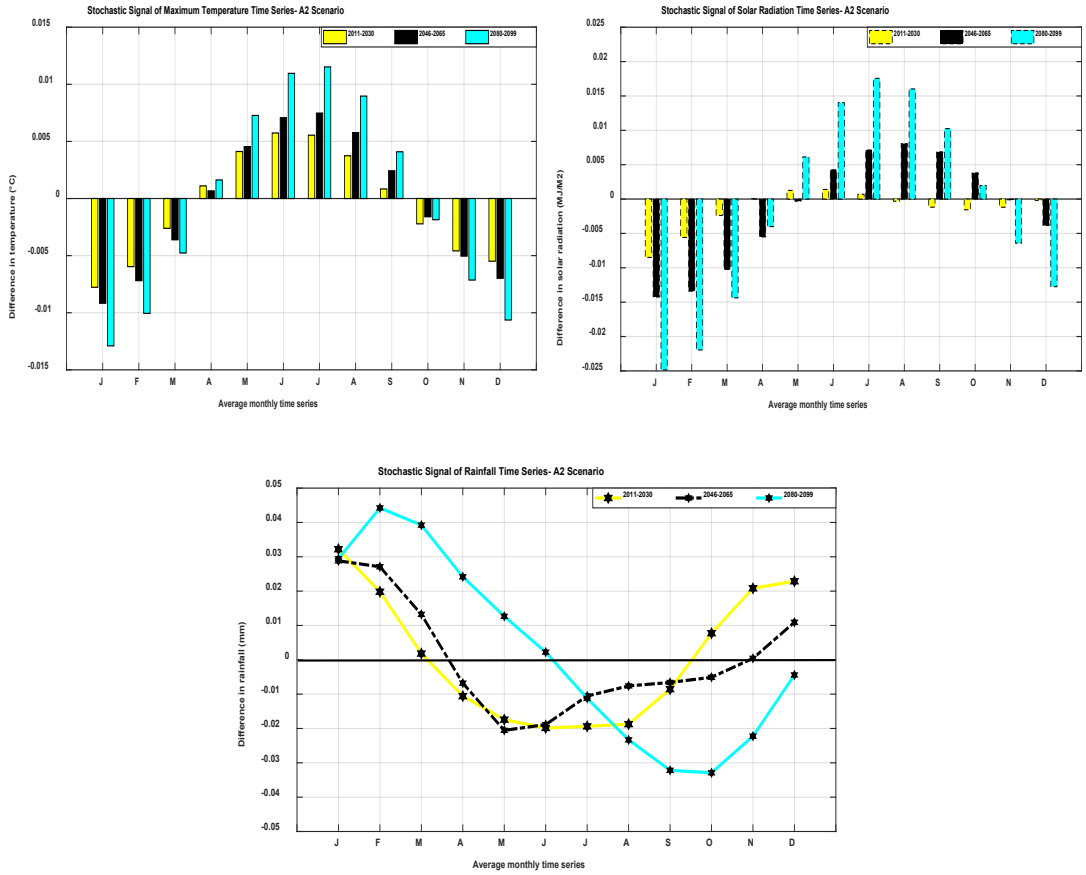

Figure 5-26: The differences in average monthly stochastic signal for three climate factors under A2 scenario between the future periods (2011-2030, 2046-265 and 2080-2099) and the current period (1980-2010)

The differences between the expected stochastic signal of the ensemble means for B1, A1B and A2 scenarios over all simulated periods and the stochastic signals of the baseline (1980-2010) for all climate variables were plotted in the monthly time series. Four months were chosen along the year to display the projected climate factor in each period. These months are January, April, July and October to represent summer, autumn, winter and spring seasons respectively (in the southern hemisphere). The figures regarding the rest of the months are displayed in Appendix 5-E.

A) First Period 2011-2030

The differences in stochastic signal of the maximum temperature under B1, A1B and A2 scenarios for the first period (20 years) for four months is shown in Figure 5.27. The stochastic signals in January will decrease under all IPCC scenarios compared with the baseline period. There is no clear trend for reducing, and B1 scenario has the coldest values over around half of the time series. On another hand, a stochastic signal of Tmax will increase over all time series in July, and B1 scenario represents the hottest scenario over around half of the time series. Stochastic signals of Tmax will fluctuate (i.e. increase and decrease) along with the time series in April and October.

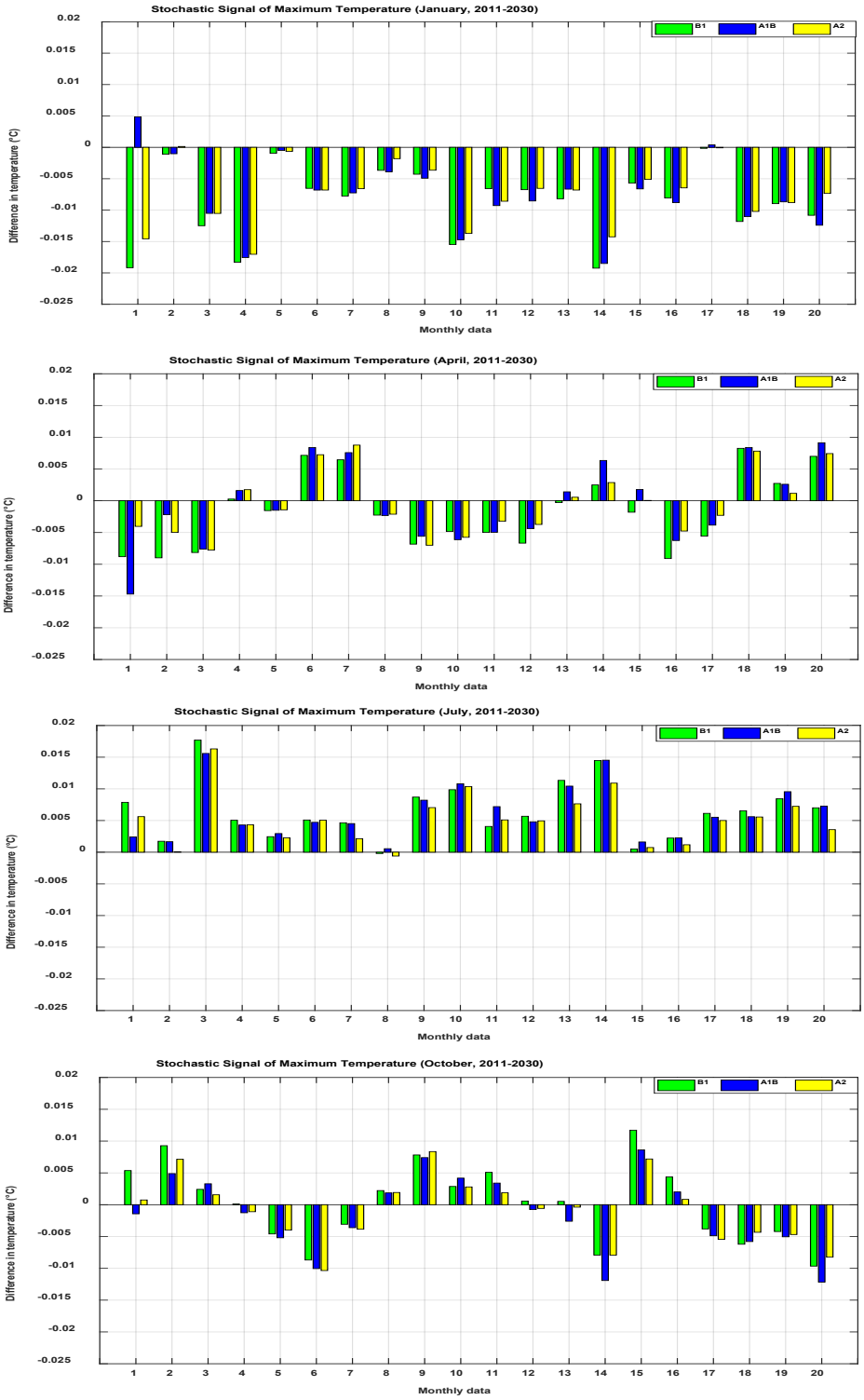

Figure 5-27: Stochastic signals of the maximum temperature projection under B1, A1B and A2 scenarios for the period (2011-2030)

Figure 5.28 shows the differences between the expected stochastic signals of rainfall under three scenarios and the stochastic signals of the 1980-2010 period. Generally, precipitation is likely to increase in summer, decrease in winter and be oscillatory in

spring and autumn seasons and tend to reduce. In addition, all scenarios have the same pattern and are close to each other.

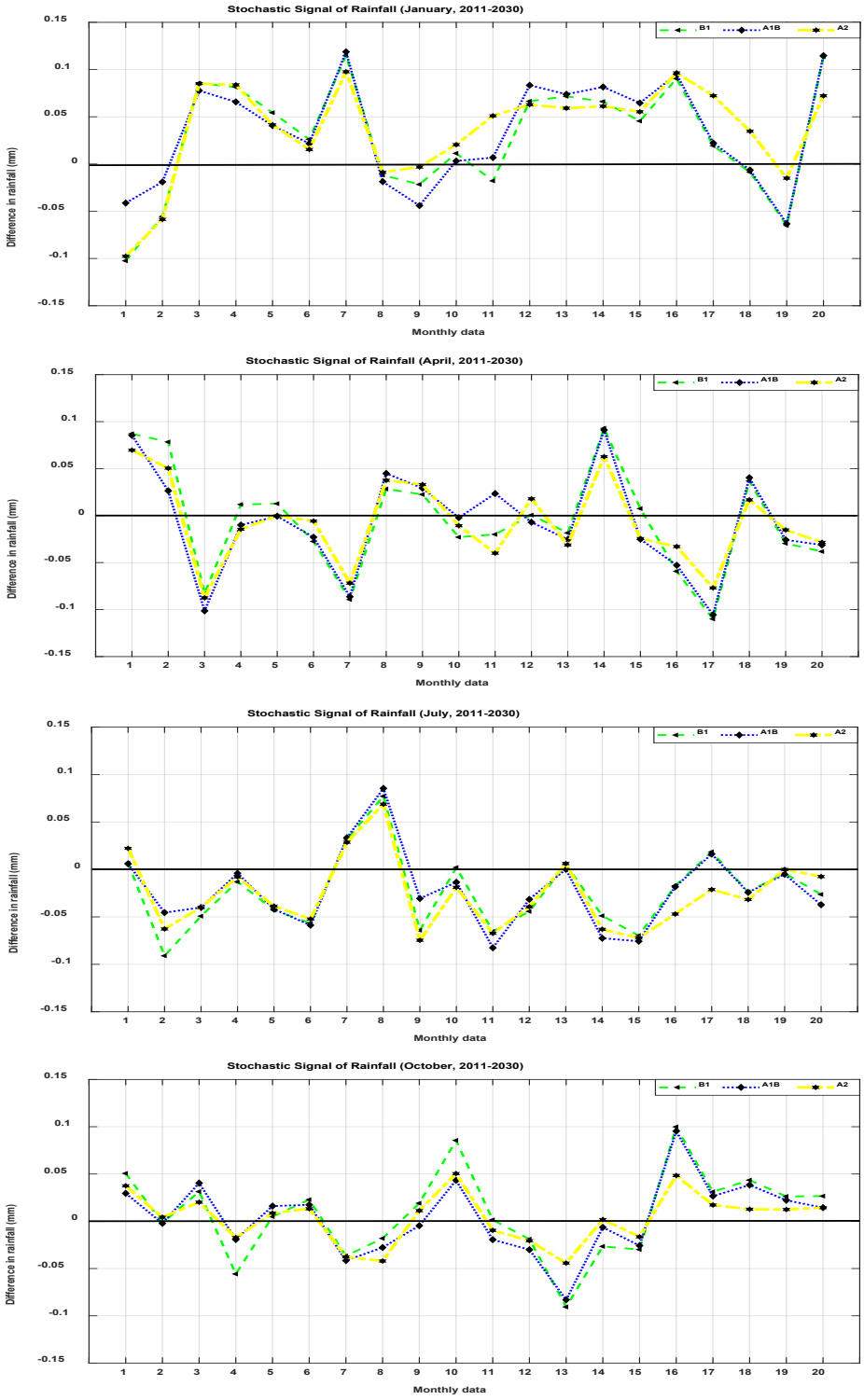

Figure 5-28: Stochastic signals of the rainfall projection under B1, A1B and A2 scenarios for the period (2011-2030)

The expected differences in stochastic signals of the solar radiation are shown in Figure 5.29. It can be seen that solar radiation is likely to reduce in January and the A1B scenario has the lowest values over around half of the time series. In addition, Radi rises in July except for some months in the time series. Moreover, the signal of solar radiation fluctuates along the time series in April and October.

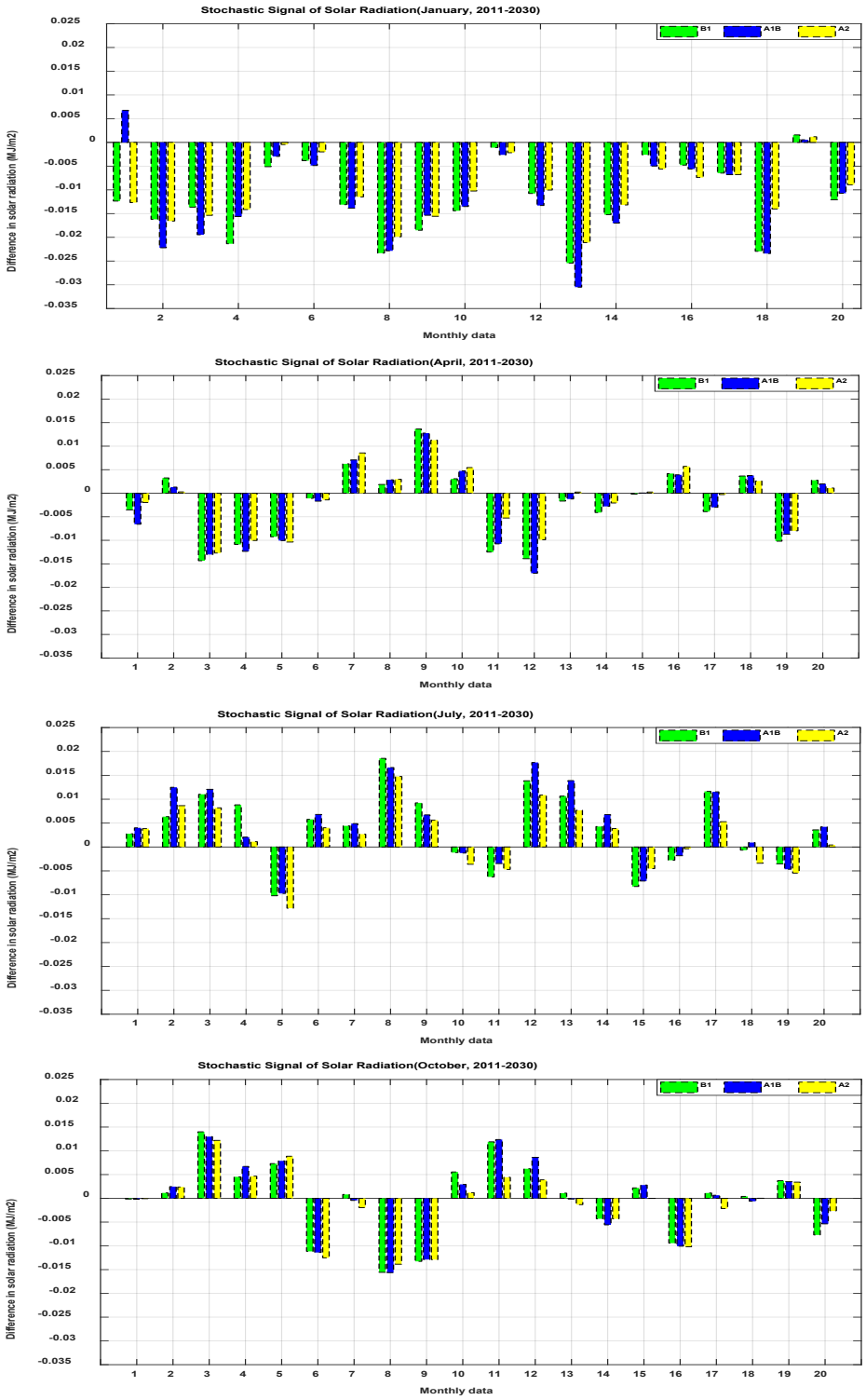

Figure 5-29: Stochastic signals of the solar radiation projection under B1, A1B and A2 scenarios for the period (2011-2030)

B) Second Period 2046-2065

The expected differences between stochastic signals of the maximum temperature under B1, A1B and A2 scenarios for the 2nd period (20 years) and the baseline period

for four months are shown in Figure 5.30. The results of differences are likely to reduce for (January, summer) for B1, A1B and A2 scenarios for 20 years with varying values from one scenario to another and from month to month. The B1 represents the coldest and the A1B the hardest scenario over around half of the time series. The stochastic signal rises in July, (winter) under all IPCC scenarios over the selected period, and the A2 scenario tends to be the hottest one. The signals for April and October are oscillating, but it tends to increase in April and reduce in October.

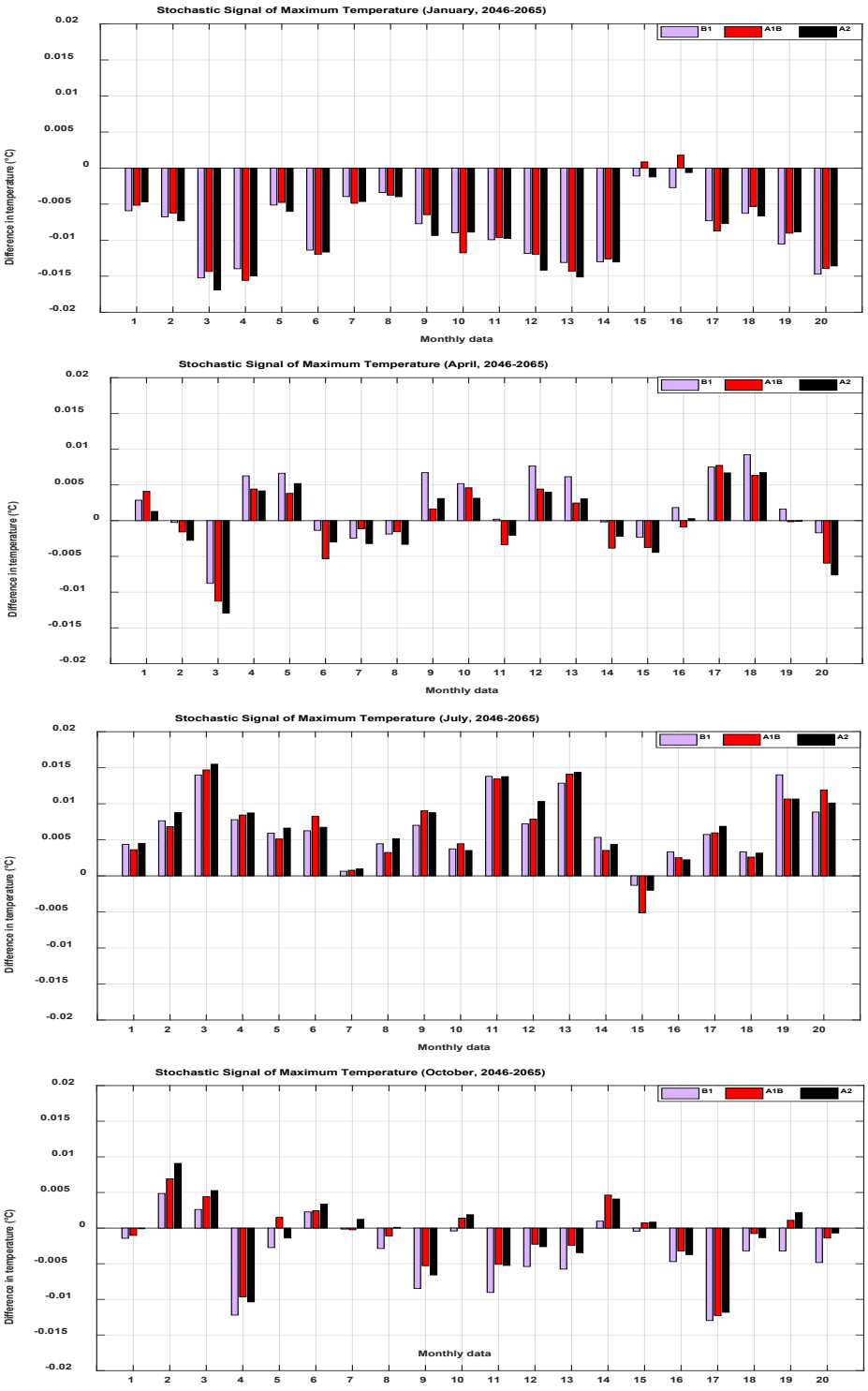

Figure 5-30: Stochastic signals of the maximum temperature projection under B1, A1B and A2 scenarios for the future period (2046-2065)

Figure 5.31 provides the probable differences between stochastic signals of the future IPCC scenarios and the 1980-2010 period of rainfall. The IPCC scenarios generally have the same pattern. However, the A1B and A2 scenarios are closer to each other

than the B1 scenario. There is neither a clear trend nor dominance for any scenario. Summer is wetter than other seasons, whereas winter is the driest season. Both autumn and spring share a number of key features, but these vary with the magnitude of precipitation.

The projected differences for the stochastic signal of solar radiation for the second period are set out in Figure 5.32. The signal drops markedly in January and rises in July. In addition, it varies from positive to negative for the rest months, but it tends to decrease in April and increase in October.

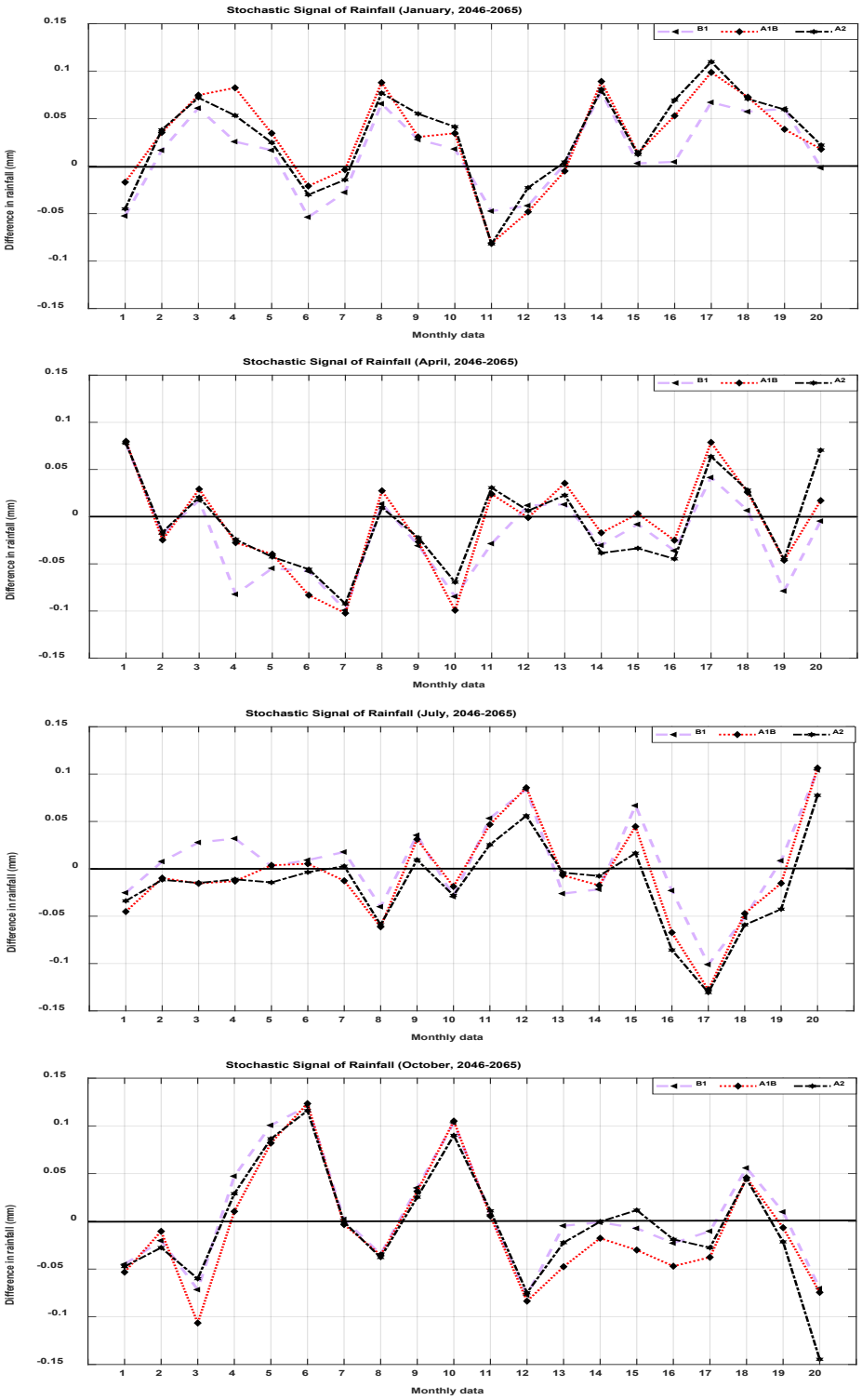

Figure 5-31: Stochastic signals of the rainfall projection under B1, A1B and A2 scenarios for the future period (2046-2065)

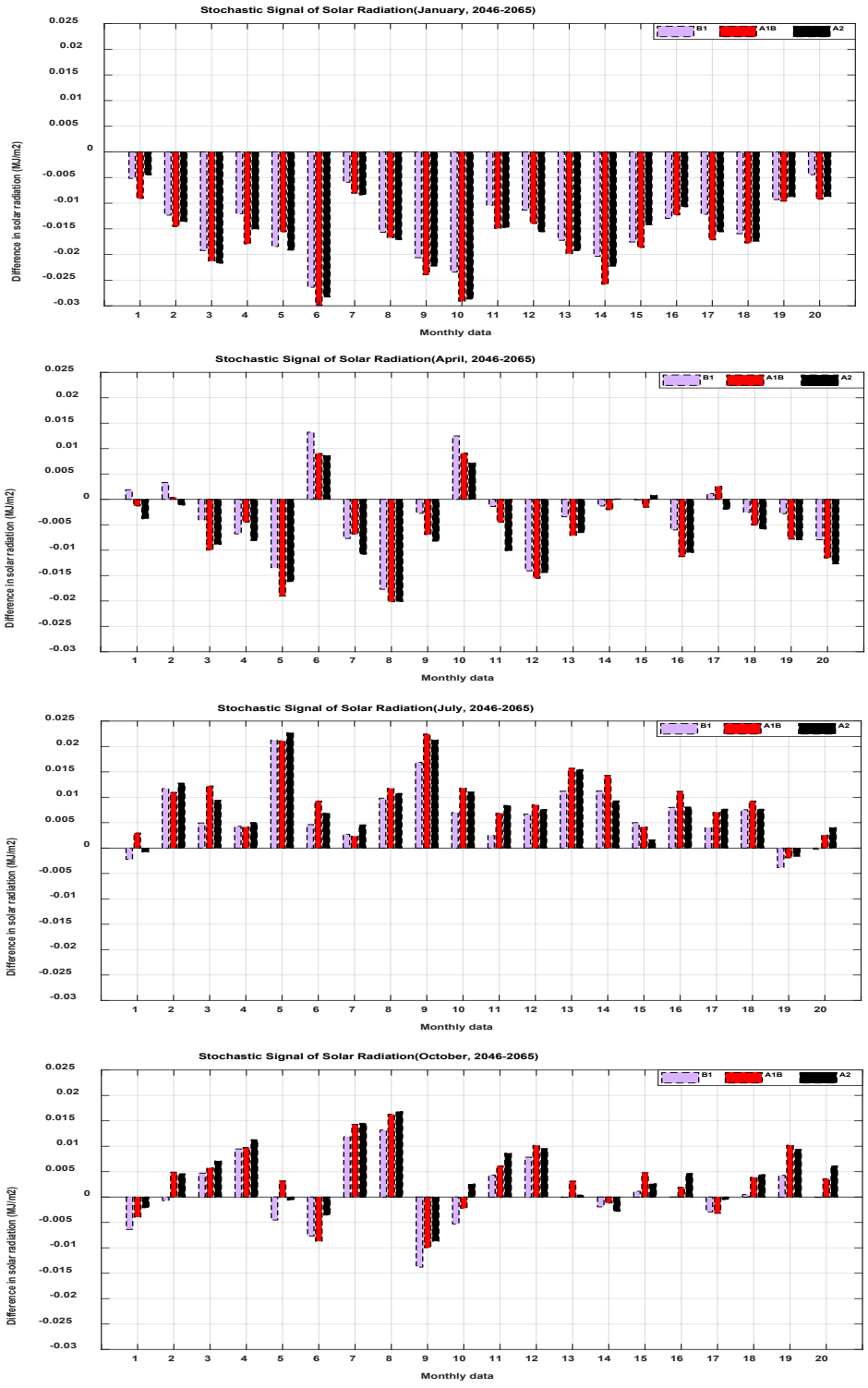

Figure 5-32: Stochastic signals of the solar radiation projection under B1, A1B and A2 scenarios for the future period (2046-2065)

C) Third Period 2080-2099

Figure 5.33 shows the expected differences results for the stochastic signal of maximum temperature for the third period. It increases in July, fluctuates in April and falls in January and October, but January differs from October in the magnitude of dropping. The values of the A2 scenario dominates the months of January, July and October, while the B1 dominates April only.

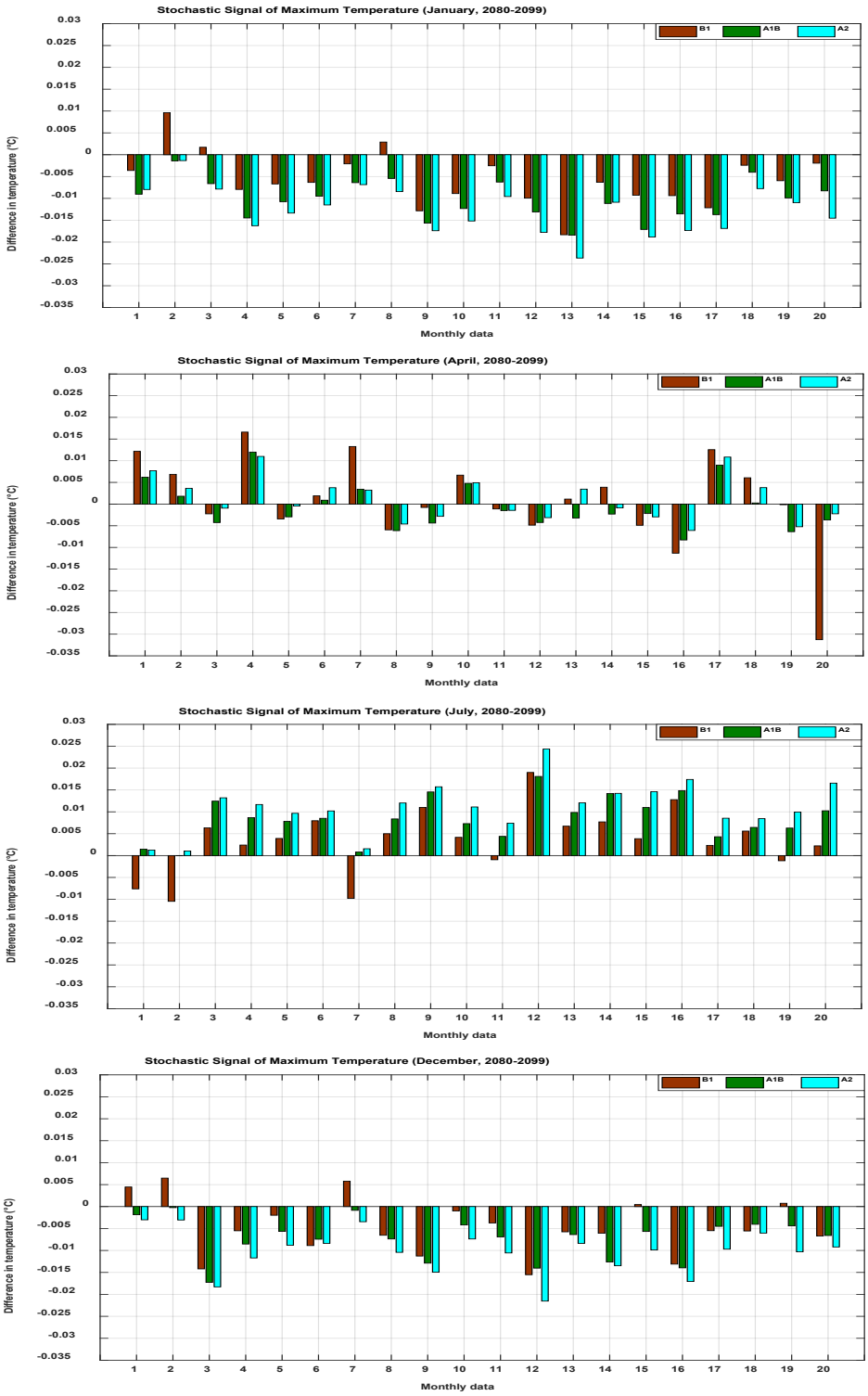

Figure 5-33: Stochastic signals of the maximum temperature projection under B1, A1B and A2 scenarios for the future period (2080-2099)

Figure 5.34 presents the projected differences values for the stochastic signal of rainfall for the 2080-2099 period. It can be seen that the signal fluctuates (between positive and negative) for January and the A2 scenario is likely to be the wettest one.

The higher positive signal is expected for April compared with the other months, and the A1B scenario is the best one. In July, signals oscillate around and close to zero, and the B1 scenario has the highest positive peaks. The highest negative signal happens in October that is considered the driest month.

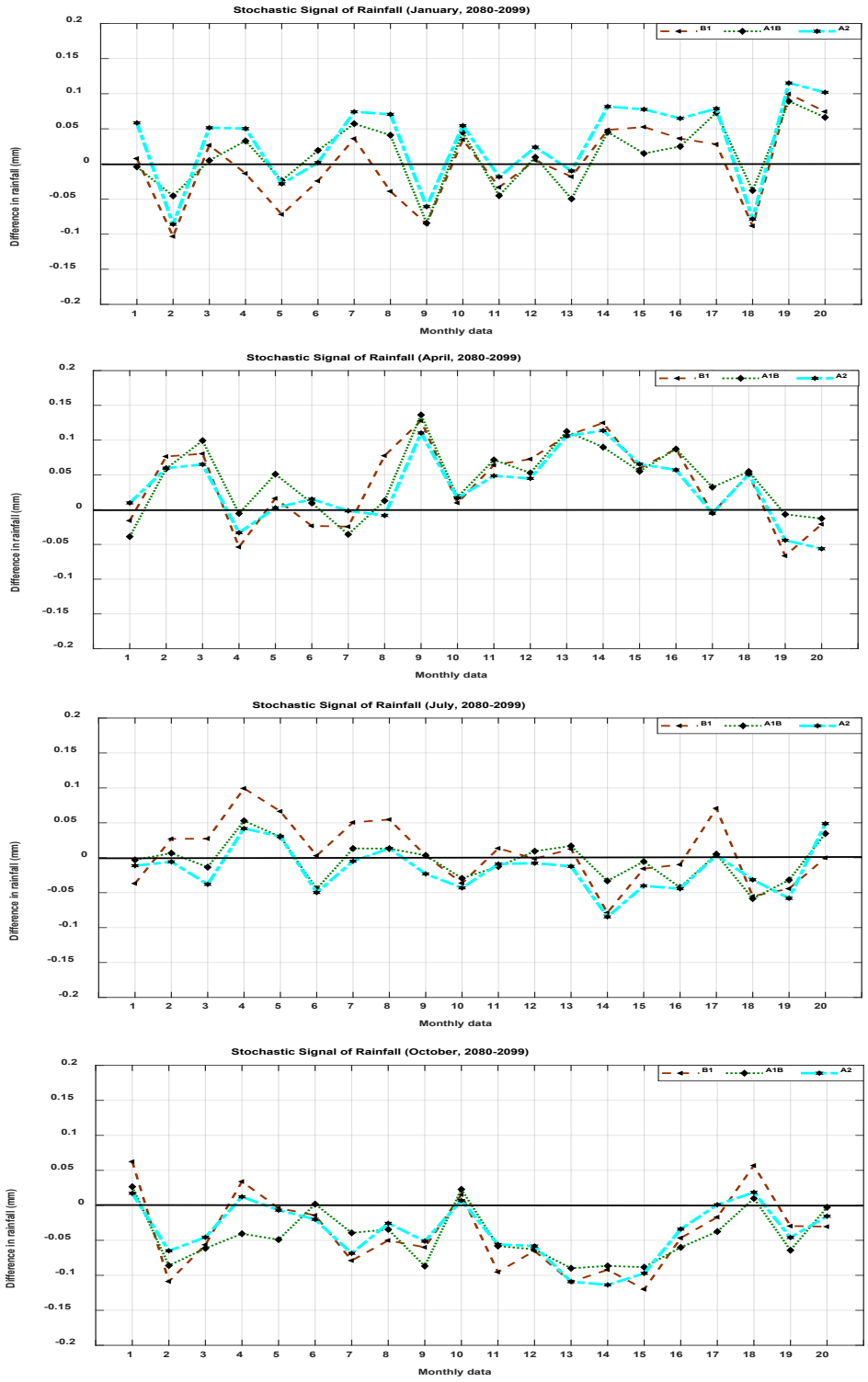

Figure 5-34: Stochastic signals of the rainfall projection under B1, A1B and A2 scenarios for the future period (2080-2099)

The probable differences results for the stochastic signal of solar radiation in the 2080-2099 period are displayed in Figure 5.35. What stands out in the figure is that the signal drops markedly in January and slightly in April. In addition, it rises clearly in

July and slightly in October. The values of the A2 scenario dominates in January (reduction) whereas, there is an increase in July.

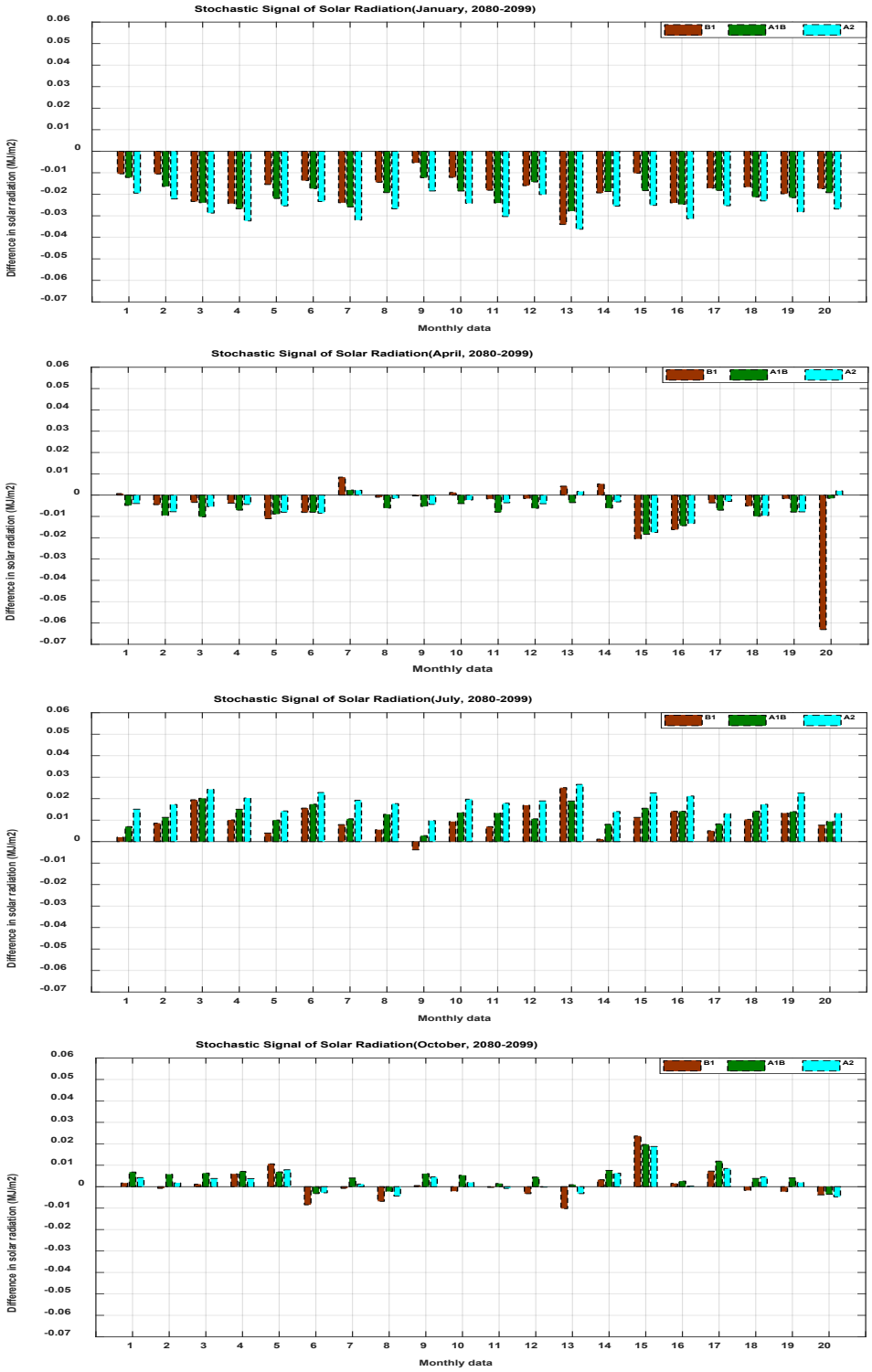

Figure 5-35: Stochastic signals of the solar radiation projection under B1, A1B and A2 scenarios for the future period (2080-2099)

Severe weather, increased Tmax and decreased Rain, may become more common in the future. Therefore, a stochastic signal of climate factors for three future periods under B1, A1B and A2 scenarios is employed to examine to what extent climate change will impact on future monthly municipal water demand.

5.4. Expected Future Municipal Water Demand

This section corresponds to step E of our proposed methodology (figure 3.1). For the monthly data of water consumption over the baseline period 1980-2010, the average mean of the 12 signals was calculated based on monthly bases (i.e. it can be seen that one average year represents 31 years, each month has 12 average signals). The monthly average water consumption time series over baseline period 1980-2010 are reconstructed and rescaled as shown in Figure 5.36.

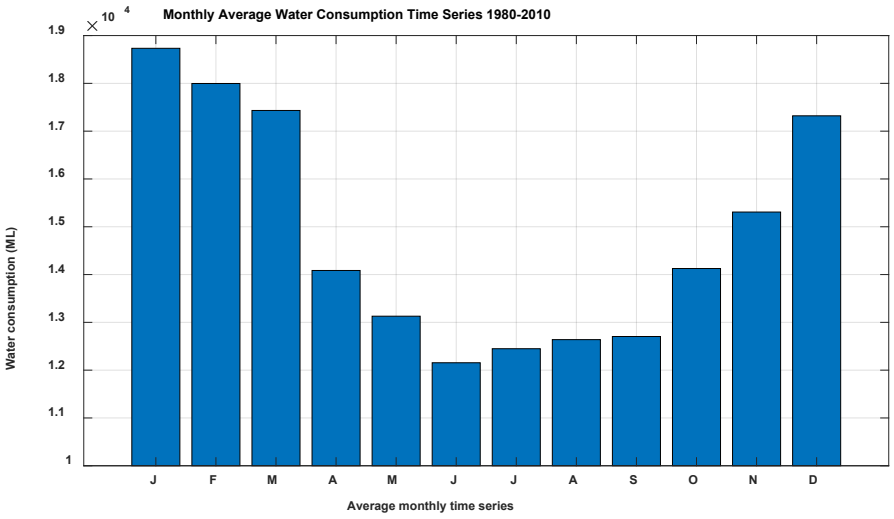

Figure 5-36: The monthly average water consumption time series over period 1980-2010

Stochastic signal of climate variables over three future periods, and under three IPCC scenarios, were employed to forecast the stochastic signal of monthly municipal water demands by using ANN. For each period, which is spanning over 20 years, the

stochastic signals of water demand were filtered based on months (e.g., 20 signals represent January months for each period). Two sets of each month in the average year of the baseline period that has 12 signals were made. The first set kept the same components; the stochastic component of the second set was replaced by future stochastic signal; this process was repeated for all months over the 20 years.

After reconstructing and rescaling of signals for both sets, we calculate the monthly percentage difference between the future and baseline water demand. Based on this calculation, the socio-economic variables were fixed to have the same effect for baseline and future periods. Therefore, the difference between the future and baseline water demands include the impact of climate change only (represented by stochastic signal) without the socio-economic effect. The monthly percentage difference between the expected future (for B1, A1B and A2 scenarios) and baseline water demands can be categorised into three periods 2011-2030, 2046-2065 and 2080-2099.

5.4.1. First Period 2011-2030

Figures 5.37, 5.38, 5.39 and 5.40 present the difference percentage for monthly water demands between the expected (B1, A1B and A2 scenarios) and baseline water demands for the first period (2011-2030). The Water Percentage Demands (WPDs) of December , January and February (summer season) are illustrated in Figure 5.37.

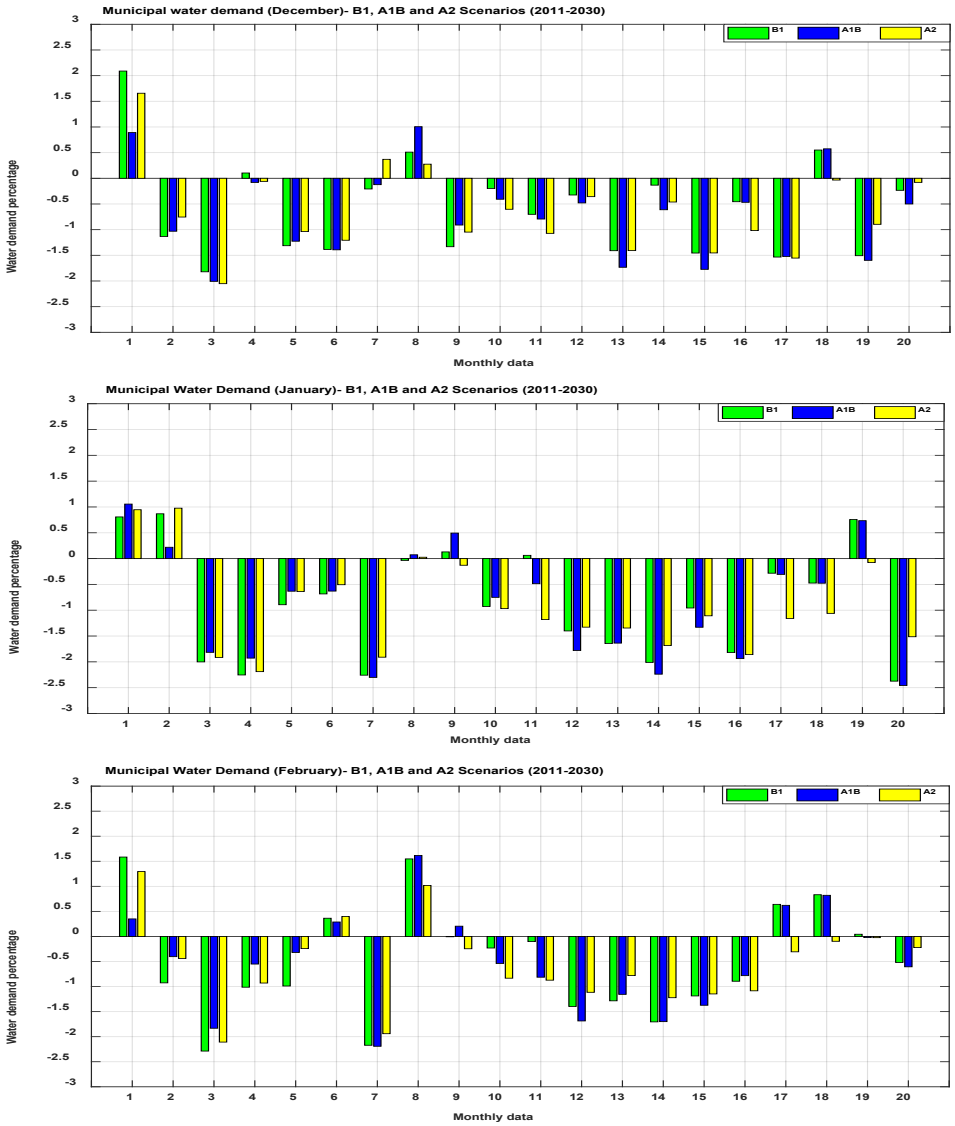

Figure 5-37: The projected WPDs under three scenarios for the period (2011-2030) based on the average monthly baseline period (1980-2010) (summer season)

Close inspection of this figure shows that the water demands in the summer season overall decrease and this reduction is consistent with the stochastic signal of climate variables for each scenario (see Figures 5.24, 5.25 and 5.26). That resulted due to the fact that the climate variables such as the Tmax and Radi are dropped, and the Rain rises in summer and under the B1, A1B and A2 scenarios. For more details, we describe the results depending on the monthly basis.

The highest decrease of WPDs happens in the third year which is (-2.05% = -355ML) under the A2 scenario in December while it is (-2.46% = -460ML) in the final year

under the A1B scenario in January. In addition, it occurs in the third year which is (-2.29% = -412ML) under the B1 scenario in February. The highest increase of WPDs happen in the first year which is (2.09% = 362ML) under the B1 scenario in December whereas, it is (1.06% = 198ML) in the first year under the A1B scenario in January. In addition, it occurs in the eighth year which is (1.62% = 291ML) under the A1B scenario in February. The majority of reduction percentage signals are distributed between (-0.25% and -1.5%), (-0. 5% and -2%) and (-0.25% and -1.5%) for the months of December, January and February respectively.

Figure 5.38 shows the WPDs of March, April and May that represent the autumn season. It can be noticed from the figure that the simulated municipal water demand in general decreases in March and fluctuates in April and May. The trend of water demand gradually increases going from March to May regarding the impact of climate variables. In March, the negative peak of WPDs is (-2.4% = -403ML) in the second year and under the B1 scenario, whereas the WPDs reach the maximum value (1.32%=231ML) in the seventeenth year and under the same scenario. In addition, about 74% of the negative signals of WPDs fall between (-0.25% and -1.5%).

The WPDs in April start with a slight rise compared with the previous month, and the negative and positive peaks of WPDs are (-2.43%=-342ML) and (1.57%=221ML) in the first and seventh years respectively under the A1B scenario. The range of most negative signals for WPDs are distributed between (0% and -1.25%). In May, the WPDs continuously increase, and the boundary limits for most signals are (-1% to 1%). The maximum WPDs value in the third year under A2 scenario is (1.76%=231ML), and the minimum WPDs value in the first year under the B1 scenario is (-2.6%=-337ML).

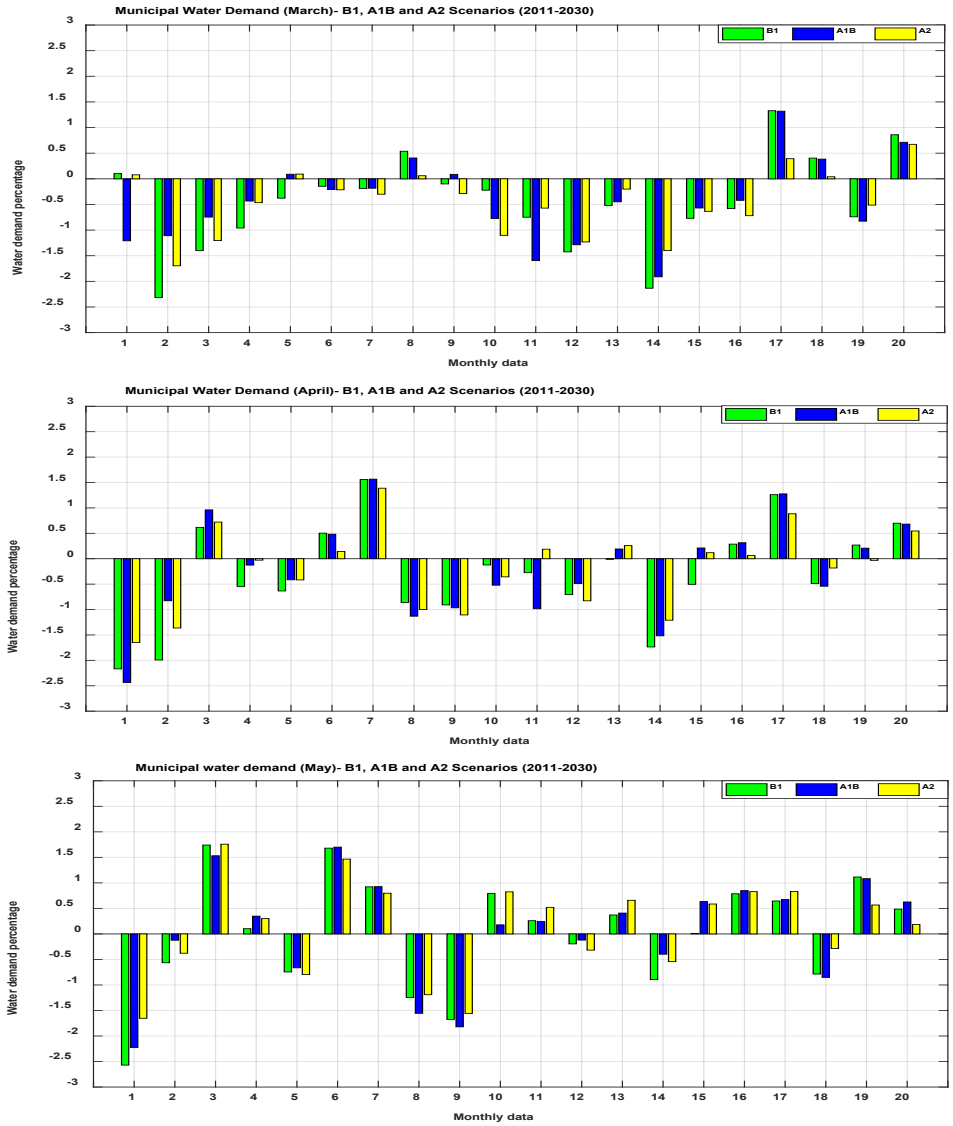

Figure 5-38: The projected WPDs under three scenarios for the period (2011-2030) based on the average monthly baseline period (1980-2010) (autumn season)

The WPDs results of the winter season which is the months of June, July and August can be seen in Figure 5.39. What is interesting about the signals in this figure is that the WPDs values increase in the winter season and this increase in WPDs is linked to the pattern of stochastic signals of climate factors (increase Tmax and Radi, and decrease Rain signals) (see Figures 5.24, 5.25 and 5.26).

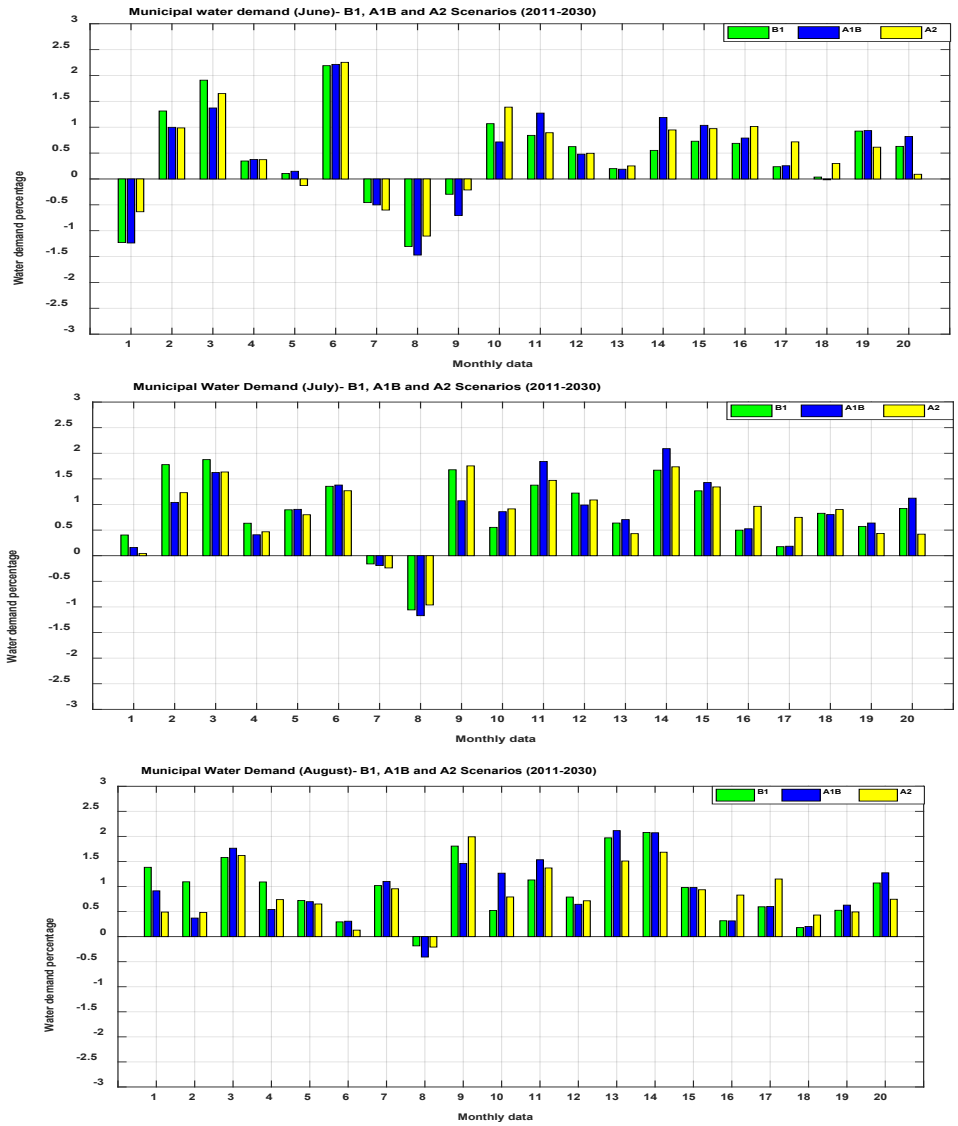

Figure 5-39: The projected WPDs under three scenarios for the period (2011-2030) based on the average monthly baseline period (1980-2010) (winter season)

The pattern of WPDs results increases for June, except in the first, seventh, eighth and ninth years, and its range of distribution is (0% to 1%). The maximum peak of WPDs is (2.26%=274ML) in the sixth year (A2 scenario). On the other hand, the lower WPDs is (-1.47%=-178.8) in the eighth year (A1B scenario). The effects of climatic factors on WPDs in July are similar to those of June. Both months approximately have the same pattern, but most of the WPDs values in July fall between (0.25% and 1.5%) and its positive peak is (2.1%=260.2ML) in the fourteenth year (A1B scenario). In addition, WPDs reduce in two years only (seventh and eighth) and its peak of reduction

is equal to (-1.17%=-146ML) in the eighth year (A1B scenario). The results of WPDs in August are similar to those reported in June and July. The increasing rates of WPDs range from (0.25% to 1.25%) with a maximum value of (2.1%=267.3ML) in the thirteenth year (A1B scenario). The WPDs decline in the eighth year only (A1B scenario) with value equal to (-0.4%=-51.4ML).

The WPDs of the months of September, October and November (autumn season) are summarised in Figure 5.40. The most interesting aspect of this figure is the WPDs values present in three modes. It increases in September (which is similar to winter season), fluctuates in October and decreases in November that is similar to the summer season. The results, as shown in the figure, indicate that the fluctuations in WPDs results are due to climate variability from winter to the summer season.

The range of WPDs results in September is likely to fall between (0% and 1%), but the peak value of WPDs is (2.55%=323ML) in the thirteenth year (A1B scenario), while the highest reduction in WPDs value is (-0.6%=-76ML) in the sixteenth year (same scenario). The values of WPDs for October oscillate between (-0.75% and 0.5%), its positive peak is equal to (1.53%=216.6ML) in the thirteenth year (B1 scenario) whereas, the negative peak is equal to (-1.56%=-221.6ML) in the sixteenth year (A1B scenario). The reduction range of WPDs results in November is (-0.25% to -1%), but the peak decline is (-1.6%=-243.2ML) in the tenth year (B1 scenario) while, the highest WPDs values is (0.56%=85.3ML) in the twelfth year (A1B scenario).

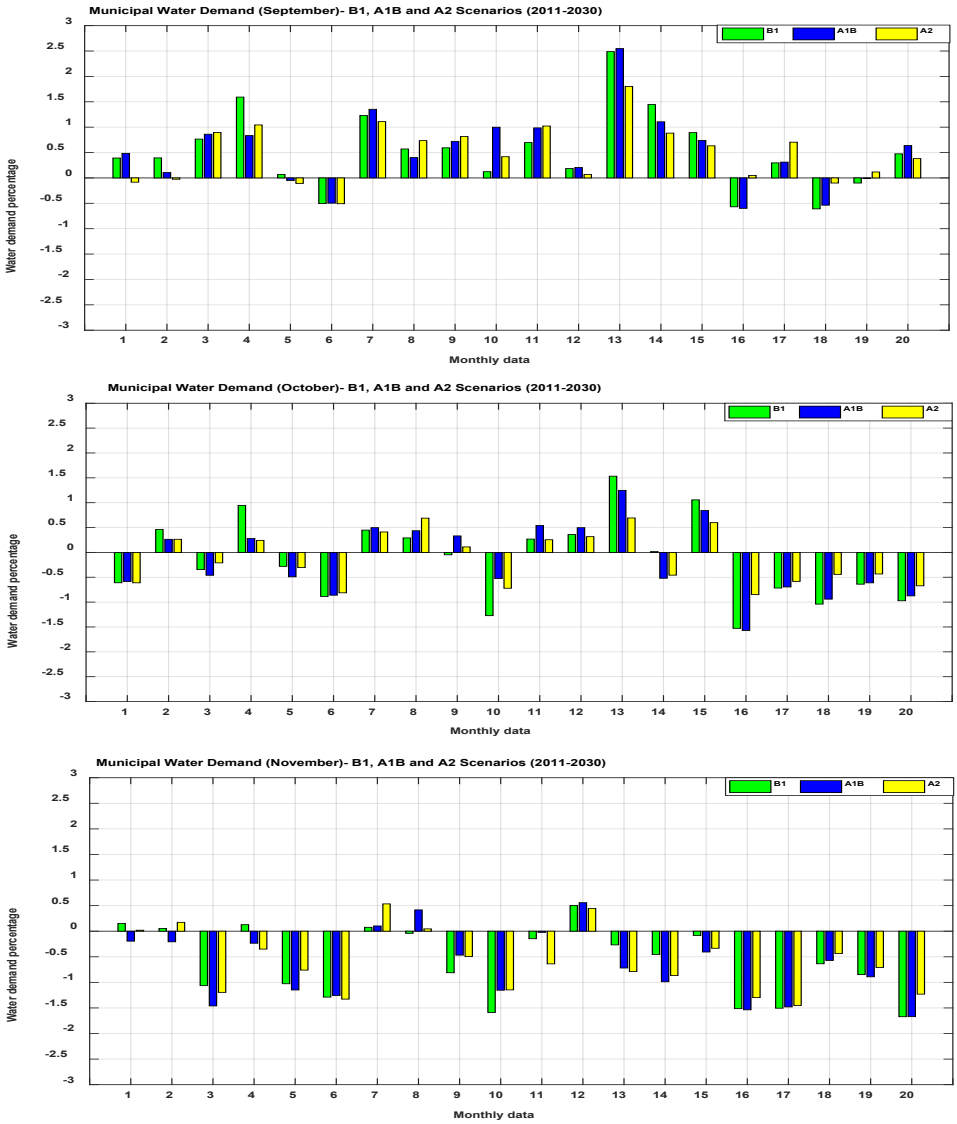

Figure 5-40: The projected WPDs under three scenarios for the period (2011-2030) based on the average monthly baseline period (1980-2010) (spring season)

Overall for this period, WPDs decrease from November to April and the best range of reduction is (-0.5% to -2%) in January whereas, it increases from June to September and the worst range of WPDs are distributed between (0.25% and 1.5%) in July, and the WPDs fluctuate in May and October. All these results are based on the variability of the stochastic signals for the climate factors.

5.4.2. Second Period 2046-2065

The expected results of WPDs for summer, autumn, winter and spring seasons under three IPCC scenarios (B1, A1B and A2) for the second period 2046-2065 are displayed

in Figures 5.41, 5.42, 5.43 and 5.44. The first Figure 5.41 provides the WPDs for the months of December, January and February (summer season).

The WPDs for December decline generally with peak negative value equal to (-2.17%=-376.1ML) in the ninth year (A2 scenario) and the majority of reduction values are distributed between (0% and -1.5%). In addition, the positive peak of WPDs is (1.77%=307ML) in the eleventh year (A1B scenario). The WPDs in January are similar to those in December, but in January WPDs tend to have more reduction than in December. The lower value of WPDs is (-2.19%=-410ML) in the seventeenth year (A2 scenario) while, the maximum increase of WPDs is (0.9%=169.1ML) in the eleventh year (same scenario). The range that has the most decline of WPDs value is (-0.25% to -1.75%). Approximately (75%) of WPDs results drop in February and most of these values are distributed between (-0.5% and -1.5%). The maximum reduction of WPDs is (-2.35%=-422.6ML) in the fourth year (A1B scenario) whereas, the positive peak of WPDs is (1.84%=331.5ML) in the fifth year (B1 scenario).

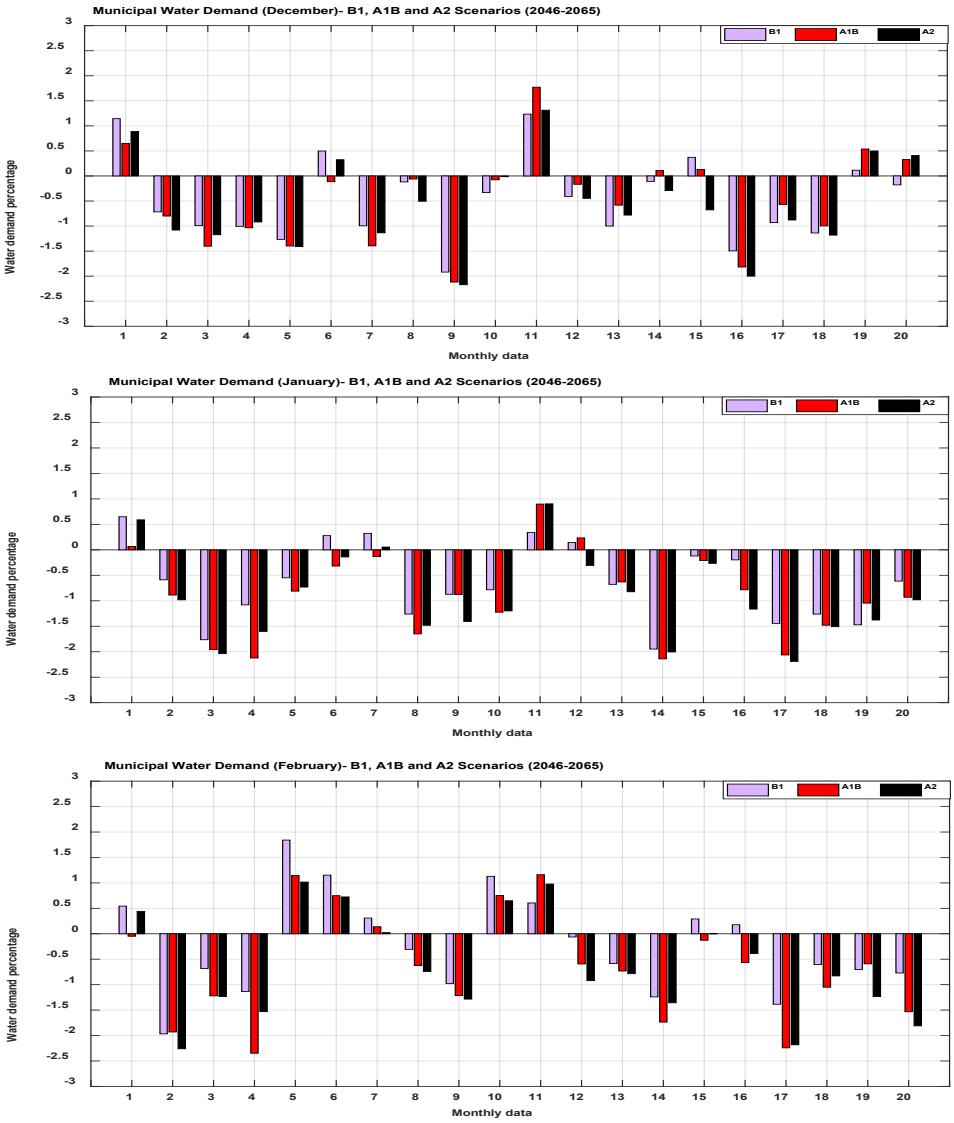

Figure 5-41: The projected WPDs under three scenarios for the period (2046-2065) based on the average monthly baseline period (1980-2010) (summer season)

Figure 5.42 shows the WPDs results for autumn season (March, April and May). It can be seen from the data in the figure that the WPDs rise slightly as time moves from March to May. In general the WPDs drop in March with a peak of (-2.24%=-390.3ML) in the twentieth year (A2 scenario). On another hand, the highest value of WPDs is (2.4%=418.5ML) in the fifth year (B1 scenario). The range of most of the decline values is (-0.25% to -1.25%). In April, the WPDs rise gradually compared with the previous month and that leads to the start of fluctuation in the values of WPDs, and most of these values fall between (-1% and 0.75%). The positive peak of WPDs is

(1.65%=233ML) in the tenth year (A1B scenario) while, the lower value of WPDs is (-1.9%=-267ML) in the final year (A2 scenario). The WPDs in May continue to fluctuate and tend to increase with a high percentage of WPDs values falling between (-0.5% and 1%). The highest reduction is (-1%=-135.8ML) in the final year (A2 scenario). In contrast, the maximum increase is (1.8%=237ML) in the nineteenth year (B1 scenario).

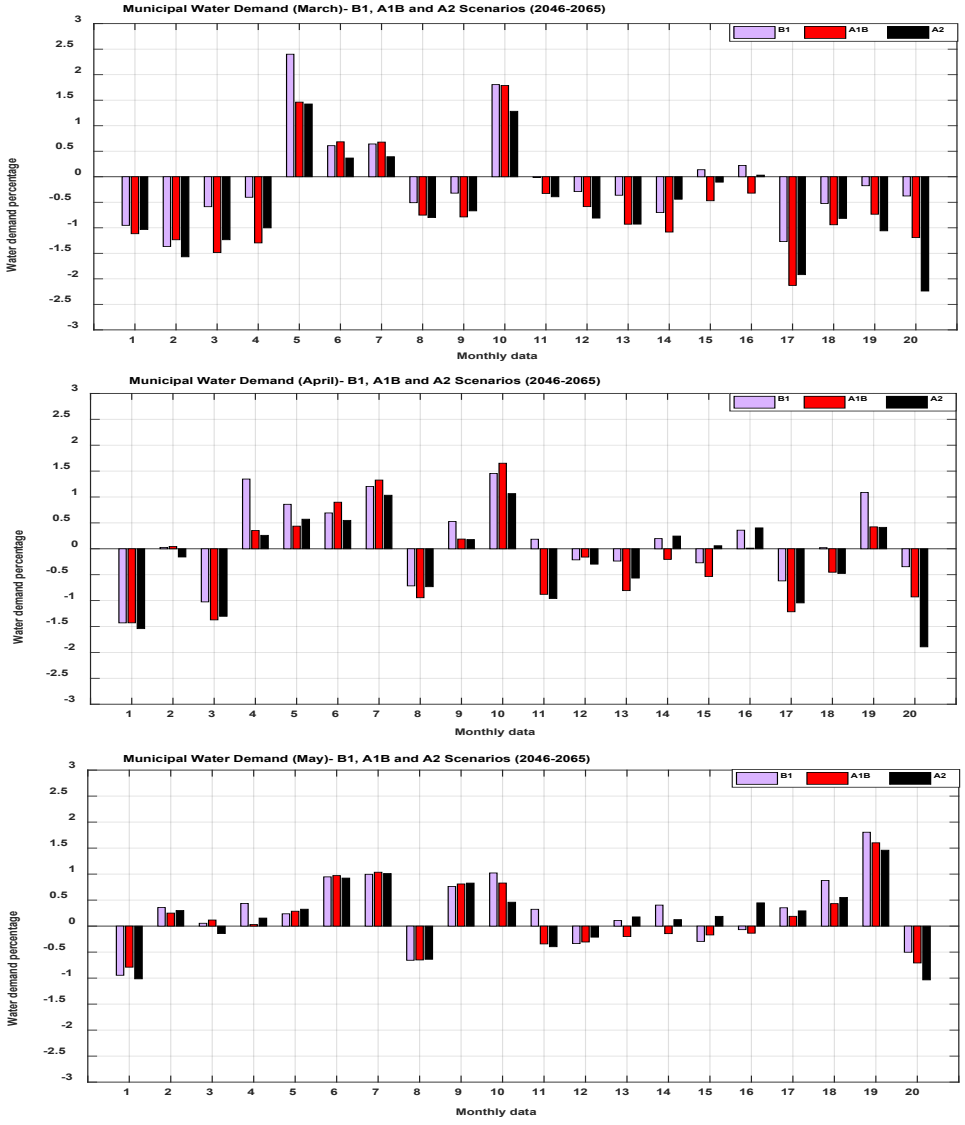

Figure 5-42: The projected WPDs under three scenarios for the period (2046-2065) based on the average monthly baseline period (1980-2010) (autumn season)

Figure 5.43 illustrates the probable WPDs results for June, July and August (winter season). What stands out in this figure is the growth of the WPDs' values is more

precise in July. The WPDs in June increase with the maximum value of WPDs reaching (1.65%=201ML) in the eighteenth year (B1 scenario) and the range of WPDs is (0% to 1.5%). On another hand, the lowest WPDs value is (-1.34%=-162.6ML) in the twentieth year (same scenario). The highest positive ratio of WPDs value occurs in July, and most of these values are located between (0.25% and 1.5%). The positive peak value of WPDs is (2.7%=338ML) in the seventeenth year (A2 scenario). However, the best status is (-1.2%=-148.4ML) in the final year (B1 scenario). The WPDs in August are similar to those of July, but it is different from the WPDs in July in a number of respects. The majority of WPDs values are distributed between (0% and 1.5%), the worst value of WPDs is (2.6%=329.5ML) in the seventeenth year (A1B scenario). In contrast, the best value of WPDs is (-0.68%=-86.5ML) in the fifteenth year (B1 scenario).

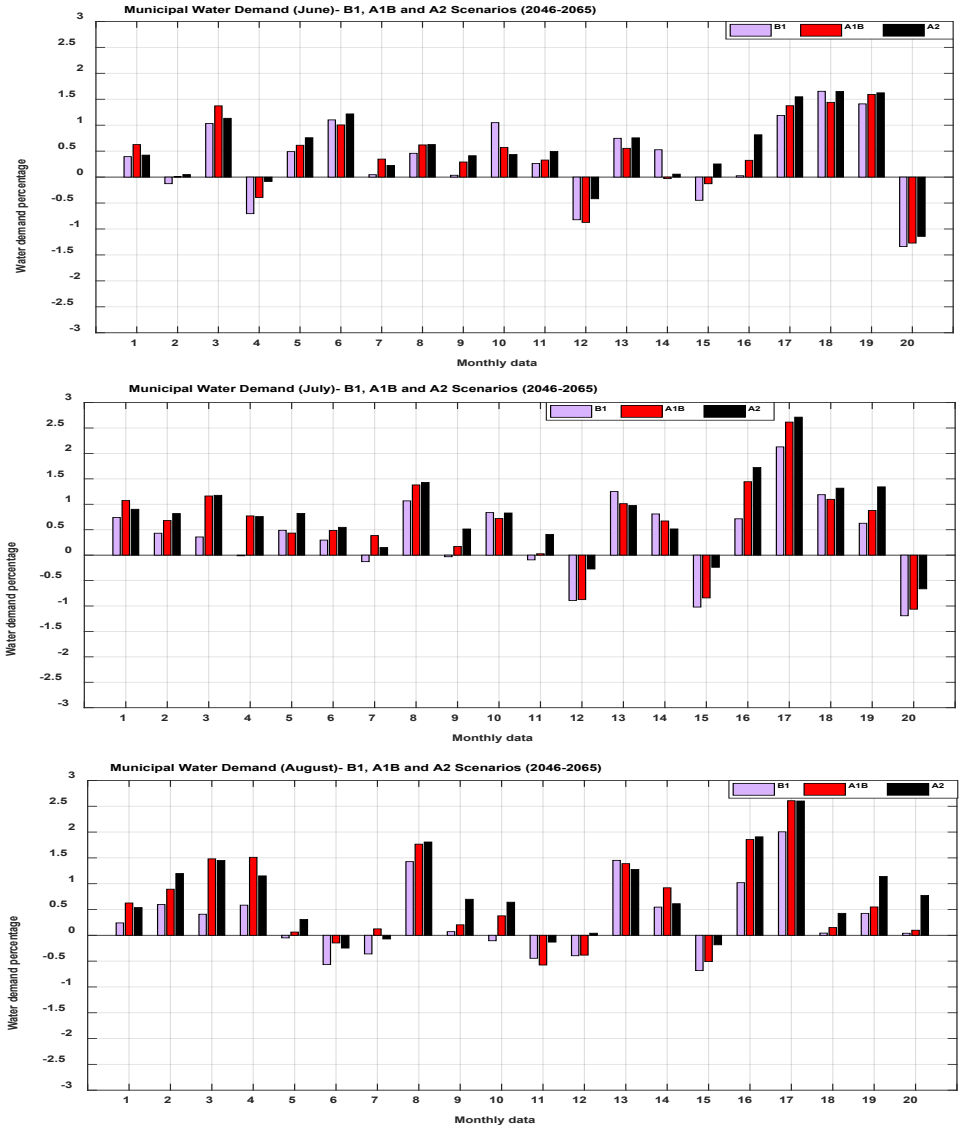

Figure 5-43: The projected WPDs under three scenarios for the period (2046-2065) based on the average monthly baseline period (1980-2010) (winter season)

The results of WPDs for the spring season (the months of September, October and November) are set out in Figure 5.44. It has been noted that there are three patterns regarding WPDs (increase, oscillate and decrease the values of WPDs) in this season. These patterns are consistent with the fluctuation of climatic factors from winter to summer season.

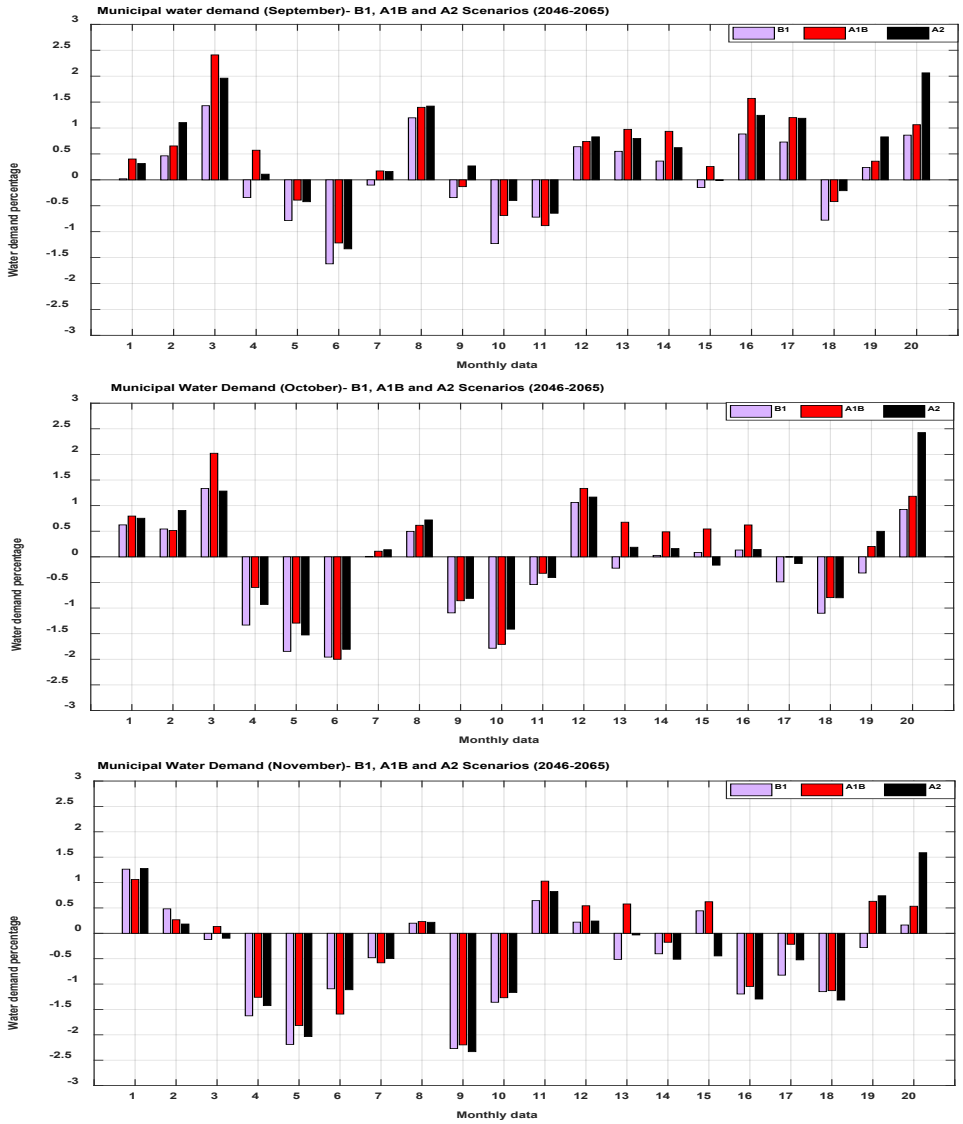

Figure 5-44: The projected WPDs under three scenarios for the period (2046-2065) based on the average monthly baseline period (1980-2010) (spring season)

The WPDs results in September are similar to those proposed in the winter season, it increases generally, and the range of most WPDs values is (0.25% to 1.5%). The maximum value of WPDs is (2.41%=306.2ML) in the third year (A1B scenario) whereas, the minimum value of WPDs is (-1.62%=-206ML) in the sixth year (B1 scenario). The WPDs fluctuate in October, it has a positive peak in the final year equal to (2.4%=342.6ML) (A2 scenario) and negative peak in the sixth year is (-2%=-282.5ML) (A1B scenario). In addition, the majority of WPDs results fall into a wide range equal to (-1.5% to 1.5%). The WPDs results in November follow the pattern of

the summer season. It decreases in general with a peak value equal to (-2.3%=-357ML) in the ninth year (A2 scenario) while, the positive peak is (1.6%=243ML) in the twentieth year (same scenario).

Generally for this period, WPDs decrease from November to March and the best range of reduction is (-0.25% to -1.75%) in January. However, it increases from June to September and the worst range of WPDs results are distributed between (0.25% and 1.5%) in July and WPDs fluctuate in April, May and October. Accordingly, the second period differs from the first period in the range of reduction in January. In addition, the pattern of the month of April changes from decreasing to fluctuating style. The future water demand is affected by the variability of the stochastic signals for the climate factors from season to another.

5.4.3. Third Period 2080-2099

Figures 5.45, 5.46, 5.47 and 5.48 show the probable monthly WPDs results for the third period (2080-2099) under IPCC scenarios (B1, A1B and A2) and baseline period (1980-2010).

Figure 5.45 displays the WPDs for the summer season (December, January and February). Looking at the figure, it is apparent that the WPDs' values decrease in general and the A2 scenario presents a significant reduction more than the other two scenarios. In addition, the continuous extreme decrease in WPDs results is probable to occur between the twelfth and seventeenth years for the months of January and February. In December, the WPDs results tend to decline with a different ratio based on IPCC scenarios, and it is 30%, 50% and 75% for B1, A1B and A2 scenarios respectively. The highest WPDs value is (1.91%=330.5ML) in the second year (B1 scenario) while, the minimum value is (-2.4%=-416ML) in the nineteenth year (A2

scenario). In addition, most WPDs are distributed between (-1% and 1%). The behaviour of WPDs in January tends to decrease except (25%) of B1 scenario values. The boundary of most decline values is (-0.25% to -1.75%), and the best value is (-2.5%=-468ML) in the nineteenth year (A2 scenario). In contrast, the extreme positive value of WPDs is (2.23%=419ML) in the second year (B1 scenario).

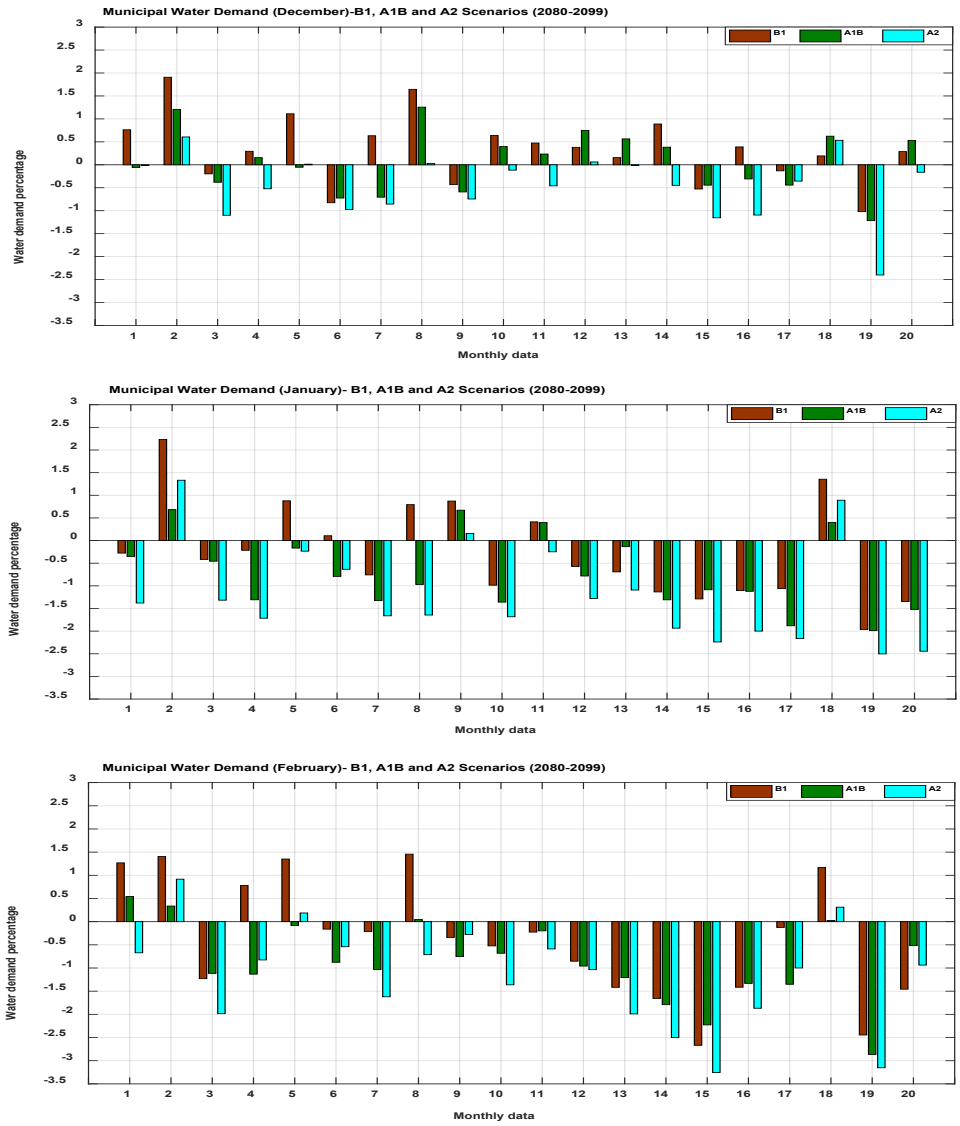

Figure 5-45: The projected WPDs under three scenarios for the period (2080-2099) based on the average monthly baseline period (1980-2010) (summer season)

The WPDs for January and February are shared in a number of key features. However, in February, WPDs tend to see more of a reduction than in January because of the impact of the climate factors' behaviour. The majority of WPDs are distributed

between (-0.25% and 2%) but the maximum reduction falls in the fifteenth year which is (-3.26%=-586ML) under the A2 scenario. In contrast, the worst case of the WPDs falls in the eighth year that is (1.46%=262ML) and under the B1 scenario.

The projected WPDs results for the months of March, April and May (autumn season) can be seen in Figure 5.46. One interesting finding is WPDs decline in all months except about (30%) of the B1 scenario results in March and April. Another significant finding is that the continuous extreme reduction in WPDs results is likely to happen between the eleventh and sixteenth years for March and April. The maximum WPDs values in March occur in the first year under the B1 scenario about (1.87%=326.1ML) while, the lowest WPDs value is (-3.14%=-548ML) in the fifteenth year (A2 scenario) and the range of most WPDs' value is (-0.5% to -2.75%). The values of WPDs in April are similar to those values in March. However, it is less reduction, and the most WPDs values are distributed between (-0.5% and -2.5%). It has the best value in the ninth year under the A1B scenario about (-2.77%=-390.4ML). On the other hand, the worst WPDs value is (1.39%=195.3ML) in the fourth year (B1 scenario). The WPDs results in May present less reduction than WPDs values in both months March and April and most WPDs values in May fall between (-0.25% and -1.5%). The maximum decrease in WPDs value is (-2.82%=-369.7ML) in the eighth year (B1 scenario), and the highest increase in WPDs value is (1.2%=157.7ML) in the nineteenth year (same scenario).

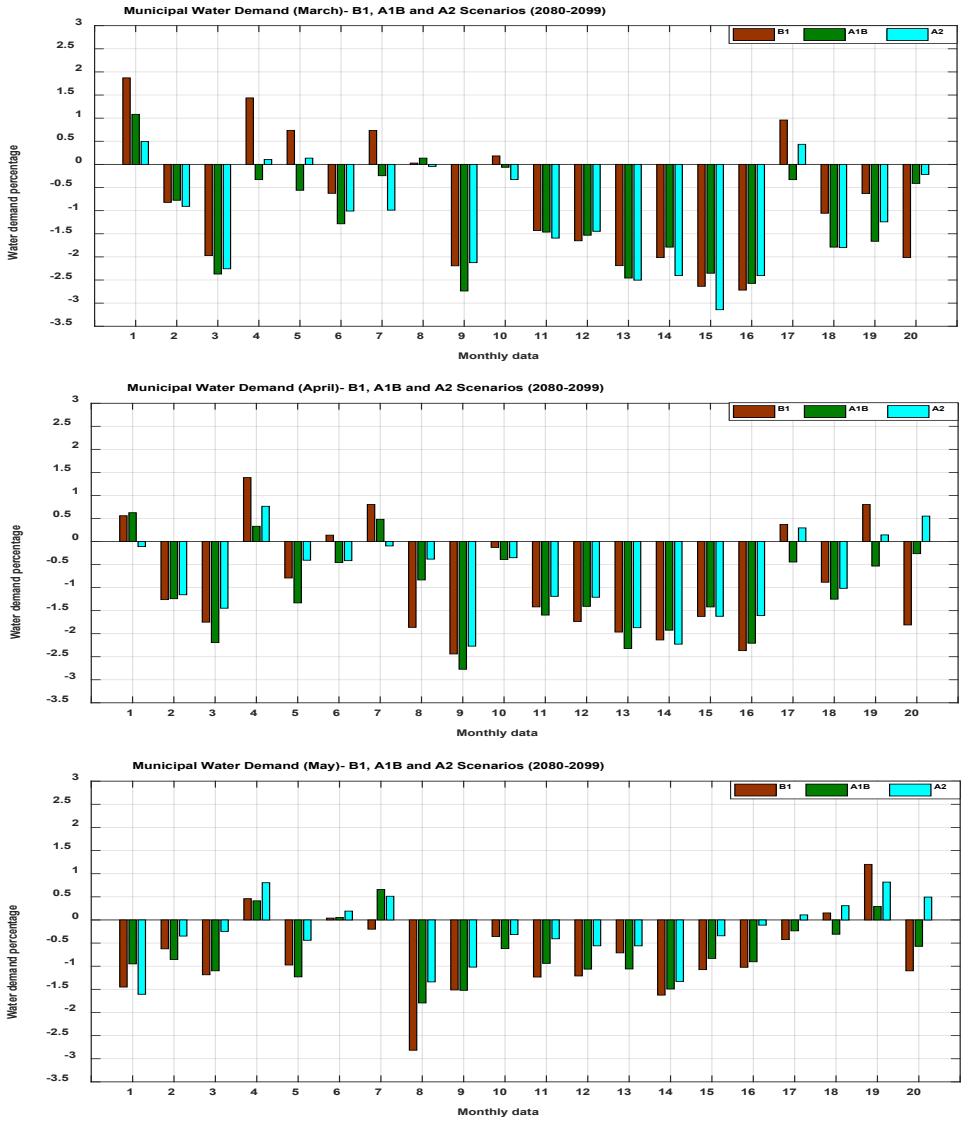

Figure 5-46: The projected WPDs under three scenarios for the period (2080-2099) based on the average monthly baseline period (1980-2010) (autumn season)

Figure 5.47 provides the expected results of WPDs in the winter season (the months of June, July and August). As can be seen from the figure the WPDs fluctuate in June and increase in July and August, and the highest continuous demand is from the twelfth to the sixteenth year in August. The WPDs results in June show various styles based on each IPCC scenario. The WPDs results of the B1 scenario decrease with (70%) but it rises for an A2 scenario about (80%), and it fluctuates for the A1B scenario (i.e. it increases about (50%)). The highest WPDs result is (2.04%=248.1ML) in the nineteenth year (A2 scenario) and lowest WPDs value is (-2.25%=-273.9ML) in the

eighth year (B1 scenario). The WPDs in July rise except (35%) of B1 scenario results, the range of most WPDs values fall between (0% and1.5%) but the maximum value is (2.33%=290ML) in the fourteenth year (A2 scenario) while the minimum value is (-1.35%=-168.3ML) in the fourth year (B1 scenario). The WPDs results in August are similar to those in July. However, the WPDs values in August tend to increase more than the WPDs value in July. The WPDs results are distributed between (0.25% and 2.25%), but the maximum value of WPDs is (2.87%=363ML) in the fourteeenth year (A2 scenario) whereas, the minimum value is (-1.2%=-151ML) in the fourth year (B1 scenario).

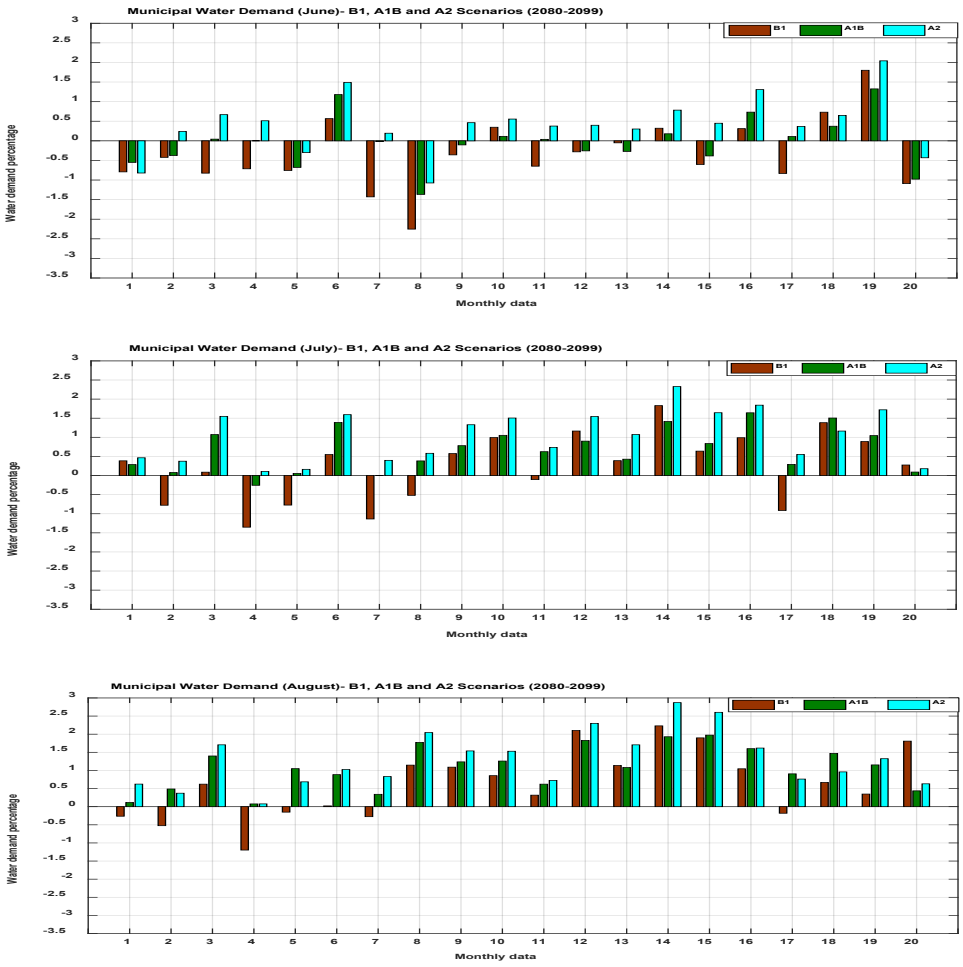

Figure 5-47: The projected WPDs under three scenarios for the period (2080-2099) based on the average monthly baseline period (1980-2010) (winter season)

The WPDs results of the spring season (September, October and November) are set out in Figure 5.48. In this figure, there is a clear trend of increases in WPDs results for September and October that are similar to the winter season, and WPDs fluctuate for November, which is a result of changing the impact of climate factors from one season to another. The pattern of WPDs values in September is similar to those WPDs values in August with a maximum positive peak in the fifteenth year under the B1 scenario equal to (2.93%=372ML), but the most WPDs values fall between (0.25% and 2%). On the other hand, the negative peak value of WPDs is (-1.27%=-161ML) in the fourth year (same scenario). The WPDs in October still have the same style of rising with the majority of its values distributed between (0.25% and 1.75%), but the worst WPDs value is (2.8%=394ML) in the fifteenth year under the B1 scenario. In contrast, the best WPDS value is (-1.65%=-233.6ML) in the first year (same scenario). The WPDs values have an oscillating mode, which results from the fluctuation of the climate variables from season to season. The highest reduction of WPDs value is (-2.4%=-416ML) in the nineteenth year (A2 scenario). However, the maximum WPDs value is (1.91%=330.5ML) in the second year under the B1 scenario, but the boundary on most WPDs results is (-1% to 1%).

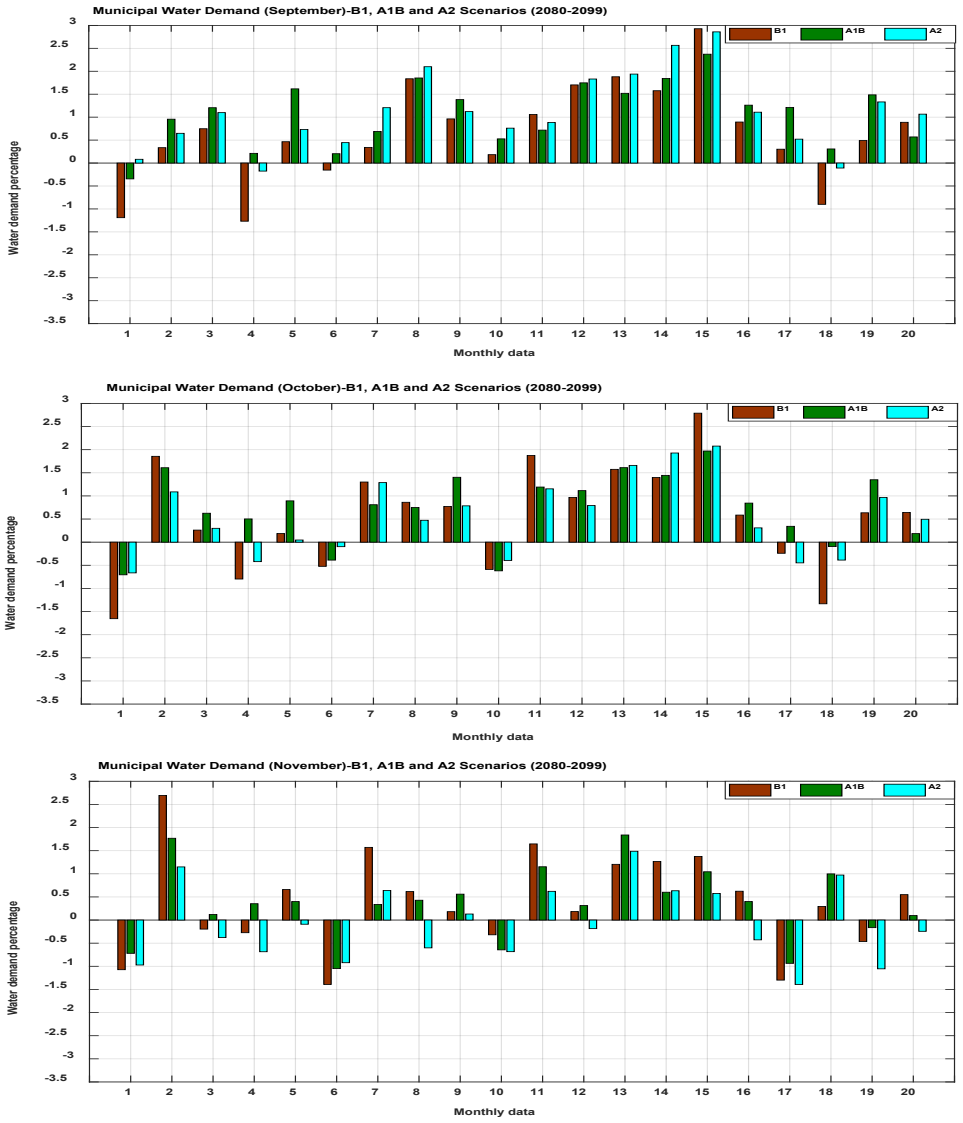

Figure 5-48: The projected WPDs under three scenarios for the period (2080-2099) based on the average monthly baseline period (1980-2010) (spring season)

Overall for the 2080-2099 period, the WPDs results decline from January to May, and the highest limit of decreasing is (-0.5% to -2.75%) in March. In contrast, it rises from July to October, and the maximum range of increasing is (0.25% to 2.25%) in August, and WPDs fluctuate in November. The WPDs values in June and December have different patterns based on IPCC scenarios. The WPDs results in June decrease, vary and increase for B1, A1B and A2 scenarios respectively. However, it rises, drops for B1 and A2, and stays the same (fluctuates) for an A1B scenario in December. The future water demand is driven by the high variability of the stochastic signals for the

climate factors from season to another particularly in this period. Therefore, the WPDs results in the third period differ from those results in the first and second periods in patterns and magnitudes that result from the style of expecting climate factors in the third period especially for the A2 scenario.

The means of seasonal municipal water percentage demands with confidence interval level, 0.95% for B1, A1B and A2 scenarios were calculated to increase the knowledge about how the climate change affects the water demand depending on a seasonal basis, in addition, to examine and select the best and worst IPCC scenarios for each season over three future periods.

For the first period, the expected mean of the water percentage demands (MWPDs) are shown in Figure 5.49.

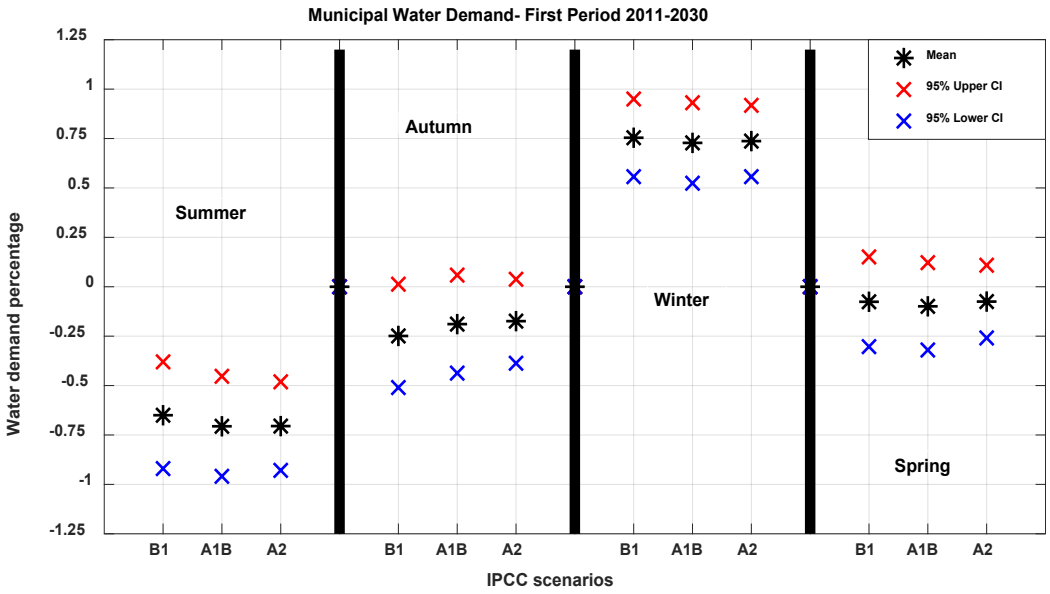

Figure 5-49: The average monthly mean for the seasonal municipal water demands percentage under B1, A1B and A2 scenarios for the 1st periods

It can be seen that the MWPDs value is -0.65, -0.71 and -0.71% for B1, A1B and A2 scenarios respectively. The water demand is likely to decrease in the summer season

under all IPCC scenarios and (A1B and A2) are the best scenarios. The MWPDs in autumn is equal to -0.25, -0.19 and -0.17% for B1, A1B and A2 scenarios. The water demands still decline under all scenarios, but the B1 scenario is the best one. The magnitudes of MWPDs in winter is 0.75, 0.73 and 0.74% for B1, A1B and A2 scenarios. The water demands are expected to rise for all situations and the worst case is the B1 scenario. For the spring season, the MWPDs drop to -0.076, -0.099 and -0.075% for B1, A1B and A2 scenarios. Therefore, the A1B scenario is the best one based on the MWPDs values. In general, no dominant scenario offers the best or the worst case but we can choose A1B as the best and B1 as the worst scenario based on what the scenario is likely to present in each season.

Figure 5.50 presents the seasonal MWPDs for the second period under B1, A1B and A2 scenarios. The results of MWPDs, in general, show a difference in values and style compare with the first period. The MWPDs results show a decrease in summer that is equal to -0.44, -0.66 and -0.71% for B1, A1B and A2 scenarios and A2 is the best case. The MWPDs value is 0.12, -0.19 and -0.2% for B1, A1B and A2 scenarios in autumn. Accordingly, the A2 is the best one, and B1 is the worst scenario. In winter, the MWPDs results increase for all situations and its value is 0.36, 0.56 and 0.71% for B1, A1B and A2 scenarios. Therefore, all IPCC scenarios are increased, but the A2 is the worst scenario. The MWPDs values are -0.24, 0.08 and 0.04% for B1, A1B and A2 scenarios in the spring season. The B1 scenario offers a reduction in the MWPDs whereas, both A1B and A2 scenarios present a slight increase in the MWPDs values. Accordingly, the A2 scenario shows a decrease in summer and autumn but it shows an increase in winter and spring.

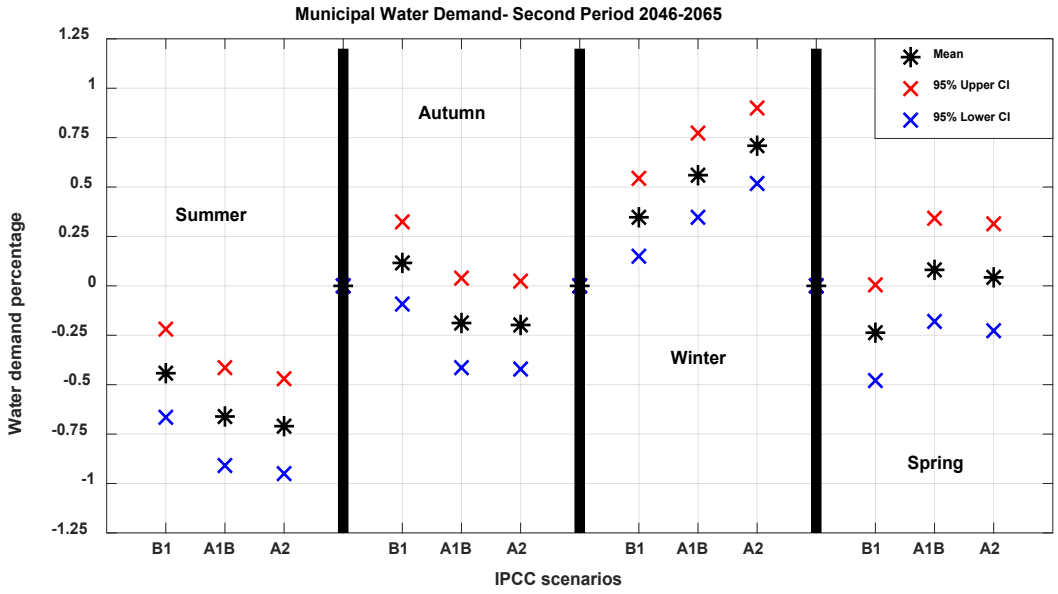

Figure 5-50: The average monthly mean for the seasonal municipal water demands percentage under B1, A1B and A2 scenarios for the 2nd periods

The seasonal MWPDs results for the third period under different IPCC scenarios are displayed in Figure 5.51. The A2 scenario presents a lower reduction in MWPDs values (-0.93%) than B1 and A1B scenarios in summer. The style of data in autumn differs from the summer but still decreases, and the lowest case is -0.98% under the A1B scenario. The MWPDs values rise in winter, and worst is 0.92% under the A2 scenario. In the spring season, the data still increase, and the highest is 0.72% under the A1B scenario. Overall, the A2 scenario still offers the same pattern in the second period (i.e. it drops in summer and autumn and increases in winter and spring). It can be noted that this period has the lowest and highest values of MWPDs in the autumn (A1B) and winter (A2) respectively.

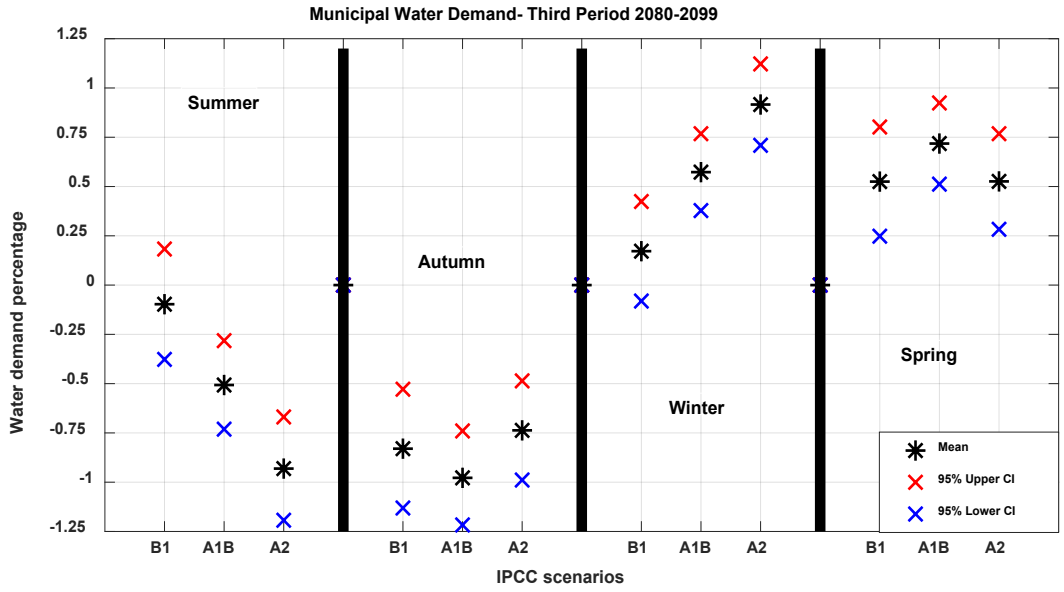

Figure 5-51: The average monthly mean for the seasonal municipal water demands percentage under B1, A1B and A2 scenarios for the 3rd periods

5.5. Discussion

The RMSE for the LSA-ANN algorithm (after 40 iterations) is 0.0236, whereas GSA-ANN does not improve the RMSE of 0.0241, and PSO-ANN algorithm only reaches its best RMSE of 0.0245 after 62 iterations. Therefore, the LSA-ANN algorithm outperforms the GSA-ANN and PSO-ANN algorithms, due to the fact that LSA-ANN achieves a smaller error (better performance) within a smaller number of iterations (making it a less complex model).

The use of a novel combination of techniques, including SSA and hybrid LSA-ANN model has also proven to be a successful choice for this particular application. This technique has resulted in stronger correlation coefficients (R=0.98 for independent data set) and less error (MSE= 6.3911 e^{-04}), for the long-term prediction of municipal water demands based only on climatic factors. Our findings compared with results of previous studies that were used traditional technique to preprocessing data and ANN model (e.g. Sebri (2013) with RMSE= 1,741.12 and Behboudian et al. (2014) with

R=0.92). Another comparison was conducted with Mohammed and Ibrahim (2013) that used climate variables as model input and ANN model with R= 0.87. The comparison of the findings with those of the other studies confirms the present methodology to forecast municipal water demand under climate change for the long term.

The model was used for different data in Columbia City, USA and it offers significant results as shown in Appendices 4-A and 5-A. According to this data analysis and statistical criteria, it can be inferred that these results provide further support for the hypothesis that our novel combination techniques can be applied successfully in any continent and under different environments. In addition, the most striking result to emerge from the results is the confirmation of the association between climate change and municipal water demands over the long-term.

Two statistical criteria (K-S, p-value) tests and graphics comparisons were performed to examine the equality of the distributions of daily climate factors calculated from measured and simulated data for the baseline period 1980-2010. Based on these results, the LARS-WG model reveals an adequate performance in simulating the future climate variables (Tmax, Rain and Radi). These results are comparing with the finding of other studies that used LARS-WG in different environments such as Chen et al. (2011) in Sudan, Behboudian et al. (2014) in Iran, Osman et al. (2017) in Iraq and Fenta Mekonnen and Disse (2018) in Ethiopia. The result of comparison broadly supports the work of other studies in this area downscaling climate factors by the LARS-WG model.

The monthly average of probable future maximum temperature has the same pattern under B1, A1B and A2 scenarios for 2011-2030, 2046-2065 and 2080-2099 periods.

However, Tmax has variation in the magnitude of degrees Celsius from period to another depending on the scenarios' assumptions. Tmax is expected to increase as we move toward the future, and the A2 scenario offers the warmest scenario (e.g. Tmax (in July) = 14.5, 15 and 15.6°C for the B1, A1B and A2 scenarios respectively).

The potential effects of climate change on the future solar radiation under B1, A1B and A2 scenarios are similar in the all periods, but there is a little difference among the three periods for any month in respect to all IPCC scenarios. Radi is expected to increase slightly over all the periods and reaches a peak solar radiation in January under the A2 scenario for the first period at 23.3MJ/m^2.

The monthly average data of future expected under B1, A1B and A2 scenarios for 2011-2030, 2046-2065 and 2080-2099 periods are likely to decline in rainfall amount as a move toward the future (i.e. the first period has rainfall more than the second and third periods) for all three scenarios. The A2 scenario projects to be a drier scenario (35 to 78) mm compared to the B1 and A1B scenarios. Moreover, February expects to be the driest month compared to other months of the year for all IPCC scenarios.

The differences between the stochastic signals of the ensemble mean of Tmax for B1, A1B and A2 scenarios over all simulated periods and the stochastic signal of the baseline (1980-2010) present that Tmax rises, generally, in winter and spring and drops in summer and autumn. In addition, the third period (2080-2099) is the hottest one and the A2 scenario presents the highest reduction in summer and a maximum increase in winter compared with the other scenarios. Solar radiation stochastic signals are similar to Tmax signals with slight variation from period to period and one scenario to another. The A2 scenario, in the third period, shows the lowest signal in summer and highest signal in winter compared with other periods and scenarios. Rainfall

stochastic signals have a non-uniform pattern for the three periods and under all IPCC scenarios. In all scenarios, the third period displays the highest decrease, which happens in spring. In contrast, it shows the highest increase that occurs in autumn for B1 and A1B scenarios whereas, it happens in summer for the A2 scenario.

The WPDs results for all periods and under all scenarios are likely to drop in summer, and the highest limit of decrease happens in January for the first and second periods, while it occurs in March for the third period. In addition, it rises in winter, and the maximum range of increase happens in July for the first and second periods, whereas it occurs in August for the third period. For autumn, the WPDs values either drop or fluctuate and tend to fall. In contrast, the WPDs in spring either increase or oscillate and tend to rise. Both the first and second period have a number of similarities. However, the third period is different from the first and second periods in some respects, especially for the A2 scenario. In addition, it has the highest and lowest values of WPDs compared with the other periods. Some of our significant findings comparing with previous study (Behboudian et al. (2014)) can by briefly highlighted here, where the projection of water conception is over period 2011-2030. Moreover, in this study there are many issues include: 1) it considers 12 years to build the prediction model of water demand instead of 31 years as baseline period; 2) it employs maximum temperature with some socio-economic factors as model input, while we consider Tmax, Rain and Radi as a model input; 3) it uses one GCM to project the Tmax over 2011-2030, where as we uses 7 GCMs to reduce the uncertainty of assumptions.

Based on the seasonal values of MWPDs under all scenarios and over the three periods, no dominant scenario offers the best or the worst case. For the first period,

the seasonal values of MWPDs drop in all seasons except winter, while in the second and third periods, it decreases in summer and autumn and rises in winter and spring except for two values of the B1 scenario in the second period (autumn and spring). In addition, the lowest and highest values of MWPDs are in the autumn (A1B) and winter (A2) for the third period respectively.

Climatological variability has a significant impact on the in economic terms, e.g., the Water Company in Melbourne City depends on water harvested from protected catchments as freshwater resources and the city faced a drought that has pushed the city water authorities to enforce water restrictions. Based on IPCC scenarios in this thesis, the Tmax and Radi are likely to increase and Rain to decrease that lead to adversely impact on the freshwater resources. Accordingly, additional restrictions on water consumption and raise the water price is expected. On another hand, municipal water demand expects to increase to around 3% based on baseline period 1980-2010. The significance of this percent is related to several issues such as availability of fresh water resource at that time, the population of the city in the future and capacity of the municipal water system to deliver the rapid increase of water demand due to rise the climate effects. Therefore, all these issues associated with economic terms to tackle the problem of increasing water demand and water scarcity at the same time. The 3% gives the stakeholders a scientific view about what is likely to occur in future that reduces the uncertainty result from the impact of climate change on the municipal water demand and find the alternatives base on IPCC scenarios. Therefore, it should be support and activated the climate change agreements such as (Paris agreement) to mitigate the impact of climate change and support the sustainability at the strategic level.

5.6. Summary

This chapter highlights the process of assessing the long-term impact of climate change on the municipal water demands under various IPCC scenarios. We consider three climate factors over the baseline period 1980-2010 to determine to what extent that climate change affects the municipal water demands.

The findings' results are classified into three sets: the first results refer to the development of a water demand model, which uses a novel combination technique Singular Spectrum Analysis (SSA) and hybrid Artificial Neural Network (ANN) to predict the monthly municipal water demands regarding climate change. Then results of the historical daily climate variables data over the period 1980-2010 (31 years) with seven GCMs and three IPCC scenarios are used to support the LARS-WG model to simulate future climate factors under B1, A1B and A2 scenarios over the 2011-2030, 2046-2065 and 2080-2099 periods. Finally, the final sets of results represent the forecasting of municipal water demands under the three IPCC scenarios over the three periods. These results came from substituting the second set of results for future climate factors with the first set of results, which represent the water demand model.

Chapter 6: Conclusions and Future Works

This chapter summarises the key findings concerning the research goals and describes the conclusions based on the results of this study. In addition, it illustrates the contributions outcome, which come from the combination model of singular spectrum analysis (SSA) and hybrid artificial neural network to forecast municipal water demands considering climate change over the baseline period 1980-2010. Finally, this chapter explains different aspects as recommendations to extend the research work of this thesis in future.

6.1. Conclusions

The need for estimating water demands is an essential component for planning and managing the water resources, because this can help to identify suitable alternative resources to guarantee a balance between water consumption and supply in the future. A high degree of seasonality and trend variability in municipal water demands not only intensifies this need but also creates a demand for predictive methods that are able to accurately deal with these variations. Returning to the findings, which were posed in this study, it is now possible to state that:

Municipal Water Demand Model Development

- Data preprocessing techniques have a significant role to play in the model inputs, specifically in the SSA technique to uncover the stochastic signal and remove the effect of socio-economic factors and noise of long-term municipal water consumption time series. In addition, another key strength of data

preprocessing is that the selection of best model inputs components based on statistical criteria is better than using a trial and error method.

- Maximum temperature (Tmax), solar radiation (Radi) and rainfall (Rain) are reliable and robust predictors to forecast long-term municipal water demands.
- The LSA-ANN algorithm performance is more accurate than the GSA-ANN and PSO-ANN algorithms in terms of water demands estimation accuracy.
- The combination SSA and LSA-ANN model was a reliable, efficient and successful choice for this particular application (water demand forecasting). This technique has resulted in stronger correlation coefficients and less error for simulating municipal water demands based on climatic factors only and for a long-term time series in different two continents.
- The most striking conclusion to emerge from the results is supporting the conceptual premise that municipal water demands are driven by climatic factors in the long-time period, thus decreasing the uncertainties around the impact of climate change.

Climate factors model

- The Long Ashton Research Station Weather Generator (LARS-WG) model provides an excellent performance for generating a maximum temperature, solar radiation and rainfall, based on statistical tests for the baseline period 1980-2010. Therefore, it is a valid model to simulate the future climate variables under different emission scenarios.
- The maximum temperature and solar radiation are expected to increase as we move toward the future, in the same context, the rainfall is likely to decline in amount as we a move toward the future that is impacted by Co_2 emissions. In

addition, the third period and A2 scenario are the worst situations compared with other periods and scenarios.

- We calculate the difference between the stochastic signals of (Tmax, Radi and Rain) for the expected ensemble mean and the baseline period (1980-2010). Then, the results show that the values of Tmax and Radi are rising in general in winter and spring seasons, while they drop in summer and autumn seasons. In the same context, the Rain values have a non-uniform style for all periods and under all emission scenarios. In general, the A2 scenario is the hottest and driest scenario especially in the 3rd period.

Future water demands

- The water percentage demands (WPDs) are expected to increase in winter and decrease in summer for all periods and under all emission scenarios. Besides, WPDs rises or fluctuates upwards in spring while it drops or fluctuates downwards in autumn. The A2 scenario shows the highest positive and negative values compared with A1B and B1 scenarios, in particular, in the third period. In addition, this study has identified that the WPDs values fall between -3.5% and 3% based on all periods and emission scenarios.
- There is no dominant scenario which shows the best or the worst case of water demands based on the mean of seasonal water percentage demands values (MWPDs). The values of MWPDs, in general increase in winter and drop in summer while fluctuating in spring and autumn seasons for all periods and scenarios. The positive peak value happens in winter and in the third period of the A2 scenario. In contrast, the lowest MWPDs value occurs in autumn and in the third period of the A1B scenario.

6.2. Research Novelty and Contribution to Knowledge

Recently, the municipal water prediction under climate change has been considered as one of the promising and significant techniques in the municipal water industry. The development of this methodology introduces a new approach in water management resulting in a sustainable development. This study contributes as follows:

- Introduce novel techniques to forecast municipal water demands for the long term to perform accurate, economical and applicable modelling.
- Forecasting the municipal water demands under different emission scenarios (B1, A1B and A2) over three periods 2011-2030, 2046-2065 and 2080-2099 to investigate the impact of climate change on the municipal water demands for both short and long-term periods.
- Estimating urban water demands improves the water industry; that is, the short-term forecasting enhances the quality of municipal water by improving the scheduling operations of pumping water and decreases the time of retention in storage tanks; while, the long-term forecast is beneficial for planning the water supply system expansion and formulating the policy of water management.
- Provide policy-makers with a clear sight about the impact of climate change on municipal water demands for both short and long-term periods.

6.3. Thesis Recommendations

- Further works can be conducted on this methodology by testing the impact of applying more climate variables depending on the availability of data on water consumption for different locations around the world.

- Implementing the statistical and dynamical downscale approaches to get the future climatic variables for comparing the outcomes and eliminating the uncertainty that results from different assumptions.
- Also, the findings of this study have clarified the relevance of climate change on water consumption, which is significant to both practitioners and policy-makers. However, more research studies are required to develop a deeper understanding of the relationships between climate change and municipal water demands over the long term and at different locations.

References

Abd Ali, J., Hannan, M. & Mohamed, A. 2015. A Novel Quantum-Behaved Lightning Search Algorithm Approach to Improve the Fuzzy Logic Speed Controller for an Induction Motor Drive. *Energies,* 8**,** 13112-13136.

Abdellatif, M., Atherton, W., Alkhaddar, R. M. & Osman, Y. Z. 2015. Quantitative assessment of sewer overflow performance with climate change in northwest England. *Hydrological Sciences Journal,* 60**,** 636-650.

Abrahart, R. J., Kneale, P. E. & See, L. M. 2004. Neural Networks for Hydrological Modelling. UK. Taylor & Francis Group plc.

Adamowski, J., Fung Chan, H., Prasher, S. O., Ozga-Zielinski, B. & Sliusarieva, A. 2012. Comparison of multiple linear and nonlinear regression, autoregressive integrated moving average, artificial neural network, and wavelet artificial neural network methods for urban water demand forecasting in Montreal, Canada. *Water Resources Research,* 48**,** 1-14.

Adamowski, J. F. 2008. Peak daily water demand forecast modeling using artificial neural networks. *Journal of Water Resources Planing and Management,* 134**,** 119-128.

Ahmed, M., Mohamed, A., Homod, R. & Shareef, H. 2016. Hybrid LSA-ANN Based Home Energy Management Scheduling Controller for Residential Demand Response Strategy. *Energies,* 9**,** 716.

Ahmed, M. S., Mohamed, A., Khatib, T., Shareef, H., Homod, R. Z. & Ali, J. A. 2017. Real time optimal schedule controller for home energy management system using new binary backtracking search algorithm. *Energy and Buildings,* 138**,** 215-227.

Ajbar, A. & Ali, E. M. 2015. Prediction of municipal water production in touristic Mecca City in Saudi Arabia using neural networks. *Journal of King Saud University - Engineering Sciences,* 27**,** 83-91.

Al-Bugharbee, H. & Trendafilova, I. 2016. A fault diagnosis methodology for rolling element bearings based on advanced signal pretreatment and autoregressive modelling. *Journal of Sound and Vibration,* 369**,** 246-265.

Al-Zahrani, M. A. & Abo-Monasar, A. 2015. Urban Residential Water Demand Prediction Based on Artificial Neural Networks and Time Series Models. *Water Resources Management,* 29**,** 3651-3662.

Araghinejad, S. 2014. Data-Driven Modeling: Using MATLAB® in Water Resources and Environmental Engineering. USA. Springer.

ASCE, American Society of Civil Engineers, 2000 *Artificial neural networks in hydrology. I: preliminary concepts, Journal of Hydrologic Egineering.* April 2000,

Azadeh, A., Ghaderi, S. F. & Sohrabkhani, S. 2007. Forecasting electrical consumption by integration of Neural Network, time series and ANOVA. *Applied Mathematics and Computation,* 186**,** 1753-1761.

Azadeh, A., Neshat, N. & Hamidipour, H. 2012. Hybrid Fuzzy Regression–Artificial Neural Network for Improvement of Short-Term Water Consumption Estimation and Forecasting in Uncertain and Complex Environments: Case of a Large Metropolitan City. *Journal of Water Resources Planning and Management,* 138**,** 71-75.

Babel, M. S., Gupta, A. D. & Pradhan, P. 2007. A multivariate econometric approach for domestic water demand modeling: An application to Kathmandu, Nepal. *Water Resources Management,* 21**,** 573-589.

Babel, M. S. & Shinde, V. R. 2011. Identifying prominent explanatory variables for water demand prediction using artificial neural networks: a case study of Bangkok. *Water Resources Management,* 25**,** 1653-1676.

Bakker, M., Van Duist, H., Van Schagen, K., Vreeburg, J. & Rietveld, L. Improving the performance of water demand forecasting models by using weather input. 12th International Conference on Computing and Control for the Water Industry, 1-1-2014 2014. 93-102.

Baratta, D., Cicioni, G., Masulli, F. & Studer, L. 2003. Application of an ensemble technique based on singular spectrum analysis to daily rainfall forecasting. *Neural Networks,* 16**,** 375-387.

Basheer, I. A. & Hajmeer, M. 2000. Artificial neural networks: fundamentals, computing, design, and application. *Journal of Microbiological Methods,* 43**,** 3-31.

Behboudian, S., Tabesh, M., Falahnezhad, M. & Ghavanini, F. A. 2014. A long-term prediction of domestic water demand using preprocessing in artificial neural network. *Journal of Water Supply: Research and Technology—AQUA,* 63**,** 31-42.

Bennett, C., Stewart, R. A. & Beal, C. D. 2013. ANN-based residential water end-use demand forecasting model. *Expert Systems with Applications,* 40**,** 1014-1023.

Bhavani, R. 2013. Comparision of Mean and Weighted Annual Rainfall in Anantapuram District. *International Journal of Innovative Research in Science, Engineering and Technology,* 2**,** 7.

Bland, J. M. & Altman, D. G. 2007. Agreement between methods of measurement with multiple observations per individual. *J Biopharm Stat,* 17**,** 571-82.

Borbora, J. & Das, A. K. 2014. Summertime Urban Heat Island study for Guwahati City, India. *Sustainable Cities and Society,* 11**,** 61-66.

Bougadis, J., Adamowski, K. & Diduch, R. 2005. Short-term municipal water demand forecasting. *Hydrological Processes,* 19**,** 137-148.

Box, G. E. P., Jenkins, G. M., Reinsel, G. C. & Ljung, G. M. 2016. Time Series Analysis Forecasting: Forecasting and Control. Canada. John Wiley & Sons, Inc., Hoboken, New Jersey.

Brentan, B. M., Luvizotto Jr, E., Herrera, M., Izquierdo, J. & Pérez-García, R. 2017. Hybrid regression model for near real-time urban water demand forecasting. *Journal of Computational and Applied Mathematics,* 309**,** 532-541.

Campisi-Pinto, S., Adamowski, J. & Oron, G. 2012. Forecasting Urban Water Demand Via Wavelet-Denoising and Neural Network Models. Case Study: City of Syracuse, Italy. *Water Resources Management,* 26**,** 3539-3558.

Chaker, A., El-Fadl, K., Chamas, L. & Hatjian, B. 2006. A review of strategic environmental assessment in 12 selected countries. *Environmental Impact Assessment Review,* 26**,** 15-56.

Chen, H., Guo, J., Zhang, Z. & Xu, C.-Y. 2012. Prediction of temperature and precipitation in Sudan and South Sudan by using LARS-WG in future. *Theoretical and Applied Climatology,* 113**,** 363-375.

Chen, J., Brissette, F. P. & Leconte, R. 2011. Uncertainty of downscaling method in quantifying the impact of climate change on hydrology. *Journal of Hydrology,* 401**,** 190-202.

Cutore, P., Campisano, A., Kapelan, Z., Modica, C. & Savic, D. 2008. Probabilistic prediction of urban water consumption using the SCEM-UA algorithm. *Urban Water Journal,* 5**,** 125-132.

Daniels, A. E., Morrison, J. F., Joyce, L. A., Crookston, N. L., Chen, S. C. & Mcnully, S. G. 2012. Climate projections FAQ. United States Department of Agriculture / Forest Service.

Davies, E. G. R. & Simonovic, S. P. 2011. Global water resources modeling with an integrated model of the social–economic–environmental system. *Advances in Water Resources,* 34**,** 684-700.

Deng, X., Huang, J., Rozelle, S., Zhang, J. & Li, Z. 2015. Impact of urbanization on cultivated land changes in China. *Land Use Policy,* 45**,** 1-7.

Diebel, J., Norda, N. & Kretchmer, O. 2013. *Average Weather in Columbia Missouri, United States* [Online]. United States Cedar Lake Ventures, Inc. Available: https://weatherspark.com/ [Accessed 23/02 2018].

Donkor, E. A., Mazzuchi, T. H., Soyer, R. & Roberson, J. A. 2014. Urban water demand forecasting: review of methods and models. *Journal of Water Resources Planing and Management,* 140**,** 146-159.

Duman, S., Güvenç, U., Sönmez, Y. & Yörükeren, N. 2012. Optimal power flow using gravitational search algorithm. *Energy Conversion and Management,* 59**,** 86-95.

Eberhart, R. C. & Shi, Y. Tracking and optimizing dynamic systems with particle swarms. Evolutionary Computation, 27-30 May 2001 2001 USA. IEEE, 94-100.

Ethaib, S., Omar, R., Mazlina, M. K. S., Radiah, A. B. D. & Syafiie, S. 2016. Development of a hybrid PSO–ANN model for estimating glucose and xylose yields for microwave-assisted pretreatment and the enzymatic hydrolysis of lignocellulosic biomass. *Neural Computing and Applications*.

Fenta Mekonnen, D. & Disse, M. 2018. Analyzing the future climate change of Upper Blue Nile River basin using statistical downscaling techniques. *Hydrology and Earth System Sciences,* 22**,** 2391-2408.

Ferguson, B. C., Brown, R. R., Frantzeskaki, N., De Haan, F. J. & Deletic, A. 2013a. The enabling institutional context for integrated water management: lessons from Melbourne. *Water Research,* 47**,** 7300-14.

Ferguson, B. C., Frantzeskaki, N. & Brown, R. R. 2013b. A strategic program for transitioning to a Water Sensitive City. *Landscape and Urban Planning,* 117**,** 32-45.

Firat, M., Turan, M. E. & Yurdusev, M. A. 2010. Comparative analysis of neural network techniques for predicting water consumption time series. *Journal of Hydrology,* 384**,** 46-51.

Firat, M., Yurdusev, M. A. & Turan, M. E. 2009. Evaluation of artificial neural network techniques for municipal water consumption modeling. *Water Resources Management,* 23**,** 617-632.

Fogden, J. & Wood, G. 2009. Access to Safe Drinking Water and Its Impact on Global Economic Growth. *HaloSource Inc*.

Gato, S. 2006. *Forecasting Urban Residential Water Demand.* PhD, RMIT University.

Gato, S., Jayasuriya, N. & Hadgraft, R. 2005. A simple time series approach to modelling urban water demand. *Australian Journal of Water Resources,* 8**,** 153-164.

Gato, S., Jayasuriya, N. & Roberts, P. 2007a. Forecasting residential water demand: case study. *JOURNAL OF WATER RESOURCES PLANNING AND MANAGEMENT,* 133**,** 309-319.

Gato, S., Jayasuriya, N. & Roberts, P. 2007b. Temperature and rainfall thresholds for base use urban water demand modelling. *Journal of Hydrology,* 337**,** 364-376.

Gharghan, S. K., Nordin, R. & Ismail, M. 2016a. A Wireless Sensor Network with Soft Computing Localization Techniques for Track Cycling Applications. *Sensors (Basel),* 16.

Gharghan, S. K., Nordin, R., Ismail, M. & Ali, J. A. 2016b. Accurate wireless sensor localization technique based on hybrid pso-ann algorithm for indoor and outdoor track cycling. *Institute of Electrical and Electronics Engineers Sensors Journal,* 16**,** 529-541.

Ghiassi, M., Zimbra, D. K. & Saidane, H. 2008. Urban water demand forecasting with a dynamic artificial neural network model. *Journal of Water Resources Planing and Management,* 134**,** 138-146.

Ghil, M., Allen, M. R., Dettinger, M. D., Ide, K., Kondrashov, D., Mann, M. E., Robertson, A. W., Saunders, A., Tian, Y., Varadi, F. & Yiou, P. 2002. Advanced spectral methods for climatic time series. *Reviews of Geophysics,* 40**,** 3-1-3-41.

Ghodsi, M., Hassani, H., Sanei, S. & Hicks, Y. 2009. The use of noise information for detection of temporomandibular disorder. *Biomedical Signal Processing and Control,* 4**,** 79-85.

Golyandina, N., Nekrutkin, V. & Zhigljavsky, A. 2001. Analysis of Time Series Structure: SSA and Related Techniques. Chapman & Hall/CRC.

Hagan, M. T., Demuth, H. B., Beale, M. H. & Jesús, O. D. 2014. Neural Network Design. 1012.2nd Edtion.

Hassani, H., Heravi, S. & Zhigljavsky, A. 2009. Forecasting European industrial production with singular spectrum analysis. *International Journal of Forecasting,* 25**,** 103-118.

Hassani, H., Webster, A., Silva, E. S. & Heravi, S. 2015. Forecasting U.S. Tourist arrivals using optimal Singular Spectrum Analysis. *Tourism Management,* 46**,** 322-335.

IPCC, The Intergovernmental Panel on Climate Change (IPCC), 2007 *Climate Change 2007: Impacts, Adaptation and Vulnerability*

Jacobs & St. Louis, M. 2015. Long Range Water System Study. Water & Light Department. Columbia, Missouri, USA.

Jain, A. & Ormsbee, L. E. 2002. Short-term water demand forecast modeling techniques conventional methods versus AI. *American Water Works Association,* 94**,** 64-72.

Jain, A., Varshney, A. K. & Joshi, U. C. 2001. Short-term water demand forecast modelling at IIT Kanpur using artificial neural networks. *Water Resources Management,* 15**,** 299–321.

Jayaraman, T. 2015. The Paris Agreement on Climate Change: Background, Analysis, and Implications. *Review of Agrarian Studies,* 5**,** 42-59.

Jewitt, D., Erasmus, B. F. N., Goodman, P. S., O'connor, T. G., Hargrove, W. W., Maddalena, D. M. & Witkowski, E. T. F. 2015. Climate-induced change of environmentally defined floristic domains: A conservation based vulnerability framework. *Applied Geography,* 63**,** 33-42.

Kadiyala, M. D., Nedumaran, S., Singh, P., S, C., Irshad, M. A. & Bantilan, M. C. 2015. An integrated crop model and GIS decision support system for assisting

agronomic decision making under climate change. *Science of the Total Environment,* 521-522**,** 123-34.

Kanzow, C., Yamashita, N. & Fukushima, M. 2004. Levenberg–Marquardt methods with strong local convergence properties for solving nonlinear equations with convex constraints. *Journal of Computational and Applied Mathematics,* 172**,** 375-397.

Khan, M. a. R. & Poskitt, D. S. 2017. Forecasting stochastic processes using singular spectrum analysis: Aspects of the theory and application. *International Journal of Forecasting,* 33**,** 199-213.

Kilundu, B., Chiementin, X. & Dehombreux, P. 2011. Singular Spectrum Analysis for Bearing Defect Detection. *Journal of Vibration and Acoustics,* 133**,** 1-7.

Kingston, G. B., Maier, H. R. & Lambert, M. F. 2005. Calibration and validation of neural networks to ensure physically plausible hydrological modeling. *Journal of Hydrology,* 314**,** 158-176.

Kotsiantis, S. B., Kanellopoulos, D. & Pintelas, P. E. 2006. Data preprocessing for supervised leaning. *International Journal of Computer Science,* 1**,** 111-117.

Lavanya, D. & Udgata, S. K. 2011. Swarm intelligence based localization in wireless sensor networks. *Multi-disciplinary Trends in Artificial Intelligence.* Springer-Verlag Berlin Heidelberg.

Li, W., Xie, Y. & Hao, F. 2014. Applying an improved rapid impact assessment matrix method to strategic environmental assessment of urban planning in China. *Environmental Impact Assessment Review,* 46**,** 13-24.

Liu, J., Savenije, H. H. G. & Xu, J. 2003. Forecast of water demand in Weinan City in China using WDF-ANN model. *Physics and Chemistry of the Earth, Parts A/B/C,* 28**,** 219-224.

Maier, H. R. & Dandy, G. C. 2000. Neural networks for the prediction and forecasting of water resources variables: a review of modelling issues and applications. *Environmental Modelling & Software,* 15**,** 101–124.

Marlow, D. R., Moglia, M., Cook, S. & Beale, D. J. 2013. Towards sustainable urban water management: a critical reassessment. *Water Research,* 47**,** 7150-61.

Marques, C. a. F., Ferreira, J. A., Rocha, A., Castanheira, J. M., Melo-Gonçalves, P., Vaz, N. & Dias, J. M. 2006. Singular spectrum analysis and forecasting of hydrological time series. *Physics and Chemistry of the Earth, Parts A/B/C,* 31**,** 1172-1179.

Masanganise, J., Mapuwei, T. W., Magodora, M. & Basira, K. 2014. Multi-model projections of temperature and rainfall under representative concentration pathways in Zimbabwe. *International Journal of Science and Technology,* 3**,** 229-240.

Mohammadi, K., Eslami, H. R. & Dardashti, S. D. 2005. Comparison of Regression, ARIMA and ANN Models for Reservoir Inflow Forecasting using Snowmelt Equivalent (a Case study of Karaj). *Journal of Agricultural Science and Technology,* 7**,** 17-30.

Mohammed, J. R. & Ibrahim, H. M. 2013. Multilayer perceptron-multiactivation function artificial neural network model for municipal water demand forecasting. *Asian Research Publishing Network Journal of Engineering and Applied Sciences,* 8**,** 1119-1138.

Msiza, I. S., Nelwamondo, F. V. & Marwala, T. Water demand forecasting using multi-layer perceptron and radial basis functions. International Joint Conference on Neural Networks, August 12-17, 2007 2007 Orlando, Florida, USA. Institute of Electrical and Electronics Engineers.

Msiza, I. S., Nelwamondo, F. V. & Marwala, T. 2008. Water demand prediction using artificial neural networks and support vector regression. *JOURNAL OF COMPUTERS,* 3**,** 1-8.

Mutlag, A., Mohamed, A. & Shareef, H. 2016. A Nature-Inspired Optimization-Based Optimum Fuzzy Logic Photovoltaic Inverter Controller Utilizing an eZdsp F28335 Board. *Energies,* 9.

Mutlu, E., Chaubey, I., Hexmoor, H. & Bajwa, S. G. 2008. Comparison of artificial neural network models for hydrologic predictions at multiple gauging stations in an agricultural watershed. *Hydrological Processes,* 22**,** 5097-5106.

MW, Melbourne Water, 2017 *Corporate Plan 2016/17 to 2020/21.* Australia.

Nasseri, M., Moeini, A. & Tabesh, M. 2011. Forecasting monthly urban water demand using Extended Kalman Filter and Genetic Programming. *Expert Systems with Applications,* 38**,** 7387-7395.

Nawi, N. M., Atomi, W. H. & Rehman, M. Z. The effect of data pre-processing on optimized training of artificial neural networks. The 4th International Conference of Electrical Engineering and Informatics, 2013. Elsevier Ltd., 32-39.

Osman, Y. Z., Abdellatif, M., Al-Ansari, N., Knutsson, S. & Jawad, S. 2017. CLIMATE CHANGE AND FUTURE PRECIPITATION IN AN ARID ENVIRONMENT OF THE MIDDLE EAST: CASE STUDY OF IRAQ. *Journal of Environmental Hydrology,* 25**,** 1-18.

Pallant, J. 2011. SPSS SURVIVAL MANUAL : A step by step guide to data analysis using SPSS.Fourth, Australia. Allen & Unwin.

Partidário, M. D. R. 2012. Strategic Environmental Assessment Better Practice Guide - methodological guidance for strategic thinking in SEA. Lisbon. Portuguese Environment Agency and Redes Energéticas Nacionais (REN), SA.

Partidário, M. R. 2007. Scales and associated data — What is enough for SEA needs? *Environmental Impact Assessment Review,* 27**,** 460-478.

Payal, A., Rai, C. S. & Reddy, B. V. R. 2015. Analysis of Some Feedforward Artificial Neural Network Training Algorithms for Developing Localization Framework in Wireless Sensor Networks. *Wireless Personal Communications,* 82**,** 2519-2536.

Polom˘Cic´, D., Gligoric´, Z., Bajic´, D. & Cvijovic´, C. E. 2017. A Hybrid Model for Forecasting Groundwater Levels Based on Fuzzy C-Mean Clustering and Singular Spectrum Analysis. *Water,* 9.

Räisänen, J. 2015. Twenty-first century changes in snowfall climate in Northern Europe in ENSEMBLES regional climate models. *Climate Dynamics,* 46**,** 339-353.

Rashedi, E., Nezamabadi-Pour, H. & Saryazdi, S. 2009. GSA: A Gravitational Search Algorithm. *Information Sciences,* 179**,** 2232-2248.

Rini, D. P., Shamsuddin, S. M. & Yuhaniz, S. S. 2011. Particle swarm optimization: technique, system and challenges. *International Journal of Computer Applications,* 14**,** 19-27.

Rocco S, C. M. 2013. Singular spectrum analysis and forecasting of failure time series. *Reliability Engineering & System Safety,* 114**,** 126-136.

Roy, U. & Majumder, M. 2016. Vulnerability of Watersheds to Climate Change Assessed by Neural Network and Analytical Hierarchy Process. 3.

Salathe, E. P., Mote, P. W. & Wiley, M. W. 2007. Review of scenario selection and downscaling methods for the assessment of climate change impacts on

hydrology in the United States pacific northwest. *International Journal of Climatology,* 27**,** 1611-1621.

Sarker, R. C., Gato, S. & Imteaz, M. Temperature and rainfall thresholds corresponding to water consumption in Greater Melbourne, Australia. 20th International Congress on Modelling and Simulation, 1–6 December 2013 2013 Adelaide, Australia. Modelling and Simulation Society of Australia and New Zealand, 2576-2582.

Sayadi, A., Monjezi, M., Talebi, N. & Khandelwal, M. 2013. A comparative study on the application of various artificial neural networks to simultaneous prediction of rock fragmentation and backbreak. *Journal of Rock Mechanics and Geotechnical Engineering,* 5**,** 318-324.

Sebri, M. 2013. ANN versus SARIMA models in forecasting residential water consumption in Tunisia. *Journal of Water, Sanitation and Hygiene for Development,* 3.

Semenov, M. A. 2008. Simulation of extreme weather events by a stochastic weather generator. *Climate Research,* 35**,** 203-212.

Semenov, M. A. & Barrow, E. M. 2002. LARS-WG - A Stochastic Weather Generator for Use in Climate Impact Studies. Version 3.0 User Manual. Rothamsted Research, Harpenden, Hertfordshire AL5 2JQ, UK, 27 p.

Semenov, M. A., Pilkington-Bennett, S. & Calanca, P. 2013. Validation of ELPIS 1980-2010 baseline scenarios using the observed European Climate Assessment data set. *Climate Research,* 57**,** 1-9.

Shahin, M. A., Jaksa, M. B. & Maier, H. R. 2008. State of the Art of Artificial Neural Networks in Geotechnical Engineering. *Electronic Journal of Geotechnical Engineering,* 13**,** 1-26.

Shareef, H., Ibrahim, A. A. & Mutlag, A. H. 2015. Lightning search algorithm. *Applied Soft Computing,* 36**,** 315-333.

Shuaib, M., Kalavathi, S. M. & Rajan, C. A., C. 2015. Optimal capacitor placement in radial distribution system using Gravitational Search Algorithm. *International Journal of Electrical Power & Energy Systems,* 64**,** 384-397.

Sirjani, R. & Okonkwo, E. C. A New Wind Power Model U sing the Lightning Search Algorithm. 13-14 Oct. 2016 2016 Nicosia, Cyprus. IEEE, 93-97.

Tabachnick, B. G. & Fidell, L. S. 2013. Using Multivariate Statistics.Sixth, United States of America. Pearson Education, Inc.

Trzaska, S. & Schnarr, E. 2014. A review of downscaling methods for climate change projections. United States Agency for International Development. United States.

UNDP, United Nations Development Programme, 2012 *Overview of Linkages Between Gender and Climate Change*. New York, USA.

UNDP, United Nations Development Programme, 2013 *Water Governance in the Arab Region Managing Scarcity and Securing the Future*. Republic of Lebanon.

UNFCCC, United Nations Framework Convention on Climate Change, 2007 *Climate Change: Impacts, Vulnerabilities and Adaptation in Developing Countries* Bonn, Germany.

Urich, C. & Rauch, W. 2014. Exploring critical pathways for urban water management to identify robust strategies under deep uncertainties. *Water Research,* 66**,** 374-89.

Van Leeuwen, C. J., Frijns, J., Van Wezel, A. & Van De Ven, F. H. M. 2012. City blueprints: 24 indicators to assess the sustainability of the urban water cycle. *Water Resources Management,* 26**,** 2177-2197.

Vijaya Kumar, J., Vinod Kumar, D. M. & Edukondalu, K. 2013. Strategic bidding using fuzzy adaptive gravitational search algorithm in a pool based electricity market. *Applied Soft Computing,* 13**,** 2445-2455.

Walker, D., Creaco, E., Vamvakeridou-Lyroudia, L., Farmani, R., Kapelan, Z. & Savić, D. Forecasting domestic water consumption from smart meter readings using statistical methods and artificial neural networks. Procedia Engineering, 2015. Elsevier Ltd., 1419-1428.

Wang, Y., Niu, D. & Ma, X. 2010. Optimizing of SVM with hybrid PSO and genetic algorithm in power load forecasting. *Journal of Networks,* 5**,** 1192-1200.

WB, World Bank, 2005 *Integrating Environmental Considerations in Policy Formulation: Lessons from Policy-Based SEA Experience*. Washington, DC 20433 USA.

Xiong, H., Pandey, G., Steinbach, M. & Kumar, V. 2006. Enhancing data analysis with noise removal. *Institute of Electrical and Electronics Engineers Transactions on Knowledge and Data Engineering,* 18**,** 304-319.

Yurdusev, M. A., Firat, M. & Turan, M. E. 2010. Generalized regression neural networks for municipal water consumption prediction. *Journal of Statistical Computation and Simulation,* 80**,** 477-478.

YVW, Yarra Valley Water Corporation, 2017 *Yarra Valley Annual Report Water 2016-2017.* Australia.

Zhang, G. P. & Qi, M. 2005. Neural network forecasting for seasonal and trend time series. *European Journal of Operational Research,* 160**,** 501-514.

Zhang, J. J., Song, R., Bhaskar, N. R. & French, M. N. Short-term water demand forecasting: a case study. 8th Annual Water Distribution Systems Analysis Symposium, August 27-30, 2006 2006 Cincinnati, Ohio, USA. United States, 1-14.

Zhao, W. 2011. Adaptive Image Enhancement Based on Gravitational Search Algorithm. *Procedia Engineering,* 15**,** 3288-3292.

Zhoua, S. L., Mcmahon, T. A., Walton, A. & Lewis, J. 2000. Forecasting daily urban water demand: a case study of Melbourne. *Journal of Hydrology,* 236**,** 153–164.

Zhu, X. & Chen, J. Urban Water Consumption Forecast Based on PQPSO-LSSVM. Ninth International Conference on Natural Computation (ICNC), 2013. IEEE, 834-837.

Zhu, X. & Xu, B. Urban Water Consumption Forecast Based on QPSO-RBF Neural Network. Eighth International Conference on Computational Intelligence and Security, 2012. IEEE, 233-236.

Zubaidi, S. L., Dooley, J., Alkhaddar, R. M., Abdellatif, M., Al-Bugharbee, H. & Ortega-Martorell, S. 2018. A Novel approach for predicting monthly water demand by combining singular spectrum analysis with neural networks. *Journal of Hydrology,* 561**,** 136-145.

Appendices

Appendix4-A The data preprocessing results for Columbia City.

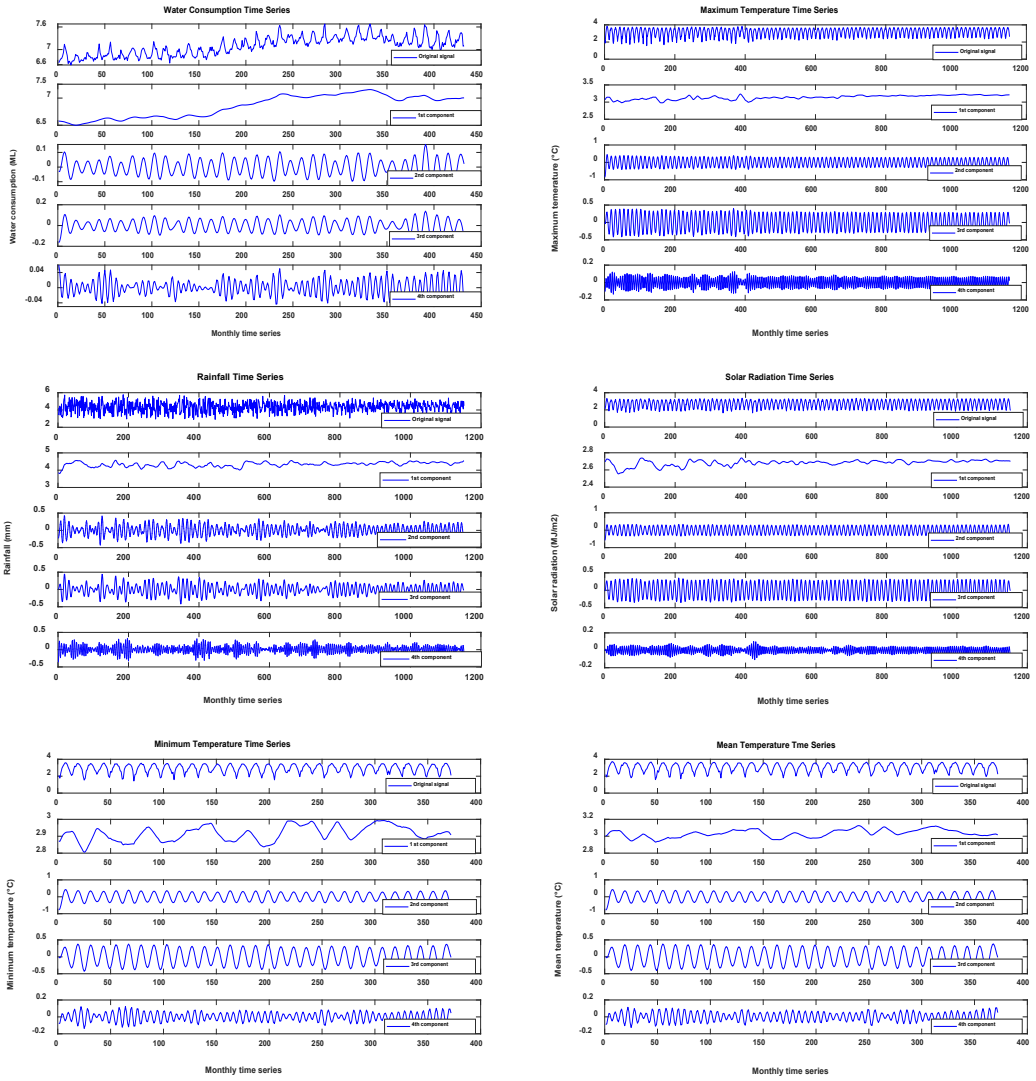

Figure 4-A.1: Original signal and the first four components obtained by SSA

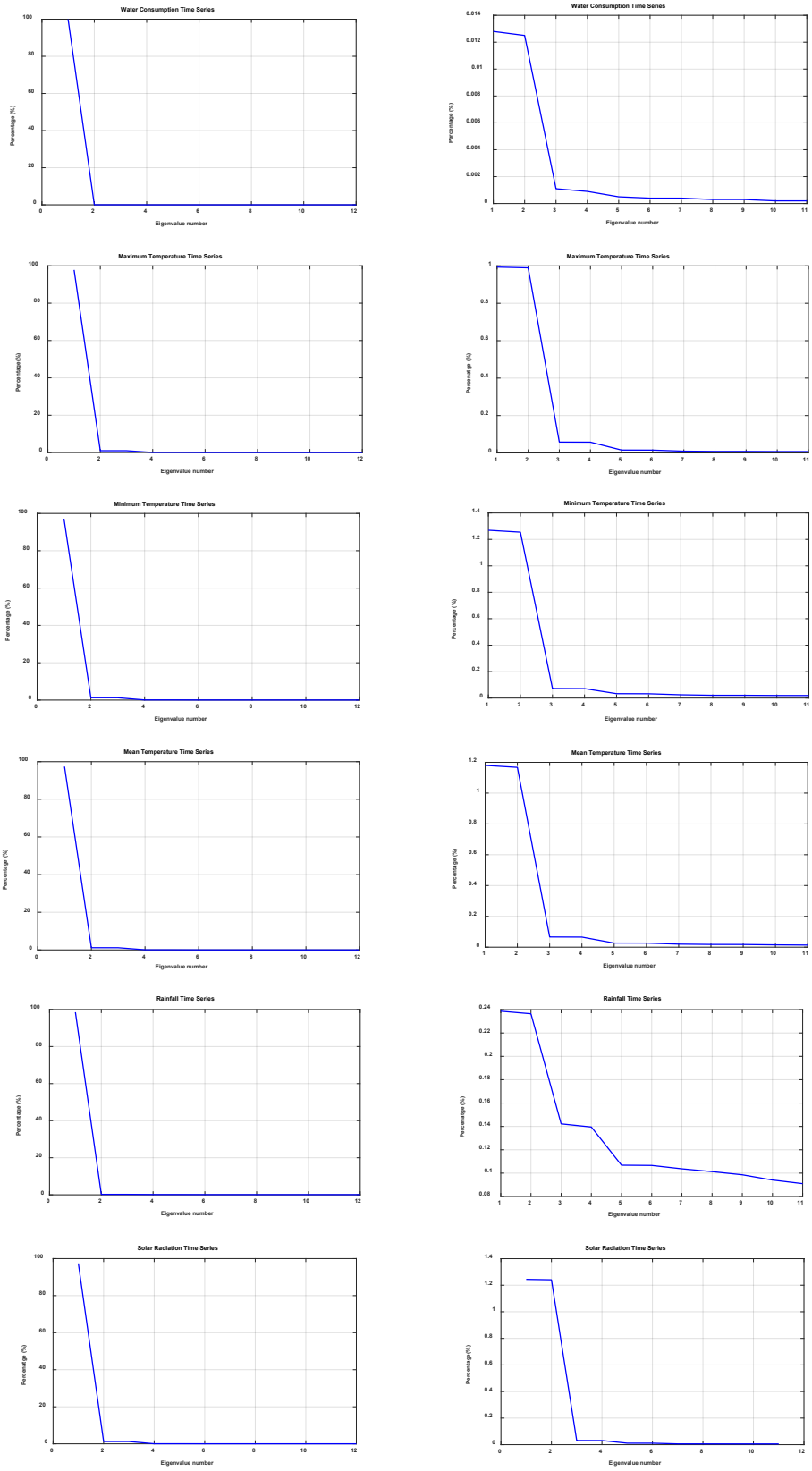

Figure 4-A.2: Eigenvalues of water consumption and climate factors time series

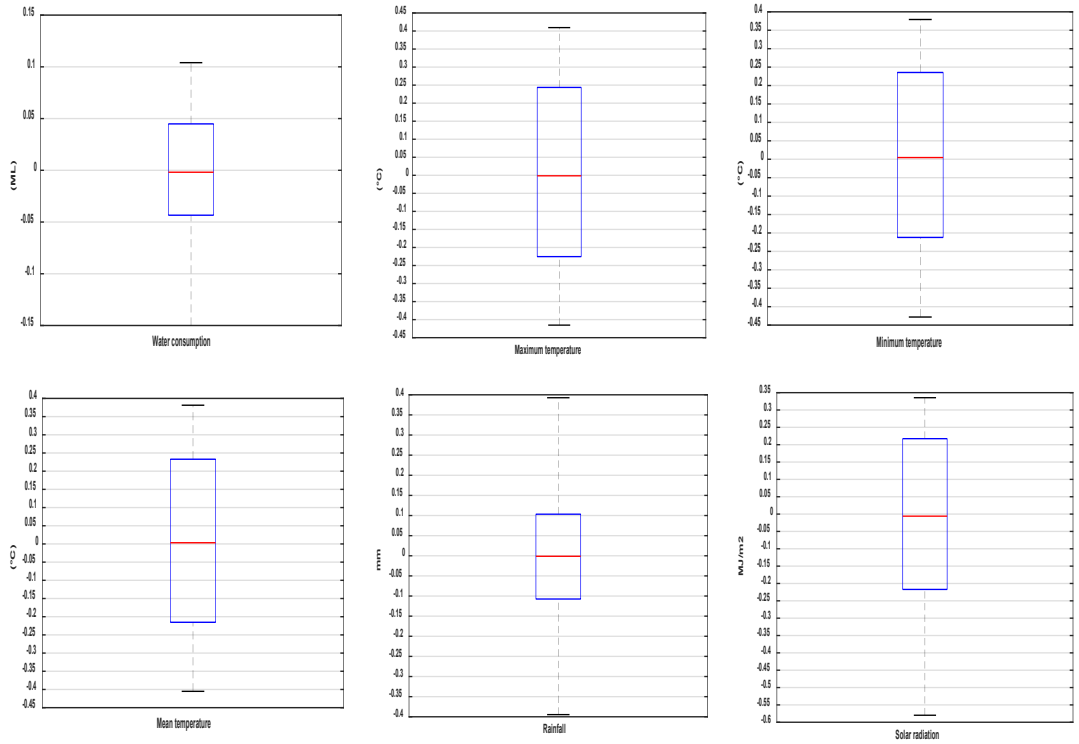

Figure 4-A.3: The monthly box plot of the stochastic signal for water consumption and all climate factors

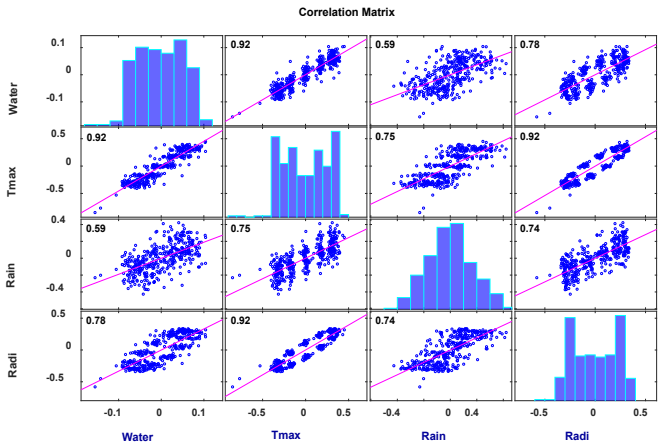

Figure 4-A.4: Correlations between water consumption and climate factors

Table 4-A.1: Correlation matrix analysis results for raw and stochastic data

Data	Municipal water	Maximum temperature	Rainfall	Radiation
Raw	1	0.42**	0.005**	0.37**
Stochastic		0.92**	0.59**	0.78**

**Correlation is significant at the 0.01 level (2-tailed).

Appendix 4-B

The average monthly data for water consumption and all climate factors after normalisation and cleaning (Melbourne and Columbia Cities).

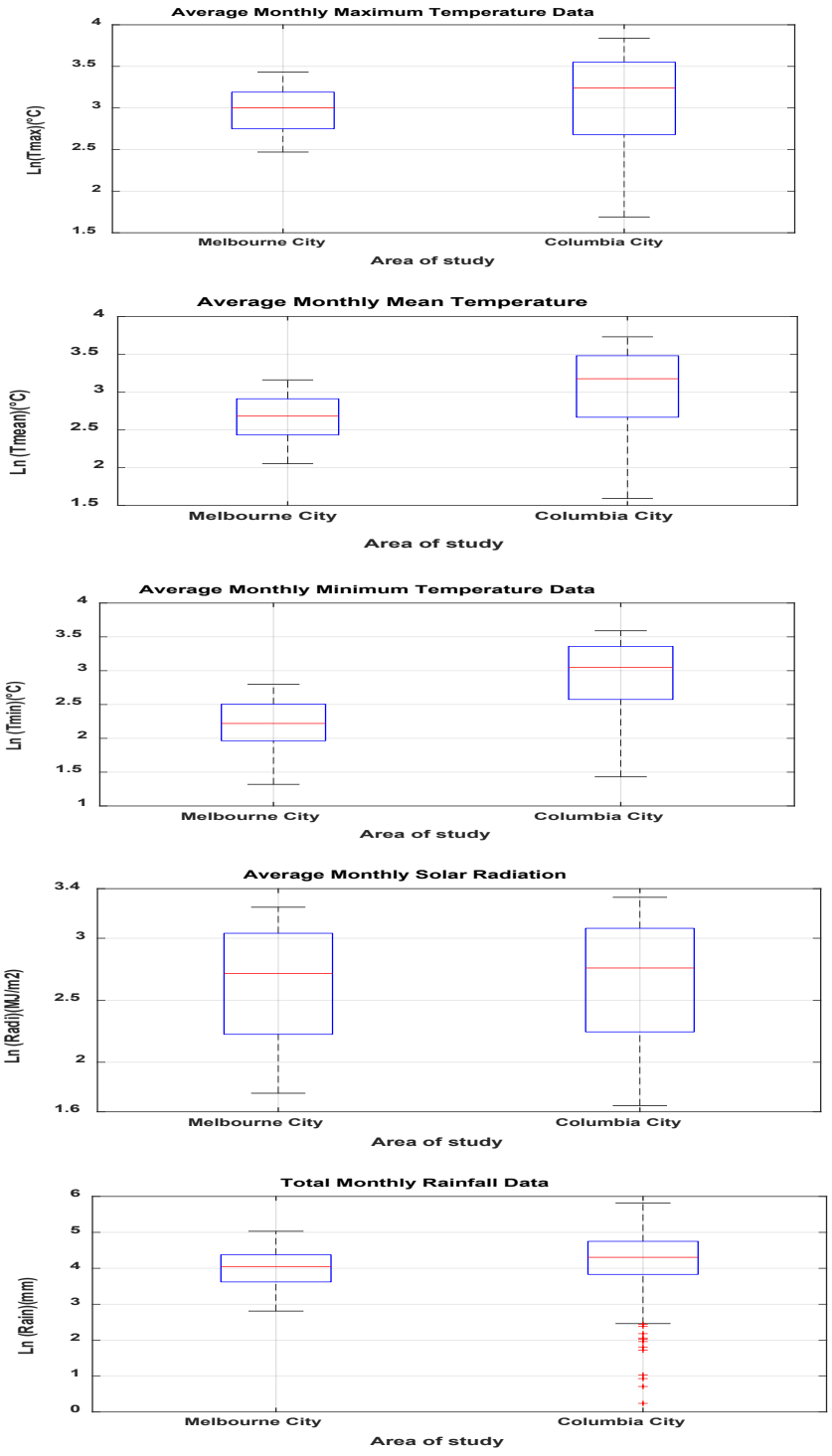

Figure 4-B.1: The average monthly data for climate factors after normalisation

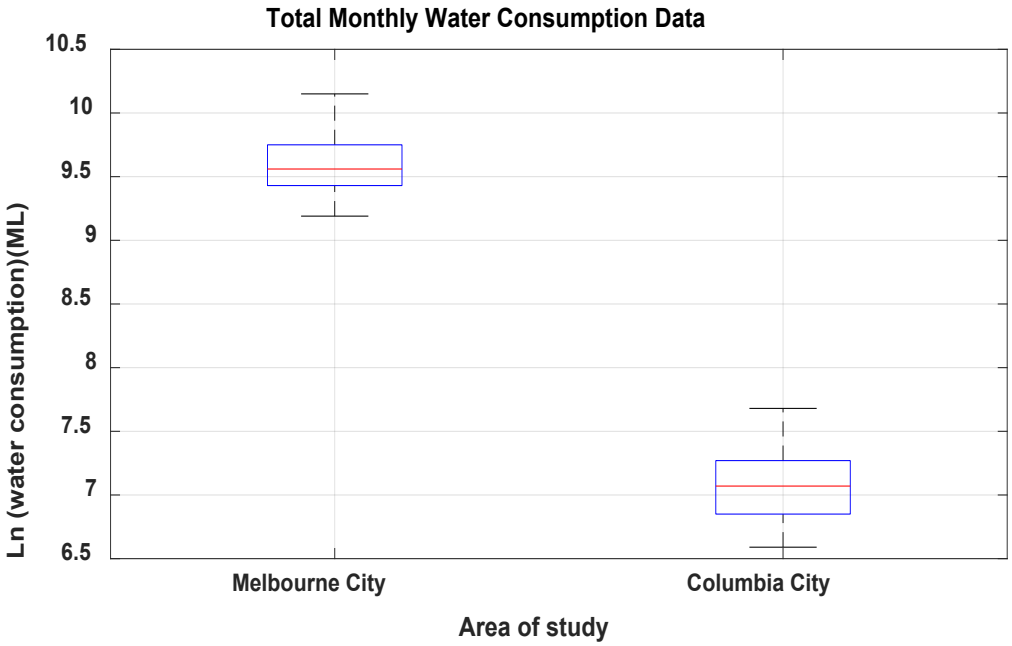

Figure 4-B.2: The average monthly data for water consumption after normalisation

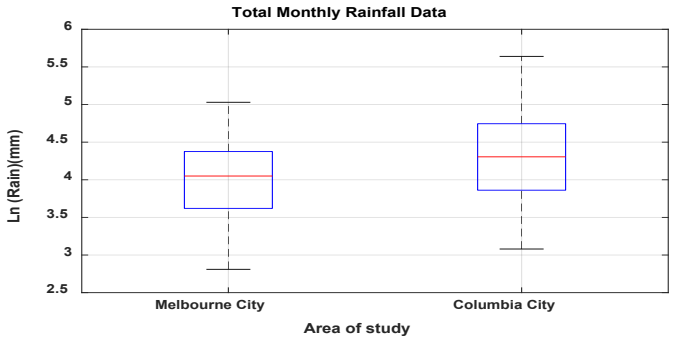

Figure 4-B.3: The average monthly data for rainfall after normalisation and cleaning data

Appendix 4-C

The graphs of eigenvalues spectra for the water consumption and climate factors time series (Melbourne City).

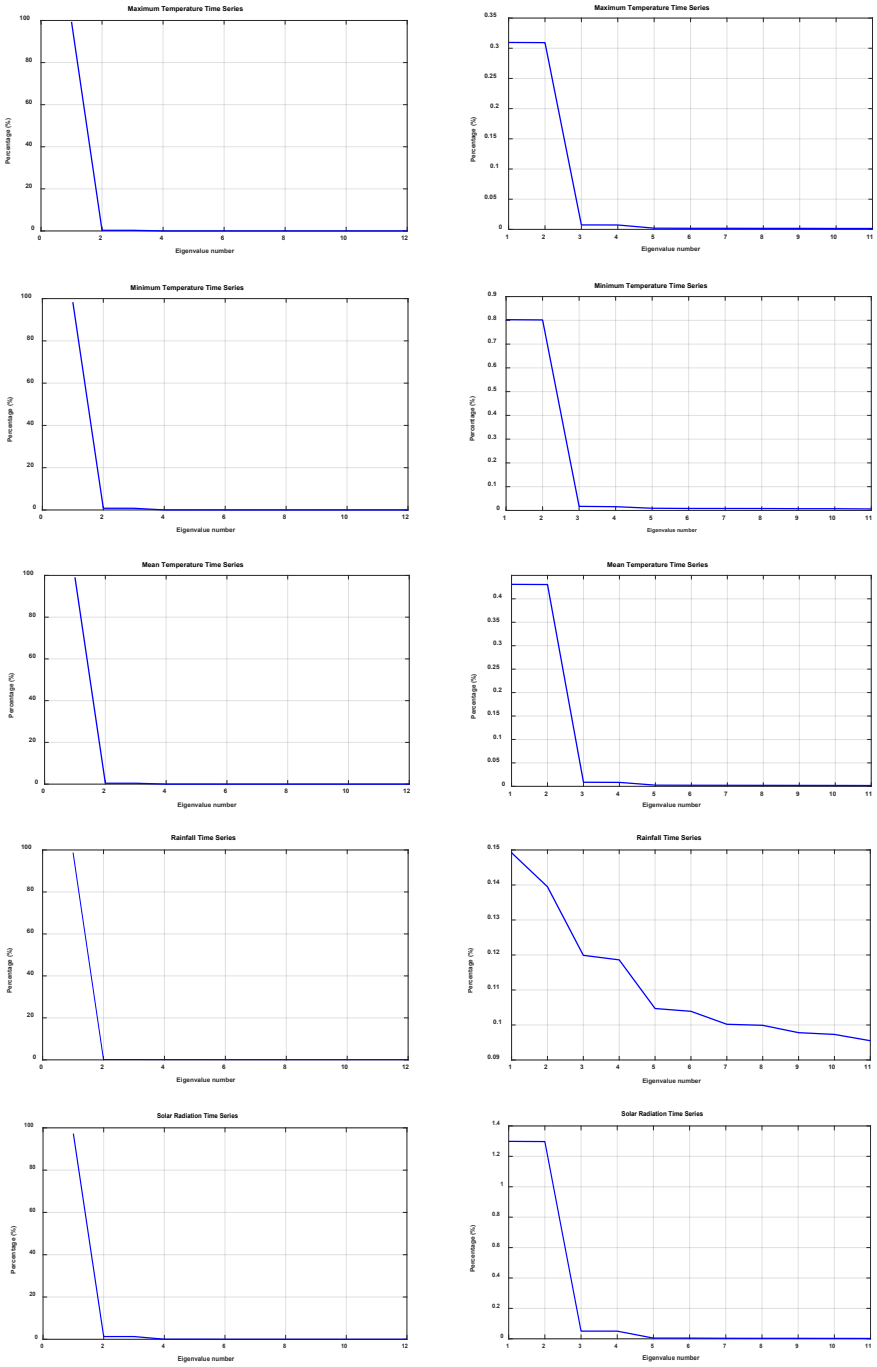

Figure 4-B.1: Eigenvalues of water consumption and climate factors time series

Appendix 5-A

The results for developing municipal water demands model for Columbia City.

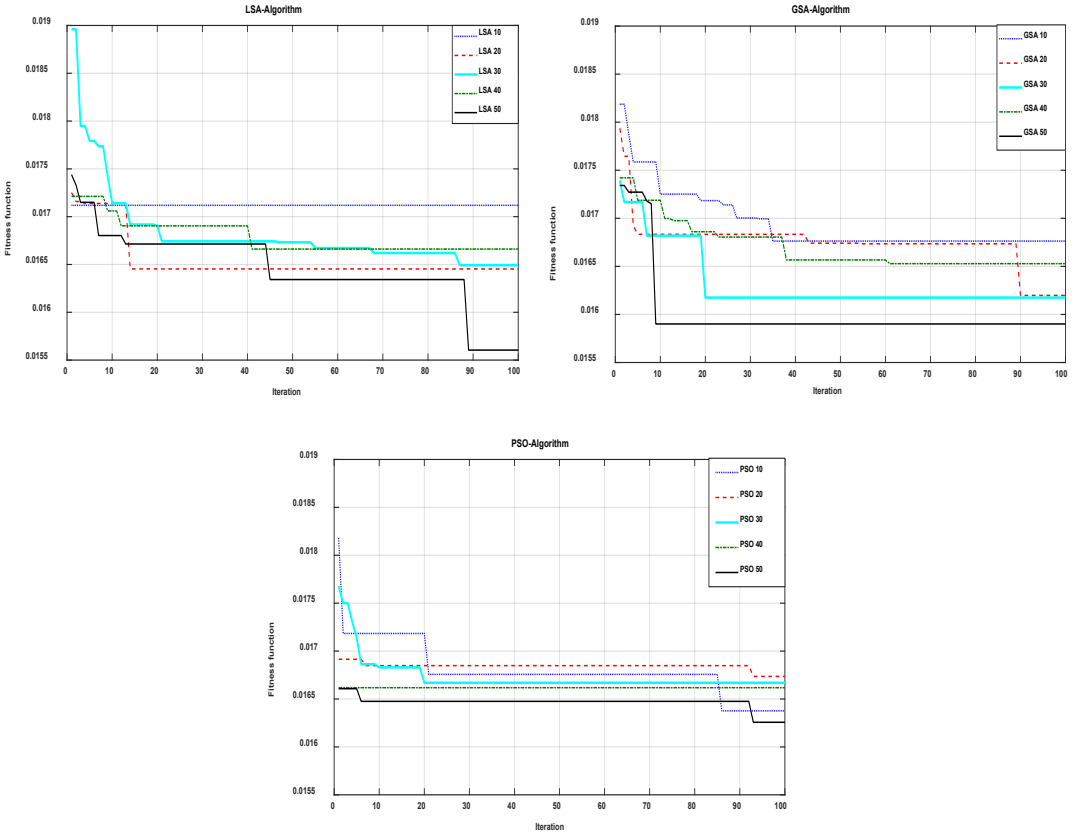

Figure 5-A.1: Fitness function for various populations using the computational intelligence algorithms

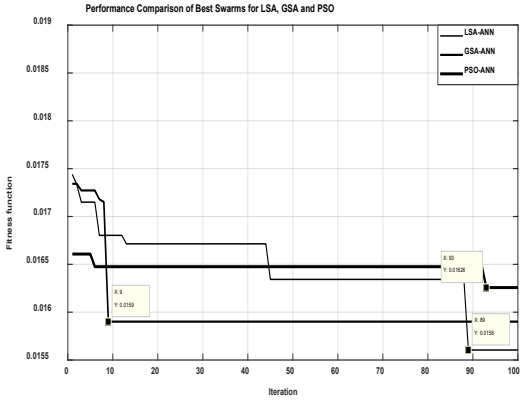

Figure 5-A.2: Comparison of the performance of the best swarm size of LSA, GSA and PSA algorithms

Table 5-A.1: ANN-designed parameters

Parameter	Value	Type
Number of inputs	3	As presented in Appendix 4-A
Number of outputs	1	Our target, which is water demand
Number of hidden layers	2	As used in Zubaidi et al. (2018)
Number of neurons in hidden layer N1	5	Estimated by LSA
Number of neurons in hidden layer N2	5	Estimated by LSA
Learning rate coefficient	0.4500	Estimated by LSA

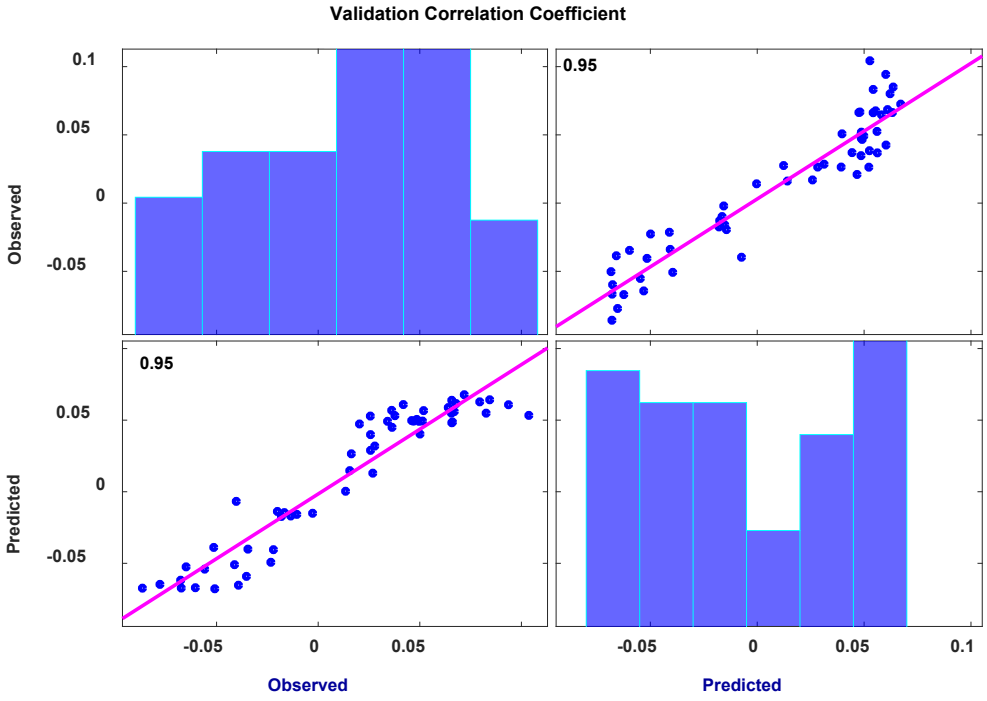

Figure 5-A.3: LSA-ANN algorithm performance for the validation data

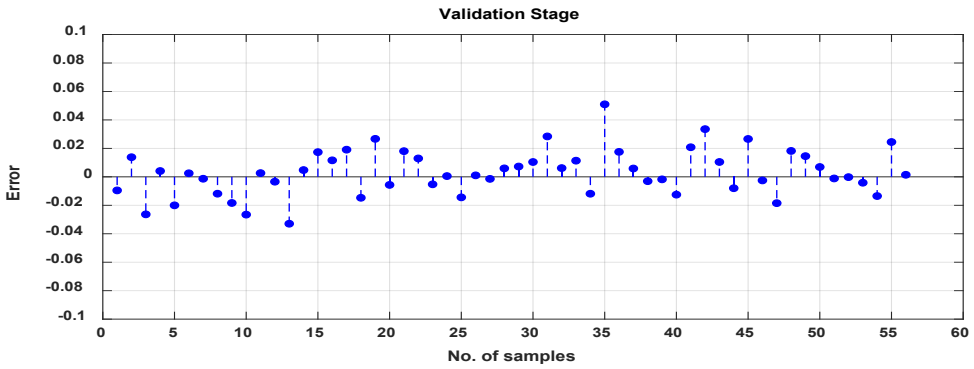

Figure 5-A.4: Residual scatterplots for validation data stage

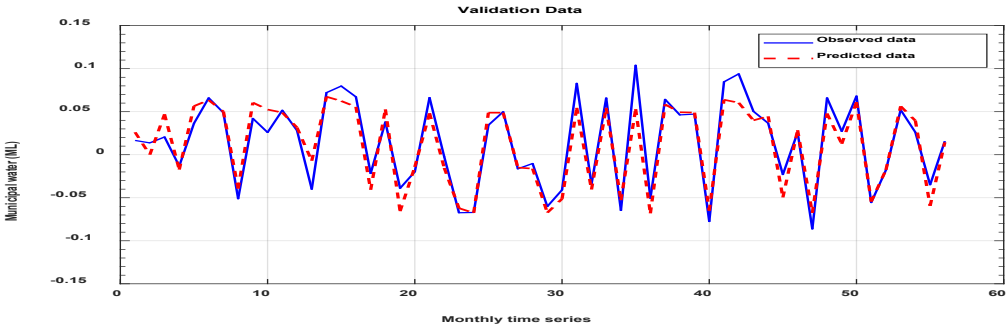

Figure 5-A.5: Observed and predicted stochastic signal of municipal water demands for the validation data

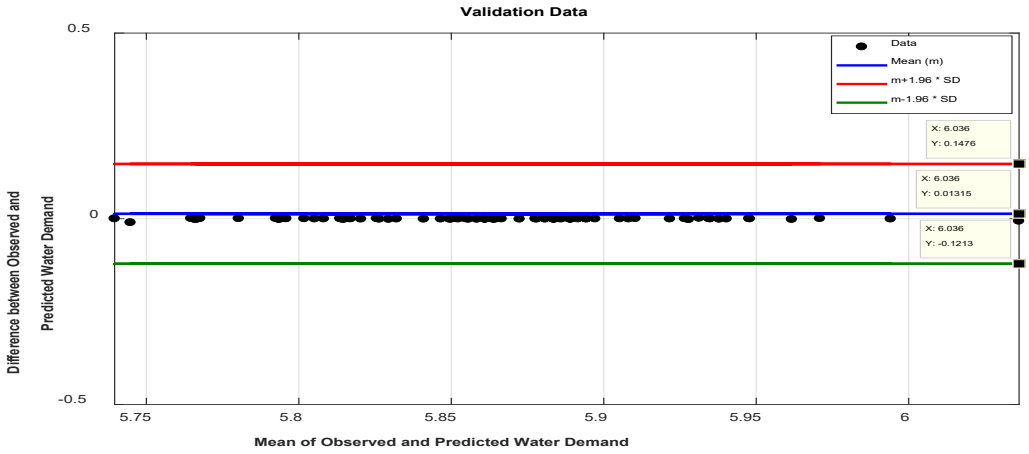

Figure 5-A.6 : Bland–Altman plot of the relation between observed and predicted stochastic signal of municipal water

Table 5-A.2: Three statistical criteria for the validation data

Data	MAE	MSE	RMSE
Validation	0.0126	2.6431 e^{-04}	0.0163

MAE: mean absolute error, MSE: mean square error, RMSE: root mean square error

Appendix 5-B

The results of yearly data for maximum temperature (Tmax.), rainfall (Rain.) and solar radiation (Radi) under A1B, B1 and A2 scenarios over three future for Melbourne City

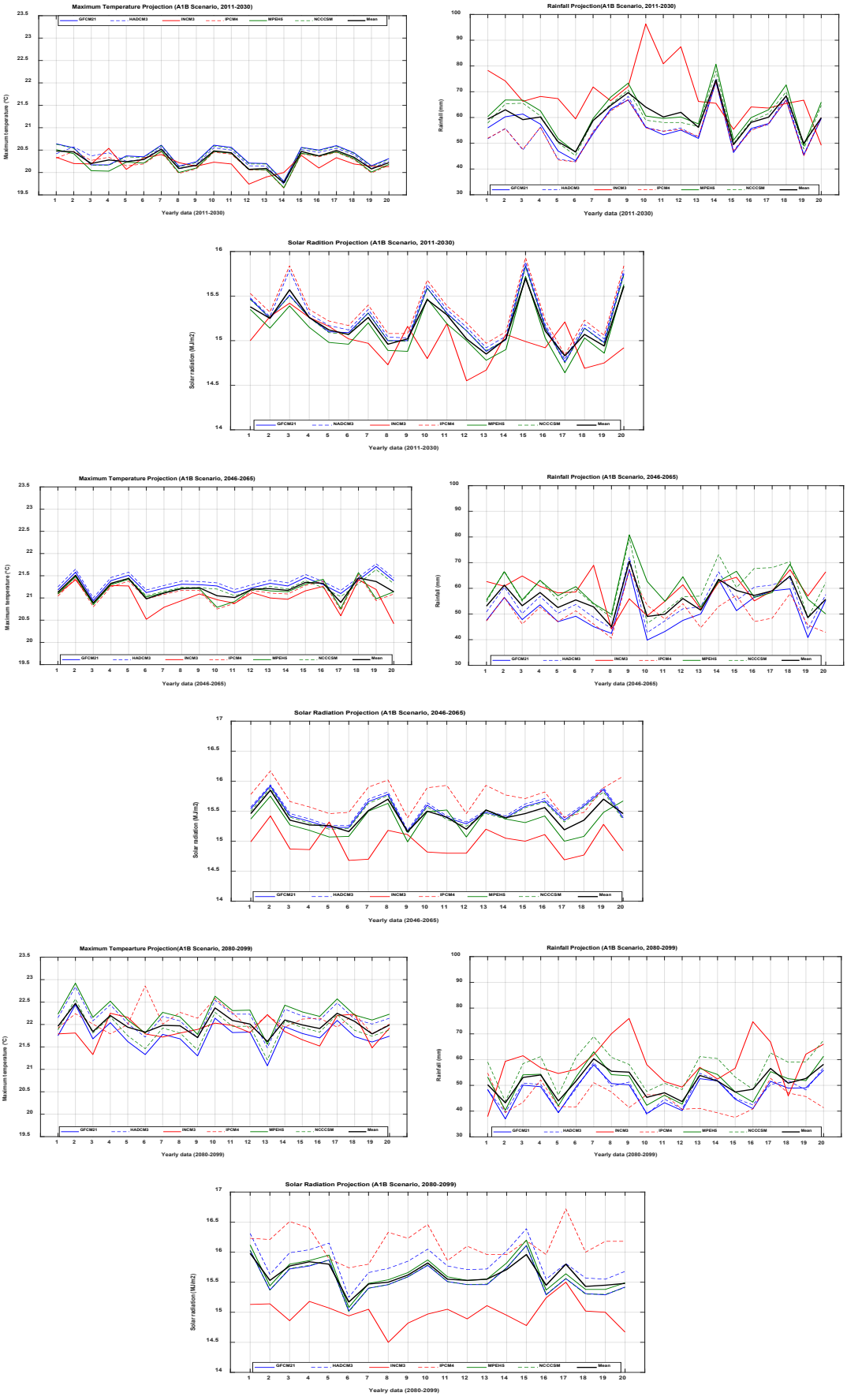

Figure 5-B.1: Projected yearly Tmax, Rain and Radi data under A1B scenario

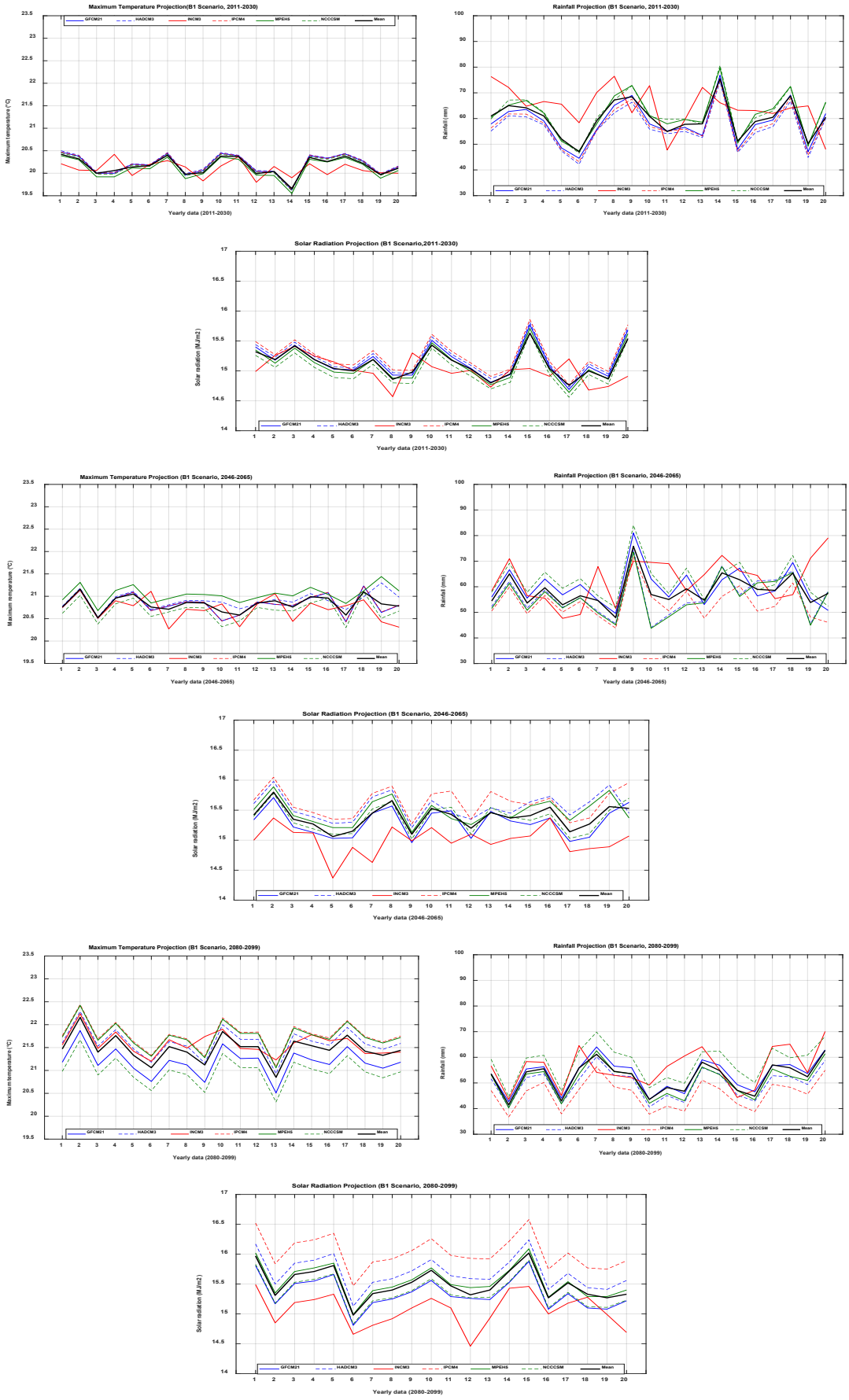

Figure 5-B.2: Projected yearly Tmax, Rain and Radi data under B1 scenario

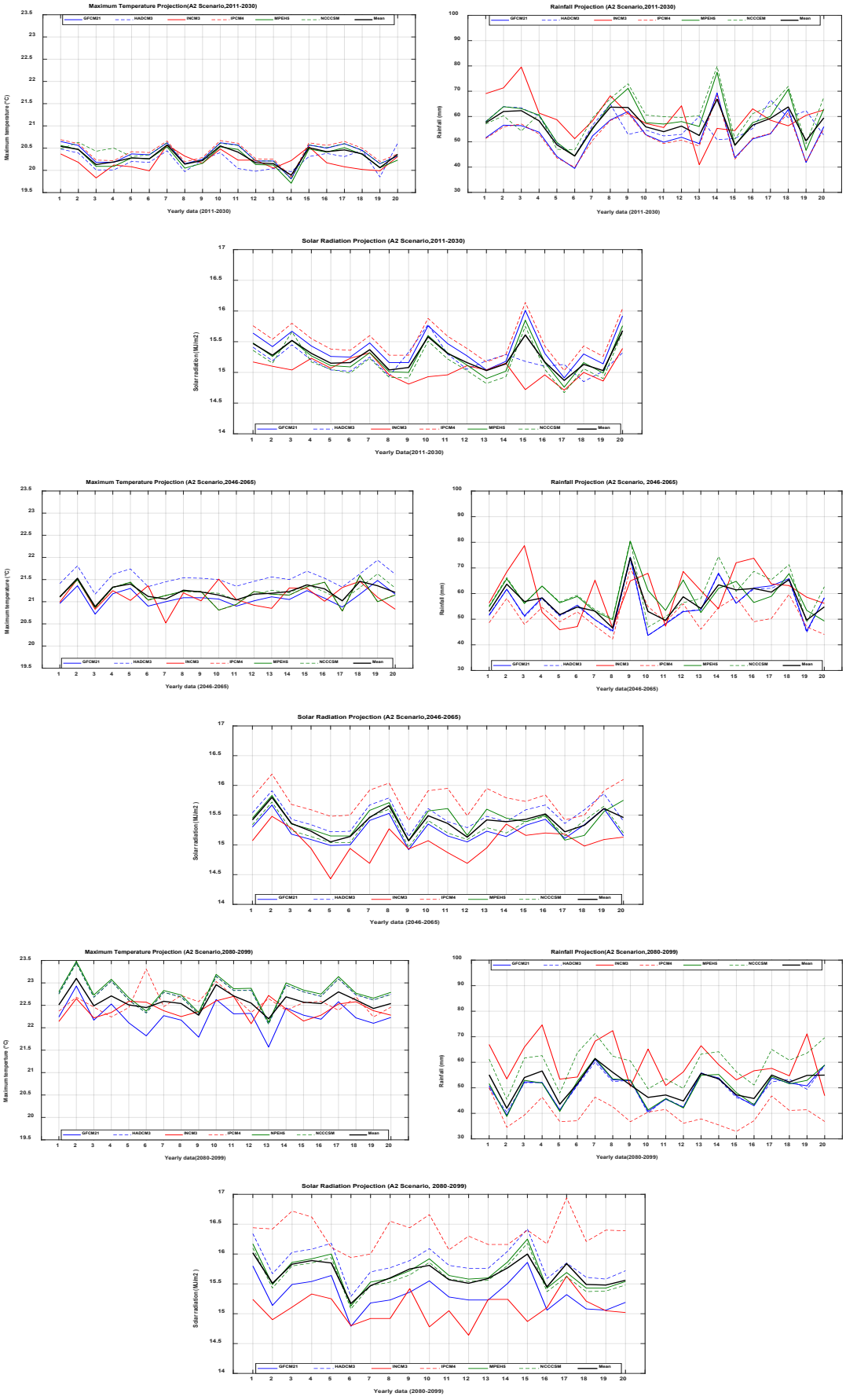

Figure 5-B.3: Projected yearly Tmax, Rain and Radi data under A2 scenario

Appendix 5-C

The results of monthly average mean with confidence interval level, 0.95% for B1 and A2 scenarios, for all climate factors over the three periods for Melbourne City.

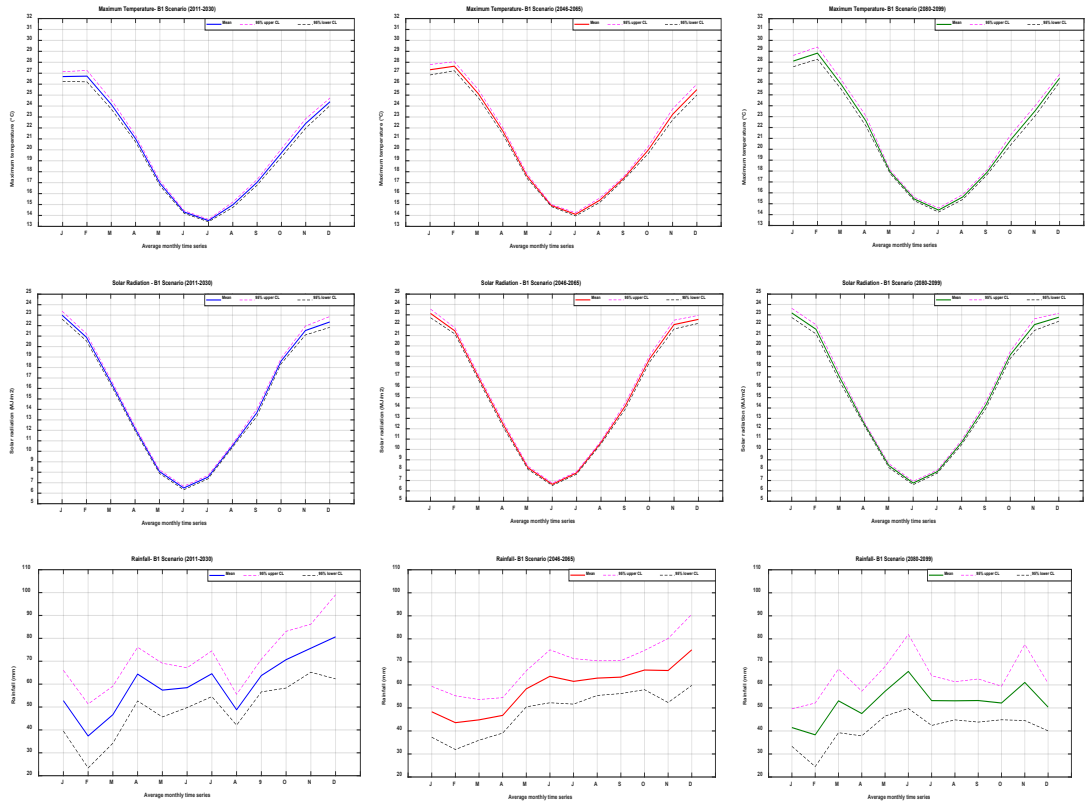

Figure 5-C.1 : The average monthly mean for three simulated climate factors of B1 scenario over the future periods (2011-2030, 2046-265 and 2080-2099)

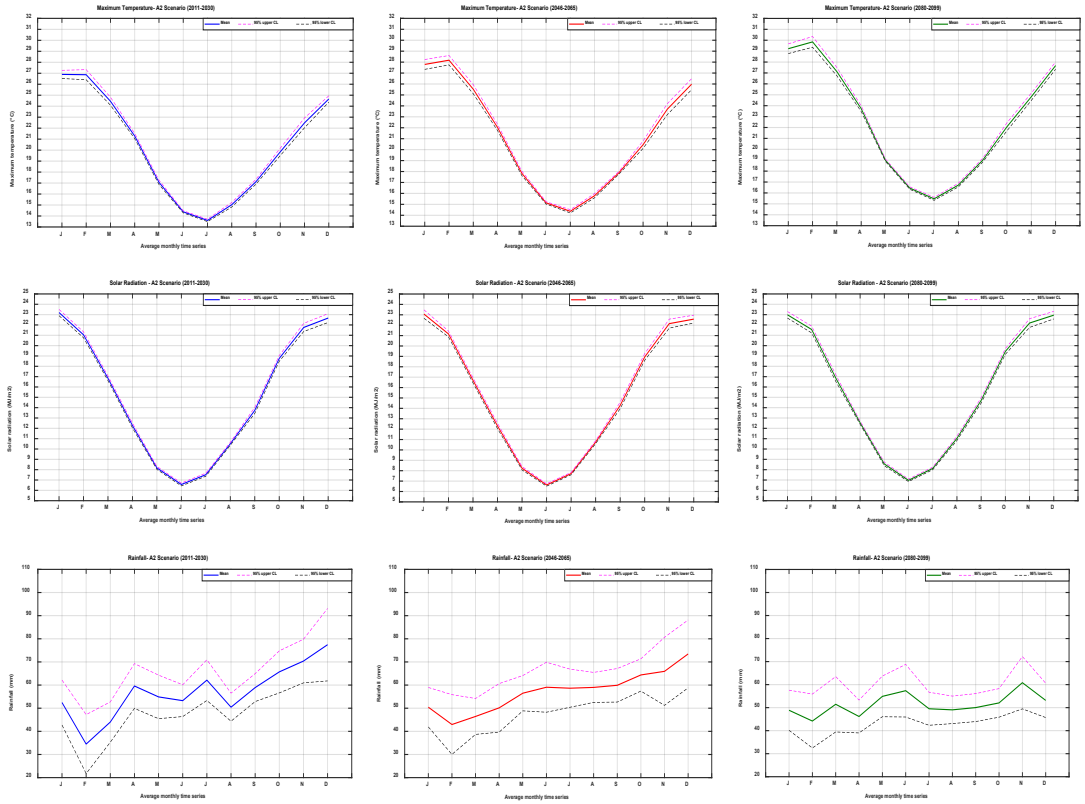

Figure 5-C.1: The average monthly mean for three simulated climate factors of A2 scenario over the future periods (2011-2030, 2046-265 and 2080-2099)

Appendix 5-D

The expected climate factors under B1, A1B and A2 scenarios for three periods (Melbourne City).

Figure 5-D.1:The maximum temperature projection under B1, A1B and A2 scenarios for the period (2011-2030)

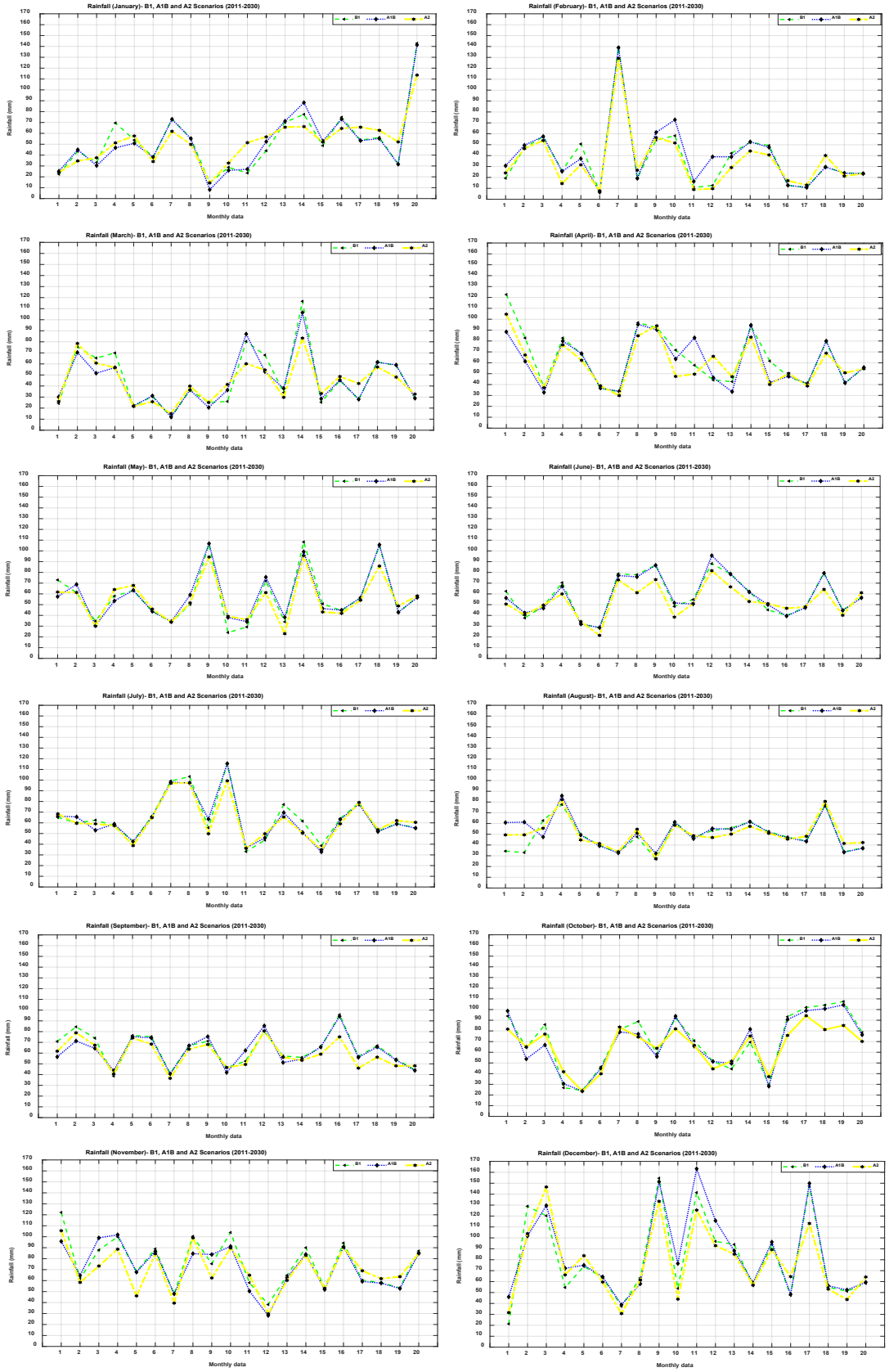

Figure 5-D.2:The rainfall projection under B1, A1B and A2 scenarios for the period (2011-2030)

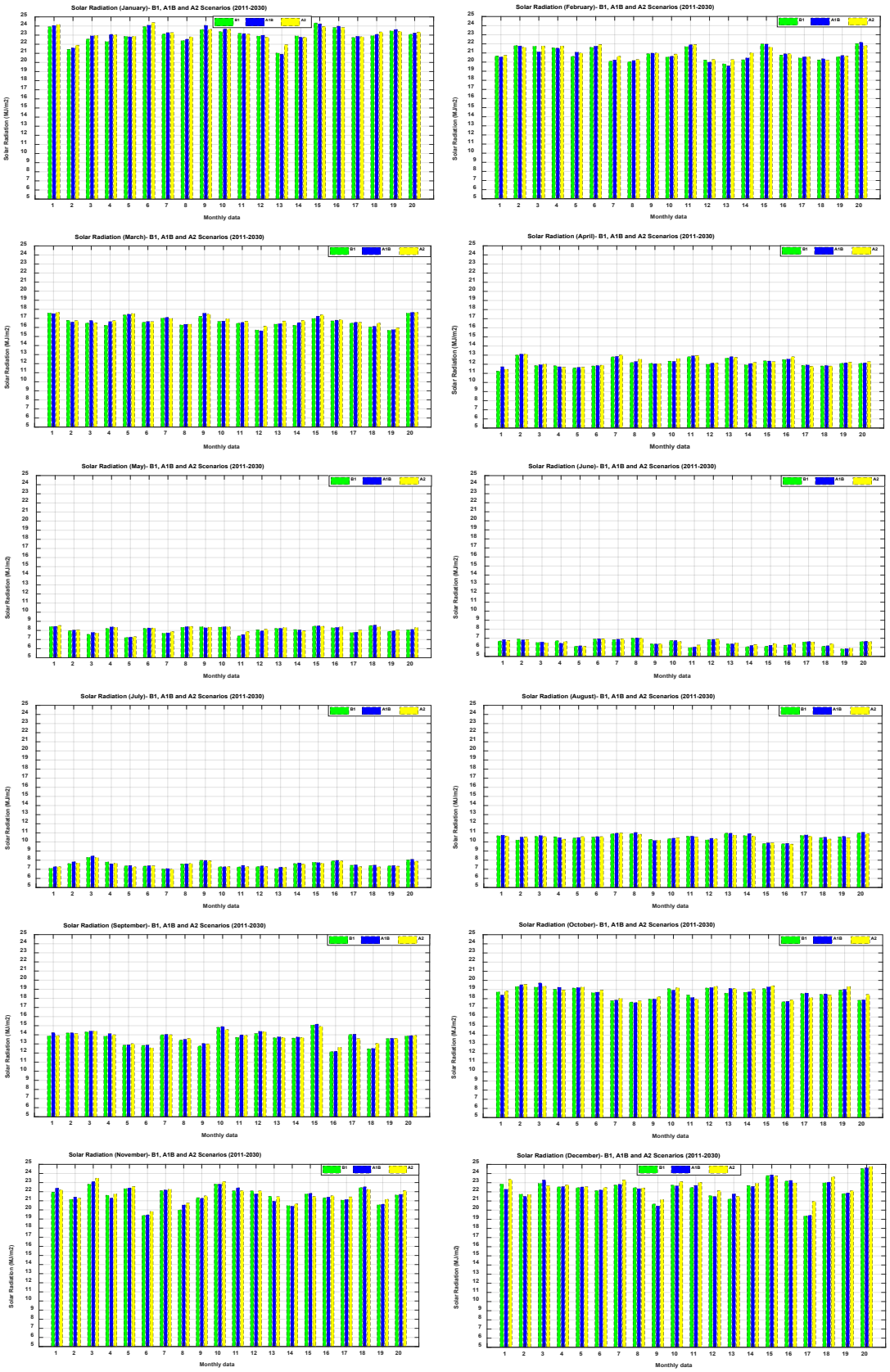

Figure 5-D.3:The solar radiation projection under B1, A1B and A2 scenarios for the period (2011-2030)

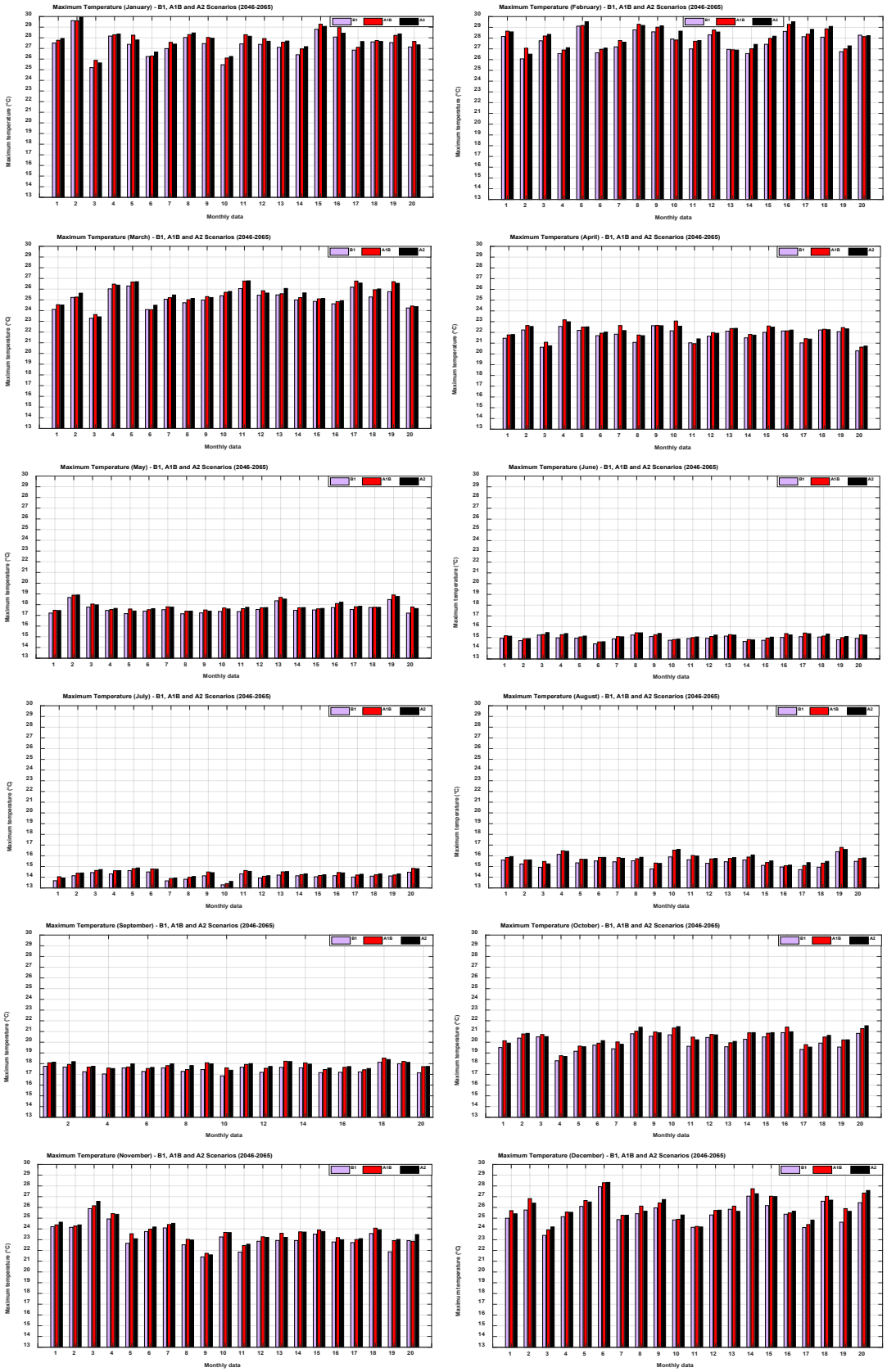

Figure 5-D.4:The maximum temperature projection under B1, A1B and A2 scenarios for the future period (2046-2065)

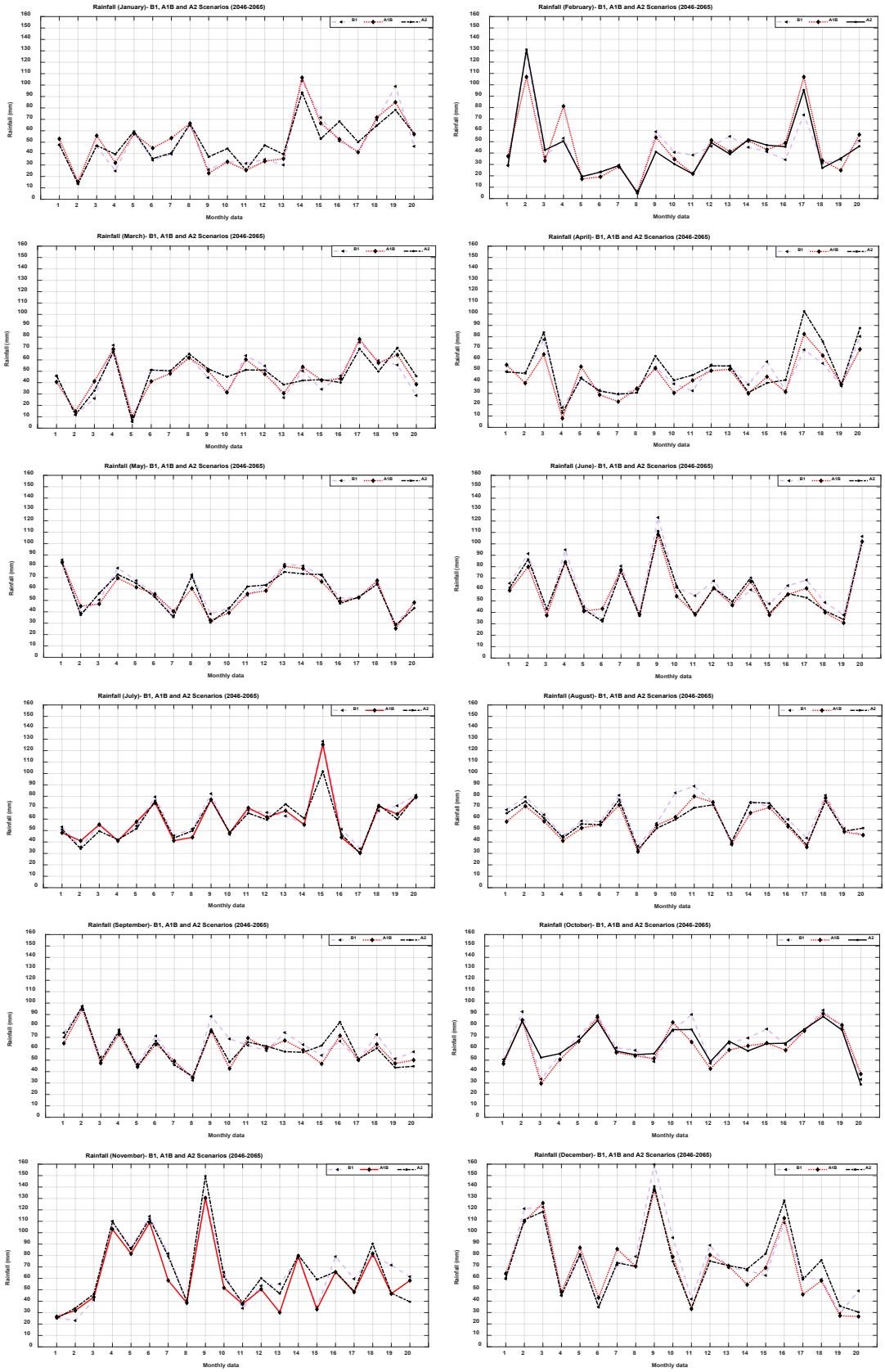

Figure 5-D.5:The rainfall projection under B1, A1B and A2 scenarios for the future period (2046-2065)

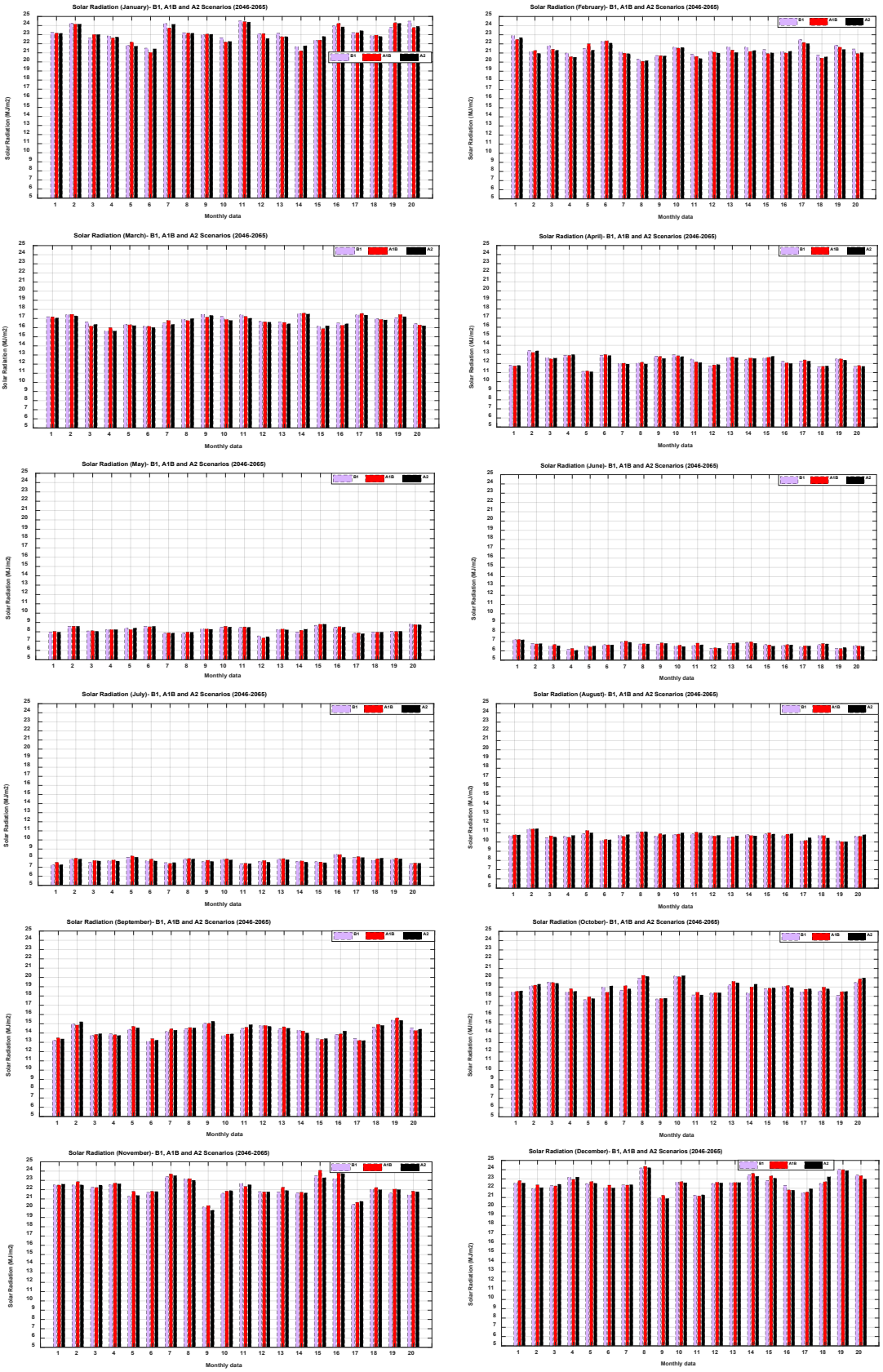

Figure 5-D.6:The solar radiation projection under B1, A1B and A2 scenarios for the future period (2046-2065)

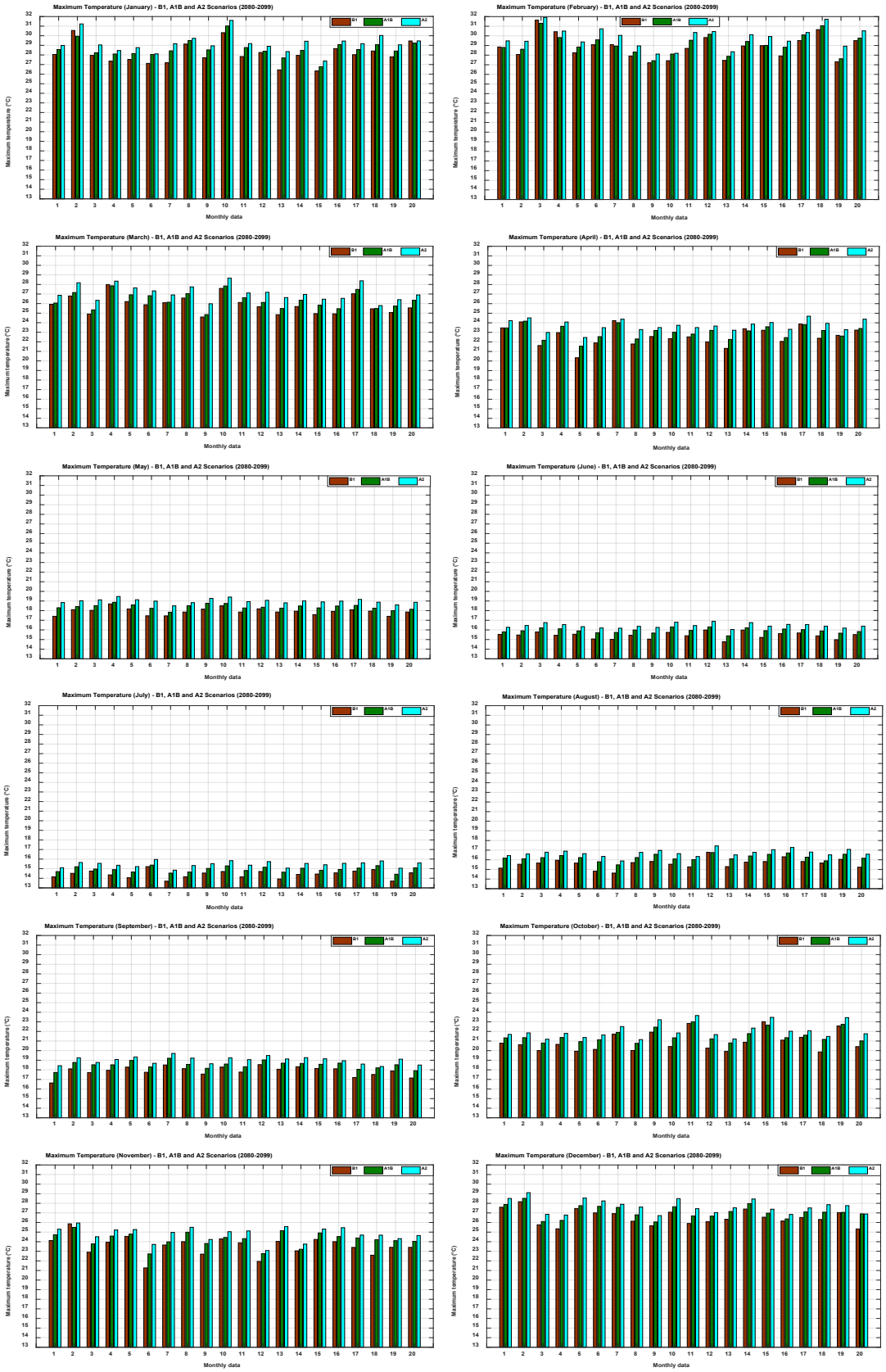

Figure 5-D.7:The maximum temperature projection under B1, A1B and A2 scenarios for the future period (2080-2099)

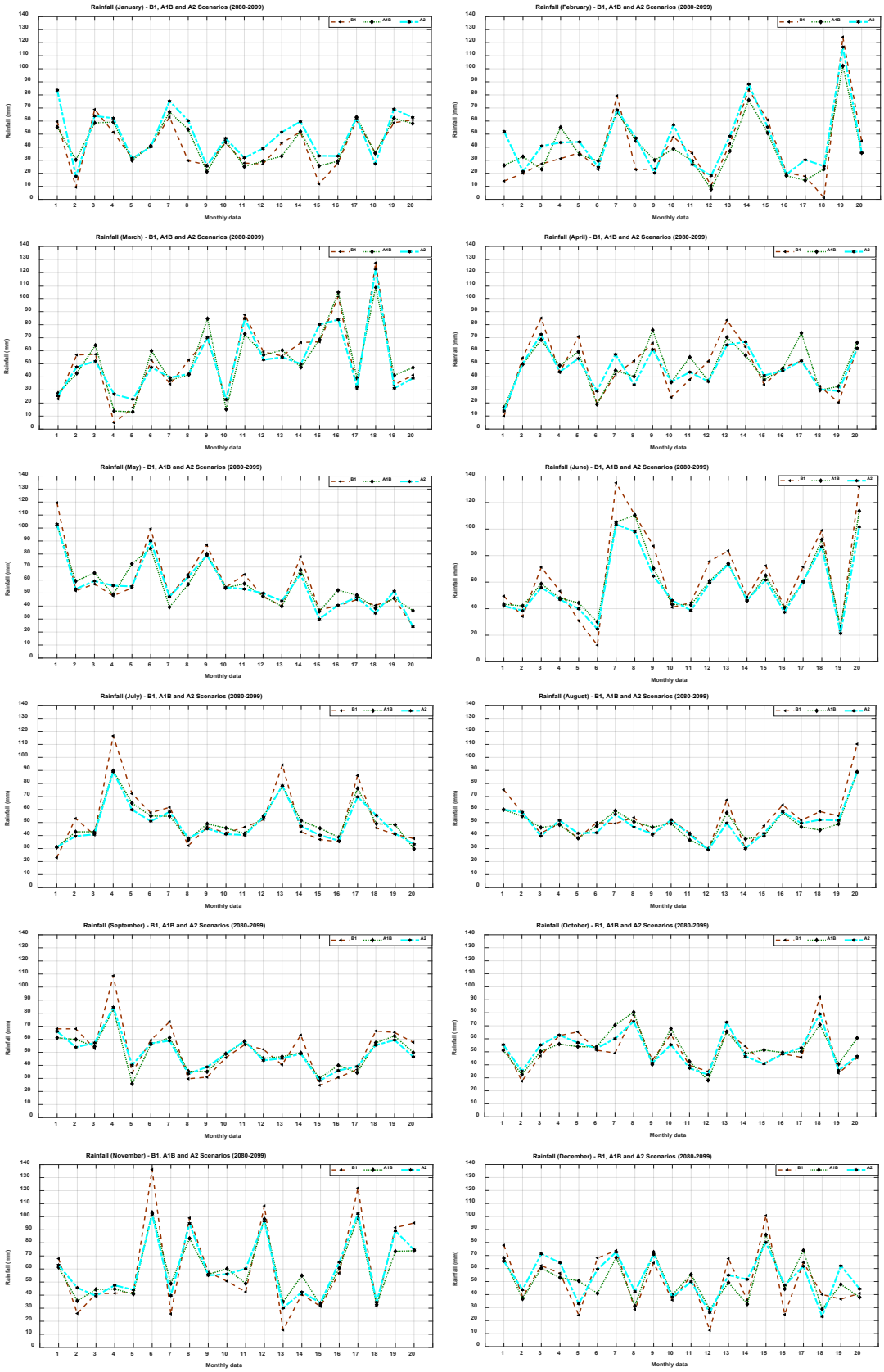

Figure 5-D.8:The rainfall projection under B1, A1B and A2 scenarios for the future period (2080-2099)

Figure 5-D.9:The solar radiation projection under B1, A1B and A2 scenarios for the future period (2080-2099)

Appendix 5-E

The differences between the expected stochastic signals of the ensemble means and the baseline (1980-2010) for all climate factors under B1, A1B and A2 scenarios for all periods (Melbourne City).

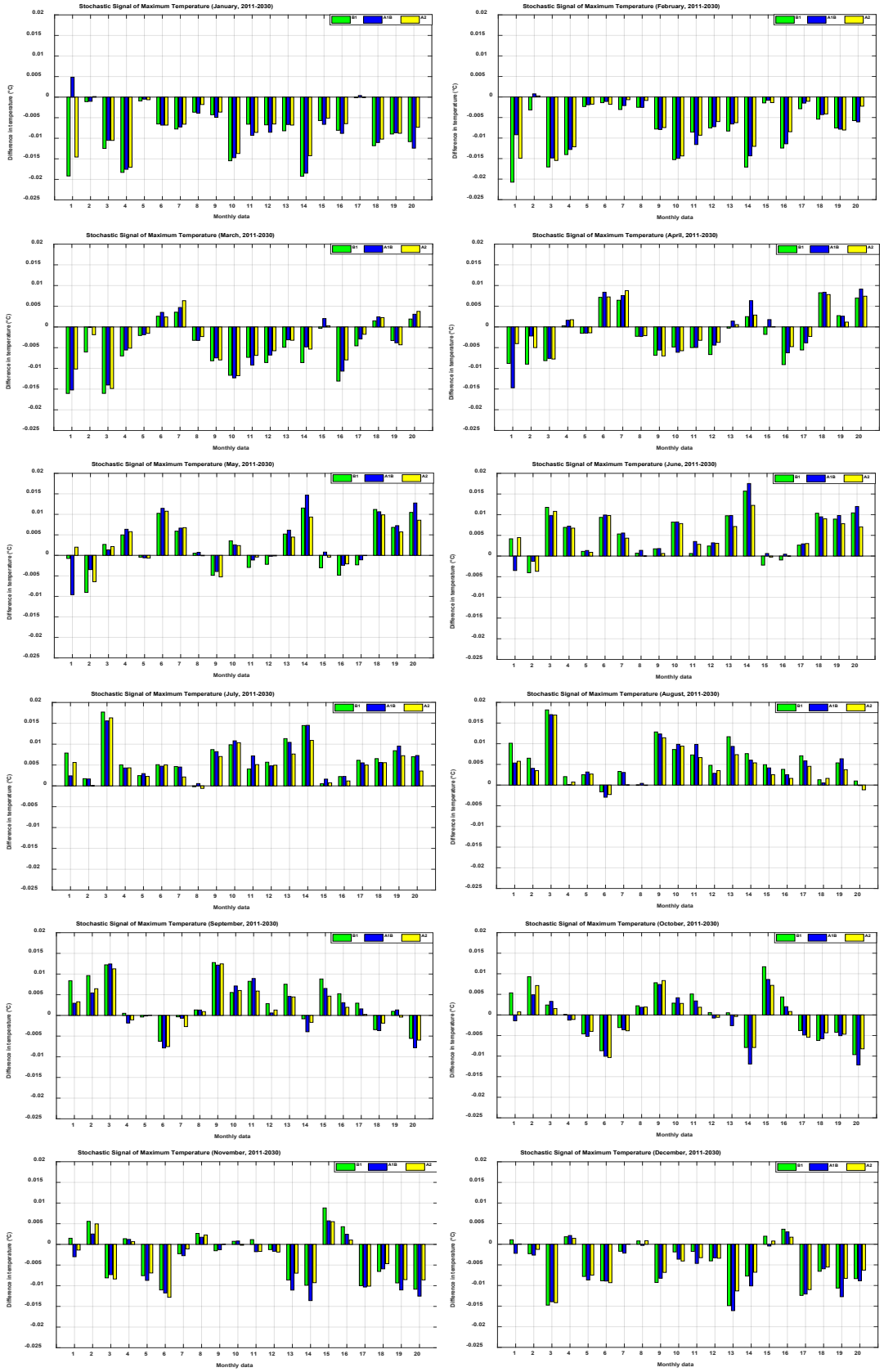

Figure 5-E.1: Stochastic signals of the maximum temperature projection under B1, A1B and A2 scenarios for the period (2011-2030)

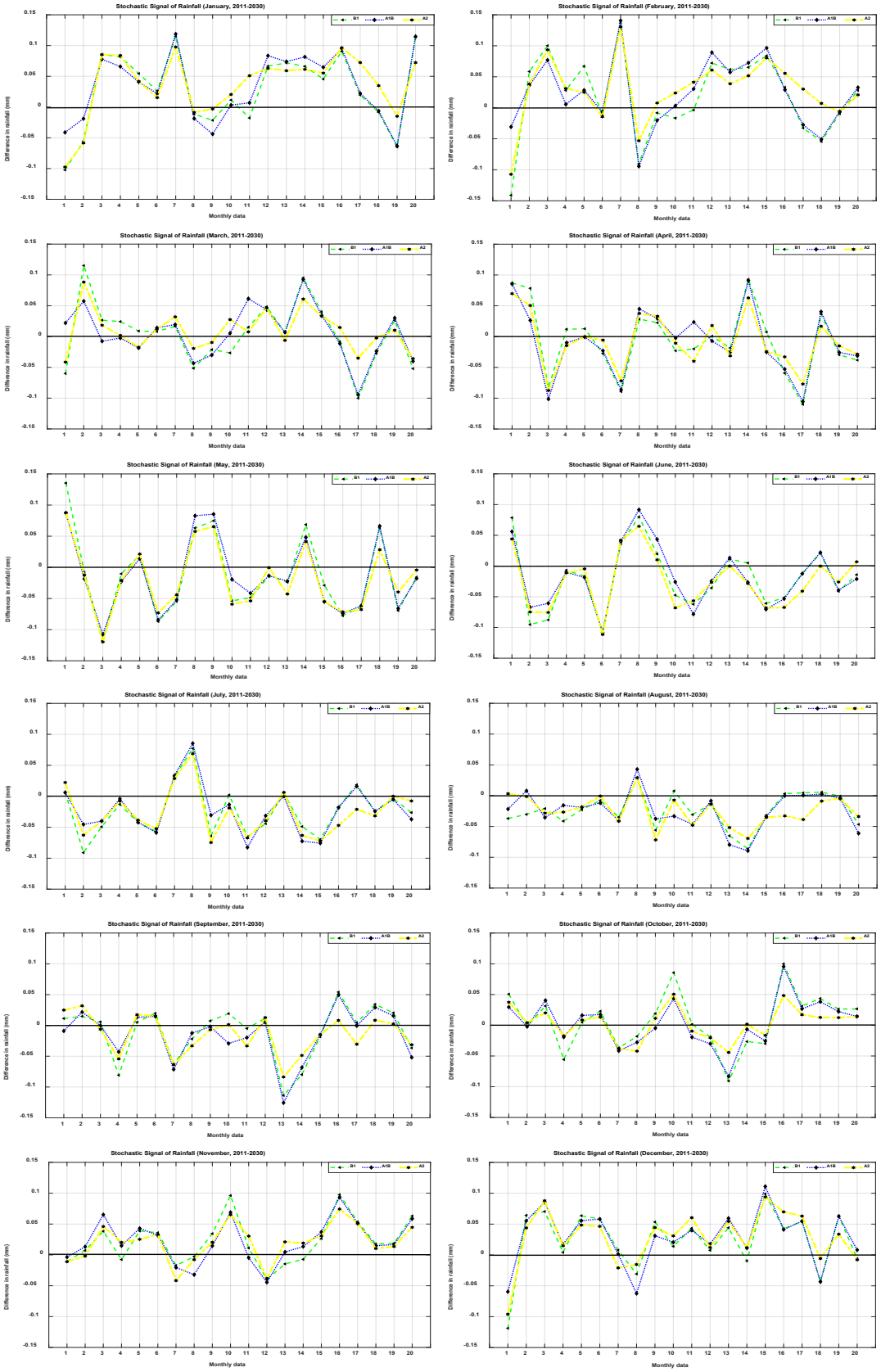

Figure 5-E.2: Stochastic signals of the rainfall projection under B1, A1B and A2 scenarios for the period (2011-2030)

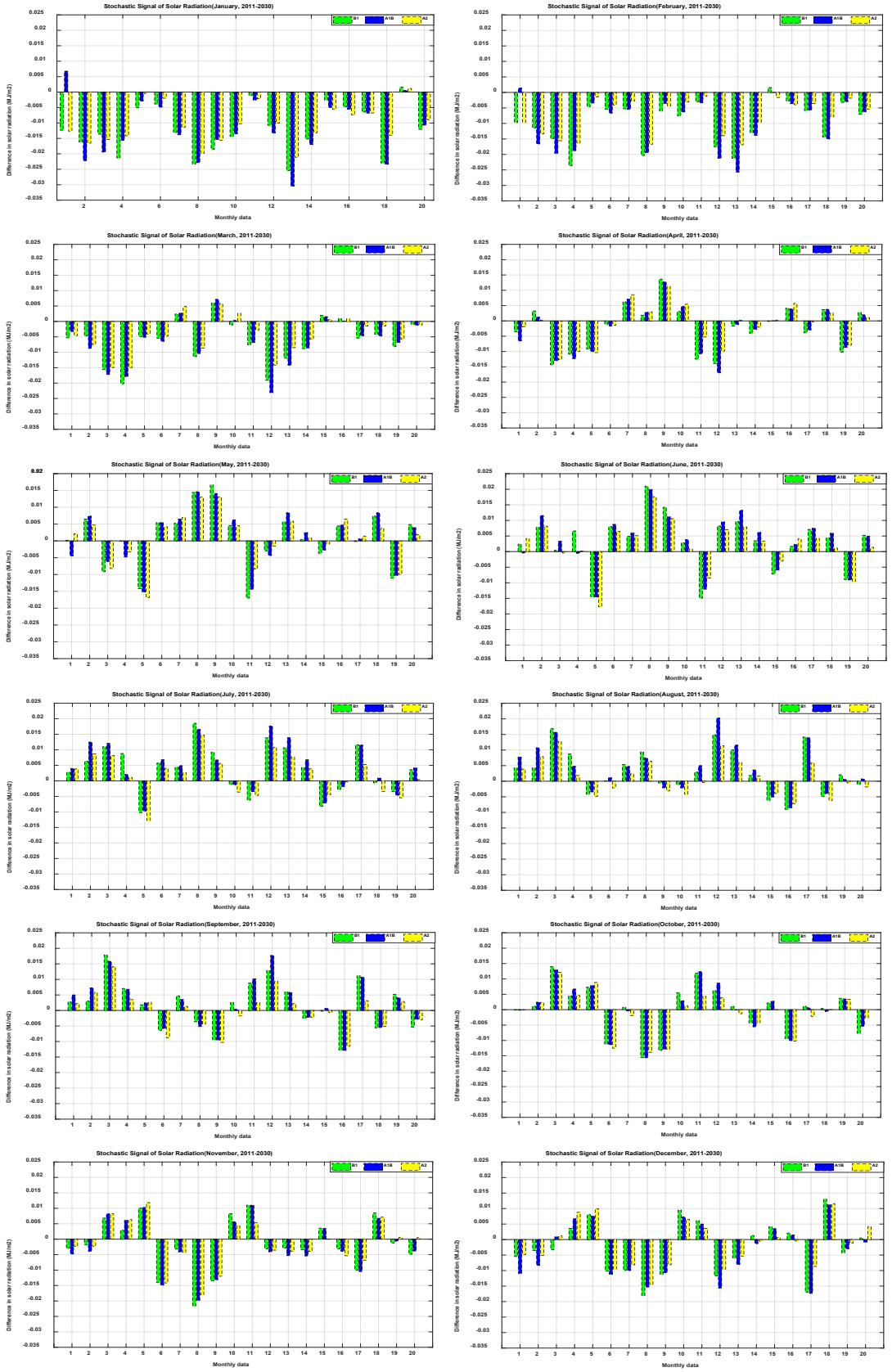

Figure 5-E.3: Stochastic signals of the solar radiation projection under B1, A1B and A2 scenarios for the period (2011-2030)

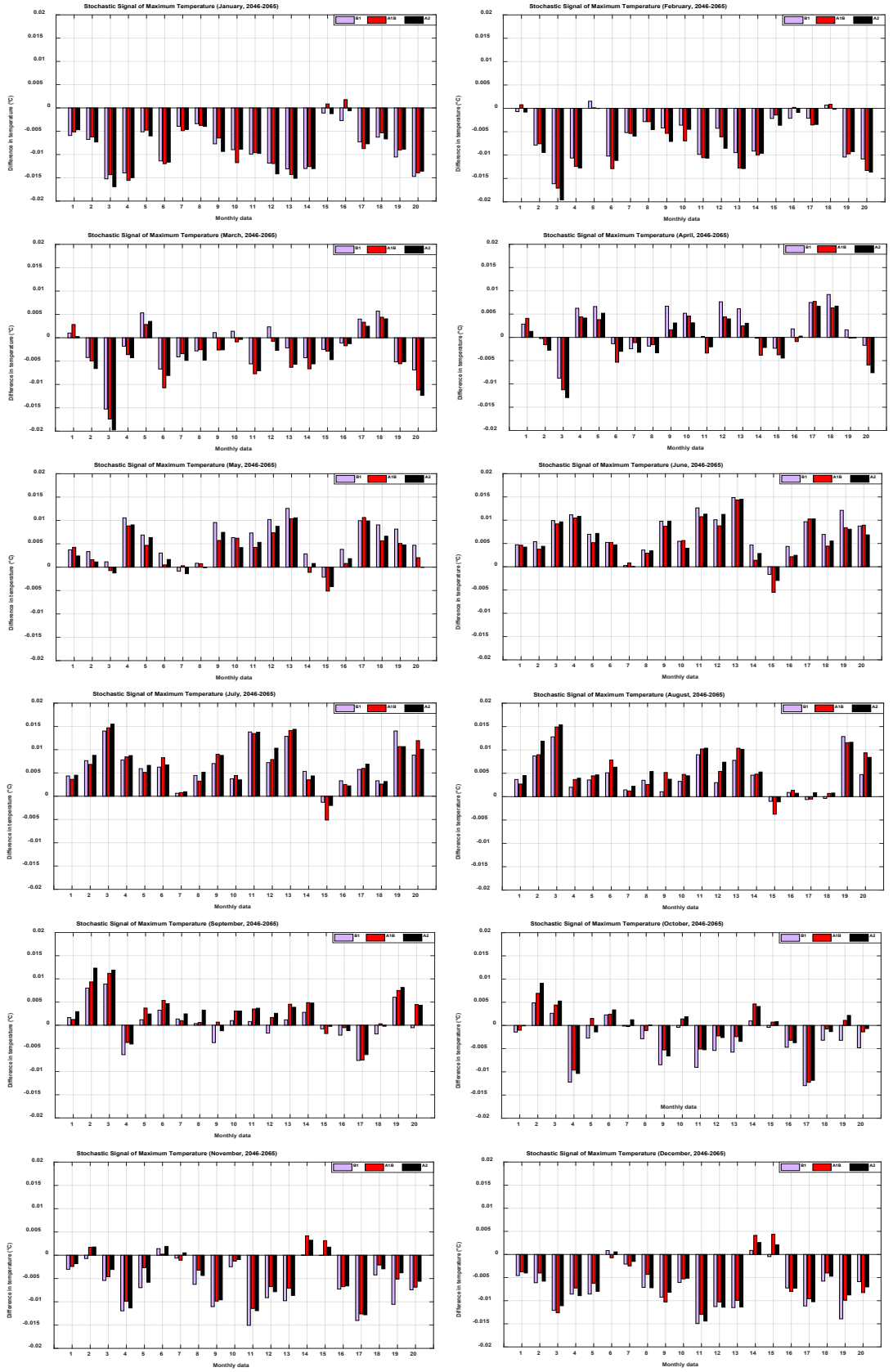

Figure 5-E.4: Stochastic signals of the maximum temperature projection under B1, A1B and A2 scenarios for the future period (2046-2065)

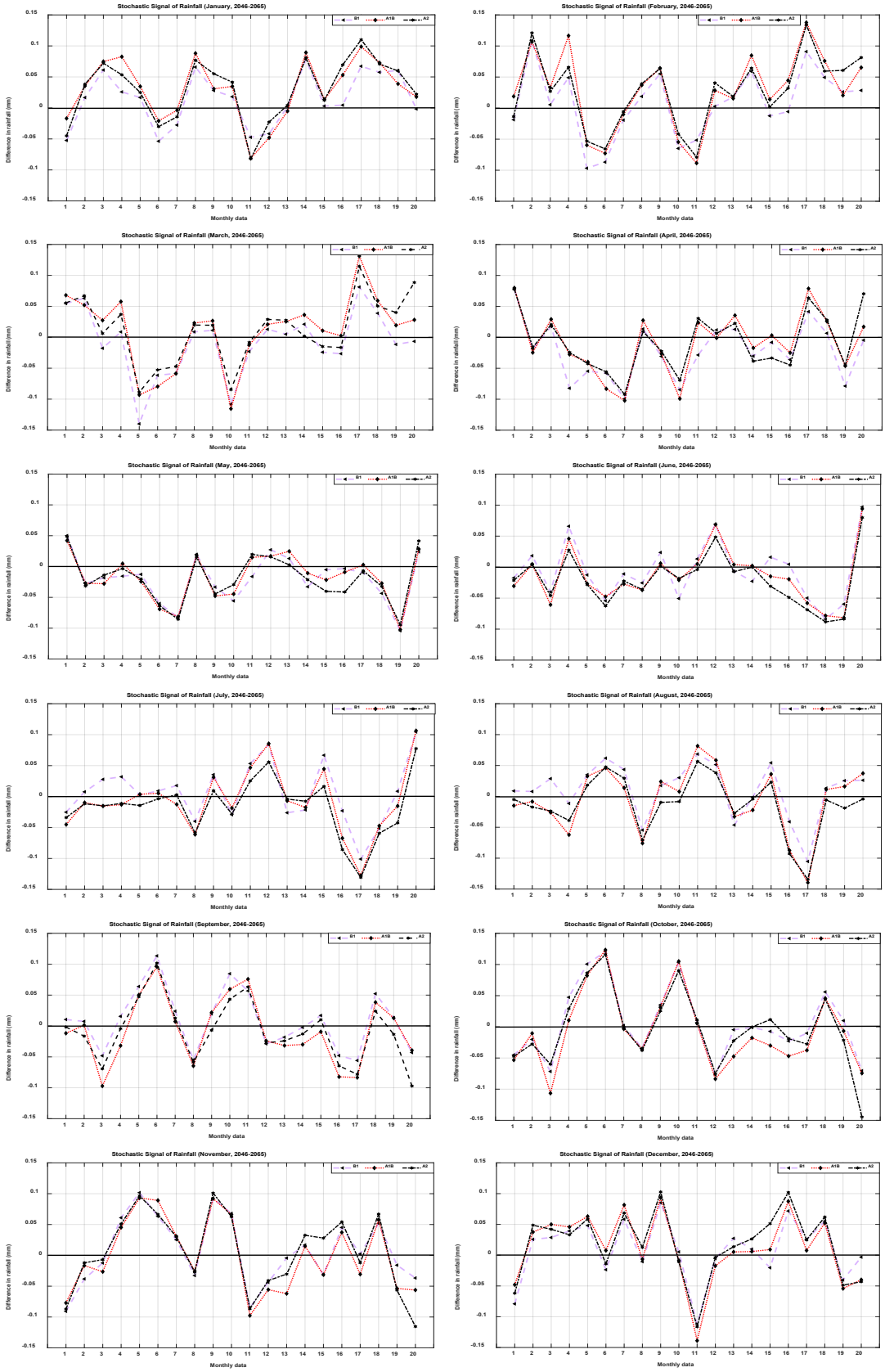

Figure 5-E.5: Stochastic signals of the rainfall projection under B1, A1B and A2 scenarios for the future period (2046-2065)

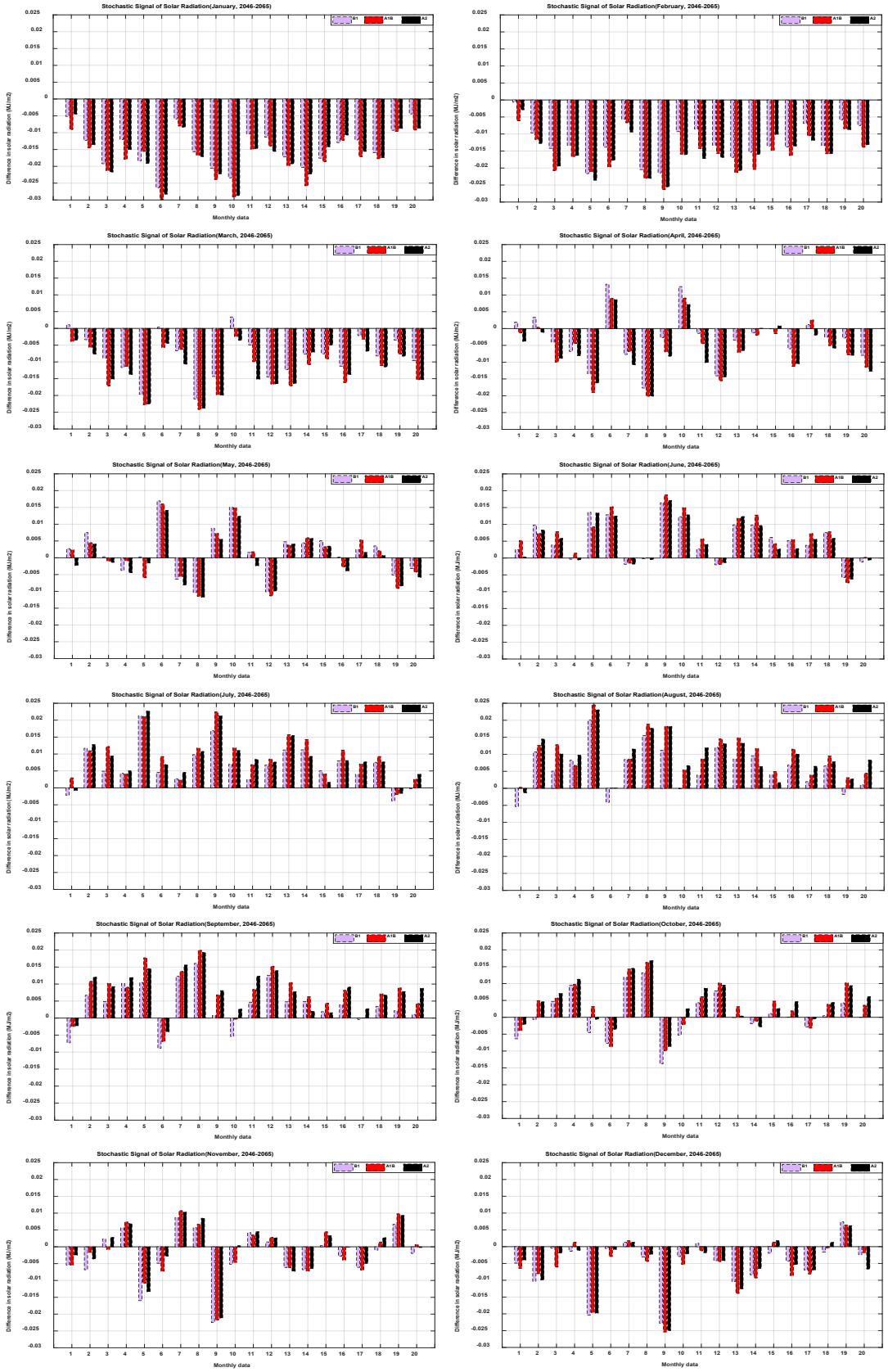

Figure 5-E.6: Stochastic signals of the solar radiation projection under B1, A1B and A2 scenarios for the future period (2046-2065)

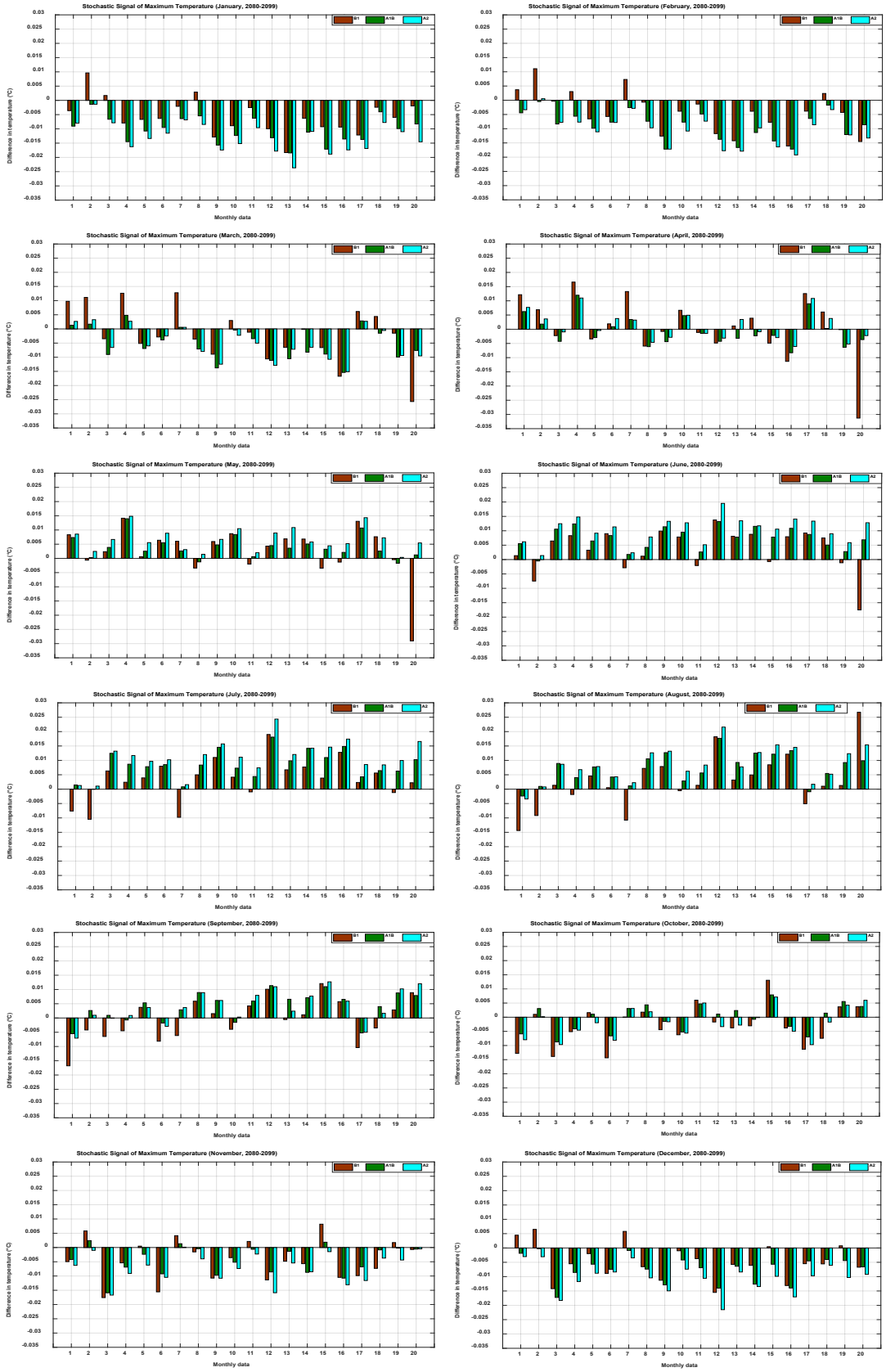

Figure 5-E.8: Stochastic signals of the maximum temperature projection under B1, A1B and A2 scenarios for the future period (2080-2099)

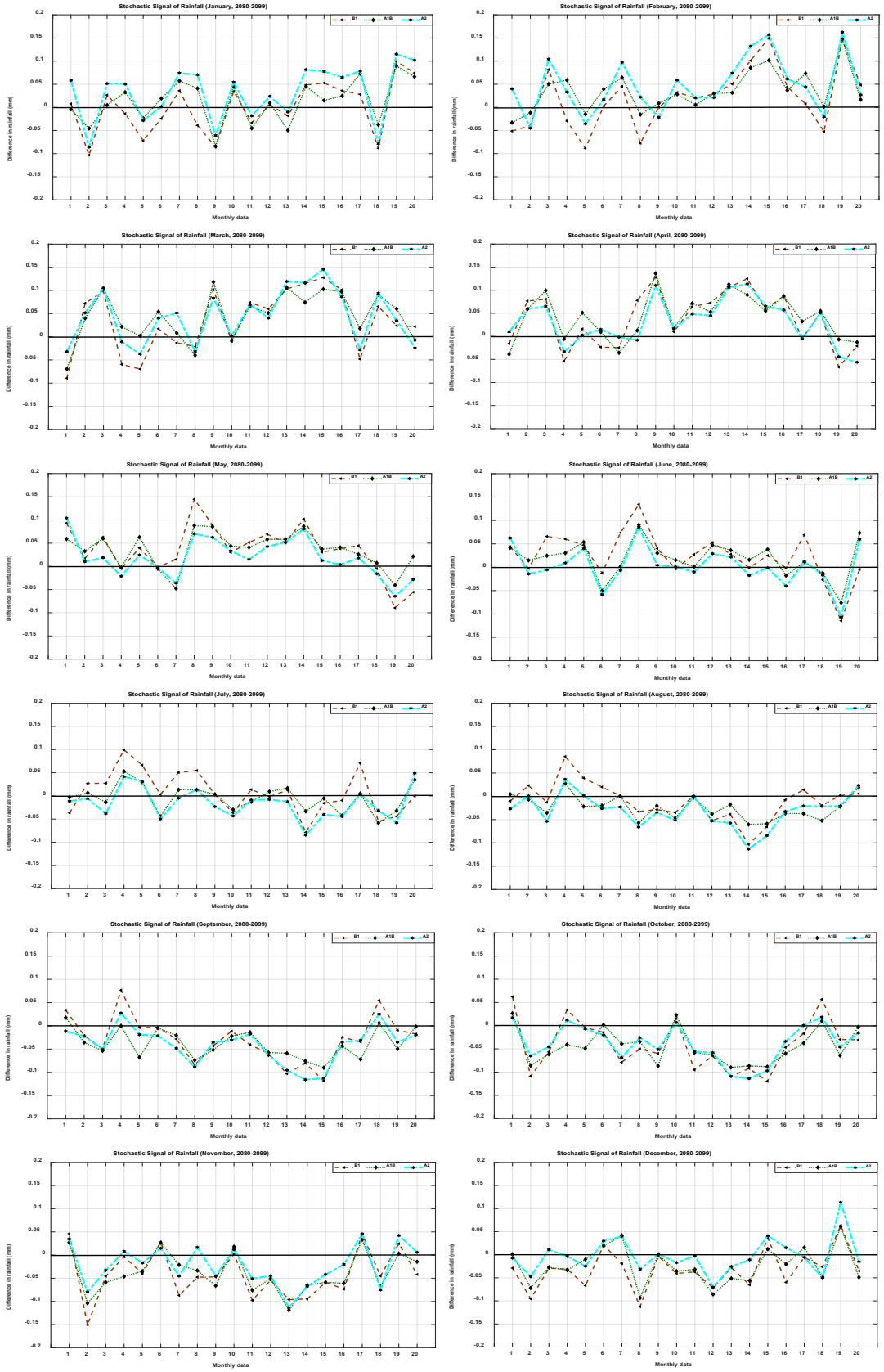

Figure 5-E.8: Stochastic signals of the rainfall projection under B1, A1B and A2 scenarios for the future period (2080-2099)

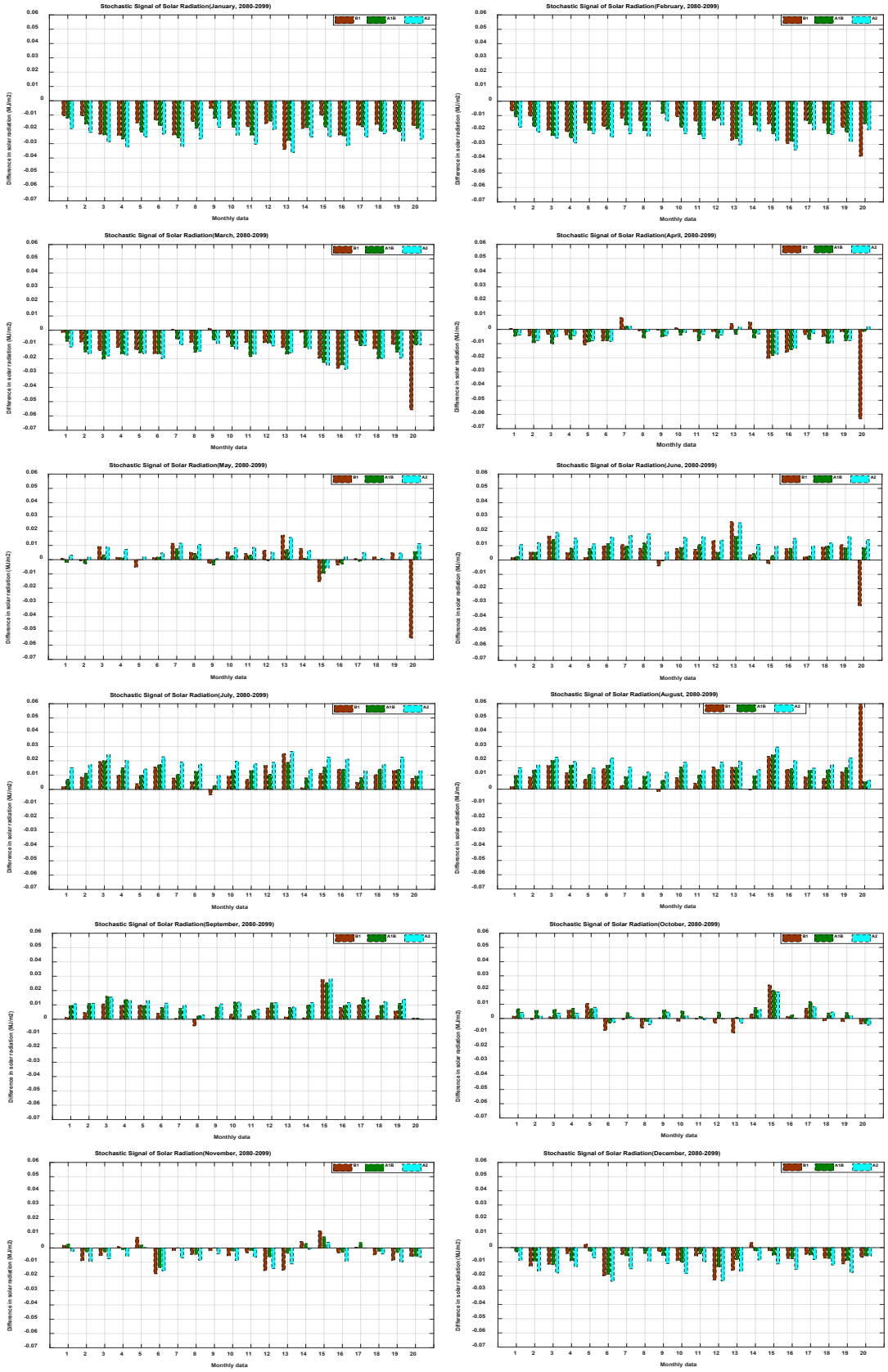

Figure 5-E.9: Stochastic signals of the solar radiation projection under B1, A1B and A2 scenarios for the future period (2080-2099)